

Functional roles of synaptic inhibition in auditory temporal processing

Dissertation

zur Erlangung des Grades eines Doktors der Naturwissenschaften

an der Fakultät für Biologie

der Ludwig-Maximilians-Universität München

vorgelegt von

Michael Pecka

München, Juli 2008

Erstgutachter: Prof. Dr. Benedikt Grothe
Zweitgutachter: Prof. Dr. Mark Hübener
Tag der mündlichen Prüfung: 27.10.2008

Für Oldřich Pecka

Table of Contents

SUMMARY	7
ZUSAMMENFASSUNG	11
INTRODUCTION	15
General motivation	15
The encoding of auditory stimuli in the mammalian brain	16
The mammalian ascending auditory pathway	17
Sound localization cues in the horizontal plane	19
ITD processing in the MSO	20
ITD coding in the Nucleus Laminaris in Birds	24
IID processing in the LSO	25
The medial nucleus of the trapezoid body	26
The dorsal nucleus of the lateral lemniscus	27
Persistent Inhibition in the DNLL and the Precedence Effect	28
Synaptic inhibition in neuronal processing	30
Goals of this study and contributions of the author to the individual chapters	32
RESULTS	35
CHAPTER 1	37
CHAPTER 2	51
CHAPTER 3	69
CHAPTER 4	85
GENERAL DISCUSSION	97
Functional roles of inhibition in coincidence detection	97
Sustained inhibition as a functional role for GABAergic transmission	100
Gain of information by disinhibition: Implications on coding strategies	101
Future perspectives	102
REFERENCES	105
List of abbreviations	115
Curriculum Vitae	117
List of publications	118
Acknowledgments	119
Ehrenwörtliche Erklärung	121

SUMMARY

Hearing and vision are important senses that mammals – including humans – use to orientate in their environment. The accurate localization of a sound source represents a particular challenge to the central nervous system, because unlike for vision, a particular location in auditory space is not mapped onto a specific location in the brain. Instead, locations in space are neuronally computed by the evaluation of physical parameters of the sound. The detection and processing of some of these physical parameters requires extreme temporal precision. Specifically, low frequency sound sources along the azimuth are localized by utilizing differences in the arrival time of the sound at the two ears (interaural time differences, ITDs) in the range of microseconds. In contrast, the duration of action potentials – the electrical signals by which neurons transmit information – is in the range of a millisecond. To overcome this discrepancy, specialized neurons of the auditory brainstem evolved to function as coincidence detectors between the inputs they receive from the left and right ear. These neurons modulate their response rate as a function of ITD with microsecond precision. Recent findings revealed that synaptic inhibition tunes these coincidence detector neurons to achieve optimal ITD sensitivity. However, the functional mechanism by which inhibition enhances ITD processing is unclear. In particular, it is unknown whether the timing of the inhibitory inputs relative to the excitatory inputs is crucial for the enhancement.

In addition to the extreme temporal sensitivity required for faithful sound source localization, the auditory system is additionally confronted with spurious spatial cues stemming from reflections and echoes. The system copes with this challenge by suppressing the directional information of these secondary sounds without eliminating their overall perception. Hence, identification and facultative evaluation of echoes is another fundamental requirement for accurate orientation in space. However, the neuronal mechanisms underlying the exquisite ability of the brain to cope with this challenge are not yet understood.

To gain insight into the functional roles of synaptic inhibition for sound localization and to identify relevant neuronal circuits, we made *in vivo* extracellular single cell recordings in anesthetized gerbils, at times combined with pharmacological manipulations. Additionally, we obtained human behavioral and modeling data, confirming our physiological results in a general framework. In the following, the result section of this thesis is divided into four chapters, reflecting the different studies that were conducted:

Chapter 1

In this study, we investigated the mechanisms of ITD processing at the initial binaural stage within the ascending auditory pathway, the medial superior olive (MSO), where ITD sensitivity is first created. The data acquired by *in vivo* single cell recordings in the MSO strongly corroborated a recently formulated hypothesis about the ITD-coding strategy in mammals. This hypothesis was predominately based on data from recordings of the auditory midbrain and stated that low frequency sound localization is accomplished by rate-coding of the entire population of ITD sensitive neurons. Moreover, to probe the role of the prominent inhibitory inputs to the MSO, we performed pharmacological experiments. Tonic application of the inhibitory transmitter glycine affected the ITD tuning of MSO neurons in an analogous way to pharmacological blockade of the endogenous glycinergic inhibition. Specifically, both drugs degraded the ITD sensitivity in the MSO cells. Thus, these experiments suggest that endogenous inhibition at the MSO is not acting tonically, but rather that precise timing of the glycinergic inputs in relation to the excitatory inputs on a cycle-by-cycle basis is essential for the ITD detection mechanism.

Chapter 2

As mentioned before, the MSO is the initial stage at which ITD sensitivity is created. Unfortunately, *in vivo* recordings from the MSO are notoriously difficult because of its relatively small size and distant location in the brainstem, surrounded by auditory fiber bundles which further hinder the isolation of single neuronal responses. MSO neurons project directly to the dorsal nucleus of the lateral lemniscus (DNLL), a nucleus that is readily accessible in *in vivo* preparations. Performing *in vivo* extracellular recordings, we determined that the ITD sensitivity of DNLL neurons is similar to the ITD sensitivity of MSO neurons, hence that no major transformations are present at the level of the DNLL. Hence, we showed that the DNLL is a surrogate model nucleus to investigate ITD processing. Subsequently, we investigated the relative timing of inhibition and excitation for ITD processing in DNLL neurons and found indirect evidence for contralateral inhibition preceding the net contralateral excitation on the level of the MSO.

Chapter 3

The findings described in chapters 1 and 2 demonstrated that inhibition is an integral part of the ITD processing mechanism. The majority of the inhibitory inputs to the MSO originate from the neurons of the medial nucleus of the trapezoid body (MNTB). MNTB neurons receive excitatory input from the contralateral cochlear nucleus via a giant calyx-shaped synapse showing remarkable specializations for both high temporal precision and reliable transmission. However, *in vitro* studies using brain-slice preparations have reported very high depression in the output strength and unexpectedly long recovery times from this depression.

To investigate the response characteristics of MNTB neurons in the intact brain, we performed *in vivo* extra-cellular single cell recordings and found that the recovery time constants of MNTB neurons to sustained sound stimulation *in vivo* were much shorter than those derived from *in vitro* measurements. Furthermore, MNTB neurons exhibited a wide spectrum of spontaneous activity, i.e. activity that was not driven by sound stimulation. Simulation of this spontaneous activity in *in vitro* experiments caused a pre-adaptation in the response strength in the MNTB neurons. Consequently, full *in vitro* recovery from depression during sustained activity was shorter in these experiments than in previous studies in which spontaneous activity was missing. Moreover, the *in vitro* recovery time courses obtained with simulated spontaneous activity matched the *in vivo* recovery time courses that we obtained.

Chapter 4

The ability to identify echoes and the context-dependent suppression of directional information in echoes is a prerequisite for faithful sound localization. However, so far the neuronal mechanisms that underlie this ability are unknown. To investigate a circuit potentially dedicated to context-dependent suppression of echo directional information, we performed *in vivo* extracellular single cell recordings in the DNLL. DNLL neurons that were sensitive to differences in the intensity of sounds at the two ears were excited by contralateral stimuli and inhibited by ipsilateral stimuli. Remarkably, in many neurons this inhibition persisted for tens of milliseconds beyond stimulus offset and suppressed responses to trailing stimuli that were excitatory if presented alone. Employing a computational model as well as human psychophysics, we showed that this persistent inhibition created sufficient information at higher auditory stages to generate context dependent echo suppression that agreed closely with the percepts of human subjects.

ZUSAMMENFASSUNG

Um sich in ihrer Umgebung orientieren zu können, sind Säugetiere - wie auch der Mensch - neben der visuellen auf ihre akustische Wahrnehmung angewiesen. Für das Zentralnervensystem stellt die akustische Ortung einer Schallquelle eine besondere Herausforderung dar, da im auditorischen System – im Gegensatz zum visuellen System – eine bestimmte Position im Raum nicht auf einer bestimmten Stelle im Gehirn abgebildet wird. Stattdessen wird die Position aus physikalischen Parametern des Schalls neuronal errechnet. Die Detektierung und Verarbeitung mancher dieser physikalischen Parameter erfordert dabei eine ungemeine zeitliche Präzision. So erfolgt beispielsweise die Ortung tieffrequenter Schallquellen in der Horizontalen über die Detektierung der Laufzeitdifferenzen des Schalls zwischen den beiden Ohren (interaural time differences, ITDs). Die Spanne der auftretenden ITDs befindet sich allerdings nur im Mikrosekundenbereich, während im Gegensatz dazu die Dauer eines Aktionspotenzials, also dem elektrischen Signal, das der Informationsübertragung im Gehirn dient, bereits >1 Millisekunde beträgt. Diese Diskrepanz in der zeitlichen Auflösung wird im auditorischen Stammhirn überwunden, indem spezialisierte Neurone als Koinzidenz-Detektoren ihrer Eingänge von linkem und rechtem Ohr fungieren und dadurch eine mikrosekundengenaue Zuordnung von ITD und Antwortrate erzeugen. Kürzlich wurde entdeckt, dass synaptische Hemmung eine wesentliche Rolle bei der Optimierung der ITD-Sensitivität dieser Koinzidenz-Detektor-Neurone spielt. Der zugrunde liegende Wirkmechanismus der Hemmung ist allerdings noch nicht verstanden. Insbesondere ist unklar, in wiefern eine präzise zeitliche Abfolge von hemmenden und erregenden Eingängen ausschlaggebend für die Optimierung ist, die durch die synaptische Hemmung erzeugt wird.

Neben den enormen Anforderungen in Bezug auf die zeitliche Sensitivität bei der Detektierung relevanter physikalischer Parameter wird das auditorische System zusätzlich mit dem Auftreten von Schallreflexionen und Echos konfrontiert. Eine Einbeziehung deren physikalischer Parameter würde unweigerlich zu einer fehlerhaften Positionsbestimmung der Schallquelle führen. Daher stellt die Identifizierung dieser sekundären Schalle sowie ihre kontextbezogene Interpretierung eine weitere Grundvoraussetzung zur korrekten Orientierung im Raum dar. Die neuronalen Korrelate im auditorischen System, die dieses komplexe Verhalten ermöglichen, sind jedoch unbekannt.

Die Studien dieser Arbeit wurden mit dem Ziel durchgeführt, ein besseres Verständnis für die funktionellen Wirkmechanismen synaptischer Hemmung bei der Schalllokalisierung zu erlangen sowie die beteiligten neuronalen Schaltkreise zu identifizieren. Dazu wurden *in vivo* Ableitungen an der anästhesierten Mongolischen Wüstenrennmaus durchgeführt, teils in

Kombination mit pharmakologischen Manipulationen. Des Weiteren wurden Daten aus Verhaltensversuchen mit Menschen erhoben sowie Computersimulationen durchgeführt, durch die die generelle Relevanz der Ergebnisse aus den physiologischen Experimenten verdeutlicht wurde. Der Ergebnisteil im Folgenden dieser Arbeit ist in vier Kapitel aufgeteilt, wobei jedes Kapitel einer eigenständigen Studie entspricht:

Kapitel 1

In dieser Studie wurden die funktionellen Mechanismen der ITD-Verarbeitung in der medialen oberen Olive (MSO) untersucht, dem Kerngebiet des Stammhirns, deren Neurone für die Generierung der ITD-Sensitivität im Gehirn verantwortlich sind. Mit unseren Daten, die wir in *in vivo* Experimente gewonnen haben, konnten wir eine unlängst aufgestellte Hypothese über die Kodierung von Positionen im Raum bei Säugetieren bestätigen. Diese Hypothese, die zum größten Teil auf Daten von Ableitungen aus dem Mittelhirn basierte, besagt, dass jegliche Position einer tieffrequenten Schallquelle in der Aktivitätsrate der gesamten Population aller ITD-sensitiver Neurone kodiert wird. Darüber hinaus wurde in dieser Studie in Kombination mit den Einzelzelleableitungen durch iontophoretischer Applikation des hemmenden Transmitterstoffes Glyzin oder eines Antagonisten der Zeitverlauf der endogenen Inhibition beeinflusst, um so die Rolle der synaptischen Hemmung bei der ITD-Verarbeitung zu erforschen. Insbesondere wurde die Bedeutung des Timings der hemmenden Eingänge in Relation zu den erregenden Eingängen untersucht. Es stellte sich heraus, dass die tonische Applikation von Glyzin eine ähnliche Wirkung hat wie die pharmakologische Blockierung der endogenen glyzineren Hemmung, da beide Manipulationen zu einer Verschlechterung der ITD-Sensitivität bei den MSO-Zellen führten. Folglich lässt sich aus diesen Ergebnissen ableiten, dass die Wirkung der endogenen glyzineren Hemmung in der MSO nicht auf tonischer Inhibition beruht, sondern dass vielmehr eine zeitlich präzise Abstimmung der hemmenden und erregenden Eingänge essenziell für den Mechanismus der ITD-Verarbeitung ist.

Kapitel 2

Wie bereits erwähnt, wird die interaurale Zeitdifferenzsensitivität in den Neuronen der MSO erzeugt. Allerdings sind Einzelzelleableitungen *in vivo* in der MSO äußerst schwierig, da die MSO ein relativ kleines Kerngebiet im schwer erreichbaren Stammhirn darstellt und zusätzlich von einer Vielzahl von Hörfaserbündeln umgeben ist, deren elektrische Aktivität die Isolierung von Aktionspotentialen einzelner Neurone weiter erschwert. Ein Kerngebiet, das direkte Eingänge von der MSO erhält, ist der dorsale Nucleus des lateralen Lemniscus (DNLL) und im Gegensatz zur MSO ist der DNLL mit den Methoden der *in vivo* Ableitungen leicht zugänglich. Wir konnten in dieser Studie durch Einzelzelleableitungen zeigen, dass es

zu keinen bedeutenden Umgestaltungen der ITD-Sensitivität auf Ebene des DNLL im Vergleich zur MSO kommt. Somit kann der DNLL ersatzweise für die MSO herangezogen werden, um Untersuchungen über ITD-Verarbeitung durchzuführen. So konnten wir im Folgenden im DNLL indirekte Indizien darüber erlangen, dass auf der Ebene der MSO bei Stimulation des kontralateralen Ohrs der Erregung eine Hemmung vorausgeht.

Kapitel 3

Unsere Studien in Kapitel 1 und 2 ergaben, dass synaptische Hemmung eine wichtige Rolle bei der interauralen Zeitdifferenzverarbeitung spielt. Der Großteil der hemmenden Eingänge, die die MSO erhält, stammt von den Neuronen des Medialen Nucleus des Trapezkörpers (MNTB). Die MNTB-Neurone wiederum erhalten erregende Eingänge aus dem kontralateralen Nucleus cochlearis über je eine riesige kelchförmige Synapse. Diese synaptische Verbindung ist wohl einzigartig sowohl in ihrer zeitlichen Präzision als auch in der Zuverlässigkeit ihrer Übertragung. *In vitro* Studien an Hirnschnitten ermittelten allerdings in der Vergangenheit sowohl eine sehr hohe Depression in der Antwortstärke von MNTB Neuronen als auch eine ungewöhnlich langsame Erholung von dieser Depression. Wir führten nun in dieser Studie extrazelluläre Einzelzelleableitungen *in vivo* durch, um die Antworteigenschaften von MNTB Neuronen im intakten Gehirn zu charakterisieren. Unsere Messungen ergaben, dass die Erholung der Antwortdepression *in vivo* deutlich schneller erfolgt als es die Daten der *in vitro* Experimente vermuten haben lassen. Darüber hinaus stellten wir ein breites Spektrum an Spontanaktivität bei den MNTB-Neuronen fest, also Aktivität, die nicht durch Schallstimulation hervorgerufen wurde. Durch die Simulation solcher Spontanaktivität bei *in vitro* Experimenten konnte schließlich eine Prä-Adaptation der Antwortstärke hervorgerufen werden, die dazu führte, dass die Erholung der Antwortstärke von der Depression *in vitro* eine ähnlich kurze Dauer aufwies wie wir sie in den *in vivo* Experimenten zuvor bestimmt hatten.

Kapitel 4

Ein Echo als solches identifizieren zu können sowie seine kontextbezogene Interpretierung ist eine Grundvoraussetzung zur zuverlässigen Ortung einer Schallquelle. Obwohl diese Fähigkeit aus Verhaltensversuchen hinlänglich bekannt ist, konnte hierfür bislang keine physiologischen Korrelate im Gehirn gefunden werden. Wir führten in dieser Studie extrazelluläre Ableitungen *in vivo* im DNLL durch und untersuchten einen neuronalen Schaltkreis, der potenziell für die kontextbezogene Unterdrückung von Richtungsinformationen von Echos verantwortlich sein könnte: DNLL Neurone, die empfindlich für interaurale Lautstärkeunterschiede waren, wurden von Stimuli erregt, die kontralateral lauter waren, und gehemmt, wenn die Intensität auf dem ipsilateralen Ohr höher

war. Im Gegensatz zur Erregung hielt allerdings die Hemmung nach Ende der Stimulierung in vielen Neuronen für mehrere Millisekunden an. Diese anhaltende Hemmung war dabei in der Lage, Antworten auf nachfolgende, normalerweise erregende Stimuli zu unterdrücken. Wir ermittelten im Folgenden in einer Computersimulation, dass durch die anhaltende Hemmung von DNLL Neuronen in höheren Zentren der Hörbahn Informationsmuster aufgebaut werden, die ausreichen, um kontextbezogenen Echounterdrückung zu generieren. Der Zeitverlauf der Ergebnisse aus diesen simulierten Versuchen stimmte dabei mit den Resultaten aus Verhaltensversuchen mit Menschen, die wir ebenfalls durchgeführt hatten, überein.

INTRODUCTION

General motivation

A principal understanding of the functioning of the mammalian brain represents one of the most fascinating as well as demanding challenges of contemporary natural science. Typically, the high complexity of the neuronal structures and their diverse connectivity allows the investigation of only those conceptual questions in which all relevant parameters as well as the structures that are involved can be defined *a priori*. The auditory system - in particular the neuronal circuits involved in sound localization - offer a unique possibility to investigate common rules and mechanisms of neuronal computation in great detail: The various cues that are used by the brain to localize a given sound source are processed by morphologically distinct pathways, creating a straightforward structure-function relationship. For instance, the neurons in the auditory brainstem that are involved in high frequency sound localization are not the same as those that process localization cues of low frequency sounds, because high frequency sounds are localized by evaluating physical cues in the sound that are not present for low frequencies. However, a theme that is common to the entire auditory brainstem system devoted to sound localization is the importance of temporal sensitivity and precision in the processing of binaural inputs (review: Grothe, 2000). Another feature that is recurring throughout the auditory brainstem is synaptic inhibition and recent findings linked inhibition closely to the formation of temporal sensitivity (review: Grothe, 2003). Hence, the investigation of synaptic inhibition in the auditory brainstem might not only yield a better understanding of the neuronal processing of sound localization, but might also help to identify functional mechanisms of synaptic inhibition that facilitate temporal processing.

The ability of an animal to localize a sound source is fundamental for prey detection or predator avoidance as well as mate attraction and, hence, has high evolutionary relevance. Therefore, high precision in spatial sound source localization can be found in most animals and humans. Neuronally, this precision is generated by comparing the physical parameters of the acoustic signals between the two ears: In the horizontal plane, low frequency signals are localized by detection of differences in the arrival time of the sound at the ears while for high frequency signals differences in the intensity of the sound are used for their localization (Rayleigh, 1907). Behavioral and neuronal sensitivity to these differences is remarkably high. For example, differences in the arrival time of a sound at the two ears in the range of only microseconds can be faithfully detected (Moore, 2004). This holds true despite the fact that even in the case of a single sound source, the auditory system is confronted with a multitude of reverberations and echoes that create spurious localization cues. Remarkably, although

these spurious cues are present at all times, the auditory system is able to distinguish them from “valid” cues and even perceptually suppress their directional information (review: Litovsky et al., 1999).

Before focusing on the functional mechanisms that might contribute to the formation of these rather complex aspects of sound localization, we give a general introduction to the binaural pathways of the auditory brainstem and the processing of sound that occurs there.

The encoding of auditory stimuli in the mammalian brain

Sound can be physically described as pressure variations in a medium propagating at a finite speed (approx. 340 meter/s in air). At the ears, these pressure variations cause vibrations of the tympanic membrane, which is coupled to the middle ear bones. Deflection of the middle ear bones then results in the transmission of the airborne sound waves onto the cochlea. The cochlea is a snail-shaped structure that can be simplified as a fluid-filled tube separated along its length-axis by the “basilar membrane”. Deflection of the chain of middle ear bones causes vibration of the basilar membrane in the form of a wave that travels from the basal part of the membrane (i.e. from the site of the coupling to the middle ear bones) towards the apical part. Since the basilar membrane has decreasing stiffness and increasing width from its base to the apex, the wave increases in amplitude due to resonance effects until it reaches a maximum at the part of the basilar membrane that is most sensitive to the particular sound frequency (von Békésy 1947). Hence, a frequency analysis of the sound is performed by the basilar membrane, in which different frequencies are mapped onto spatially distinct locations along the cochlea. The transduction of the mechanical movements into electrical signals is performed by the inner hair cells that are located on the basilar membrane and connect to the auditory nerve fibers. The deflection of the basilar membrane causes movement of the hair cell cilia, leading to ion-influx into the hair cell, which results in intracellular potential changes that – at least for lower frequencies - faithfully resemble the stimulus waveform within the particular frequency channel. These potential changes cause the release of transmitter into the synaptic cleft between the basal part of the hair cell and auditory nerve fibers. A supra-threshold post-synaptic depolarization will result in the generation of an action potential (AP) in the post-synaptic cell. Contrary to the graded changes in potential in the hair cells, APs represent a uniform and binary form of information coding in which all information about the stimulus waveform and its properties that shall be processed at later stages must be encoded. One important and characteristic temporal feature of APs is referred to as “phase-locking” (Galambos and Davis, 1943; Kiang et al., 1965). It describes the phenomenon that auditory nerve fibers (and most auditory neurons involved in temporal coding) tend to fire an AP at a preferred phase of individual cycles of a

pure tone (Fig. 1). Therefore the occurrence of a particular phase of an acoustic signal can be encoded with very high temporal precision. However, inner hair cells exhibit relative high internal noise due to their high sensitivity to cilia movements, resulting in the generation of so-called spontaneous activity in the auditory system (Kiang et al., 1965), i.e. APs that are not caused by sound stimulation (Fig. 1). After the initiation at the auditory nerve fiber, the sound information travels in the form of APs to the nuclei of the ascending auditory pathway. The work in this thesis will concentrate on the binaural pathways of the brainstem up to the auditory midbrain. The various nuclei within the binaural pathway will be described in the following section.

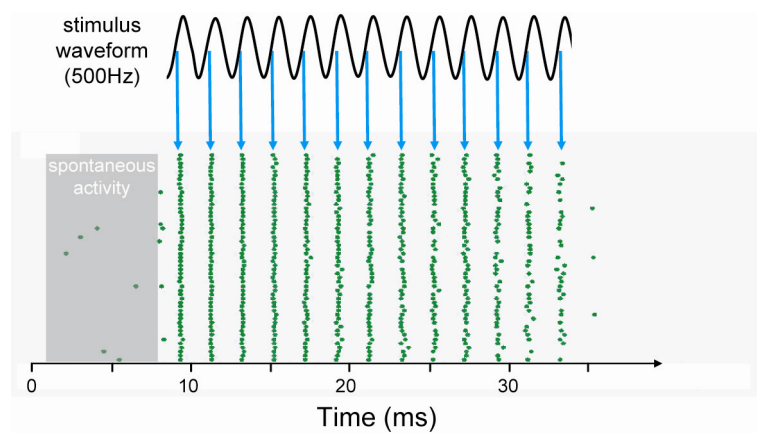


Figure 1

Phase-locking and spontaneous activity. Each dot in the dot-raster-display in green marks the occurrence of an AP for multiple presentations of a 500Hz pure-tone (shown in black). APs are precisely locked to a particular phase of each cycle of stimulation (blue arrows). APs in gray shaded area are not sound-evoked and hence, represent spontaneous activity. (Unpublished recording of a MNTB neuron by Pecka M.).

The mammalian ascending auditory pathway

The first nucleus of the ascending auditory pathway is the cochlear nucleus (CN). Neurons in the CN are innervated by the ipsilateral auditory nerve fibers (Lorente de No, 1933), the excitatory transmitter being Glutamate (as with all excitatory synapses in the auditory brainstem). The CN is divided into two major sub-parts, the dorsal cochlear nucleus (DCN) and the ventral cochlear nucleus (VCN, Rose et al., 1959; Brawer et al., 1974). For binaural processing in the brainstem, the neurons of the VCN are the most important. Here, one particular cell type that is located in the anterior part of the VCN (AVCN), the bushy cells, project to the binaural nuclei that are responsible for the processing of localization cues (Cant and Morest, 1984; Smith et al., 1991; 1993; Fig. 2). Within the population of bushy cells, morphological distinctions can be made between two sub-types, namely spherical bushy cells (SBC) and globular bushy cells (GBC). SBCs and GBCs can be distinguished morphologically by their distinct staining patterns after Nissl staining (Osen 1969), and physiologically by a distinct response characteristics to sinusoidal stimuli: SBCs exhibit a pure primary-like response pattern, similar to that of the auditory nerve (pronounced onset of response followed by rapid adaptation), while GBCs show an additional notch (i.e. a

breakdown of the response rate) after the onset in their otherwise likewise primary-like response pattern (Rhode and Smith 1986). SBCs receive very large auditory nerve fiber terminals, the so-called endbulbs of Held (Ryugo and Sento, 1991), and project to the main nuclei of the superior olivary complex (Cant and Morest, 1984; see Fig. 2). GBCs receive smaller terminals and project mainly to the glycinergic neurons of the lateral nucleus of the trapezoid body (LNTB) on the ipsilateral side and the medial nucleus of the trapezoid body (MNTB) on the contralateral side (Friauf and Ostwald, 1988; Smith et al 1991; see Fig. 2).

The first neurons in the ascending pathway to be innervated from both ears and thus to receive binaural information relevant for sound localization processing, are the main nuclei of the superior olivary complex (SOC), the medial superior olive (MSO, Fig. 2a) and the lateral superior olive (LSO, Fig. 2b). Principal neurons of the LSO receive – in addition to the aforementioned excitatory inputs from the ipsilateral SBCs - inhibitory projections from the MNTB of the same side, which in turn is innervated from the contralateral side (Boudreau and Tsuchitani, 1968; Moore and Caspary 1983; Smith et al., 1991). Thus, LSO neurons receive Excitatory/Inhibitory (E/I) innervation (Fig. 2b), the inhibitory transmitter being glycine. In contrast, principal neurons of the MSO receive SBC input from both sides and, hence, Excitatory/Excitatory (E/E) innervation (Stotler 1953; Warr, 1966; Lindsey 1975; Smith et al., 1993). Additionally, inhibitory, glycinergic inputs are provided to the MSO from both the ipsilateral MNTB and LNTB (Clark, 1969; Perkins, 1973; Wenthold et al., 1987; Cant, 1991; Cant and Hyson, 1992; Kuwabara and Zook, 1992; see Fig. 2a). The significance of these innervation patterns will be introduced in more detail below.

Both MSO and LSO neurons innervate the nuclei of the lateral lemniscus and the midbrain, but in different ways. MSO neurons send excitatory, glutamatergic projections mainly to the ipsilateral dorsal nucleus of the lateral lemniscus (DNLL) and inferior colliculus (IC, Fig. 2a; Adams, 1979; Glendenning et al., 1981; Aitkin and Shuck, 1985; Shneiderman et al., 1988). Excitatory, glutamatergic projections of the LSO in turn terminate in the contralateral DNLL and IC, while ipsilateral LSO projections to these nuclei are glycinergic and thus inhibitory (Fig. 2b; Brunso-Bechtold et al., 1981; Glendenning et al., 1992; Saint Marie and Baker 1990). DNLL neurons themselves send inhibitory projections using the transmitter GABA (γ -aminobutyric acid) to their contralateral (and to a lesser extent to their ipsilateral) counterpart and the contralateral IC (Fig. 2; Kudo, 1981; Moore and Moore, 1987; Shneiderman et al., 1988). From the midbrain neurons of the IC, at which point all principal localization cues are already evaluated, information is passed on to the geniculate body and the cortical structures.

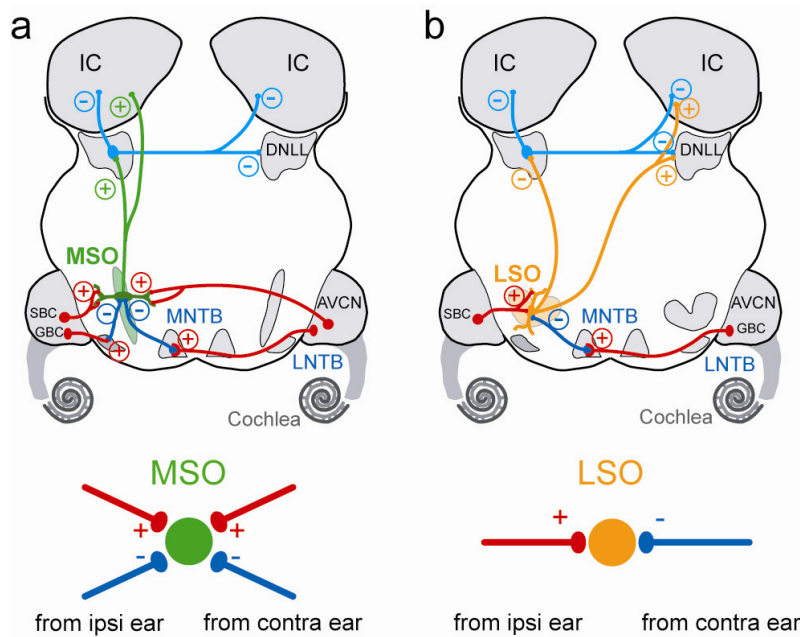


Figure 2
The binaural pathway. (a) The MSO receives excitatory and inhibitory inputs from both ears and sends excitatory projections ipsilaterally to the DNLL and IC. (b) The LSO receives excitatory input from the ipsilateral ear and inhibitory input from the contralateral ear. LSO neurons send inhibitory projections to the ipsilateral DNLL and excitatory projections to the contralateral DNLL and IC. See text for details.

Sound localization cues in the horizontal plane

Sounds that are emitted to the left or right of a listener's head will reach the ears with different intensities and/or at different times. These physical parameters are called interaural intensity differences (IID) and interaural time differences (ITD), respectively. IIDs are created because of shadowing effects of the head, meaning that sound waves are partially reflected by the head causing lower intensities of the sound at the ear more distant to the sound source (Fig. 3a). IIDs are specific in their value (given in dB units) to a particular location in the azimuth with IID=0 dB coding for sound sources from directly ahead and positive and negative values describing locations in the contralateral and ipsilateral hemisphere, respectively. However, high frequencies are more attenuated than low frequencies (Feddersen et al., 1957). For frequencies below approx. 2 kHz, the attenuation becomes insignificant and ITDs are utilized for sound source localization. ITDs are created due to the finite speed of sound and the difference in the distance between the sound source and the ears (Fig. 3b): a sound takes longer to reach the ear turned away than the ear turned towards the sound source with each ITD being specific for a location in the azimuth (relative to the listener's head). Maximal ITD values are dependent on the subject-specific distance between the two ears, but can be approximated for humans to be $\pm 690\mu\text{s}$ (Moore, 2004). For the Mongolian gerbil (*Meriones unguiculatus*), which is the model animal of this thesis, the “physiological range” of ITDs, as it is commonly called, is even smaller ($\pm 135\mu\text{s}$, Maki and Furukawa, 2005) because of the smaller head size. Again, positive ITD values indicate locations on the contralateral side and negative values conversely indicate ipsilateral sound source locations. ITDs are only used for low frequency signals (approx. below 2 kHz). At higher frequencies ITDs become

ambiguous, because the distance between the two ears can account for a multiple of the wavelength of the signal, making it impossible to distinguish trailing and leading incidences for a given period of the signal. This division of different acoustic cues that are used for sound localization in different frequency bands was first introduced in the duplex theory of sound localization proposed by Rayleigh (1907). It should be mentioned that in general a categorical division of ITD and IID processing with frequency is valid; nevertheless significant IIDs are created for low frequencies when the sound source is located within the near-field of the listener (Brungart and Rabinowitz 1999). Conversely, ITDs in the envelope structure represent an important cue of high frequency signals (Batra et al., 1993; Bernstein 2001). As mentioned earlier, the different cues are processed in distinct pathways in the auditory system, i.e. by different nuclei. For IID and ITD processing, the relevant nuclei are the LSO and MSO, respectively (Masterton and Diamond, 1967). Next, the physiological properties of these nuclei and their circuitries will be described, beginning with ITD processing in the MSO.

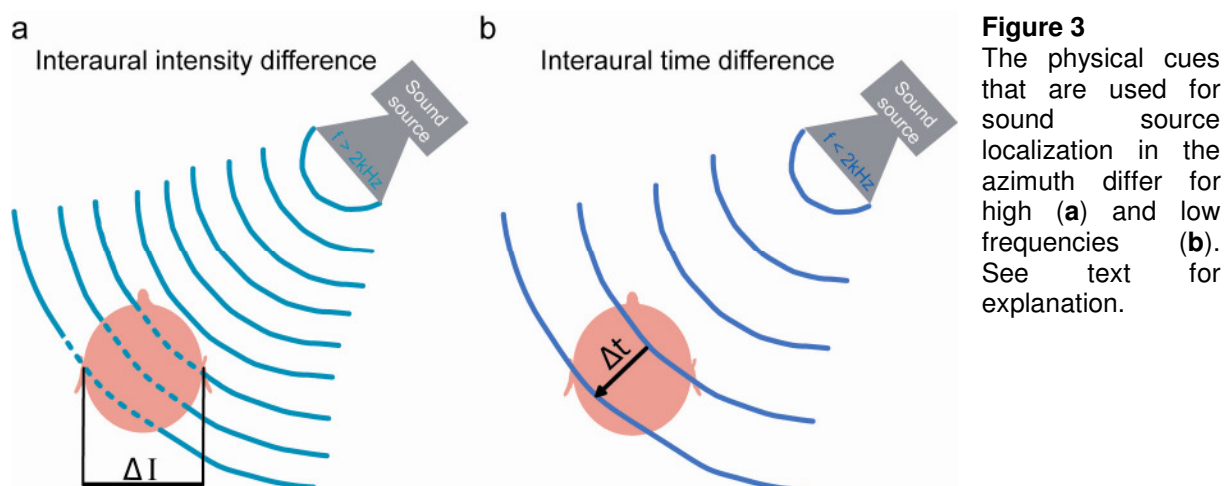


Figure 3
The physical cues that are used for sound source localization in the azimuth differ for high (a) and low frequencies (b). See text for explanation.

ITD processing in the MSO

The MSO is located at the ventral side of the auditory brainstem, medial and rostral to the LSO and lateral to the MNTB (Fig. 2). The principal neurons of the MSO are precisely aligned along the dorso-ventral axis, forming a mostly single cell lamina and their dendrites are typically extended in the medio-lateral axis in bipolar fashion (Schwartz, 1992). Excitatory input to MSO cells is provided by the glutamatergic SBCs from both sides, with the axons terminating primarily on the dendritic areas of the MSO cells (Stotler, 1953; Warr, 1966; Clark, 1969; Perkins, 1973; Lindsey, 1975). Additionally, prominent glycinergic, thus inhibitory inputs innervate the MSO cells, terminating predominately at the somatic areas (Clark, 1969; Perkins, 1973; Wenthold et al., 1987; Cant, 1991; Cant and Hyson, 1992; Kuwabara and Zook, 1992; Kapfer et al., 2002). These inhibitory inputs are provided by the MNTB and to a lesser extend the LNTB (Grothe and Sanes, 1993).

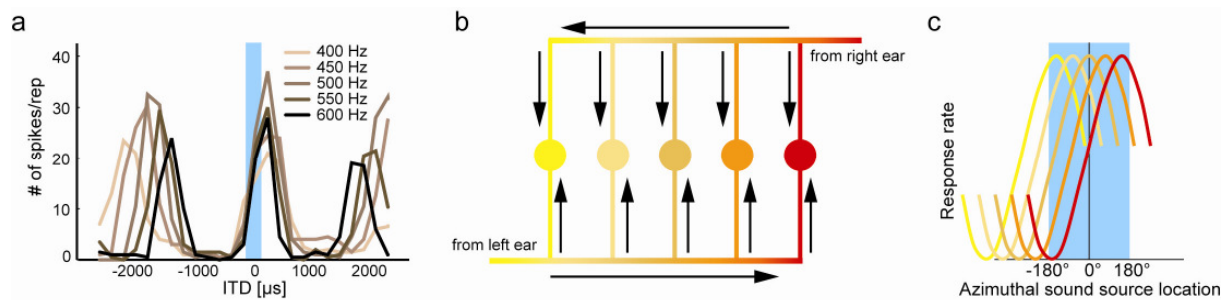


Figure 4

ITD coding in the MSO and the Jeffress model. (a) ITD functions of an MSO single cell recorded at five different frequencies. The best ITD (central peak of the function) was constant with frequency and outside the physiological range (depicted in blue). (b) Delay line arrangement as proposed by Jeffress (1948). Coincident arrival of ipsi- and contralateral inputs is systematically varied by the axonal length from both ears. (c) Such a delay line arrangement would create neuronal ITD functions with best ITDs that are equally distributed across the physiological range (blue bar). Best ITDs outside the physiological range (as in the recordings from the MSO shown in panel a) would not be expected in the Jeffress model.

MSO principal cells are highly sensitive to ITDs (Rose et al., 1966; Goldberg and Brown, 1969; Moushegian et al., 1975; Crow et al., 1978; Yin and Chan, 1990; Spitzer and Semple, 1995; Brand et al., 2002). When presented with different ITDs, the neuronal response magnitude, which is expressed in number of APs (or “spikes”, as they are commonly called), shows a prominent peak at one particular ITD (“best ITD”) and decreases monotonically for more positive and more negative ITDs. When presented with pure tones, these ITD functions take the form of a periodic function with multiple peaks, clear troughs and peak-to-peak distances that reflect the wave length of the stimulus frequency (Rose et al., 1966; Goldberg and Brown, 1969). The peaks to the left and right of the best ITD are created, however, only under dichotic conditions by introducing artificial ITDs that exceed the wave length of the pure tone. Importantly, best ITDs are independent of stimulation frequency, thus remain stable for a particular cell when tested with multiple frequencies (Rose et al., 1966; Yin and Chan, 1990, Fig. 4a).

As displayed in figure 4a, MSO neurons typically exhibit full response rate modulation for an ITD range of only hundreds of μ s, thus are extremely sensitive to differences in the arrival time of the inputs from both ears. This sensitivity is generally believed to be generated by a E/E coincidence detector mechanism (Jeffress, 1948; Yin and Chan, 1990): When the phase-locked excitatory inputs from left and right ear arrive simultaneously at the MSO neuron, the firing rate of this neuron will be maximal, while it will be minimal when the inputs from left and right ear arrive temporally separated by half a cycle. While this principal idea of coincidence detection in the MSO is widely accepted, it was recently put into question what functional mechanism is underlying this processing and how information is subsequently processed to compute the location of a sound source. The textbook view of mammalian ITD processing

has been dominated by a theoretical model that was put forward by Lloyd Jeffress in 1948. In this model, besides the concept of coincidence detection of phase-locked excitatory inputs, two more general assumptions were made: (I) Inputs to the coincidence-detector neurons vary in their axonal length and consequently in their transmission time until they reach the target neuron. These “delay lines” compensate internally for particular external ITDs. Through systematic variation of the length of the delay lines, coincidence of ipsi- and contralateral inputs is created over the whole range of physiological ITDs, with each ITD eliciting maximal response in a particular neuron (Fig. 4b). (II) For each frequency channel, a systematic representation or “topographic map” of auditory space is created, which is characterized by the peak activity of a distinct single neuron for each ITD (Fig. 4c).

The neuronal implementation of this elegant model has since been heavily investigated both in the avian system and in mammals. However, while evidence for the realization of the Jeffress model is considerable for birds (e.g. Parks and Rubel, 1975; Rubel and Parks, 1975; Carr and Konishi, 1990), the situation for mammals is unclear. While earlier findings had been interpreted as being consistent with the delay-line organization of the contralateral excitatory MSO inputs (Smith et al., 1993; Beckius et al., 1999), more recent findings from studies in the auditory midbrain of several mammals, supplemented by sparse data from the gerbil MSO, challenged the validity of the Jeffress model for mammalian hearing (McAlpine et al., 2001; Brand et al., 2002; Hancock and Delgutte, 2004; Siveke et al., 2006). In these studies, the common observation was made that the neuronal best ITDs were not evenly distributed throughout the physiological range of the respective animal, but instead were clustered at the contralateral border and even outside of the physiological range (compare Fig. 4a). Even more surprising, best ITD locations were dependent on the BF of the neuron with the lowest BFs having the largest best ITDs. As a consequence of this dependency, the linear slopes of the ITD-functions were aligned within the physiological range of ITD for most neurons with the steepest part of the slopes centered on midline. Such an arrangement not only contradicts a delay-line type topographic mapping of auditory space, but also negates a possible representation of ITDs by the peak activity of a neuron, because peak activity would only rarely be experienced under natural conditions. As a result, these data led to the formation of an alternative hypothesis of neuronal ITD coding, commonly referred to as population-rate-coding hypothesis (McAlpine et al., 2001). It states that sound source locations are encoded in the overall activity of the population of MSO neurons on each side. Since MSO neurons modulate their firing activity linearly within the whole physiological range and thereby convey information about all ITDs in this range (Harper and McAlpine, 2004), each ITD is represented by a particular activity pattern in each MSO, with reciprocal activity levels for both sides.

In such a population-rate-code regime, the ITD sensitivity of every MSO neuron is tuned in the way that the linear slope of its ITD function crosses the physiological range of ITDs. However, the physiological range of ITDs of an individual changes during development because its head size changes. To ensure proper localization ability at all stages, plasticity in the mechanism that is responsible for tuning ITD sensitivity is required. A simple projection of two excitatory inputs onto a coincidence detector cell with hard-wired axonal connectivity is hardly capable of adjusting ITD tuning in a plastic manner. Accordingly, recent findings revealed the importance of the prominent inhibitory inputs to the MSO in tuning the ITD sensitivity. It was shown *in vivo* that blocking the endogenous glycinergic inhibition with strychnine shifted the response distributions (and hence the best ITDs) of MSO neurons toward 0 ITD, causing the slopes to shift outside the physiological range (Brand et al., 2002). Therefore, this study showed that the glycinergic inputs re-tune the ITD of coincident input of net-excitations from both ears, positioning the slope of the ITD-function to the physiological range. It was further shown that this re-tuning is an experience-dependent mechanism involving anatomical changes in the distribution of excitatory and inhibitory synapses on the MSO neurons during a critical period in the development of the animals (Kapfer et al., 2002). Because of the emergence of the population-rate-code model in combination with the new findings about the importance of glycinergic inhibition in ITD processing, an alternative functional mechanism to the Jeffress-type delay-line mechanism was recently proposed. This new model not only explains the contralateral position of best ITDs which was observed experimentally, but at the same time also incorporates the role of inhibition in ITD coding. The basic idea of coincidence detection of excitatory inputs is maintained, however the model additionally states that the inputs of the phase-locked inhibition from the MNTB interact with the inputs of the contralaterally driven excitation in discrete events on a cycle-by-cycle basis (Brand et al., 2002; Grothe, 2003).

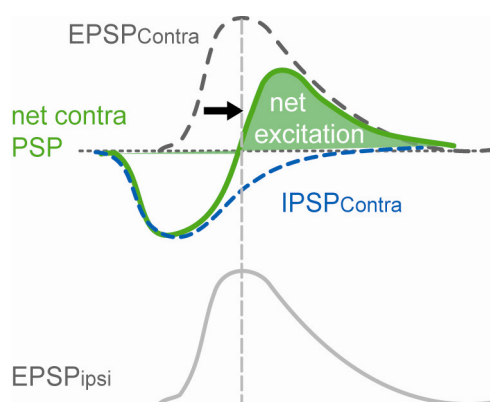


Figure 5

The preceding inhibition scenario.
See text for explanation.

The basic principle of this hypothesis is that the inhibitory post-synaptic potential (IPSP) arrives earlier at the cell soma than the excitatory post-synaptic potential (EPSP). This preceding of the IPSP effectively delays the net post-synaptic potential from the contralateral side (figure 5). This way, the binaural coincidence window of the MSO cell is not only shortened but also shifted to more positive ITDs (contralateral stimulus leading) and as a result, ITD functions are also shifted to more positive ITDs. Hence, ITD functions would be tuned by inhibition to align the slopes within the physiological range, which consequently positions the best ITDs outside the physiological range. By this mechanism, which depends on the temporally precise, phasic, hyperpolarizing action of the inhibitory inputs, the system would be able to adapt ITD sensitivity during maturation and reposition the ITD functions in respect to the physiological range. A crucial element of this model is the preceding of the IPSP from the contralateral ear relative to the contralateral EPSP despite the additional synapse between GBCs and the MNTB as has been previously demonstrated in the MSO *in vitro* (Grothe and Sanes, 1993) and *in vivo* (Grothe, 1994;Grothe and Park, 1998).

ITD coding in the Nucleus Laminaris in Birds

Analogous to the MSO in mammals, the Nucleus Laminaris (NL) represents the ITD detection system in birds. The primary neurons of the NL have striking morphological similarities to those of the MSO. NL neurons are also of bipolar shape, aligned in a single lamina, are innervated by excitatory projections from both ears and act as coincidence detectors (Parks and Rubel, 1975;Rubel and Parks, 1975;Sullivan and Konishi, 1986). NL neurons also receive inhibitory innervation (Carr et al., 1989;von Bartheld et al., 1989;Hyson et al., 1995). However, the mechanisms of ITD processing and coding are quite different in birds compared to mammals. Most importantly, the avian system shows clear indications for a Jeffress-like delay-line organization of the excitatory axonal inputs to NL neurons (Parks and Rubel, 1975;Overholdt et al., 1992;Carr and Konishi 1988,1990). Hence, the ITD tuning of NL neurons is determined by the offset in axonal delay between their binaural inputs (figure 4b): By systematic variation of the contralateral axonal length a topographic map of auditory space is constructed in the NL with each neuron representing a particular location in the horizontal plane by its peak activity (Carr and Konishi 1990;Overholt et al., 1992). NL neurons also receive inhibitory inputs, a feature that is not included in the Jeffress model. In contrast to the inhibition in the MSO the inhibitory NL inputs are GABAergic and de-correlated from the phase-locked excitation (Yang et al., 1999) and have depolarizing effects on their target NL neurons (Hyson et al., 1995;Yang et al., 1999). The main function of this inhibition is to enhance the phase-locking precision and thus ITD sensitivity in NL neurons (Funabiki et al., 1998) and to act as gain control (Pena et al., 1996;Dasika et al., 2005).

IID processing in the LSO

Next to the MSO the other main nucleus of the SOC is the LSO. The LSO is located lateral and caudal to the MSO, with its primary neurons arranged in a V or S-shaped fashion, depending on the species (Schwartz, 1992). LSO neurons receive ipsilaterally excitatory innervation by the SBCs of the VCN and contralateral inhibitory innervation via the MNTB (Fig. 2b; Cant and Casseday, 1986; Friauf and Ostwald, 1988, Matsubara, 1990). This E/I connectivity enables LSO neurons to perform the processing of IIDs (Masterton and Diamond, 1967; Boudreau and Tsuchitani, 1968; Tsuchitani and Boudreau, 1969). As shown in figure 6a, LSO neurons respond vigorously to sounds emitted from the ipsilateral side and are gradually suppressed when the location of the sound source is moved towards the contralateral side. Hence, the output rates of LSO neurons can be approximated by a subtraction mechanism of the contralaterally driven inhibition from the ipsilaterally evoked excitation. Consequently, the strength of the inhibitory inputs has to be equal to the strength of the excitatory inputs in order to achieve total suppression of the cell. The minimal IIDs at which total suppression occurs vary within the population of LSO neurons as do the IIDs at which response rates saturate (e.g. Park et al., 2004). Thus, on the population level a wide range of IIDs can be encoded within the modulatory response range of LSO neurons (Fig. 6b).

However, changing the IIDs changes not only the strength of the inputs to the LSO, but also their latency: The louder a sound, the shorter the time span between stimulation and the neuronal response. Since excitatory and inhibitory latencies have to match in order to achieve total suppression (Jeffress, 1948; Pollak, 1988; Park et al., 1996), low-frequency LSO neurons are also sensitive to differences in the timing of ipsilateral and contralateral inputs, hence to ITDs (Finlayson and Caspary, 1991; Tollin and Yin, 2005). In contrast to MSO neurons, it is not the best ITDs of ITD functions from LSO neurons that are constant with different frequencies, but rather the troughs (Fig. 6c). This difference in ITD sensitivity can be attributed to the differences in connectivity between MSO and LSO: The ITD that creates coincidence of binaural inputs in the LSO results in minimal responsiveness – the trough – independent of stimulation frequency. In contrast, coincidence of binaural excitatory inputs in the MSO results in maximal responsiveness – hence the peak or best ITD.

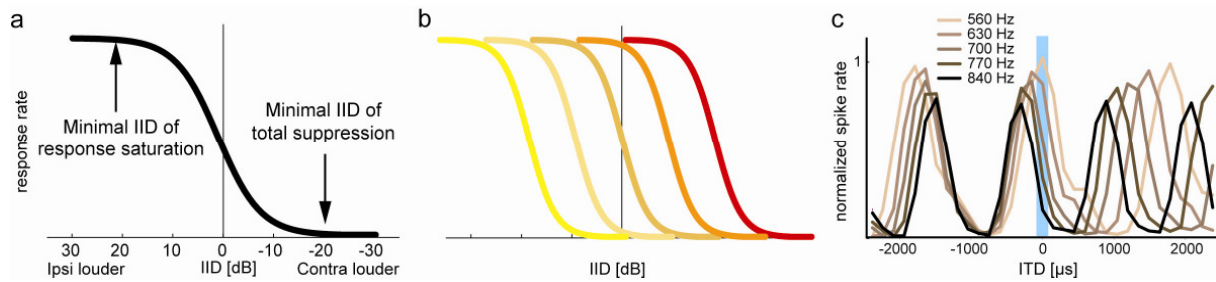


Figure 6

IID coding in the LSO. **(a)** Schematic IID function of a LSO neuron tested at BF. The response rate varies monotonically over a wide range of IIDs between the minimal IID of saturation and total suppression. **(b)** The entire range of naturally occurring IIDs can be covered within the population of LSO neurons by variation of total suppression and saturation IIDs between cells. **(c)** Low BF LSO neurons are sensitive to ITDs by coincidence detection of ipsilateral excitation and contralateral inhibition.

LSO neurons send excitatory projections to the contralateral DNLL and IC (Brunso-Bechtold et al. 1981; Saint-Marie and Baker, 1990; Glendenning et al., 1992). Therefore the target neurons in the respective regions inherit IID sensitivity from the LSO (Pollak et al., 2002). However, because of the contralateral projections, the IID functions in DNLL and IC are reversed as compared to the LSO (contralateral ear= excitatory, ipsilateral ear= inhibitory). A significant consequence of this reversal of IID sensitivity will be explained in a separate section about the DNLL. First, the main inhibitory source to the LSO and MSO is introduced.

The medial nucleus of the trapezoid body

The MNTB is located medial to the MSO and LSO and spans almost the entire SOC in its rostro-caudal expansion. As introduced before, its neurons, which are innervated by the contralateral GBCs, give rise to the prominent inhibitory input of both the MSO and the LSO that are located on the same side of the brain (Fig. 2). The synapse between a GBC and a MNTB neuron exhibits a number of interesting specializations that enhance fidelity and temporal precision of transmission: First, each MNTB cell is typically innervated by only one GBC synapse, which terminates directly onto the cell soma. Second, a GBC-MNTB synapse is exceptionally large, spanning over about half of the postsynaptic somatic region (approx. 20 μm in width). The pre-synaptic terminals were named calyx of Held after the original report of its existence and shape by Hans Held in the cat in 1893. It was later shown that the terminals actually form a finger-like structure with pronounced protrusions around the post-synaptic somata (Morest, 1968). The enormous size of the calyces afford a third specialization, namely a exceptionally large synaptic area that allows for the release of very large amounts of transmitter (glutamate) and thus assures a high probability of post-synaptic spike generation. Moreover, the high amount of transmitter release also leads to very short synaptic delays of the AP transmission between GBCs and MNTB neurons and to low variability (jitter) in the delay (e.g. Borst et al., 1995; Sabatini and Regehr, 1999). Accordingly,

it was established by extracellular recordings *in vivo* that MNTB neurons exhibit very high degrees of phase-locking, similar to the precision that is first established in the AVCN (Guinan and Li, 1990; Smith et al., 1998; Kopp-Scheinpflug et al., 2003). Because of these interesting properties and its size, the calyx of Held synapse received soaring attention in recent years when patch-clamp techniques enabled a thorough investigation of the biophysical properties of synaptic transmission (review: von Gersdorff and Borst, 2002). However, all these measurements *in vitro* were conducted on rested synapses that are only active when stimulated by current injections during the experimental measurements. These experiments established the prevailing view of the calyx of Held as a simple synaptic relay in which each pre-synaptic impulse is faithfully responded with a supra-threshold EPSP. However, in contrast to the paradigm of these *in vitro* experiments it is actually well known that auditory neurons in the intact brain are active even in a completely silent environment (compare Fig. 1, which shows an extra-cellular recording from a MNTB neuron). This so-called spontaneous activity is inherited from the auditory nerve and is thought to be a consequence of the extreme sensitivity of the inner hair-cells in the cochlea (Kiang et al., 1965). The influence of spontaneous activity on synaptic properties is neglected in *in vitro* experiments because all inputs from the cochlea are cut and, hence spontaneous activity is absent.

The dorsal nucleus of the lateral lemniscus

The DNLL represents an accumulation of neurons in the dorsal region of the lateral lemniscus, which is located dorsally to the rostral part of the SOC and ventrally to the caudal part of the IC (Fig. 2). Both the MSO and the LSO project directly to the DNLL. These connections are well established anatomically and have been confirmed physiologically by the finding of ITD- as well as IID-sensitive cells in the DNLL. The MSO projections are purely excitatory and stem mainly from the ipsilateral side (Adams, 1979; Glendenning et al., 1981; Aitkin and Shuck, 1985; Shneiderman et al., 1988), although contralateral MSO projections are reported as well (Adams, 1979; Glendenning et al., 1981). In contrast, the LSO projections are more diverse: The DNLL receives excitatory inputs from the contralateral LSO while the ipsilateral LSO inputs are glycinergic and thus, inhibitory (Brunso-Bechtold et al., 1981; Glendenning et al., 1992; Saint Marie and Baker 1990). Moreover, the DNLL receives additional inhibitory inputs from the contralateral DNLL via the so-called commissure of Probst (Kudo, 1981; Moore and Moore, 1987; Shneiderman et al., 1988). These inputs are GABAergic, as are most DNLL neurons (Adams and Mugnaini, 1984; Roberts and Ribak, 1987; Thompson et al., 1985). Along with the commissural

connections, the main target of the GABAergic DNLL projections are the contralateral IC and to a lesser extent the ipsilateral IC (Moore and Moore, 1987; Shneiderman et al., 1988).

ITD-sensitive neurons in the DNLL have been reported in a number of species (Brugge et al., 1970; Kelly et al., 1998; Fitzpatrick and Kuwada, 2001; Kuwada et al., 2006), yet a systematic evaluation of the ITD sensitivity of the DNLL compared to the MSO is missing. So far, comparative studies on ITD sensitivity between the two areas have focused mainly on a apparent sharpening of the ITD functions from the MSO via DNLL to IC and thalamic areas (Fitzpatrick and Kuwada, 2001; Kuwada et al., 2005). Studies on ITD processing are typically carried out in the IC, because recording in the MSO is notoriously difficult (Guinan et al., 1972). However, it is known that the degree of convergence between multiple neurons with distinct ITD-sensitivity is rather high in the IC, thus conclusions about the origin of a particular property of ITD processing are difficult to draw (McAlpine et al., 1998). In the DNLL on the other hand, convergence should be less of a problem because of the minor number of input sources and their un-modified nature.

IID-sensitivity in the DNLL has been demonstrated in multiple species as well (Brugge et al., 1970; Markovitz and Pollak 1994; Kelly et al., 1998). In accordance with the fact that excitatory projections from the LSO stem from the contralateral side, IID-sensitive DNLL neurons are excited by sounds that are louder at the contralateral ear and are inhibited by sounds that are louder at the ipsilateral ear. Interestingly, the un-responsiveness of an IID-sensitive DNLL neuron to ipsilaterally louder sounds has multiple causes (review: Pollak et al., 2003): First, the excitatory LSO input will be inactive during this particular stimulation. Second, the DNLL neuron might receive glycinergic, i.e. inhibitory input from the LSO on the same side, effectively hyperpolarizing the DNLL neuron. Third, since the DNLL on the other side will be excited, the DNLL neuron might additionally receive GABAergic inhibition via the commissure of Probst. Hence, IID-sensitive DNLL neurons are subjected to a dual inhibition during stimulation of the ipsilateral ear, consisting of glycinergic input from the ipsilateral LSO and GABAergic input from the contralateral DNLL (Fig. 7b). The significance of this dual inhibition will be explained below.

Persistent Inhibition in the DNLL and the Precedence Effect

When Pollak and his co-workers carried out recordings from IID-sensitive cells in the DNLL of bats in the 1990s (Yang and Pollak, 1994a,b; 1998), they found that ipsilateral stimulation was able to cause suppression in these cells that lasted several tens of milliseconds longer than the inhibitory sound itself (Fig. 7c). Usually, the duration of a sound-evoked excitation or suppression on auditory brainstem neurons is tightly bound to the duration of the stimulation. Nevertheless, these IID-sensitive neurons not only remained inhibited after the end of

stimulation, but this inhibition even suppressed responses to immediately trailing sounds which were excitatory when presented alone (Fig. 7d). Accordingly, Pollak and colleagues termed this suppressive effect “persistent inhibition” (PI). Using pharmacological techniques in combination with extra-cellular recordings, they were able to dissect the contributions of glycinergic and GABAergic inhibition to PI (Yang and Pollak, 1994 JNeurophys). By blocking the respective transmitters, they showed that the glycinergic LSO projections only contributed to the suppression of the DNLL cells within the duration of the sound stimulation, but not longer. In contrast, when they blocked the GABAergic inputs (presumably stemming from the contralateral DNLL, Fig. 7b), they observed that PI, meaning ongoing suppression after the end of stimulation, was absent. They concluded that synaptic properties of the contralateral DNLL inputs are responsible for creating PI, because these inputs are the only known GABAergic projections onto the DNLL. Subsequently, a possible purpose of PI was revealed when looking at the target cells of the DNLL in the IC. Here, the E/I property of some IID-sensitive neurons is created *de novo* by convergence of contralateral excitatory projections from the AVCN and ipsilateral inhibitory projections via the pathway of the contralateral DNLL (Vater et al., 1992; Park and Pollak, 1993; 1994; see figure 7e). Burger and Pollak (2001) were able to show that these *de novo* E/I cells in the IC are released from their inhibitory input, the contralateral DNLL, not only during contralateral stimulation, but also for the duration of PI. Thus, when first stimulated contralaterally, these IC cells were able to respond to a trailing ipsilateral stimulation, a normally inhibitory stimulus due to the contralateral DNLL input, because the initial stimulus created PI in the contralateral DNLL. In other words, *de novo* E/I IC cells exhibited an enhancement of responsiveness to trailing stimuli that arrived from the hemisphere opposite to the initial stimulus. Burger and Pollak inferred from these results that the circuit of E/I cells in the DNLL and IC might be involved in producing a prominent psychophysical phenomenon called “the precedence effect” (PE). The PE summarizes a number of psychophysical effects that allow for the selective suppression of directional information in echoes and reverberations without eliminating their overall perception (reviews: Blauert, 1997; Litovsky et al., 1999). In other words, PE describes that we are aware of the presence of echoes, but do not localize them. This applies when lagging sounds trail leading sounds in the range between 2 to tens of milliseconds. For delays of <2 ms, the two sounds are fused to one location midway between the two sound sources and for delays greater than the upper threshold, two separate sounds with distinct locations are perceived (figure 7f). Importantly, depending on the context, PE can break down so that both leading and trailing sounds are localized (Clifton, 1987), indicating that spatial information about echoes is not lost, but selectively disregarded in higher brain centers. Hence, a simple suppression of trailing signals is insufficient to explain the neuronal computation of the PE. Intriguingly, PI results in a response enhancement in *de novo* E/I IC cells rather than a

suppression of information (Burger and Pollak, 2001). Also, the range of delays at which PE is existent, matches the duration of PI in the DNLL of the bat. Therefore, the DNLL-IC circuitry seems to be a prime candidate for the neuronal implementation of the selective and context-dependent suppression of directional information of trailing signals in the PE.

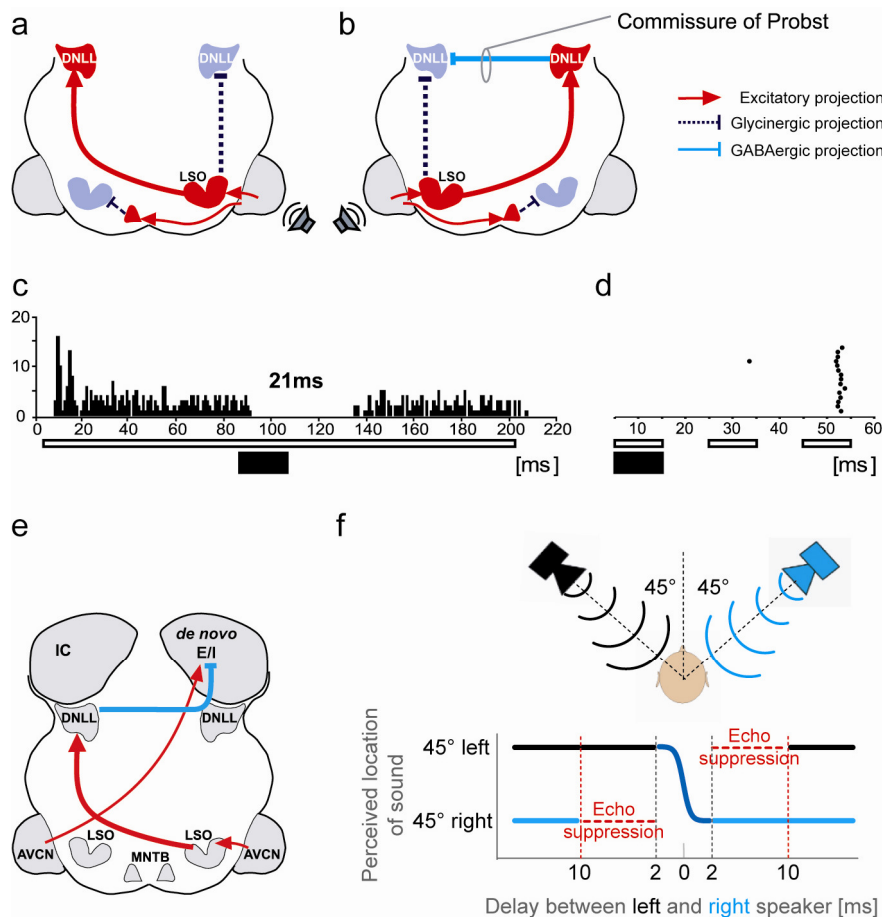


Figure 7

Persistent inhibition (PI) in the DNLL and echo suppression. **(a)** DNLL cells sensitive to IIDs are excited by contralateral stimulation by projections from the contralateral LSO. **(b)** Inhibition to these DNLL cells during ipsilateral stimulation is provided by two sources: the ipsilateral LSO and the contralateral DNLL via the commissure of Probst. **(c)** Poststimulus-time histogram of a E/I DNLL neuron for 200ms contralateral stimulation at BF (open bar). 20 ms long ipsilateral stimulation (filled bar) midway through the contralateral stimulation produced an suppression of response for 41 ms; hence, the inhibition persisted 21 ms longer than the ipsilateral stimulation **(d)** Dot-raster display of response of a E/I DNLL neuron to three

10 ms stimuli: The initial stimulus was louder on the ipsi ear (filled bar) and generated PI that suppressed responses to a trailing contralateral stimulation (open bar). After PI had ended, contralateral stimulation (second open bar) causes responses. **(e)** De novo E/I cell in the IC are created by convergence of an excitatory projection from the contralateral AVCN and an inhibitory projection from the contralateral DNLL, which is innervated by the LSO ipsilateral to the IC neuron. **(f)** Echo suppression can be experimentally demonstrated by playing identical stimuli with varying delays from two speakers that are positioned 45° to the left and right of a listeners head. For delays of approx. >2ms to <10ms, the subject will report only one sound source location.

Synaptic inhibition in neuronal processing

Synaptic inhibition in the central nervous system is mediated by two transmitters, namely the amino acid glycine and the γ -aminobutyric acid (GABA). Glycine receptors (GlyR) and A-type GABA receptors (GABA_AR) share many structural as well as functional features. Both receptors are pentameric ligand-gated ion-channels (reviews: Betz, 1990; Legendre, 2001) and their activation results in an influx of chloride ions, generating an inhibitory post-synaptic

current (IPSC) in most mature neurons (Krnjevic and Schwartz, 1967;Curtis et al., 1968;Hamill et al., 1983). Also, both receptors are anchored at the post-synaptic membrane via the same sub-membrane scaffold protein called gephyrin (Tretter et al 2008). Despite these similarities, there are also significant differences between glycinergic and GABAergic inhibition. Glycine and GABA are typically associated with distinct areas in the brain. Glycinergic inhibition is primarily thought to be present in the spinal cord and brainstem, while GABA is assigned mainly to cerebellar, sub-cortical and cortical processing (Aprison and Werman, 1965;Betz, 1990). However, more recently glycine was found in many cortical areas (Rampon et al., 1996;Malosio et al., 1991;Friauf et al., 1997) and conversely, roles of GABAergic transmission were identified in the brainstem and spinal cord (Pollak et al., 2002;Wu et al., 1992;Ziskind-Conhaim, 1998). Nonetheless, in regard to timing and the generation of temporal patterns, a basic functional differentiation between glycine and can be made that is also related to different neural structures: Glycinergic inhibition is typically involved in the temporal modulation of single neurons or small circuits, as found in the brainstem or spinal cord. Often, a precise temporal sequence of excitation and glycinergic inhibition generates a specific function e.g. the band-pass selectivity to amplitude modulations or inter-stimulus-intervals in bat MSO neurons (Grothe, 1994;Grothe et al., 2001) or the generation of motor rhythm patterns responsible for locomotion as well as for reflex responses in the spinal cord (review: Kirsch 2006). GABAergic inhibition on the other hand is generally not associated with such precise temporal refinement on the single cell level, but rather with the synchronization of large-scale networks (e.g in the olfactory bulb, see Laurent 2002, or the cerebellum, see Geurts et al., 2003) or with the generation of oscillations in such networks as for instance in the hippocampus (e.g. see Farrant and Nusser 2005). These functional differences between the two transmitters, which are mainly reflected in the temporal extent of their action, are established by differences in the repolarization kinetics of the two receptors: repolarization time constants of glycinergic IPSCs can be twice or even an order of magnitude shorter than GABAergic IPSCs (although the actual time constants vary substantially with channel sub-unit composition, Gingrich et al, 1995;Smith et al., 2000;Legendre, 2001;Magnusson et al, 2005). In other words, glycinergic inhibition allows for higher temporal precision than GABAergic inhibition in respect to modulation of neuronal firing and therefore, different functional roles are associated with the two transmitters.

Goals of this study and contributions of the author to the individual chapters

As mentioned before, the work of this thesis is divided into four chapters, which represent four independent studies that were conducted. They are related by the common theme of synaptic inhibition, which either represented a crucial element in the neuronal processing task that we investigated (Chapter 1, 2 and 4) or we examined the response properties of the inhibitory source (Chapter 3).

Chapter 1:

Glycinergic inhibition has been recently identified to play a crucial role in tuning the ITD sensitivity of MSO neurons (Brand and Grothe 2001, Grothe 2003). However, it is unknown by which mechanism glycine is able to facilitate the ITD tuning. Specifically, it is unclear whether the phase-locked glycinergic inputs interact with the likewise phase-locked excitatory inputs as discrete events or if tonic inhibition is sufficient to explain the observed effects. We addressed this question by performing *in vivo* extra-cellular recordings from the MSO of the anesthetized Gerbil. We studied the importance of timing of the endogenous glycinergic inputs by tonic iontophoretical application of glycine or the glycine-antagonist strychnine during the presentation of pure-tone stimuli with varying ITDs. Moreover, by demonstrating a BF-dependency of best ITDs in MSO neurons, the results of this work provide strong evidence for the population-rate-coding model, which has been previously mainly based on data from higher brain centers.

For this study, I performed all MSO recordings and pharmacological experiments except for the subset of experiments of strychnine applications, which were performed by A. Brand and O. Behrend. I performed the data analysis as well as figure design and preparation. The manuscript was written by me and B. Grothe, who also devised the concept of the study and was responsible for the design of the pharmacological experiments.

Chapter 2:

Because of the small size and distant location of the MSO combined with the small action potential sizes and big field potentials surrounding the MSO, *in vivo* studies on ITD processing are typically conducted in the IC. However, the level of convergence of inputs from different areas is rather high in the IC, making it difficult to draw direct conclusions about ITD processing in MSO cells. Similar to the IC, DNLL neurons receive direct projections from the MSO, however the level of convergence is supposedly much lower in the DNLL compared to the IC because of the smaller number of input nuclei to the DNLL. By conducting *in vivo* extra-cellular recordings in the DNLL of anesthetized gerbils, we assessed the ITD sensitivity of low-frequency DNLL neurons in order to determine the suitability of the

DNLL as a surrogate model nucleus to investigate ITD processing. Subsequently, we indirectly investigated the relative effective timing of inhibition and net excitation in the MSO by recording from DNLL neurons. Also, we collected data on IID sensitivity in low-frequency DNLL neurons and compared this data to the IID sensitivity of the LSO.

The data for this study were obtained by I. Siveke, me, A. Seidl and S. Baudoux. I recorded and analyzed all data on IID sensitive cells. Data analysis on ITD sensitivity was performed by I. Siveke and me. I. Siveke, I and B. Grothe wrote the manuscript. Experimental design was devised by I. Siveke, me and B. Grothe.

Chapter 3:

In this study, we determined physiological properties of MNTB neurons by *in vivo* extra-cellular single cell recordings in anesthetized gerbils. In particular, we assessed the range of spontaneous activity rates in MNTB neurons in order to implement these data in subsequent simulations of spontaneous activity in *in vitro* experiments. This way, we were able to measure a realistic measurement of recovery times of response adaptation in MNTB cells *in vitro*. We subsequently compared the obtained values to the recovery times determined *in vivo*. Moreover, the introduction of spontaneous activity in the *in vitro* experiments allowed a re-assessment of the transmission fidelity of the calyx of Held synapse.

I contributed to this study by performing the *in vivo* experiments and by analyzing most of the *in vivo* data. *In vitro* data was obtained and analyzed by J. Hermann. The manuscript was written by A. Klug and J. Hermann and was revised by me, H. von Gersdorff and B. Grothe. A. Klug, H. von Gersdorff, J. Hermann and I designed the experiments, while A. Klug and B. Grothe devised the study.

Chapter 4:

Here, we examined the potential role of the reciprocal inhibition between the DNLLs on the perceptual suppression of echo directional information. After determining the existence of PI in E/I cells in the gerbil DNLL with *in vivo* extra-cellular single cell recordings, we assessed the effects of the DNLL PI on the responses of *de novo* E/I IC cells to trailing signals with a physiologically realistic computer model of the auditory brainstem. An ideal observer that relied solely on the output of the model ICs was not only able to identify echoes, but exhibited suppression of echo directional information in a manner that closely agreed with percepts of human subjects that were tested on the same stimuli as the model.

The physiological data was collected by me, B. Saunier-Rebori, I. Siveke, and T. Zahn. The model was designed and built by T. Zahn and I made modifications on the parameter settings and the read-out; I conducted all model simulations. The behavioral experiments were designed by L. Wiegand, B. Grothe and me and I conducted these experiments. I

analyzed the data together with B. Saunier-Rebori, I. Siveke, F. Felmy and A. Klug. The manuscript was written by me, G. Pollak, F. Felmy and B. Grothe. The experiments were designed by G. Pollak, B. Grothe, F. Felmy and A. Klug. T.P. Zahn, B. Saunier-Rebori and I share first authorship for this publication.

RESULTS

The result section is divided into 4 chapters, of which each chapter represents an independent manuscript that is published in a peer-reviewed international journal.

Chapter 1: Interaural time difference processing in the medial superior olive: the role of glycinergic inhibition (2008) by **Pecka M**, Brand A, Behrend O, and Grothe B. *Journal of Neuroscience* 28(27):6914-25.

Chapter 2: Binaural response properties of low-frequency neurons in the gerbil dorsal nucleus of the lateral lemniscus (2006) by Siveke I, **Pecka M**, Seidl AH, Baudoux S, and Grothe B. Published in the *Journal of Neurophysiology* 96:1425-1440.

Chapter 3: Synaptic transmission at the calyx of Held under *in vivo*-like activity levels (2007) by Hermann J, **Pecka M**, von Gersdorff H, Grothe B, and Klug A. Published in the *Journal of Neurophysiology* 98:807-820.

Chapter 4: Inhibiting the inhibition: a neuronal network for sound localization in reverberant environments (2007) by **Pecka M**, Zahn TP, Saunier-Rebori B, Siveke I, Felmy F, Wiegrebe L, Klug A, Pollak GD, and Grothe B. Published in the *Journal of Neuroscience* 27(7):1782-1790.

CHAPTER 1

Interaural Time Difference Processing in the Mammalian Medial Superior Olive: The Role of Glycinergic Inhibition

Michael Pecka,^{1,3} Antje Brand,² Oliver Behrend,² and Benedikt Grothe^{1,2,3}

¹Division of Neurobiology, Department Biology II, Ludwig-Maximilians University Munich, D-82152 Martinsried, Germany, ²Max Planck Institute of Neurobiology, D-82152 Martinsried, Germany, and ³Bernstein Center for Computational Neuroscience, D-81377 Munich, Germany

The dominant cue for localization of low-frequency sounds are microsecond differences in the time-of-arrival of sounds at the two ears [interaural time difference (ITD)]. In mammals, ITD sensitivity is established in the medial superior olive (MSO) by coincidence detection of excitatory inputs from both ears. Hence the relative delay of the binaural inputs is crucial for adjusting ITD sensitivity in MSO cells. How these delays are constructed is, however, still unknown. Specifically, the question of whether inhibitory inputs are involved in timing the net excitation in MSO cells, and if so how, is controversial. These inhibitory inputs derive from the nuclei of the trapezoid body, which have physiological and structural specializations for high-fidelity temporal transmission, raising the possibility that well timed inhibition is involved in tuning ITD sensitivity. Here, we present physiological and pharmacological data from *in vivo* extracellular MSO recordings in anesthetized gerbils. Reversible blockade of synaptic inhibition by iontophoretic application of the glycine antagonist strychnine increased firing rates and significantly shifted ITD sensitivity of MSO neurons. This indicates that glycinergic inhibition plays a major role in tuning the delays of binaural excitation. We also tonically applied glycine, which lowered firing rates but also shifted ITD sensitivity in a way analogous to strychnine. Hence tonic glycine application experimentally decoupled the effect of inhibition from the timing of its inputs. We conclude that, for proper ITD processing, not only is inhibition necessary, but it must also be precisely timed.

Key words: sound localization; pharmacology; strychnine; population coding; superior olivary complex; brainstem

Introduction

Auditory space is synthesized by our brain based on one-dimensional movements of the two tympanic eardrums. Spectral cues and differences in level or arrival time of a sound at the two ears are used by the brain for performing this computational task. Interaural time differences (ITDs) are the dominant cue for localizing low-frequency sounds, which are most important for larger mammals (including humans) and small mammals living in habitats that require detection of distant sounds and long-range communication (like Mongolian gerbils). These species have well developed low-frequency hearing and a well developed medial superior olive (MSO) with principal neurons highly sensitive to ITDs (Goldberg and Brown, 1969; Moushegian et al., 1975; Crow et al., 1978; Yin and Chan, 1990; Spitzer and Semple, 1995).

Until recently, considerations of mammalian ITD processing

were dominated by a model proposed by Jeffress in 1948. This model assumes coincidence detection of binaural excitatory inputs with systematically varying axonal conduction time: Neurons respond maximally to ITDs that compensate for the differences in axonal conduction time of the excitatory inputs from both ears. The systematic arrangement of axons with different conduction times tunes neurons to different ITDs, creating a place code whereby the location of peak activity forms a map of auditory space. This arrangement has been verified both structurally and physiologically for the bird ITD detection system (for review, see Carr and Soares, 2002; Grothe et al., 2004). Mammals, however, developed ITD processing independently (Manley et al., 2004) and the structural and functional mechanisms of ITD processing in mammals are not as well understood. Although findings of anatomical studies in the cat seemed to be consistent with a delay line organization for the contralateral excitatory MSO inputs (Smith et al., 1993; Beckius et al., 1999), a number of recent studies indicate other or additional mechanisms underlying ITD tuning of MSO neurons and/or suggest a neuronal representation of ITDs that is different to the place coding in the Jeffress model (for review, see Grothe, 2003; Palmer, 2004). Particularly controversial is the role of synaptic inhibition in tuning MSO neurons to specific ITDs (Joris and Yin, 2007). There is anatomical (Clark, 1969; Perkins, 1973; Wenthold et al., 1987; Cant, 1991; Cant and Hyson, 1992; Kuwabara and Zook, 1992) and physiological evidence (Grothe and Sanes, 1993, 1994; Grothe and Park, 1998) for strong glycinergic inputs onto MSO principal neurons. These inputs derive from the medial nucleus of the

Received Sept. 10, 2007; revised May 13, 2008; accepted May 23, 2008.

This work was supported by The Max Planck Society (B.G.), the German Research Foundation (Deutsche Forschungsgemeinschaft) (Gr1205/12-1; GR1205/14-1, GRK 1091), and Bundesministerium für Bildung und Forschung (Project 3.5 of the Bernstein Center for Computational Neuroscience). We thank Drs. D. H. Sanes, N. Lesica, D. McAlpine, and G. D. Pollak for helpful discussions and critical comments on this manuscript. We are thankful to Dr. R. M. Burger for technical advice. C. Schulte provided excellent assistance with the histology.

Correspondence should be addressed to Prof. Dr. Benedikt Grothe, Department Biology II, Biocenter, Ludwig-Maximilians University Munich, Grosshaderner Strasse 2, D-82152 Martinsried, Germany. E-mail: neurobio@lmu.de.

A. Brand's present address: Helmholtz Zentrum München—Deutsches Forschungszentrum für Gesundheit und Umwelt, GmbH, D-85764 Neuherberg, Germany.

O. Behrend's present address: Munich Center for Neurosciences—Brain and Mind, D-82152 Martinsried, Germany. DOI:10.1523/JNEUROSCI.1660-08.2008

Copyright © 2008 Society for Neuroscience 0270-6474/08/286914-12\$15.00/0

trapezoid body (MNTB) and, to a lesser extent (Grothe and Sanes, 1993), the lateral nucleus of the trapezoid body (LNTB). The MNTB in particular (von Gersdorff and Borst, 2002), but also the LNTB (Spirou et al., 1998), show pronounced specializations for high-fidelity temporal transmission. Moreover, the glycinergic MSO inputs are restricted to the cell somata (Clark, 1969; Perkins, 1973; Kapfer et al., 2002), and this seems to be crucial for shaping the range of ITDs to which MSO neurons are tuned (Seidl and Grothe, 2005). The range of ITDs that neurons are sensitive to has led to a second controversy about the strategy of encoding location: is it the peak of the ITD function that encodes a location, and thus the place of maximal activity that shifts with location as proposed by Jeffress, or is it the slope of the function, in which firing rates change markedly with location, and thus the coding is by rate rather than place?

Here, we recorded from MSO neurons in the gerbil and present evidence in support of a rate code and for a strong influence of glycinergic inhibition on ITD tuning of MSO neurons to stimulus onset as well as to ongoing activity. We argue that these effects cannot be explained by tonic but only by precisely timed inhibition. Part of this data were published previously as a short communication (Brand et al., 2002).

Materials and Methods

Animals and surgery. Experiments were approved by the German animal welfare law (209.1/211-2531-40/01 and 55.2-1-54-2531-57-05). Adult Mongolian gerbils (*Meriones unguiculatus*), weighing between 60 and 100 g, were initially anesthetized with an intraperitoneal injection (0.5 ml/100 g body weight) of a mixture of ketamine (20%) and xylazine (2%) diluted in 0.9% NaCl solution. During surgery, analgesia was reinforced by administration of additional doses of anesthesia. An adequate analgesic state of the animal was ascertained regularly throughout the experiment by testing for absence of motor reflexes and monitoring breathing rate. To secure a constant state of anesthesia during electrophysiological recordings, supplementary doses of 0.05–0.1 ml of the same mixture were given subcutaneously every 30 min or when needed. The animal was transferred to a sound-attenuated chamber and mounted in a custom-made stereotaxic instrument (Schuller et al., 1986). Constant body temperature (37–39°C) was maintained using a thermostatically controlled heating blanket. A craniotomy ($\sim 2.5 \times 2$ mm) was performed just lateral to midline of the skull and caudal to the posterior aspect of the transverse sinus. The dura was opened and the underlying cerebellum partially aspirated to expose the floor of the fourth ventricle. For a subset of experiments (pharmacology with strychnine), access to the brain was obtained by an opening of the dura at the foramen magnum. Ringer's solution was frequently applied to the opening to prevent dehydration of the brain. After recordings (10–15 h) and a lethal injection of anesthesia, the animals were perfused intracardially with heparinized NaCl solution (0.9%) followed by 4% paraformaldehyde (PFA) solution. Afterward, the brain was retained in 4% PFA for histological processing.

Acoustic stimuli and sound delivery. Acoustic stimuli were digitally generated at a sampling rate of 50 kHz by TDT System II or III (Tucker-Davis Technologies), converted to analog signals (DA3-2/RP2-1; Tucker-Davis Technologies), attenuated to desired levels (PA4/PA5; Tucker-Davis Technologies), and delivered to the earphones (ES1; Tucker-Davis Technologies/TD990; Beyer Dynamics/Sony; Stereo Dynamic Earphones; MDR-EX70LP). For details and calibration procedures, see Sivek et al. (2006). Stimuli had \cos^2 -function gated rise–fall times of 5 ms that were added to given stimulus durations and were presented with equal intensities at the two ears. To search for acoustic responses, 100 or 200 ms uncorrelated noise bursts were delivered binaurally. When a neuron was encountered, its characteristic frequency (CF) and threshold were determined. The frequency that elicited responses at the lowest sound intensity was defined as CF; the lowest sound intensity evoking a noticeable response at CF was defined as threshold of the neuron. These properties were determined by a frequency-versus-level stimulus matrix using 200 ms pure tones. All stimuli were presented in a randomized, interleaved

order. CFs ranged from 165 to 4800 Hz with thresholds between 0 and 65 dB sound pressure level (SPL). In addition to binaural presentation, for the majority of neurons the same stimulus matrix was presented monaurally so that the excitatory or inhibitory nature of the inputs from both ears could be determined. Most low-frequency neurons were then tested for ITD sensitivity first by presenting an ITD-versus-intensity stimulus matrix (duration, 100 ms) at CF (or below for CFs >1300 Hz). The intensity at which the neuron showed best modulation in response to different ITDs was determined (typically 20–30 dB above threshold). This intensity was subsequently applied for all additional stimulations. ITD-versus-frequency stimulus matrices were presented with either 50 or 200 ms long pure tones. Five or nine frequencies centered on CF were tested over a range of ITDs equivalent to at least two cycles of the stimulation frequency and 10 interaural phase differences (IPDs) per period of the CF of a neuron. The frequency that elicited the highest response at the central peak of the ITD function was defined as best frequency (BF). During experiments involving iontophoretic application of glycine, ITDs were presented at BF with 50 ms stimulus duration and 10 ITDs per period. During iontophoretic application of strychnine, which were conducted before a modification of the setup for reasons not related to this study, 100 ms long pure tones (including 5 ms rise and 5 ms fall time) were presented with ITDs of -1 to $+1$ ms with 0.1 or 0.2 ms increments. In two cells, ITD functions were obtained using trains of narrowband pulses (duration, 5 ms; center frequency, BF; five pulses per sweep).

Electrophysiological recordings and data analysis. Action potentials from single neurons were recorded extracellularly using glass electrodes (impedance, 5–20 M Ω) filled with 1 M NaCl or 2% HRP (Sigma-Aldrich) diluted in 10% NaCl. For the dorsal approach, the recording electrode was tilted caudally by 18 or 20°, whereas for the approach through the foramen magnum the animals head was tilted by 60°. Electrodes were advanced under remote control, using a motorized micromanipulator (Digimatic) and a piezodriven [PM-10-1 (World Precision Instruments) or Inchworm controller 8200 (EXFO Burleigh Products Group)]. Recordings were amplified, filtered, and A/D-converted (RP2-1; Tucker-Davis Technologies), and the digitized signals were fed to the computer. Clear isolation of action potentials from single neurons was guaranteed by visual inspection on a spike-triggered oscilloscope (to assure a stable shape and amplitude of the action potential) and by off-line spike cluster analysis (Brainware; Tucker-Davis Technologies).

Responses to ITD stimuli were analyzed for best IPD and vector strength (VS) for each frequency using vector analysis (Goldberg and Brown, 1969; Yin and Kuwada, 1983). Significant best IPDs were scored based on the $p < 0.001$ significance level of the Rayleigh test of uniformity (Mardia, 1972). Significant best IPDs were plotted against stimulation frequency, and the linear regression of these values was calculated (at least three significant frequencies). Thereby the characteristic delay (CD) and the characteristic phase (CP) of the neuron were obtained (Yin and Kuwada, 1983). The CD value denotes the estimated ITD at which the ITD function showed constant relative amplitude with different frequencies. The CP value describes the mean interaural phase at which the CD occurred. A CP value near or at 0 cycles indicates that the CD occurred near or at the peak of an ITD function and is indicative of a coincidence of binaural excitation (peak-type). Conversely, CP values near 0.5 cycles indicate a CD at the trough of an ITD function, which can be explained by a coincidence of excitatory and inhibitory inputs (trough-type). We calculated CD and CP both with a weighted regression as described by Kuwada et al. (1987) or Spitzer and Semple (1995) and with a non-weighted regression. The two ways of calculation yielded similar results for both CD and CP in all neurons. Thus, we only present CD and CP values calculated without weighting. The best ITD, the most favorable ITD of a neuron, was obtained by multiplying the best IPD with the period of the stimulation frequency. The ITD at which the ITD function of a neuron had its steepest slope was calculated by fitting a Gaussian function with an additional offset parameter to the central period of the ITD function at BF (the central period was defined as one cycle of IPDs centered on best IPD). The average R^2 value of the fit was 0.94 ± 0.06 (SD). For pharmacological experiments, the significance of changes in the distribution of spikes over the measured ITDs within the central period of the ITD function was assessed using the $p < 0.05$ criterion of

Watson's U^2 test (software, Oriana 2; Kovach Computing Services). Population statistics on differences in normalized response rates were computed by normalizing ITD or IPD functions of control and drug condition of each neuron and calculating the changes in normalized response rates between control and drug condition at three ITDs (for strychnine) or IPDs (for glycine) to the left-hand side as well as to the right-hand side of the best ITD/IPD of each cell under control conditions. Subsequently, significance of the changes in the population of cells was assessed separately for left- and right-hand side and for each drug condition using the Student t test.

For analysis of the onset component of responses, only the first 10 ms of the stimulus-related responses were considered. For ongoing components, the first 10 ms of the stimulus-related response were discarded, if not stated otherwise. CD, CP, and best IPD of each frequency were determined in the way described above. Neurons were included in the analysis only if CD and CP could be calculated for both onset and ongoing component. Analysis of "first spike" onset component was only performed on responses of neurons for which first spikes in response to all repetitions presented could be binned into one 2 ms time window.

Iontophoresis and drugs. To mark a recording site after successful recordings, HRP (Sigma-Aldrich) was ejected through the recording pipette using a current source (HV-TR150; NPI) connected to the recording pipette. A current of +1 μ A was applied to the pipette for 30–50 s.

Five-barrel glass pipettes with tip size of 15–30 μ m were used for drug iontophoresis. Barrels were backfilled with glycine (amino-ethanoic acid, pH 3.5–4; 100 mM; Sigma-Aldrich); strychnine, pH 3.5 (10 mM); or NaCl, pH 3 (1 M). The center barrel was filled with either 2 M sodium acetate or 1 M NaCl for current balancing. Retention and ejection currents were applied via a Neurophore BH-2 system and IP-2 current pumps (Harvard Apparatus). Strychnine was retained with a current of -24 nA and ejected with a current of ≤ 240 nA. Glycine was retained in barrels with a current of -20 nA and ejected with a current of typically $+20$ to $+200$ nA.

Histology. Brains were sectioned frontally (40 μ m thickness), and sections were stained for HRP with diaminobenzidine, intensified by cytochrome (Adams, 1977). After mounting to a glass slide, the sections were counterstained by standard protocol using Neutral Red. Sections were analyzed by light microscopy, and recording sites were captured digitally. In some cases, no distinct HRP staining was found but recording sites could be reconstructed from the track of the recording electrode that was clearly visible because of either diffuse HRP staining or diaminobenzidine-stained erythrocytes caused by lesions induced by the electrode (see Fig. 1A, black arrow).

Results

Here, we report on single-cell recordings from 62 MSO neurons. Pure-tone ITD functions were recorded with neuronal BFs ranging from 200 to 1200 Hz; note that CFs were occasionally much higher (see Materials and Methods). Recording sites for 46 of the 62 neurons were histologically confirmed or reconstructed to be within or directly adjacent to the MSO cell band (see Materials and Methods) (Fig. 1A). For 16 cells, no recording site could be determined, but these cells all showed clear evidence for binaural excitation via monaural stimulation from either ear and could be classified as peak type (for definition, see Materials and Methods). Moreover, the analysis of basic ITD sensitivity, which will be presented in the following section, revealed that the properties of cells recorded during histologically unconfirmed penetrations were indistinguishable from those of confirmed MSO recordings.

Basic ITD properties

We performed a detailed analysis of the sensitivity to ITDs in the fine structure of low-frequency pure tones in a subset of 48 MSO neurons for which we were able to obtain recordings from a complete stimulus set (Fig. 1). Figure 1B contains the distributions of CD and CP (for definitions, see Materials and Methods) among peak-type MSO neurons ($n = 48$). Both the CD and the

CP distribution were centered near zero with a slight asymmetry toward positive values. We also obtained data from 18 neurons with CPs >0.25 , but these neurons were histologically determined not to be in the MSO or their recording sites could not be determined. Overall, the distributions are in line with previous data from the gerbil, rabbit, and cat MSO (Yin and Chan, 1990; Spitzer and Semple, 1995; Batra et al., 1997). When stimulated binaurally at CF and favorable ITDs, about one-third of the neurons (18 of 48) responded only to the beginning of a stimulus with a few action potentials independent of stimulus duration. The majority of neurons (30 of 48), however, responded in a primary-like sustained manner to favorable ITDs. Spiking of the neurons was highly synchronized to the fine structure of the tonal stimuli. The average vector strength at BF and best ITD was 0.46 [± 0.19 (SD); $N = 48$; average BF, 796 Hz ± 213 (SD); distribution of vector strengths as a function of BF is given in supplemental Fig. 1A (available at www.jneurosci.org as supplemental material)]. Because the relative relevance of responses to the beginning of a stimulus for the localization of a sound source compared with ongoing responses is an issue of debate (Zurek, 1993; Akeroyd and Bernstein, 2001; Joris and Yin, 2007), we investigated whether ITD sensitivity of sustained responding neurons differed in the initial component ("onset"; first 10 ms) from its ongoing component (remaining stimulus-related discharges). Figure 1C1–C3 shows ITD functions of one MSO neuron for five different frequencies between 200 and 300 Hz (BF of the neuron, 250 Hz). In Figure 1C1, the total responses are plotted, whereas Figure 1, C2 and C3, shows the ITD functions separated into onset and ongoing component, respectively. Both onset and ongoing components exhibited strong modulation in response to different ITDs and had typical peak-type ITD sensitivity as expressed in the linear phase–frequency relationship intersecting the y -axis at IPD values close to 0 (Fig. 1C4). The CD for total, onset, and ongoing response of this neuron were 269, 436, and 283 μ s, respectively, and the CPs were 0.13, 0.03, and 0.13. Figure 1, D1 and D2, shows the distributions of CD and CP for onset and ongoing response components in 21 cells that exhibited significant ITD sensitivity in their onset as well as sustained responses. Nine of the 30 sustained responding neurons were excluded from this analysis because of high variance in their onset latency ($n = 3$) or insufficient number of spikes to calculate CD and CP in either the onset ($n = 3$) or ongoing ($n = 3$) component. The distribution of CPs and CDs was not significantly different for total, onset, or ongoing response ($p > 0.49$ for all distributions, two-sided paired Student's t test; $n = 21$) (compare Fig. 1B). Moreover, plotting CD of onset against CD of ongoing component for each cell (Fig. 1E1) ($n = 21$) revealed no tendency in divergence, albeit values scattered slightly. The same observation holds true for the CPs of onset and ongoing components (Fig. 1E2) ($n = 21$) and the VS of the two components (supplemental Fig. 1B, available at www.jneurosci.org as supplemental material). Most importantly, the preferred interaural phase differences (best IPDs) of each cell were similar for onset and ongoing component [correlation coefficient (cc), 0.8; $p < 0.001$] (Fig. 1F1) ($n = 18$). Furthermore, we analyzed the onset components in more detail by dividing them into the "first spike" (0–2 ms of response) and remaining 8 ms of the onset response. We compared the best IPDs derived from these subcomponents of the 10 ms onset response to the ongoing component. This analysis revealed that best IPDs derived from the 2–8 ms subcomponent of the onset response were very similar to ongoing best IPDs (cc, 0.89; $p < 0.001$; $n = 20$) (Fig. 1F3). "First spike" onset best IPDs were less correlated to the ongoing best IPDs (cc, 0.49; $p < 0.1$;

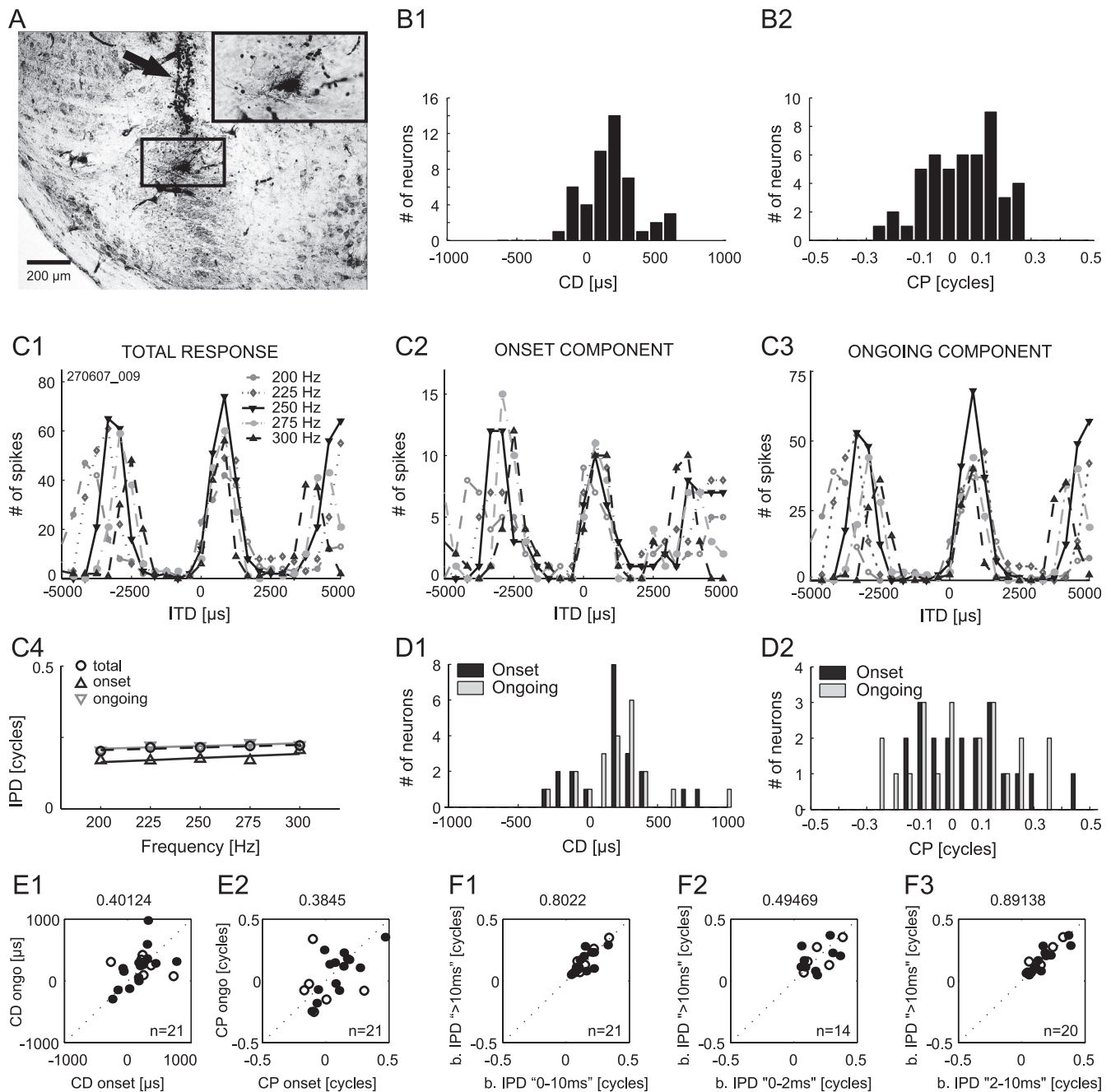


Figure 1. Basic properties of ITD sensitivity are equal for onset and ongoing responses. Stimulus durations were 50 or 200 ms. **A**, Recording site for the example neuron shown in **C**. The MSO cell band and surrounding neuropil are clearly visible. HRP staining is present in the dorsal region of the MSO cell band. The electrode track of the multibarrel electrode is marked by the black arrow. The inset in top right corner shows higher magnification of the region demarcated by the black square, with HRP staining being concentrated on the somatic area. **B**, Distributions of CDs (**B1**) and CPs (**B2**) of 48 MSO neurons based on total responses. **C1–C3**, ITD functions of a low-frequency neuron (BF, 250 Hz) in response to pure tones (5 test frequencies; 8 repetitions; 50 ms duration). ITD functions are shown for total response (**C1**), onset component only (first 10 ms of total response) (**C2**), and ongoing component only (first 10 ms of total response excluded) (**C3**). **C4**, Phase–frequency plots for the ITD functions shown in **C1–C3**. **D**, Distributions of CD (**D1**) and CP (**D2**) for 21 of the 48 neurons in **B**, separately analyzed for onset and ongoing response components. **E**, Comparison between onset and ongoing response for CD (**E1**) and CP (**E2**). **F**, Best IPDs of first 10 ms of response were similar to best IPDs of ongoing responses (**F1**). Correlation was strongest if the first 2 ms of responses were excluded (**F3**). Correlation coefficients are given on top of each panel. The open symbols indicate neurons with unconfirmed recording sites.

$n = 14$) (Fig. 1F); however, this result is most likely attributable to the low spike number for this subcomponent (typically <20 spikes).

Next, we examined the representation of the peak of the ITD functions within our population of MSO neurons and subsequently related it to the frequency tuning of the neurons, hence their BF, for 56 of the 62 MSO neurons (for the remaining 6 cells, no BF but only the CF was determined). We found a large pref-

erence for ITD functions to peak at contralateral leading ITDs (55 of 56), a finding that is consistent with previous reports from the MSO (Yin and Chan, 1990; Spitzer and Semple, 1995; Batra et al., 1997). Normalizing best ITDs to the BFs of the neurons, the mean best IPD was $0.17 \text{ cycles} \pm 0.08 \text{ (SD)}$. Only one cell had an ipsilateral leading best ITD, which, however, was very close to 0 ITD ($-8 \mu\text{s}$). The best ITD of most neurons was outside the “physiological range” (ITDs that naturally occur for single sound

sources without interference of echoes or other stimuli; for the gerbil with its small interaural distance, approximately $\pm 135 \mu\text{s}$) (Maki and Furukawa, 2005), because only 10 of the 56 cells had best ITDs $< 135 \mu\text{s}$. Moreover, best ITDs depended significantly on BF in that neurons with lower BFs exhibited longer best ITDs (cc, -0.66 ; $p < 0.001$) (supplemental Fig. 2A, available at www.jneurosci.org as supplemental material). In contrast, sensitivity to modulations in ITD was maximal ("ITD of steepest slope," first derivative of the ITD function) within the physiological range of ITDs for the majority of ITD functions (39 of 56) and was independent of BF (correlation coefficient, -0.16 ; $p > 0.293$) (supplemental Fig. 2B,C, available at www.jneurosci.org as supplemental material).

Measurements of ITD tuning are typically performed at only one intensity (20 or 30 dB above threshold). However, little is known about the influence of absolute intensity on ITD tuning of MSO neurons. Therefore, we also obtained ITD functions over a wide range (35 dB) of absolute sound intensities (ASIs) and assessed best IPDs at each of the intensities. We successfully tested this paradigm on 36 MSO neurons, and an example recording of one MSO neuron is provided in Figure 2A1: Clearly, the maximum number of spikes increased with increasing ASI. In contrast, the best IPD of the neuron was unaffected by changing the ASI. When plotting the best IPDs against the corresponding ASIs, the slope of a linear regression fit was only -0.001 phase/dB, indicating robustness of best IPD against variations in ASI (Fig. 2A2). As summarized in Figure 2B1, the best IPD of the majority of neurons did not change at all or just slightly with increasing intensity. This high robustness was also exhibited when expressed in time delays, because shifts of best ITD were typically less than $\pm 10 \mu\text{s}/\text{dB}$ (Fig. 2B2).

Pharmacological experiments

MSO neurons receive prominent inhibitory, glycinergic inputs, mainly from the MNTB and, to a lesser extent, from the LNTB (Cant and Hyson, 1992; Kuwabara and Zook, 1992; Grothe and Sanes, 1993; Kapfer et al., 2002). To test the influence of the glycinergic inhibition on ITD sensitivity, we iontophoretically applied either the glycine antagonist strychnine or glycine itself onto MSO neurons while presenting different ITDs at the BFs of the cells. These are very difficult experiments, potentially because of the action potential-producing zone being rather distant up the axon (Scott et al., 2007). Nevertheless, we successfully applied drugs in 17 MSO recordings in which we assessed ITD functions before and during drug application. We were able to record from 13 cells long enough to achieve full recovery of the original ITD sensitivity after stopping drug application (supplemental Table 1, available at www.jneurosci.org as supplemental material). In 6 of the 17 MSO neurons, we tested the effect of blocking glycinergic inhibition via strychnine on ITD functions (Fig. 3). We first focus on the total response, including onset and ongoing components. Control functions before application are shown in solid blue, whereas solid red lines indicate the response functions for the

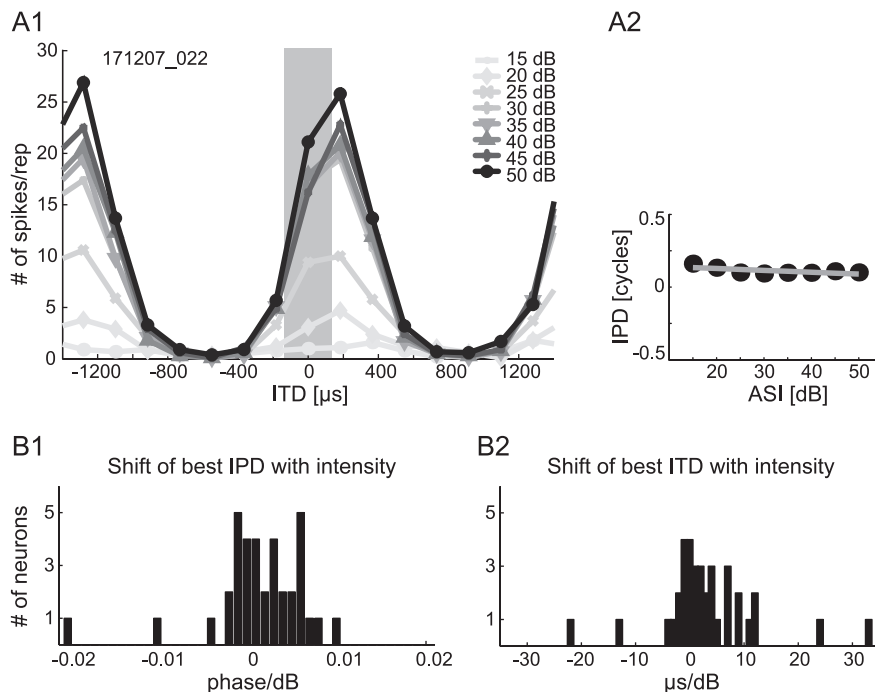


Figure 2. ITD sensitivity is robust against variations in ASI. **A1**, Responses of an example neuron that exhibited ITD sensitivity over the full test range of ASIs. Frequency of pure-tone stimulation was 683 Hz (BF). ASIs in decibels SPL are given in the top right corner (10 repetitions for each ASI). The gray bar marks the physiological range of ITDs. **A2**, Best IPDs are plotted against respective ASIs. The gray line depicts a linear fit as a basis for the histograms showing shifts in IPD (**B1**) and ITD (**B2**) for 36 neurons. Values are clustered around 0 in both measures, indicating high robustness of best IPD/ITD against changes in ASI.

strychnine condition. Note that four neurons were tested with pure tones at BF, whereas two neurons responded best to narrow-band pulses centered on BF (cell 061500mso07, bandwidth, ± 500 Hz; cell 100101mso03, bandwidth, ± 300 Hz; BFs are given in panels). In addition to the expected increase in overall spike rate, at least at some ITDs, the slopes that were closest to 0 ITD shifted to the left (toward zero or more negative ITDs) in all six cells tested. Data of one additional cell in which strychnine also induced a similar shift are not shown, because its location could not be verified. Response types were not changed by blocking inhibition. Circular statistics for analyzing the central period of the ITD functions (± 0.5 IPD centered on best IPD) revealed that the change in response distribution within the central peak of the ITD function was significant in five of the six cells ($p < 0.05$, Watson's U^2 test) (total response: Fig. 3, filled asterisks). That the obvious shift in cell 100101mso04 was not significant ($0.2 > p > 0.1$, Watson's U^2 test) is partially attributable to the fact that spike counts in this cell were low (and slightly but steadily decreased during the recordings) and its onset component was not ITD sensitive (in contrast to its ongoing component, which shifted significantly) (see below). Values of best IPD before and during strychnine application are compiled in supplemental Table 1 (available at www.jneurosci.org as supplemental material). Note that best ITDs are not necessarily equivalent to the apparent peaks of the ITD functions, but are derived from calculation of the mean vector (see Materials and Methods) that reflects the overall shape of the central period of the ITD functions. Normalizing the shifts in best ITD for the BF of the cells, the average difference in best IPD between control and strychnine condition was 0.13 (SD, ± 0.08) cycles (scatter plot in Fig. 3, filled circles). Recoveries were similar to best IPDs under control conditions with an average difference of 0.02 cycles (SD, ± 0.06). For explanation of the apparent lack of a shift in the "side peak" of the

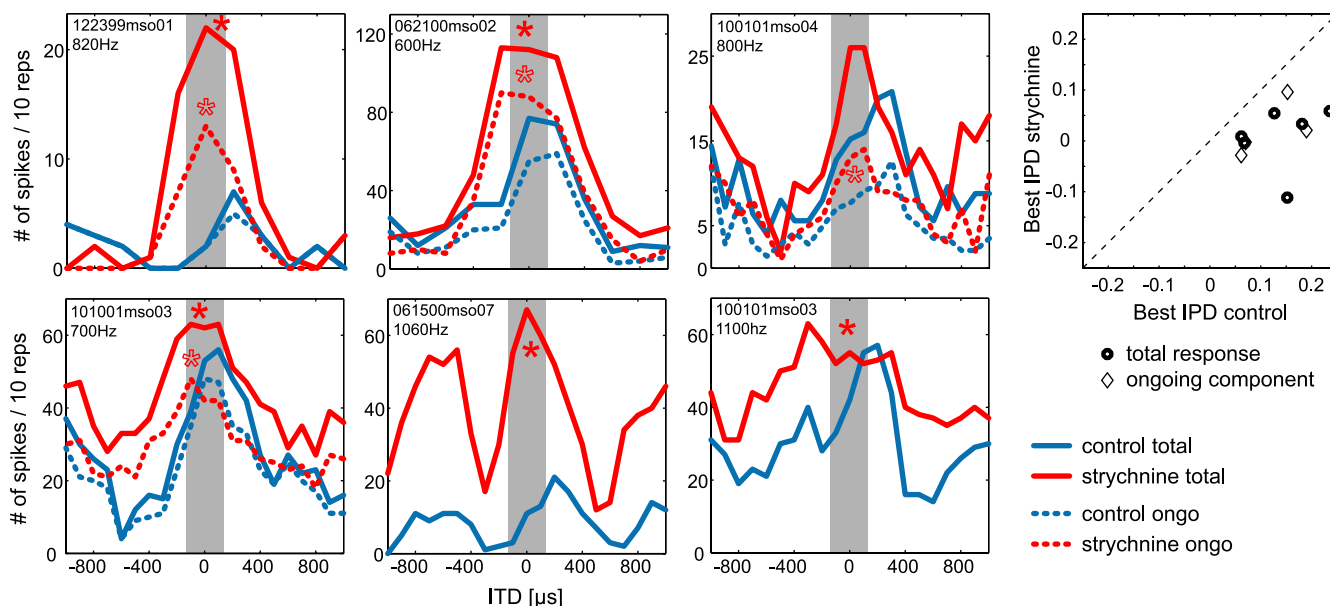


Figure 3. Strychnine induces shifts in response distribution toward 0 ITD for total and ongoing response. ITD functions for pure-tone stimulation at BF (provided at top left of panels) for four neurons and for trains of narrowband pulses centered on BF for two neurons (middle and right of bottom panels) are shown before and during or shortly after local strychnine application. The solid blue lines indicate control condition of the total responses of the cells, whereas the corresponding strychnine conditions are depicted by the solid red lines. Ongoing components of the responses are shown in dashed lines. The asterisks mark significant shifts for total (filled asterisks) or ongoing response (open asterisks). The gray bar indicates “physiological range” of ITDs ($\pm 135 \mu\text{s}$). The scatter plots in the rightmost panel show changes in best ITD during strychnine application for each cell.

response of neuron 061500mso07, see supplemental Figure 3 (available at www.jneurosci.org as supplemental material).

Responses were typically strongest at the beginning of stimulation and weaker during the ongoing component. Potentially, the effects of strychnine application could be different for the ongoing component of the response or even restricted to the stronger onset response. Therefore, we tested whether blocking glycinergic inhibition equally affects ITD sensitivity of all response components. Four of the six cells showed a clear ongoing component in their response to ITDs, which we analyzed separately by removing the first 10 ms of the response. The same overall effect of strychnine, namely a shift of the response distribution to the left, was apparent for these ongoing responses. In Figure 3, the ITD functions of the ongoing components are shown in dashed lines (blue lines depict control; red lines depict strychnine conditions). Importantly, the shifts in response distribution toward 0 ITD were significant for all four neurons ($p < 0.05$, Watson’s U^2 test). Figure 4 exemplifies the effect by showing one neuron in which ITD sensitivity for ongoing responses (Fig. 4A, blue dots in the dot raster plots) was identical with the ITD sensitivity of the total response (compare Fig. 3, bottom left panel). Figure 4B shows the ITD functions of the ongoing response, which clearly shifted because of blocking of inhibition (red line) by firing at higher rates at ipsilateral leading ITDs, which were “unfavorable” before strychnine application as well after recovery (dashed gray line). In Figure 4C, significant mean phase angles of the phase-locked response to the pure-tone frequency of the ongoing responses before and during strychnine application are presented as dashed lines. Note that, in particular when the contralateral stimulus was leading (positive ITD values), the mean angle decreased; hence the neuron tended to respond earlier within each period of the pure tone than under control (or recovery) (data not shown) conditions. For three ITDs tested, this effect was statistically significant ($p < 0.05$, Watson’s U^2 test). The vector strength of the ongoing compo-

nent was very high with and without strychnine application (Fig. 4C, solid lines). The same effect was found in a second neuron (062100mso02) with well phase-locked, ongoing responses yielding a sufficient number of spikes to perform this analysis.

The findings from strychnine application demonstrated that glycinergic inhibition is strongly involved in internally delaying the coincidence of the net excitation of the binaural inputs, thereby tuning the ITD functions of MSO neurons in relation to the physiological range. The shifts of best ITD in the ongoing components further showed that the effect of inhibition is not restricted to the onset, but that it is active throughout the duration of sound stimulation. These experiments, however, cannot distinguish between two principle possibilities that explain how this tuning is achieved by glycinergic inhibition: (1) Stimulus driven but tonic inhibition (accumulating over cycles) could change the sensitivity of the MSO neurons to coincidence of excitatory inputs (cf. Zhou et al., 2005). (2) The MNTB projection could provide well timed, contralaterally driven phase-locked inhibition that interacts with the timing of the contralaterally driven excitation on a cycle-by-cycle basis (cf. Grothe, 2003). The basic principle of this hypothesis is an earlier arrival of the IPSP relative to the EPSP, which effectively delays the net PSP from the contralateral side. Thereby the binaural coincidence window is not only shortened but also shifted to more positive ITDs (contralateral stimulus leading) (Fig. 7A). These two hypotheses make distinct predictions, which can be experimentally tested: (1) If timing of inhibition does not matter, tonically applied glycine would either enhance the effect of the tonic synaptic inhibition and shift the ITD function even further to the right (Zhou et al., 2005) or, alternatively, would simply lower the response rate because of a hyperpolarization of the cell. (2) If timing of inhibition does matter, tonic application of glycine would diminish the effectiveness of endogenous inhibition by “masking” the discrete events of the phase-locked synaptic inhibition (Fig. 7C). As a result, ITD functions would also shift to the “left” (more negative

ITDs) but the sides of the ITD functions would be affected differently from those during strychnine applications. Blocking inhibition with strychnine would broaden the coincidence window by expanding it to more ipsilateral leading ITDs, which in turn would increase neuronal response rates mainly at ITDs to the left of the original best ITD (Fig. 7B). This prediction is consistent with our findings shown above. In contrast, tonic glycine application induces constant hyperpolarization in the neurons, which in turn would not only mask the timing of the endogenous inhibition, but, at the same time, only a smaller fraction of the net PSP would exceed threshold for binaural coincidence, effectively cutting off the declining tail of the contralateral net PSP. Hence, the accompanied shift in ITD tuning would be predominately created by decreased response rates at the right-hand side of the ITD function (Fig. 7C).

To test these hypotheses, we used iontophoresis to tonically apply glycine onto MSO neurons while presenting pure tones at BF with varying ITDs. Because the neurons were very sensitive to glycine application, we carefully controlled the amount of glycine so that the neurons were not silenced but their spike rate was lowered. This was successfully achieved in 11 of 12 peak-type neurons tested. In one neuron (data not shown), a slight reduction of spike counts was correlated with only a marginal shift in best ITD. Here, apparently, drug application was not strong enough to yield any quantifiable effects. In 9 of the 11 cells with clear drug-induced effects shown in Figure 5, tonic glycine application caused a significant shift of the ITD function toward the left ($p < 0.05$, Watson's U^2 test). Expressed in phase differences to normalize for frequency, overall the best IPDs during glycine application were significantly smaller than the control best IPDs ($p < 0.01$, one-sided paired Student's t test). The mean difference between control best IPD and the best IPD for glycine condition for 11 cells was 0.10 ± 0.10 (SD) (Fig. 5, scatter plot; supplemental Table 1, available at www.jneurosci.org as supplemental material). In contrast, the average difference between control ($n = 11$) and recovery best IPD ($n = 8$) was only 0.02 (SD, ± 0.03). Hence tonic application of glycine caused ITD functions to shift to smaller or more negative best ITDs. Three neurons were additionally tested with a NaCl solution (1 M) with pH 3, similar to the pH of the drug solutions, to control for possible effects of acidity changes in the extracellular medium on IPD functions. In all cells tested, NaCl application alone did not cause a shift of IPD functions (average difference in best IPD, 0.003) (Fig. 5, black lines) (Watson's U^2 test, $p > 0.2$), confirming that the drug-induced changes in IPD tuning were specific.

Glycine strongly reduced the ongoing components of the responses. As a consequence, most neurons only responded during the initial 10 ms of a stimulus. Therefore, we analyzed the spikes

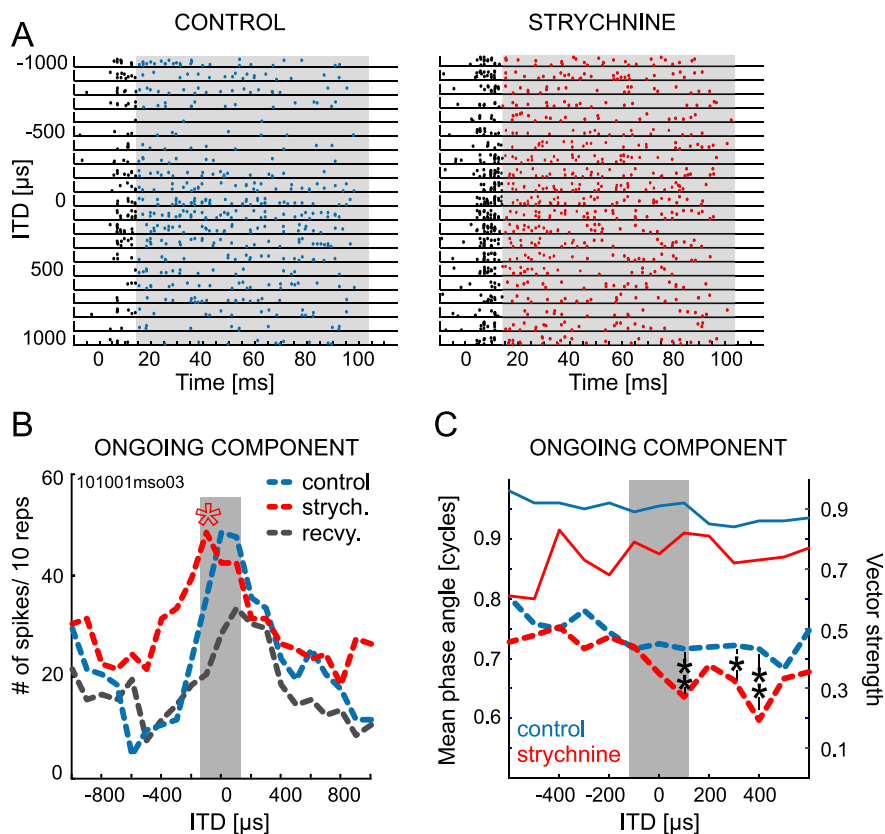


Figure 4. Ongoing response is sensitive to strychnine application. **A**, Dot raster display of one neuron stimulated with pure tones at BF (700 Hz). Shown are responses for 10 repetitions at ITDs between ± 1 ms without (left; control) and in the presence of strychnine (right). Time axis refers to start of stimulation; stimulus duration was 100 ms (including 5 ms rise/fall time). Spikes that fell into the time window for ongoing response (gray rectangle) are shown in blue and red for control and strychnine condition, respectively. Spikes within the first 10 ms of each spike train were discarded and are shown in black. **B**, ITD functions for ongoing response only, derived from spikes shown in color in **A**. Compared with control condition (blue line), the response distribution during strychnine application (red line) was significantly shifted toward the “left” (red asterisk). Several minutes after the strychnine application was terminated, the best ITD was shifted back to more positive ITD values (to the “right”; recovery, gray line). The gray bar marks “physiological range” of ITDs. **C**, The mean phase angle of the phase-locked ongoing responses was also affected by blocking inhibition. At contralateral leading ITDs in the range of $+100$ to $+400$ μ s, neuronal responses phase-locked to significantly smaller mean phase angles during strychnine application (dashed red line; left y-axis) than under control condition (dashed blue line); hence, during blockade of inhibition, the response occurred slightly earlier in each pure tone cycle. Phase-locking was high before and during strychnine application (solid blue and red lines, respectively; right y-axis). * $p < 0.05$; ** $p < 0.001$.

after the initial 2 ms of the response as ongoing component, which, following our results shown above (Fig. 1F), seems to be an appropriate alternative approach. This way we could analyze significant ongoing responses during glycine application in four cells. Analogous to strychnine, the shifting effect of glycine was also apparent for the ongoing responses alone (Fig. 5, top row, dashed lines) ($p < 0.05$, Watson's U^2 test; $n = 3$). Ongoing responses remained phase-locked during glycine application, displaying an average VS of 0.58. A detailed example for the effect of glycine is shown in Figure 6. The raster plots show highly synchronized discharges to pure-tone stimulation (630 Hz) for both onset and ongoing responses for control conditions and during application of glycine.

We showed above that both strychnine and glycine application induced left shifts in the overall ITD sensitivity. These findings do not confirm the hypothesis of endogenous glycinergic inhibition acting tonically (Zhou et al., 2005). Instead, the data are in line with the predictions made by the timed inhibition hypothesis (Fig. 7). Specifically, the timed inhibition hypothesis holds that, under normal conditions, ipsilateral stimulation

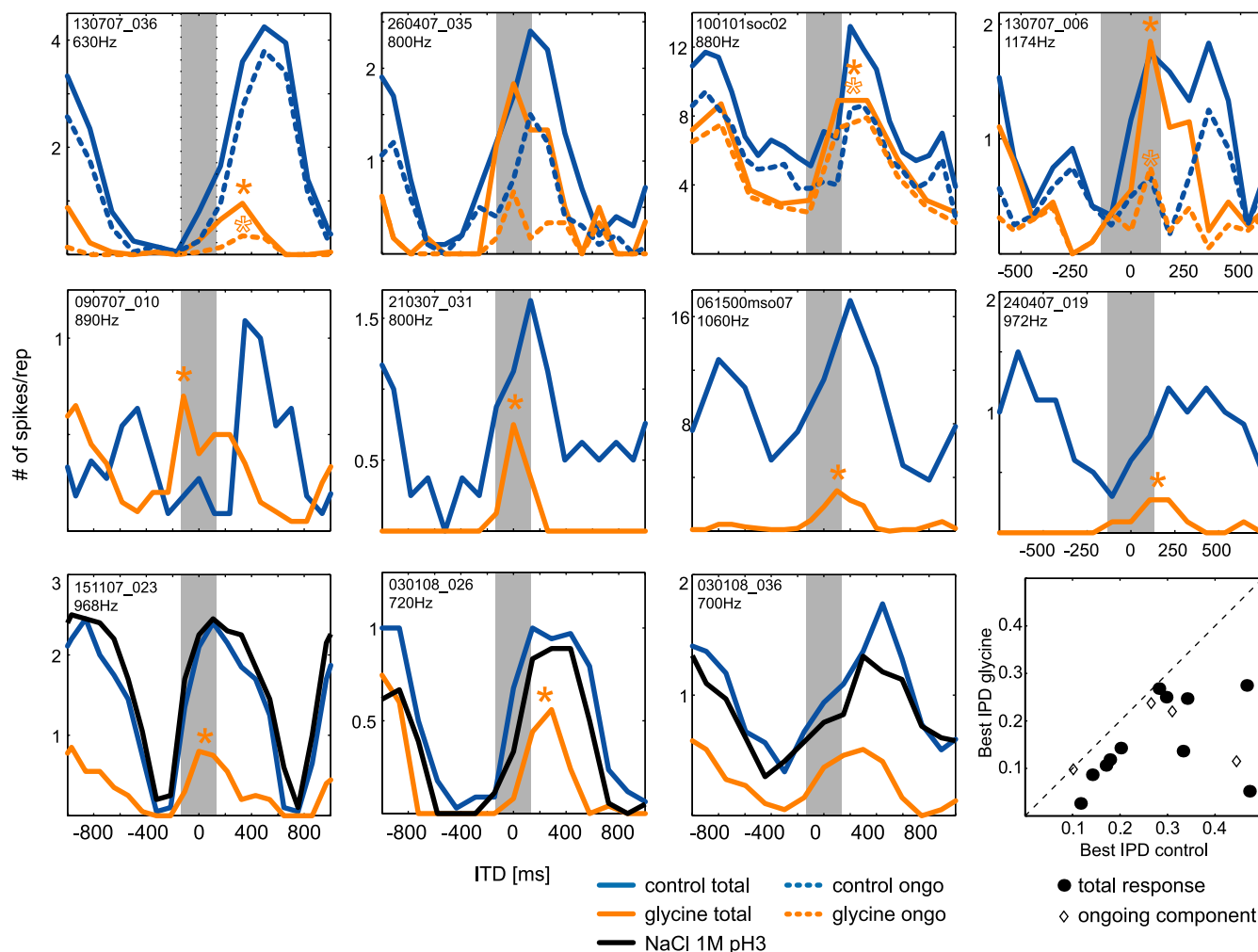


Figure 5. Tonic inhibition shifts the best ITD toward 0 ITD. ITD functions for pure-tone stimulation at BF (provided at top left of panels) for 11 neurons are shown before (solid blue lines) and during tonic glycine application (solid orange lines). During glycine application, response distributions were significantly shifted in 9 of 11 cells (filled asterisks). Shifts of best ITDs were also present in the ongoing responses (dashed blue and orange lines for control and during application, respectively). The solid black lines in the bottom panels show the ITD function during application of NaCl solution with similar acidity as the glycine solution, pH 3. “Physiological range” of ITDs is marked by gray bars. The scatter plot in the bottom-most right panel summarizes the shifts in best IPD for all 11 neurons.

evokes essentially a pure EPSP_{ipsi}. However, contralateral stimulation evokes not only an EPSP_{contra} but also an IPSP_{contra} with shorter onset latency preceding the EPSP_{contra}. The summation of the IPSP_{contra} and EPSP_{contra} generates a contralaterally evoked PSP with two components, an early hyperpolarization followed by a depolarization (Fig. 7A1). Therefore, the net excitation is delayed and binaural coincidence of the EPSP_{ipsi} and contralaterally evoked net excitation only occurs for stimulations with the contralateral sound leading (Fig. 7A2). Consequently, the peak of the IPD function is at positive values (Fig. 7A3).

The changes in IPD functions caused by blocking inhibition with strychnine or tonically enhancing inhibition with glycine can be explained by the effects of the drugs on the delays imposed on the net excitation by contralaterally evoked inhibition. The effects of blocking inhibition with strychnine are straightforward because strychnine simply eliminates the IPSP_{contra}; hence the net excitation (Fig. 7B1, PSP_{contra}) is now advanced in time and broadened compared with the net excitation in the control condition (Fig. 7B1, arrow). Therefore the IPD functions are shaped only by the coincidence of the contralateral and ipsilaterally evoked EPSPs (Fig. 7B2). Thus, the IPD function is shifted to the left, mainly by expanding on the left-hand side (ipsi ear leading)

(Fig. 7B3, arrow), just like the contralateral EPSP expanded on the left-hand side compared with the control net excitation (Fig. 7A2).

The tonically applied glycine, however, greatly reduces or even eliminates the efficacy of the IPSP_{contra} because the membrane potential is already at a hyperpolarized value (Fig. 7C1, black arrow and orange dotted line). Thus, the PSP_{contra} is reduced in overall amplitude but also advanced compared with the control condition. Coincidence of the PSP_{contra} and the ipsi EPSP is now also occurring at IPDs near 0 cycles, analogous to strychnine application (Fig. 7C2). However, the induced reduction of the EPSP amplitude has a pronounced impact on the right-hand side of the IPD function (Fig. 7C1, arrow), because the more negative PSP is insufficient for reaching binaural threshold at large contralateral IPDs. Hence the combination of these two effects (the advancing of the EPSP_{contra} in time and the pronounced amplitude reduction) results in a left-shifted IPD function that is narrowed on the right-hand side and has overall reduced spike rates compared with control (Fig. 7C3). Note that constant hyperpolarization by glycine alters the membrane conductance of the cells. This could lead to additional accelerations of the PSP kinet-

ics that would even add to the narrowing effect of tonic glycine application.

Together, the timed inhibition hypothesis predicts that during strychnine application IPD function should broaden at the left-hand side, whereas tonic glycine application should mainly induce a narrowing of the right-hand side of the IPD function. We normalized the IPD functions of all cells presented in Figures 3 and 5 to their respective control and averaged them within conditions (for details, see figure legends). Intriguingly, the mean IPD functions for control, strychnine, and glycine conditions closely resemble the qualitative predictions of the timed inhibition scenario (Fig. 7D1,D2): During strychnine application, the mean IPD function broadened mostly to the left-hand side, whereas glycine application restricted the mean IPD function mainly on the right-hand side of the control function. This qualitative result could also be statistically verified by normalizing all IPD functions individually (thereby ignoring the drug-induced overall change in spike rate) and testing for significant differences at each IPD presented. For the population of cells tested with strychnine, normalized response rates were significantly higher during drug application compared with control conditions for IPDs composing the left-hand side ($p < 0.001$, one-sided Student's t test), but not for IPDs on the right side of the original best IPD ($p > 0.5$, two-sided Student's t test) (for details, see Materials and Methods). Accordingly, compared with control conditions, normalized response rates were significantly lower during glycine application for IPDs composing the right-hand side ($p < 0.0001$, one-sided Student's t test), but did not change for IPDs on the left side ($p > 0.3$, two-sided Student's t test) (for details, see Materials and Methods). Together, these results strongly support the hypothesis of endogenous glycinergic inputs being well timed, discrete events as illustrated in Figure 7A and are inconsistent with a nonspecific, tonic effect of inhibition.

Discussion

There are three main findings in the present study: (1) The ITD tuning of gerbil MSO neurons is coherent with the idea that ITDs are encoded via a population rate code: Best ITDs depended on the neuronal BFs and were mostly outside the “physiological range” of ITDs, whereas most of the steepest slopes of the ITD functions fall within this range. (2) Blocking glycinergic inhibition with strychnine enhanced the spike rates and retuned ITD sensitivity by significantly shifting response distributions of MSO neurons toward 0 ITD and slopes out of the “physiological range.” (3) Tonic application of glycine reduced the spike rates but at the same time also induced shifts of the ITD functions toward 0 ITD, albeit with characteristics different than those observed by strychnine application.

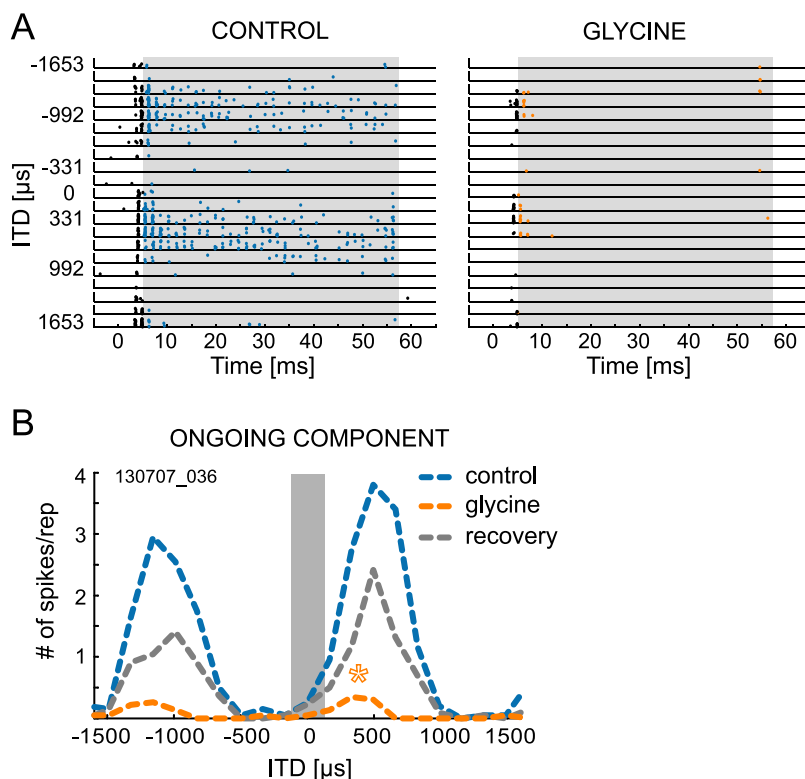


Figure 6. ITD sensitivity of ongoing response is equally sensitive to glycine application. **A**, Dot raster display of one neuron stimulated with pure tones at BF (630 Hz). Responses for multiple repetitions of ITDs between $\pm 1653 \mu\text{s}$ without (left; control) and during glycine application (right) are shown. Time axis refers to start of stimulation; stimulus duration was 50 ms (plus 5 ms rise/fall time). Spikes that fell into the time window for ongoing response (gray rectangle) are shown in blue and orange for control and glycine condition, respectively. The first 2 ms of spike trains were discarded and are shown in black. **B**, ITD functions for ongoing response only, derived from spikes shown in color in **A**. ITD tuning was shifted significantly toward the left (orange asterisk) during glycine application (orange line) compared with control condition (blue line). After glycine application was terminated, the best ITD immediately shifted back to the right (recovery; gray line). The gray bar marks the “physiological range” of ITDs.

Basic ITD properties

MSO neurons responded preferentially to contralateral leading ITDs, corroborating previous findings from both the MSO (Goldberg and Brown, 1969; Crow et al., 1978; Yin and Chan, 1990; Spitzer and Semple, 1995) and higher, subcortical structures (McAlpine et al., 2001; Hancock and Delgutte, 2004; Siveke et al., 2006, 2007). Such positions of the peaks of the ITD functions result in their slopes being positioned within the physiological range of ITDs (McAlpine et al., 2001; Harper and McAlpine, 2004). Importantly, these data corroborate the hypothesis that the population of MSO neurons encode various locations along the azimuthal plane by a monotonic modulation of their output rate along the slopes of their ITD function (McAlpine and Grothe, 2003; Palmer, 2004).

The fraction of neurons we found to respond only to the onset of stimuli was high, which could partially be attributable to anesthesia. Kuwada et al. (1989) showed prominent effects of anesthesia on neuronal response characteristics in the rabbit mid-brain. However, a recent study in the gerbil found that anesthesia-induced changes of temporal response characteristics were restricted to higher auditory centers (Ter-Mikaelian et al., 2007). Possibly the high percentage of onset responses reflects a behavioral relevance, because many natural signals have prominent onset components. To date, the relative contributions of onset and ongoing components for low-frequency sound localization is a matter of debate (Buell et al., 1991; Akeroyd and

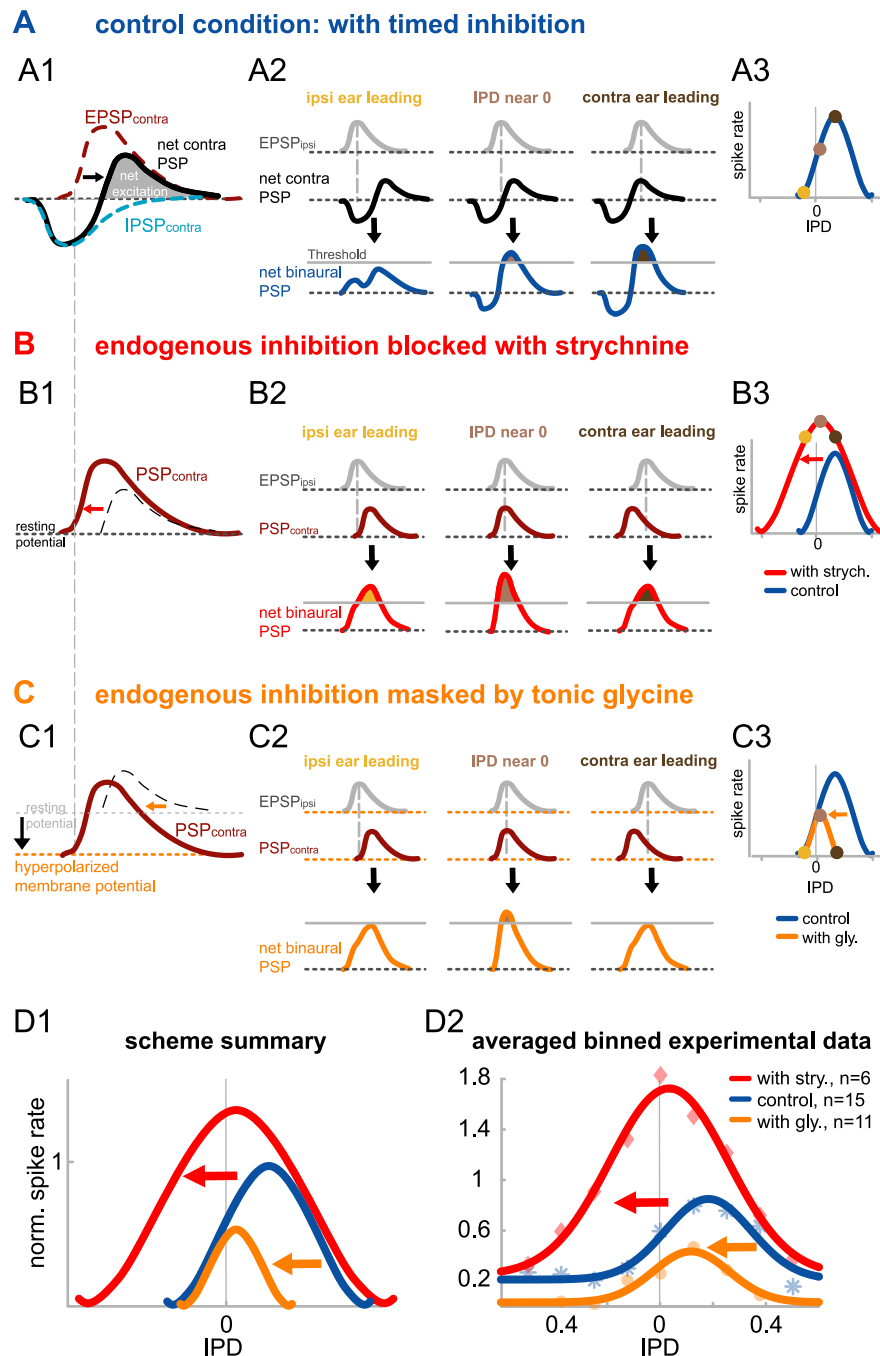


Figure 7. Predicted and measured shifts of IPD tuning during strychnine and glycine application. **A**, Control condition. **A1**, Contralateral PSP (black line). The basic principle of the timed inhibition hypothesis is that the contralateral IPSP_{contra} (light blue dashed line) precedes the contralateral EPSP (brown dashed line) on a cycle-by-cycle basis. This causes a delay of the contralaterally induced net excitation (shaded area under black line). **A2**, Binaural interaction (blue) of the net contra PSP (black) with the EPSP_{ipsi} (gray) at different IPDs. Maximal coincidence of the net excitations from both ears occurs for contra leading IPDs (right-most column of panels) compensating for the inhibition-induced delay of the contralateral excitation. **A3**, Resulting IPD function: yellow-, light brown-, and dark brown-filled circles correspond to the three stimulus conditions shown in **A2**. **B**, Effect of strychnine application. **B1**, Experimentally blocking the timed inhibition with strychnine results in a net contra PSP that is identical with the contralateral EPSP (brown line; compare with brown dashed line in **A1**). Hence the net contra PSP is advanced in time and broadened (indicated by red arrow) compared with the control condition (dashed black line). **B2**, Maximal binaural coincidence during strychnine application occurs at IPDs near 0 cycles (middle column of panels). Ipsilateral leading IPDs also create suprathreshold net binaural PSPs (left column of panels) because of partial overlap of ipsi and contra excitation. This results in overall increased response rates and a broadening of the IPD function on the left-hand side, shifting the peak toward 0 IPD (**B3**). **C**, Effect of tonic glycine application. **C1**, Tonic glycine application induces a tonic hyperpolarization (black arrow and orange dotted line), which has two important effects. First, the timed inhibition is masked; hence the net PSP_{contra} is not delayed but, second, reduced compared with the strychnine condition. Compared with control condition, this reduction has the most pronounced impact at the declining tail of the PSP (indicated by orange arrow). **C2**, This causes EPSP_{ipsi} and PSP_{contra} to coincide at IPDs near 0 cycles with only a small fraction of the net binaural PSPs exceeding threshold. **C3**, Compared with control conditions, the right-hand side of

Bernstein, 2001; Best et al., 2004). Importantly, at the level of the MSO, both onset and ongoing components exhibit similar ITD sensitivity and this ITD sensitivity is equally dependent on glycinergic inhibition (see below).

Obtaining ITD functions at multiple intensities changed overall response rates but resulted in either no or only small shifts in best ITDs. These findings are in line with previous reports from the dog MSO as well as the cat midbrain (Goldberg and Brown, 1969; Yin and Kuwada, 1983). Interestingly, in their seminal work in 1969, Goldberg and Brown argued that the invariance of best ITD with intensity is closely linked to inhibitory influences. It therefore seems conceivable that the hyperpolarizing inhibitory inputs in the MSO help to convey intensity robustness of ITD sensitivity by defining the binaural coincidence window and preventing out-of-phase responses, which otherwise increase in likelihood at higher intensities (Reed and Durbeck, 1995). Such gain control is also present in the avian analog of the MSO; however, it is achieved by tonic, GABAergic inputs providing depolarizing, shunting inhibition (Yang et al., 1999; Burger et al., 2005; Dasika et al., 2005).

Pharmacology

Because it is inherently difficult to record from MSO cells (Guinan et al., 1972), our sample size with pharmacology is small. However, in all cells in which firing rates were increased by antagonizing glycinergic inhibition with strychnine, the left side of the ITD functions shifted markedly toward 0 ITD. Similarly, whenever glycine application reduced firing rates, correlated shifts in the right-hand side of the ITD functions were observed. Importantly, in all neurons with an ongoing response, ITD functions were shifted by application of glycine or strychnine. Thus, onset and ongoing components seem to be tuned via the same circuitry and synaptic properties. It follows that glycinergic inhibition is an

the IPD function is highly reduced causing a left shift of the overall IPD function (orange arrow). **D1**, **D2**, These qualitative predictions are summarized in **D1** and are consistent with the results in our population data as depicted in **D2**, showing the average normalized spike rates of control ($n = 15$), strychnine ($n = 6$), and glycine ($n = 11$) condition (shown by asterisks, diamonds, and filled circles, respectively). For averaging, responses were binned in IPD widths of 0.125 cycles. Average normalized IPD functions were derived from these mean values by Gaussian fits. The R^2 values of the fits were 0.92, 0.98, and 0.92 for the control (blue), strychnine (red), and glycine (orange) conditions, respectively.

important mechanism for tuning ITD functions in the mammalian MSO.

There are at least two ways in which inhibitory inputs could interfere with coincidence detection of binaural excitation, both causing the contralateral inputs to be functionally delayed. One possibility was proposed by Zhou et al. (2005) and assumes both tonic inhibition and dendritic asymmetry [i.e., that the axons of MSO cells originate from the lateral dendrites (which receive the ipsilateral excitatory inputs) (Smith et al., 1993)]. The basic idea is that tonic inhibition delays the propagation of EPSPs from the contralateral input to the spike-initiating zone but does not affect ipsilateral EPSPs. However, most MSO cells are not asymmetric (Scott et al., 2005) (our unpublished observations). Additionally, our experiments showed that glycine application did not enhance the effect of endogenous synaptic inhibition, as the model would suggest, but reduced it.

A second hypothesis, proposed by Brand et al. (2002), is that precise timing of the inhibitory inputs relative to the excitatory inputs shifts the coincidence window as explained in Figure 7. The hypothesis predicts not only the shifting of ITD functions to more ipsilateral ITDs for both strychnine and tonic glycine application but also that different sides of the ITD functions are changed by glycine compared with strychnine. We emphasize that the glycine-induced shifts are not attributable to receptor desensitization, because spike rates were lowered throughout glycine application; hence the cells were hyperpolarized. Theoretically, because of the additional opening of chloride channels, this hyperpolarization might have accelerated the kinetics of the sound-evoked PSPs. However, synaptically evoked EPSPs measured in the gerbil MSO *in vitro* are essentially as fast as the underlying EPSCs (Magnusson et al., 2005; Scott et al., 2005) leaving not much space for additional acceleration. Also, we emphasize that the acceleration of PSP kinetics by tonic hyperpolarization would affect ipsilateral and contralateral inputs equally, hence would cause a narrowing of the ITD function but cannot account for the observed shifts. Turecek and Trussel (2001) described presynaptic glycine receptors that enhance neurotransmission in the calyx of Held. In principle, presynaptic glycine receptors could also be present in the MSO, which might be affected by the glycine application. However, glycinergic inputs to the MSO are restricted to the somatic area and are absent in the dendrites (Kapfer et al., 2002). Hence, presynaptic, glycine-mediated effects would affect the inhibitory inputs and would counteract the postsynaptic effects of glycine iontophoresis. Therefore, we regard this as an unlikely explanation.

Thus, our data strongly favor the scenario involving well timed inhibition. This scenario includes two critical features: One feature is the specificity in the relative onset of inhibition and excitation, whereas the other is the time course of the inhibition. With regard to timing, the scenario incorporates contralateral inhibitory inputs that arrive a few hundred microseconds before the contralateral excitatory inputs. Our data support this feature because the inhibition-induced delay in the mean phase angle of the response that was exposed by strychnine application (Fig. 4C) was exactly in this range. Moreover, the MNTB and its MSO inputs exhibit extreme specializations for exact timing and speed of transduction (Kapfer et al., 2002; von Gersdorff and Borst, 2002). For instance, it is well established that the MNTB-mediated inhibition via the even longer pathway to the lateral superior olive coincides or even precedes the excitation via the much shorter ipsilateral pathway (Grothe and Park, 1995; Tollin and Yin, 2005). Most importantly, *in vivo* recordings in the bat MSO revealed contralateral inhibition to have the capacity to arrive simultaneously or even precede the contralateral excitation (Grothe, 1994; Grothe and Park, 1998). Finally, artificial, simulta-

neous stimulation of both the excitatory and inhibitory inputs from the contralateral side *in vitro* resulted in full spike suppression in >80% of gerbil MSO neurons (Grothe and Sanes, 1993). Hence the MNTB pathway is able to compensate for the delay because of the additional synapse. The second feature is the exact time course of the inhibitory inputs, which in the model acted on a cycle-by-cycle basis. Although we could not measure the time course of inhibition directly, our findings indicate such a phasic interaction of inhibitory and excitatory inputs. Notably, our sample for pharmacological manipulations is restricted to neurons with CFs <1200 Hz, which represents the dominant frequency range of MSO cells (Yin and Chan, 1990; Spitzer and Semple, 1995). We cannot exclude the possibility that the effect of inhibition as described above is restricted to this frequency range and that inhibition is not fast enough to tune ITD sensitivity at higher frequencies. Interestingly, in our total sample of MSO recordings, we found several ITD-sensitive cells with higher CFs (up to 4800 Hz), but their BF's were all \leq 1200 Hz. *In vitro* studies on isolated glycinergic currents and potentials determined kinetics that, although very fast, were on average not fast enough to follow each stimulation cycle at higher frequencies (Smith et al., 2000; Magnusson et al., 2005). However, the effective period of glycinergic inhibition determined in MSO brain slice experiments using multiple inputs was <1 ms (Grothe and Sanes, 1994). Recently, it was shown in MNTB membrane patches that the kinetics of glycinergic inhibition is accelerated by the corelease of GABA (Lu et al., 2008). Hence, it is currently unclear how fast inhibition can act *in vivo* and how fast it would have to be to make our scenario feasible [note that Brand et al. (2002) only aimed for proof of principle, not for assessing the kinetics required].

The present data provide strong evidence for glycinergic inhibition as a key factor in setting functional delays of the binaural excitatory inputs, but it is important to note that glycine might act in concert with other factors that could cause internal delays of the MSO inputs (cf. Joris and Yin, 2007). These factors include axonal length (Jeffress, 1948; Smith et al., 1993; Beckius et al., 1999), cochlear delays if frequency tuning of the different inputs do not exactly match (Shamma et al., 1989; Joris et al., 2006), or differences in myelination or axonal diameter. Additional research is needed to address these questions using more sophisticated manipulations such as experimentally induced decorrelation of the phase-locked inhibitory inputs.

References

- Adams JC (1977) Technical considerations on use of horseradish-peroxidase as a neuronal marker. *Neuroscience* 2:141–145.
- Akeroyd MA, Bernstein LR (2001) The variation across time of sensitivity to interaural disparities: behavioral measurements and quantitative analyses. *J Acoust Soc Am* 110:2516–2526.
- Batra R, Kuwada S, Fitzpatrick DC (1997) Sensitivity to interaural temporal disparities of low- and high-frequency neurons in the superior olivary complex. I. Heterogeneity of responses. *J Neurophysiol* 78:1222–1236.
- Beckius GE, Batra R, Oliver DL (1999) Axons from anteroventral cochlear nucleus that terminate in medial superior olive of cat: observations related to delay lines. *J Neurosci* 19:3146–3161.
- Best V, van Schaik A, Carlile S (2004) Separation of concurrent broadband sound sources by human listeners. *J Acoust Soc Am* 115:324–336.
- Brand A, Behrend O, Marquardt T, McAlpine D, Grothe B (2002) Precise inhibition is essential for microsecond interaural time difference coding. *Nature* 417:543–547.
- Buell TN, Trahiotis C, Bernstein LR (1991) Lateralization of low-frequency tones: relative potency of gating and ongoing interaural delays. *J Acoust Soc Am* 90:3077–3085.
- Burger RM, Cramer KS, Pfeiffer JD, Rubel EW (2005) Avian superior olivary nucleus provides divergent inhibitory input to parallel auditory pathways. *J Comp Neurol* 481:6–18.
- Cant NB (1991) Projections to the lateral and medial superior olivary nuclei

- from the spherical and globular bushy cells of the anteroventral cochlear nucleus. In: *Neurobiology of hearing: the central auditory system* (Altschuler RA, Bobbin RP, Clopton BM, Hoffman DW, eds), pp 99–119. New York: Raven.
- Cant NB, Hyson RL (1992) Projections from the lateral nucleus of the trapezoid body to the medial superior olivary nucleus in the gerbil. *Hear Res* 58:26–34.
- Carr CE, Soares D (2002) Evolutionary convergence and shared computational principles in the auditory system. *Brain Behav Evol* 59:294–311.
- Clark GM (1969) Vesicle shape versus type of synapse in the nerve endings of the cat medial superior olive. *Brain Res* 15:548–551.
- Crow G, Rupert AL, Moushegian G (1978) Phase locking in monaural and binaural medullary neurons: implications for binaural phenomena. *J Acoust Soc Am* 64:493–501.
- Dasika VK, White JA, Carney LH, Colburn HS (2005) Effects of inhibitory feedback in a network model of avian brain stem. *J Neurophysiol* 94:400–414.
- Goldberg JM, Brown PB (1969) Response of binaural neurons of dog superior olivary complex to dichotic tonal stimuli: some physiological mechanisms of sound localization. *J Neurophysiol* 32:613–636.
- Grothe B (1994) Interaction of excitation and inhibition in processing of pure tone and amplitude-modulated stimuli in the medial superior olive of the mustached bat. *J Neurophysiol* 71:706–721.
- Grothe B (2003) New roles for synaptic inhibition in sound localization. *Nat Rev Neurosci* 4:540–550.
- Grothe B, Park TJ (1995) Time can be traded for intensity in the lower auditory system. *Naturwissenschaften* 82:521–523.
- Grothe B, Park TJ (1998) Sensitivity to interaural time differences in the medial superior olive of a small mammal, the Mexican free-tailed bat. *J Neurosci* 18:6608–6622.
- Grothe B, Sanes DH (1993) Bilateral inhibition by glycinergic afferents in the medial superior olive. *J Neurophysiol* 69:1192–1196.
- Grothe B, Sanes DH (1994) Synaptic inhibition influences the temporal coding properties of medial superior olivary neurons: an *in vitro* study. *J Neurosci* 14:1701–1709.
- Grothe B, Fritzsche B, Köppl C, Casseday JH, Carr CE (2004) The evolution of central pathways and their neural processing patterns. In: *Evolution of the vertebrate auditory system* (Manley GA, Popper AN, Fay RR, eds), pp 289–359. New York: Springer.
- Guinan JJ Jr, Norris BE, Guinan SS (1972) Single auditory units in the superior olivary complex. II. Locations of unit categories and tonotopic organization. *Int J Neurosci* 4:147–166.
- Hancock KE, Delgutte B (2004) A physiologically based model of interaural time difference discrimination. *J Neurosci* 24:7110–7117.
- Harper NS, McAlpine D (2004) Optimal neural population coding of an auditory spatial cue. *Nature* 430:682–686.
- Jeffress LA (1948) A place theory of sound localization. *J Comp Physiol Psychol* 41:35–39.
- Joris P, Yin TC (2007) A matter of time: internal delays in binaural processing. *Trends Neurosci* 30:70–78.
- Joris PX, Van de Sande B, Louage DH, van der Heijden M (2006) Binaural and cochlear disparities. *Proc Natl Acad Sci U S A* 103:12917–12922.
- Kapfer C, Seidl AH, Schweizer H, Grothe B (2002) Experience-dependent refinement of inhibitory inputs to auditory coincidence-detector neurons. *Nat Neurosci* 5:247–253.
- Kuwabara N, Zook JM (1992) Projections to the medial superior olive from the medial and lateral nuclei of the trapezoid body in rodents and bats. *J Comp Neurol* 324:522–538.
- Kuwada S, Stanford TR, Batra R (1987) Interaural phase-sensitive units in the inferior colliculus of the unanesthetized rabbit: effects of changing frequency. *J Neurophysiol* 57:1338–1360.
- Kuwada S, Batra R, Stanford TR (1989) Monaural and binaural response properties of neurons in the inferior colliculus of the rabbit: effects of sodium pentobarbital. *J Neurophysiol* 61:269–282.
- Lu T, Rubio ME, Trussell LO (2008) Glycinergic transmission shaped by the corelease of GABA in a mammalian auditory synapse. *Neuron* 57:524–535.
- Magnusson AK, Kapfer C, Grothe B, Koch U (2005) Maturation of glycinergic inhibition in the gerbil medial superior olive after hearing onset. *J Physiol* 568:497–512.
- Maki K, Furukawa S (2005) Acoustical cues for sound localization by the Mongolian gerbil, *Meriones unguiculatus*. *J Acoust Soc Am* 118:872–886.
- Manley GA, Popper AN, Fay RR (2004) *Evolution of the vertebrate auditory system*. New York: Springer.
- Mardia KV (1972) *Statistics of directional data*. London: Academic.
- McAlpine D, Grothe B (2003) Sound localization and delay lines—do mammals fit the model? *Trends Neurosci* 26:347–350.
- McAlpine D, Jiang D, Palmer AR (2001) A neural code for low-frequency sound localization in mammals. *Nat Neurosci* 4:396–401.
- Moushegian G, Rupert AL, Gidda JS (1975) Functional characteristics of superior olivary neurons to binaural stimuli. *J Neurophysiol* 38:1037–1048.
- Palmer AR (2004) Reassessing mechanisms of low-frequency sound localization. *Curr Opin Neurobiol* 14:457–460.
- Perkins RE (1973) An electron microscopic study of synaptic organization in the medial superior olive of normal and experimental chinchillas. *J Comp Neurol* 148:387–415.
- Reed MC, Durbeck L (1995) Delay lines and auditory processing. *Comm Theor Biol* 3:441–461.
- Schuller G, Radtke-Schuller S, Betz M (1986) A stereotaxic method for small animals using experimentally determined reference profiles. *J Neurosci Methods* 18:339–350.
- Scott LL, Mathews PJ, Golding NL (2005) Posthearing developmental refinement of temporal processing in principal neurons of the medial superior olive. *J Neurosci* 25:7887–7895.
- Scott LL, Hage TA, Golding NL (2007) Weak action potential backpropagation is associated with high frequency axonal firing capability in principal neurons of the gerbil medial superior olive. *J Physiol* 583:647–661.
- Seidl AH, Grothe B (2005) Development of sound localization mechanisms in the mongolian gerbil is shaped by early acoustic experience. *J Neurophysiol* 94:1028–1036.
- Shamma SA, Shen NM, Gopalaswamy P (1989) Stereausis: binaural processing without neural delays. *J Acoust Soc Am* 86:989–1006.
- Siveke I, Pecka M, Seidl AH, Baudoux S, Grothe B (2006) Binaural response properties of low-frequency neurons in the gerbil dorsal nucleus of the lateral lemniscus. *J Neurophysiol* 96:1425–1440.
- Siveke I, Leibold C, Grothe B (2007) Spectral composition of concurrent noise affects neuronal sensitivity to interaural time differences of tones in the dorsal nucleus of the lateral lemniscus. *J Neurophysiol* 98:2705–2715.
- Smith AJ, Owens S, Forsythe ID (2000) Characterisation of inhibitory and excitatory postsynaptic currents of the rat medial superior olive. *J Physiol* 529:681–698.
- Smith PH, Joris PX, Yin TC (1993) Projections of physiologically characterized spherical bushy cell axons from the cochlear nucleus of the cat: evidence for delay lines to the medial superior olive. *J Comp Neurol* 331:245–260.
- Spirou GA, Rowland KC, Berrebi AS (1998) Ultrastructure of neurons and large synaptic terminals in the lateral nucleus of the trapezoid body of the cat. *J Comp Neurol* 398:257–272.
- Spitzer MW, Semple MN (1995) Neurons sensitive to interaural phase disparity in gerbil superior olive: diverse monaural and temporal response properties. *J Neurophysiol* 73:1668–1690.
- Ter-Mikaelian M, Sanes DH, Semple MN (2007) Transformation of temporal properties between auditory midbrain and cortex in the awake Mongolian gerbil. *J Neurosci* 27:6091–6102.
- Tollin DJ, Yin TC (2005) Interaural phase and level difference sensitivity in low-frequency neurons in the lateral superior olive. *J Neurosci* 25:10648–10657.
- Turecek R, Trussell LO (2001) Presynaptic glycine receptors enhance transmitter release at a mammalian central synapse. *Nature* 411:587–590.
- von Gersdorff H, Borst JG (2002) Short-term plasticity at the calyx of Held. *Nat Rev Neurosci* 3:53–64.
- Wentholt RJ, Huie D, Altschuler RA, Reeks KA (1987) Glycine immunoreactivity localized in the cochlear nucleus and superior olivary complex. *Neuroscience* 22:897–912.
- Yang L, Monsivais P, Rubel EW (1999) The superior olivary nucleus and its influence on nucleus laminaris: a source of inhibitory feedback for coincidence detection in the avian auditory brainstem. *J Neurosci* 19:2313–2325.
- Yin TC, Chan JC (1990) Interaural time sensitivity in medial superior olive of cat. *J Neurophysiol* 64:465–488.
- Yin TC, Kuwada S (1983) Binaural interaction in low-frequency neurons in inferior colliculus of the cat. II. Effects of changing rate and direction of interaural phase. *J Neurophysiol* 50:1000–1019.
- Zhou Y, Carney LH, Colburn HS (2005) A model for interaural time difference sensitivity in the medial superior olive: interaction of excitatory and inhibitory synaptic inputs, channel dynamics, and cellular morphology. *J Neurosci* 25:3046–3058.
- Zurek PM (1993) A note on onset effects in binaural hearing. *J Acoust Soc Am* 93:1200–1201.

CHAPTER 2

Binaural Response Properties of Low-Frequency Neurons in the Gerbil Dorsal Nucleus of the Lateral Lemniscus

Ida Siveke,^{1,2} Michael Pecka,^{1,2} Armin H. Seidl,² Sylvie Baudoux,² and Benedikt Grothe^{1,2}

¹Division of Neurobiology, Department Biology II, Ludwig-Maximilians-University of Munich; and ²Max Planck Institute of Neurobiology, Martinsried, Germany

Submitted 6 June 2005; accepted in final form 22 March 2006

Siveke, Ida, Michael Pecka, Armin H. Seidl, Sylvie Baudoux, and Benedikt Grothe. Binaural response properties of low-frequency neurons in the gerbil dorsal nucleus of the lateral lemniscus. *J Neurophysiol* 96: 1425–1440, 2006. First published April 5, 2006; doi:10.1152/jn.00713.2005. Differences in intensity and arrival time of sounds at the two ears, interaural intensity and time differences (IID, ITD), are the chief cues for sound localization. Both cues are initially processed in the superior olivary complex (SOC), which projects to the dorsal nucleus of the lateral lemniscus (DNLL) and the auditory midbrain. Here we present basic response properties of low-frequency (<2 kHz) DNLL neurons and their binaural sensitivity to ITDs and IIDs in the anesthetized gerbil. We found many neurons showing binaural properties similar to those reported for SOC neurons. IID-properties were similar to that of the contralateral lateral superior olive (LSO). A majority of cells had an ITD sensitivity resembling that of either the ipsilateral medial superior olive (MSO) or the contralateral LSO. A smaller number of cells displayed intermediate types of ITD sensitivity. In neurons with MSO-like response ITDs that evoked maximal discharges were mostly outside of the range of ITDs the gerbil naturally experiences. The maxima of the first derivative of their ITD-functions (steepest slope), however, were well within the physiological range of ITDs. This finding is consistent with the concept of a population rather than a place code for ITDs. Moreover, we describe several other binaural properties as well as physiological and anatomical evidence for a small but significant input from the contralateral MSO. The large number of ITD-sensitive low-frequency neurons implicates a substantial role for the DNLL in ITD processing and promotes this nucleus as a suitable model for further studies on ITD-coding.

INTRODUCTION

Interaural disparities in time and intensity are the cues that animals use to localize sounds in the horizontal plane. Interaural intensity disparities (IIDs) are produced by a wavelength-dependent shadowing effect of the head that is more prominent for high- than for low-frequency sounds. In mammals, IIDs are initially processed by neurons in the lateral superior olive (LSO) via a subtraction mechanism based on excitatory inputs from the ipsilateral ear and inhibitory inputs from the contralateral ear (IE) (Boudreau and Tsuchitani 1968; Yin 2002). Most LSO cells are tuned to high frequencies. Because low frequencies do not create significant IIDs, interaural time differences (ITDs) are the dominant cue for localizing low-frequency sounds (Rayleigh 1907; Thompson 1882). ITDs are first processed in the medial superior olive (MSO), which receives both excitatory and inhibitory binaural inputs. The response of MSO

neurons is dominated by a coincidence of the net excitation of the inputs from the two ears (for review: Irvine 1992; Yin 2002). Additionally, it has been speculated that low-frequency LSO neurons might contribute to ITD processing (Joris and Yin 1995). A recent study confirms such an IE-based ITD sensitivity for a small number of neurons in the low-frequency limb of the cat LSO (Tollin and Yin 2005). Data from low-frequency MSO and LSO neurons are sparse because it is notoriously difficult to record from these cells in vivo. Accordingly, the few neurophysiological studies of low-frequency MSO and LSO neurons provide small sample sizes compared with studies dealing with other auditory nuclei (Batra et al. 1997b; Brand et al. 2002; Goldberg and Brown 1969; Spitzer and Semple 1995; Tollin and Yin 2005; Yin and Chan 1990). Therefore most data about ITD-processing and the neuronal representation of ITDs stems from the auditory midbrain, the inferior colliculus (IC), a direct target of the MSO and LSO projections (Caird and Klinke 1987; Kuwada and Yin 1983; McAlpine et al. 1998, 2001; Rose et al. 1966; Yin and Kuwada 1983a,b). Unfortunately, a high degree of convergence of both excitatory and inhibitory projections from numerous lower auditory nuclei, from the opposite IC and from intrinsic connections complicates the interpretation of data derived from the IC (for review Oliver and Huerta 1992). Therefore large data sets are necessary to perform reliable population statistics on IC recordings (D'Angelo et al. 2005; Fitzpatrick and Kuwada 2001; Kidd and Kelly 1996; McAlpine and Palmer 2002; McAlpine et al. 2001). In vivo recordings from IC (e.g., McAlpine et al. 1998) as well as theoretical considerations (e.g., Cai et al. 1998a,b) indicate that the convergence of only two MSO inputs, for instance, could create ITD-properties in the IC that are much more complicated than the ITD sensitivity at the level of the MSO itself.

However, the MSO and the LSO also send strong projections to the dorsal nucleus of the lateral lemniscus (DNLL) (Glendenning et al. 1981; Oliver 2000; Shneiderman et al. 1988), a hindbrain structure ventral of the IC. This nucleus is easier to record single neuron responses from than MSO and LSO and shows more linear and, hence, predictable response properties than IC neurons, at least for high-frequency neurons (Xie et al. 2005). DNLL neurons are known to be sensitive to both IIDs and ITDs (Brugge et al. 1970; Fitzpatrick and Kuwada 2001; Kelly et al. 1998; Kuwada et al. 2005; Markovitz and Pollak 1994). Nevertheless, only a little is

Address for reprint requests and other correspondence: B. Grothe, Dept. Biology II, Biocenter, Ludwig-Maximilians-University of Munich, Grosshaderner Strasse 2, D-81252 Martinsried, Germany (E-mail: grothe@lmu.de).

The costs of publication of this article were defrayed in part by the payment of page charges. The article must therefore be hereby marked "advertisement" in accordance with 18 U.S.C. Section 1734 solely to indicate this fact.

known about the role of the DNLL in low-frequency sound processing.

Here we show that many low-frequency DNLL neurons display response properties strikingly similar to those seen in the superior olivary complex (SOC). However, we also found that a substantial portion of our neurons have response features that are more similar to the properties seen in the IC rather than the SOC.

METHODS

Experimental animals

Auditory responses from single neurons were recorded from 74 Mongolian gerbils (*Meriones unguiculatus*) of both sexes. Mongolian gerbils have a well developed low-frequency hearing and can use ITDs and IIDs for sound localization (Heffner and Heffner 1988; Ryan 1976). Animals used for the experiments were 2–3 m/h of age.

All experiments were approved according to the German Tier-schutzgesetz (AZ 211-2531-40/01 + AZ 211-2531-68/03).

Surgical procedures

Before surgery, animals were anesthetized by an initial intraperitoneal injection (0.5 ml/ 100 g body wt) of a physiological NaCl solution containing ketamine (20%) and rompun (2%). During surgery and recordings, a dose of 0.05 ml of the same mixture was applied subcutaneously every 30 min. Constant body temperature (37–39°C) (Field and Siebold 1999) was maintained using a thermostatically controlled heating blanket.

Skin and tissue covering the upper part of the skull was cut and carefully pushed aside laterally, and a small metal rod was mounted on the frontal part of the skull using UV-sensitive dental-restorative material (Charisma, Heraeus Kulzer). The rod was used to reproducibly secure the head of the animal in a stereotactic device during recordings. Custom-made ear-phone holders were attached to the gerbil head close to the acoustic meatus to form a sealed pressure field sound-delivery system allowing the insertion of ear phones and probe-tube microphones. The animal was then transferred to a sound-attenuated chamber and mounted in a custom-made stereotactic instrument (Schuller et al. 1986). The animal's position in the recording chamber was standardized by stereotactic landmarks on the surface of the skull (intersections of the bregmoid and lambdoid sutures with the sagittal suture in horizontal alignment) (Loskota et al. 1974). For electrode penetrations to the DNLL, a small hole was cut into the skull extending 1.3–2.6 mm lateral from the midline and 0.5–0.8 mm caudal of the interaural axis. Micromanipulators were used to position the recording electrode according to landmarks on the brain surface, and a reference point was used for all penetrations. The dura mater overlying the cortex was removed carefully, and during the recording session, Ringer solution was applied to the opening to prevent dehydration of the brain. For some recordings, the recording electrode was tilted 10° or 5° laterally.

Typical recording periods lasted 10–14 h. After recordings, the animal was killed without awakening by an injection of 0.1 ml of T61 (BGA-Reg No. T331, Intervet), and the last electrode position was marked by a current-induced lesion (5 mA for 5 s after T61 had been applied) using metal electrodes (5 M Ω). Afterward the head was fixed in 4% paraformaldehyde for 2 days. The brain was removed and placed in 30% sucrose at 4°C for 2 days. The brains were embedded in tissue-freezing medium (Jung, Leica Instruments GmbH, Germany), frozen solid, and mounted in a standard plane for sections. Transverse sections were cut at 45 μ m in a cryostat at –21°C. Sections were Nissl-stained, and the recording sites verified using standard light microscopy.

Neuronal recordings

Single-unit responses were recorded extracellularly using tungsten electrodes (1 or 5 M Ω ; World Precision Instruments) or glass electrodes filled with 1 M NaCl (~10 M Ω). We did not detect any differences between recordings using either type of electrodes in terms of the recording quality (spike-to-noise ratio, possibility of holding the cells and number of cells recorded per penetration) or neuronal response properties (discharge properties, best frequencies, thresholds, aurality, ITD or IID sensitivity). The recording electrode was advanced under remote control, using a motorized micromanipulator (Digimatic, Mitutoyo, Neuss, Germany) and a piezodrive (Inchworm controller 8200, EXFO Burleigh Products Group). Extracellular action potentials were recorded via an electrometer (npi electronics, Germany or Electro 705, World Precision Instruments), a noise eliminator (Humbug, Quest Scientific) removing residual line noise picked up by electrode, a band-pass filter (VBF/3, Kemo) and an additional amplifier (Toellner 7607) and fed into the computer via an A/D converter (RP2-1, TDT). Clear isolation of action potentials from a single cell (signal-to-noise ratio >5) was guaranteed by visual inspection on a spike-triggered oscilloscope (stable shape and amplitude of the action potential) and by off-line spike cluster analysis based on stable amplitudes of the positive and negative peaks (volt) and stable spikes waveform (Brainware, Jan Schnupp, TDT) (see insets Fig. 5 and 7).

Stimulus presentation and recording protocols

Stimuli were generated at 50-kHz sampling rate by TDT System II or III (Tucker Davis Technologies). Digitally generated stimuli were converted to analog signals (DA3-2/RP2-1, TDT), attenuated (PA5, TDT) and delivered to the ear phones (Sony, Stereo Dynamic Earphones, MDR-EX70LP). The sound field inside the sealed system was controlled using calibrated probe tube microphones (FG 3452, Knowles Electronics). The microphone signal was amplified (RP2-1, TDT) and transferred to the computer for off-line analysis. The difference of the sound pressure level between the two headphones was <5 dB in the range of 100–2,000 Hz and the phase difference was <0.01 cycles.

The standard setting was stimulus duration of 200 ms plus squared-cosine rise/fall times of 5 ms, presented at a repetition rate of 2 Hz. For all recordings, stimulus presentation was randomized. To search for acoustically evoked responses, noise stimuli without interaural time and intensity differences were delivered binaurally. When a neuron was encountered, we first determined its best frequency (BF) and absolute threshold using binaurally identical (IID/ITD = 0) sinus tone stimulation. The frequency that elicited responses at the lowest sound intensity was defined as BF, the lowest sound intensity evoking a noticeable response at BF as threshold. These properties were determined on-line by audio-visual inspection in all neurons and, in almost all neurons (229/254), confirmed by a careful off-line analysis of the frequency versus level response areas. These parameters were used to set stimulus parameters subsequently controlled by the computer. In addition, monaural pure tones and binaural pure tones were presented so that the binaural properties (aurality) could be determined.

Sensitivity to ITDs was primarily assessed by presenting a matrix of pure-tone stimuli with varying ITDs and stimulus frequencies 20 dB above threshold. We presented different ITDs over a range equivalent to at least a cycle of the stimulus frequency (step size 100 or 62,500/0.6/BF μ s). ITD sensitivity was tested for between three and nine frequencies around BF. ITDs with the contralateral stimulus leading were defined as positive, ITDs with the ipsilateral stimulus leading as negative ITDs. ITD sensitivity was tested setting the IID to 0 dB.

A subpopulation of the binaurally excitable (EE) low-frequency cells was tested with very short downward-frequency-modulated

sweeps ("chirps"). To record the waveform of the frequency-modulated-downward sweep stimulus (chirp, see Fig. 1), we used a pressure-field 1/2-in. microphone (Type 4192, Brüel and Kjær) placed ~5 mm in front of the headphone. Headphone and microphone were tightly connected by a plastic tube to mimic the situation at the ear of the animal. The recorded signal was amplified (Calibration amplifier Type 2636, Brüel and Kjær), digitized (RP2.1, TDT), and stored on a PC. The frequency was modulated linearly from 2,000 to 100 Hz in 3 ms, including squared cosine-function rise and fall times of 0.5 ms. The repetition interval was 2.5 Hz. Although these stimuli generate considerable spectral splatter, we chose them because, unlike clicks, they did not appear to generate a prolonged ringing response; also, most of the stimulus energy is concentrated in the low-frequency band (Fig. 1). The average monaural latencies were assessed for each ear individually by presenting the chirps monaurally. These stimuli evoked either a single discharge or, at most, two discharges with high temporal precision. We could therefore unambiguously determine those discharges that were evoked by the contralateral or the ipsilateral ear, even when the stimuli were presented binaurally, due to the separation by a given ITD. Binaural chirps with varying interaural delays were presented. The stimulation time of the ipsilateral chirp was kept constant and the delay of the contralateral stimulus was varied in steps of 50, 100, or 200 μ s. Maximal interaural delays were ± 1 or 2 ms. Stimulus amplitudes were adjusted so that cells responded to monaural chirps with one or two action potentials and were then held constant for all further stimulations.

In a subpopulation of EI neurons we assessed IID sensitivity. A combination of different IIDs was presented by holding the intensity on the excitatory ear constant at 20 dB above the binaural (ITD = 0) threshold while varying the intensity on the inhibitory ear in 10-dB steps between 10 dB below and 50 dB above threshold. The resulting IIDs of -30 dB (negative values mark higher intensities on the inhibitory ear) to +30 dB were presented for five different frequencies centered on BF. The repetition rate was 4 Hz.

Data analysis

All quantifications in this study are based on off-line analysis. Spontaneous activity was defined as a firing rate > 2 Hz. For the analysis of the different response patterns, the mean response to

binaural stimuli (IID = 0, ITD = 0) at BF and 20 dB above threshold were used. For analyzing the poststimulus time histogram (PSTH), the period histogram, and the inter-spike interval histogram (ISI), of 184 DNLL neurons, we defined different response patterns. The response pattern was defined as onset (response exclusively during the 1st 50 ms) or sustained (response over the entire duration of the stimulus). Sustained activity was further divided in phase-locked sustained response and non phase-locked sustained response. Neuronal response was classified as phase-locked sustained (s-l) if the vector strength (Goldberg and Brown 1969) was > 0.3 and the $P < 0.05$ criterion in the Rayleigh test was fulfilled (Batschelet 1991). Following the description of response pattern of neurons in the cochlear nucleus by Rhode and Greenberg (1992), we divided the nonphase-locked pattern into primary-like (s-p) and tonic sustained (s-t) response patterns. Both patterns did not show regularity in the period histogram or the ISI. The s-p types were separated from the s-t types by the mean response at the beginning of the response (in the time interval of 12.5–37.5 ms) and the middle of the response (in the time interval of 87.5–112.5 ms). For the s-p types, the response at the beginning was approximately three times larger than the response to the middle portion of the stimulus, whereas the response for the s-t types was about the same in both intervals.

ITD sensitivity was carefully analyzed and quantified for cells that showed $\geq 50\%$ modulation (reduction of max. spike rate by $\geq 50\%$) in their ITD response rate function when tested at BF. For a detailed analysis of ITD functions, we increased our sample size of ITD-sensitive cells by the addition of 105 DNLL cells from earlier, unpublished and published studies (control group) (Seidl and Grothe 2005) using identical equipment and experimental procedures. The quantifications were based on the interaural phase difference (IPD) functions measured with pure tones at different test frequencies (thereby normalizing the cyclic ITD functions for test frequency). The cells mean interaural phase was calculated for each test frequency via a vector analysis following Yin and Kuwada (1983a). Because stimulus phase changes linearly with frequency, neuronal responses can be plotted as best phase versus frequency and the functions can be extrapolated to zero frequency. The phase at which the graphs intersect with the y axis (at 0 Hz) is called the characteristic phase (CP), a value between -0.5 and +0.5 cycles. Depending on the calculated CP, different groups of ITD-sensitive neurons can be distinguished. Peak-type neurons have a CP at or around 0 cycles, reflecting coincidence of binaural excitation, which results in an individual best ITD (eliciting the maximal spike rate) independent of test frequency (Yin and Kuwada 1983b). Similar reasoning is applied to trough-type neurons, although trough-type neurons are characterized by the ITD that generates the minimum responses in the ITD functions. The trough in the ITD function is expected when there is coincidence of excitation from one ear and inhibition from the other. Extrapolation of these phase-frequency plots yield characteristic phases at or around ± 0.5 cycles, reflecting that maximal responses occur when excitatory and inhibitory inputs are out of coincidence.

We defined peak-type neurons by an absolute CP of 0–0.125 cycles and trough-type neurons by 0.375–0.5 cycles. According to the locations of the peaks and the troughs, we separated these two types into ipsi- or contralateral peak- or trough-type neurons, depending on whether the peak or trough occurred for ipsi- or contralaterally leading sounds. Furthermore we defined two intermediate types: a peak-intermediate type by a absolute CP within 0.125–0.25 cycles and a trough-intermediate type by a absolute CP within 0.25–0.375 cycles. The slope of the linear fit yielded a quantitative measure of the neuron's characteristic delay (CD) (Rose et al. 1966; Yin and Kuwada 1983b). Phase plots were considered linear if the linear regression component exceeded the 0.005 level of significance using the test of nonlinearity described by Kuwada and colleagues (Kuwada et al. 1987). A subgroup of ITD-sensitive neurons ($n = 81$) was tested for the validity of the assumed linearity of our regression lines of the frequency versus best IPD functions. Of this subpopulation 74 (93%)

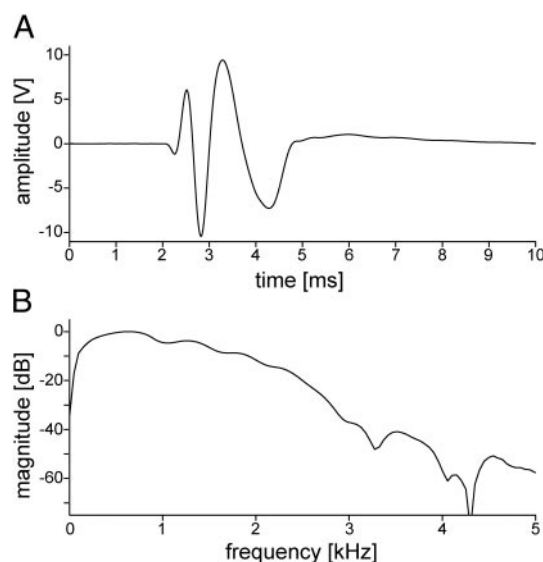


FIG. 1. Chirp stimulus used to test a subset of neurons. A: recorded waveform of the chirp stimulus that was generated by a linear frequency downward modulation from 2 to 0.1 kHz within 3 ms including 0.5 ms rise and fall times. The magnitude spectrum of the waveform in B illustrates that most of the energy was concentrated in the frequency band < 3 kHz.

neurons showed a significant linearity (following Kuwada et al. 1987). Furthermore we tested if weighting each data point (best IPD at certain frequency) by the vector strength and the mean response in a similar manner to that described by Kuwada et al. (1987) and Spitzer and Semple (1995) would change the obtained distribution of different types. We could not find any differences. Almost all calculated CPs (71/81, 88%) were not or at most slightly affected and, hence, their classification of ITD-sensitivity was independent of the method used.

To define the point of steepest slope, the ITD-rate function was fitted by a Gaussian (Matlab; The MathWorks) or sigmoid function (Statistica; StatSoft) and the inflection point closest to zero ITD was determined. Fitted ITD functions obtaining an R -square <0.7 were excluded.

Analysis of the responses to binaural chirp stimuli were conducted by defining time slots during which action potentials should occur in response to the ipsilateral or the contralateral stimulus. These time slots (starting point and width) were based on the spike time latencies measured in response to monaural stimulation. The time slots had a width of ~ 0.25 ms. Response rates in these time windows were assessed. For responses with more than one action potential per stimulation, only the first action potential was counted. The average spike time, SD, and variance was determined for analysis of the temporal accuracy of a cell's response.

Neurons were defined as IID sensitive if ipsilateral (inhibitory) stimulation reduced the maximal response elicited by contralateral (excitatory) stimulation by $>50\%$. The IID of maximal inhibition was defined as the smallest IID (lowest intensity at the ipsilateral, inhibitory ear) that caused maximal suppression of the response to the contralateral stimulus. To calculate the maximal inhibition in percent, we used the following formula: $[(\text{maximal response rate} - \text{minimal response rate}) / \text{maximal response rate}] \times 100$. The IID of 50% inhibition was graphically extrapolated from the calculated 50% response rate of the neurons IID function.

Immunohistochemistry

Three animals were used for anatomical studies in which neuronal tracers were injected into the DNLL after recording. Two different tracer cocktails were used: a mixture of biotin (10%; Molecular Probes D-1956, NL) and fluorescein-dextran (10%, Molecular Probes D-1820, NL), or tetramethylrhodamine-dextran (10%, Molecular Probes D-1817, NL) dissolved in 0.9% NaCl. Tracers were injected by iontophoresis (6 μA for 6–10 min). Nine to 10 days after the injection, the animals were killed (chloralhydrate, 50 mg/100 g) and perfused transcardially with heparinized 0.9% buffered saline solution for 5 min under deep anesthesia followed by a buffered solution containing 4% paraformaldehyde and 1% glutaraldehyde for 20–30 min. The fixed brain was removed from the skull and placed in 30% sucrose (until it had sunk) for cryoprotection. Transverse sections of 40 μm were prepared in a cryostat (Leica Microsystems CM 3050S, Nussloch).

The histological methods used in this study have been described in detail elsewhere (Malmierca et al. 2002; Oliver et al. 1997). In short, all sections were incubated in 0.05% TritonX100 for 30 min. For visualization of the biotinylated-dextran amine, the avidin-biotin-diaminobenzidine (DAB) method (ABC Kit, Vector Laboratories) coupled with nickel was used. For permanent staining of the tetramethylrhodamine-dextran, the slices were incubated with anti-tetramethylrhodamine rabbit IgG (Molecular Probes, NL) over night followed by 30 min incubation with biotinylated anti rabbit (Jackson), and avidin-biotin-DAB. Every third section was counter-stained (Nissl) to allow a clear allocation of the labeled cells. Camera lucida drawings were made with the aid of a drawing tube attached to a Leitz microscope (Dialux 20, Leitz, Wetzlar, Germany). Photomicrographs were made with a digital camera (Polaroid). The retrogradely labeled and DAB-stained neurons in the SOC of three animals were counted

under the light microscope and pooled for each nucleus (as defined via the Nissl staining).

RESULTS

General response features of DNLL cells

BFs ranged from 70 Hz to 5.6 kHz, but more than 2/3 of the neurons (185/254) had BFs $<2,000$ Hz; we refer to these as low-frequency neurons. Twenty percent of the low-frequency DNLL neurons we tested were spontaneously active (38/185; 20.5%; rate: ≥ 2 Hz).

Low-frequency DNLL neurons (BF < 2 kHz) exhibited five different discharge patterns when tested at ITD = 0. A small group of neurons (34/185, 18%) showed onset responses (Fig. 2A). Of these, two-thirds (23/34, 68%) fired one to three spikes per stimulus with an extremely short onset (on; Fig. 2B), whereas 32% (11/34) showed a phasic-on type response (on-ph; Fig. 2C). Most neurons (151/185, 82%) had sustained discharge patterns. About two-thirds of the sustained neurons (101/151, 67%) showed a significant phase-locked response (s-l) to the low-frequency pure tones (Fig. 2D). Non-phase-locked but sustained neurons exhibited either primary-like (s-p; 14/151, 9%) or tonic (s-t) discharge patterns (36/151, 24%). S-t neurons exhibited a nearly constant discharge rate throughout the entire stimulus duration (Fig. 2E), whereas s-p neurons had a stronger response at the beginning of the response period (Fig. 2F).

We tested the distribution of binaural properties using 127 low-frequency DNLL neurons (Fig. 3). Except for a small number of monaural neurons (16/127, 13%) that were excited by the contralateral ear and unaffected by ipsilateral stimulation (EO), most low-frequency DNLL neurons (111/127, 87%) were binaurally sensitive. Most of these binaural sensitive neurons (73/111, 65%) showed evidence for binaural excitation either by responding to monaural stimulation of either ear alone or by exhibiting binaural facilitation. These neurons were classified as excitatory-excitatory (EE). A substantial number of neurons (33/111, 30%) were excited by the contralateral and inhibited by stimulation of the ipsilateral ear (EI) and a smaller number of the neurons (4/111, 5%) were excited by ipsilateral and inhibited by contralateral stimulation (IE).

We looked for correlations between temporal response patterns with the binaural response type (Table 1). Interestingly we found that all onset neurons were EE or EO, whereas sustained responding neurons showed all binaural response types. All monaurally inhibited neurons (EI and IE) showed sustained response patterns. EI and IE type neurons showed s-l and s-p response types to an equal extent, whereas the EE and EO types showed more s-l type than s-p type responses. 50% of the binaural neurons exhibited s-p type activity.

Features of ITD-sensitive neurons

We evaluated responses to a wide range of ITDs in 189 binaural low-frequency DNLL neurons. ITD-sensitive neurons were divided into two main groups: peak-type neurons and trough-type neurons (as defined in METHODS). Representative ITD-functions of these two types of ITD-sensitive neurons are shown in Figs. 4 and 5. Both example neurons exhibited a sustained phase-locked discharge pattern (Fig. 4, insets) at favorable ITDs (maxima or "peak" of the functions) and a

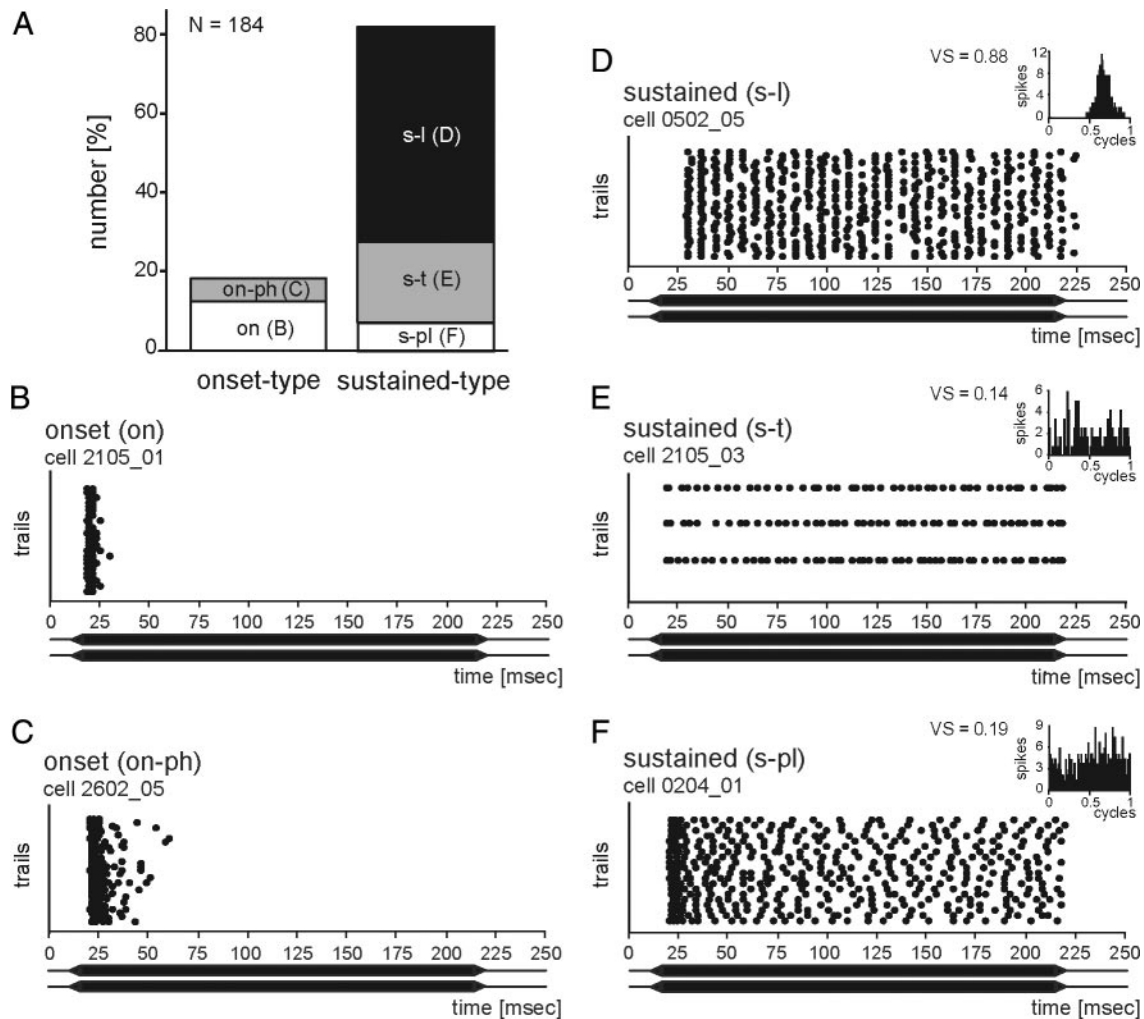


FIG. 2. Response types of binaural dorsal nucleus of the lateral lemniscus (DNLL) neurons in response to binaural 200 ms pure tones at best frequency (BF), 20 dB above threshold. **A**: distribution of response types. **B–F**: examples of different response types showing discharges as raster plots and phase histograms (*insets*) averaging the responses on a cycle-by-cycle basis. Stimuli are indicated below the dot raster as black bars. **B**: example of an on-type response with 1 or 2 action potentials per stimulus presentation (on). BF = 1,300 Hz. **C**: on-type neuron with multiple spikes at the beginning of the stimulus (on-ph). BF = 800 Hz. **D**: response of a neuron with a sustained response showing nearly perfect phase-locking as apparent from the phase histogram (*inset*) and the high vector strength (VS) derived from it (s-l). BF = 200 Hz. **E**: neuron with a sustained response which was not phase-locked to the stimulus (s-t). BF = 1,300 Hz. **F**: typical primary-like discharge pattern with a prominent on-component and a weaker ongoing component (s-p). In this case, the ongoing component was weakly phase-locked. BF = 1,000 Hz.

decreased response rate with only an on-discharge remaining at unfavorable ITDs (minima or “trough” of the function). While the peak-type neuron had a peak response at a common best ITD independent of the test frequency (Fig. 5A), the trough-type neuron showed a trough at a common ITD independent of the test frequency (Fig. 5B). The characteristic phase (CP, see METHODS) of the peak-type neuron was around 0 cycles (Fig. 5A; CP = -0.068 cycles), the CP of the trough-type neuron around ± 0.5 cycles (Fig. 5B; CP = -0.514 cycles). We found that the large majority of the peak-type neurons was contralateral (70%, 56/80) and that a smaller group was ipsilateral peak-type neurons (30%, 24/80). The trough-type neurons were roughly equally distributed between ipsilateral (44%, 14/32) or contralateral trough-type neurons (56%, 18/32).

The peak-type neurons and trough-type neurons are the most distinct examples of ITD-tuning. Peak-type neurons were the most common type of ITD function and comprised 42% of the sample (80/189). Trough-type neurons were the least common

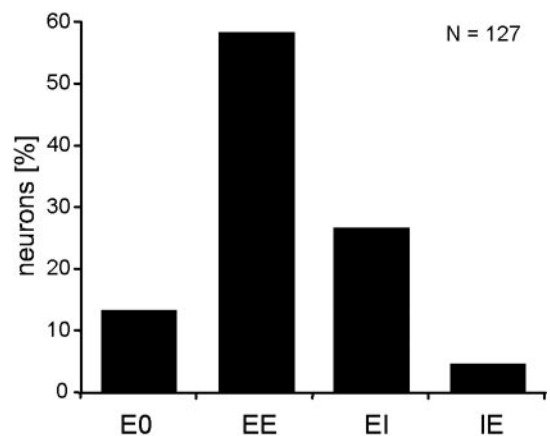


FIG. 3. Distribution of aural types of low-frequency DNLL neurons. The 1st letter indicates the overall effect of the contralateral, the 2nd letter of the ipsilateral ear. E, excitatory; I, inhibitory; 0, no effect. Note that this notation does not distinguish between excitation and facilitation.

TABLE 1. Correlation between the binaural types and the response pattern of the low-frequency neurons

Response Pattern	Binaural Types			
	OE	EE	IE	EI
Onset	1 (13)	12 (21)	0 (0)	0 (0)
Sustained (phase-locked)	5 (63)	33 (57)	3 (60)	5 (42)
Sustained (tonic/primary-like)	2 (25)	12 (21)	2 (40)	7 (58)

Total number of types is 82. $n = 8, 57, 5$, and 12 for OE, EE, IE, and EI, respectively. Parentheses enclose percentages.

and comprised 17% (32/189) of our sample (Fig. 6). A large group of neurons, however, showed an ITD sensitivity between these two extremes; 41% (77/189) of the neurons showed an intermediate type ITD-sensitivity ($0.125 < CP < 0.375$ cycles; Fig. 7A). According to our definition (see METHODS), we found 20% intermediate peak-type neurons (37/189; $0.125 < CP < 0.25$) and 21% intermediate trough-type neurons (40/189; $0.25 < CP < 0.375$ cycles; Fig. 8).

Based on qualitative visual inspections, we observed secondary peaks in the ITD functions in 23% (44/189) of our sample. An example neuron is illustrated in Fig. 7B. In some cases, the secondary peak was evoked by one frequency, but in other neurons, it was evoked by all of the tested frequencies. Secondary peaks were not evenly distributed among the groups of ITD-sensitive types. Eleven percent of the contralateral peak-type neurons (6/56) had secondary peaks and were the least likely type to have secondary peaks. Significantly more (χ^2 ; $P < 0.001$) secondary peaks were found in ipsilateral peak-type neurons (50%, 12/24).

For a small number of peak-type neurons, we compared the ITD sensitivity of the first spike to the ITD sensitivity of the ongoing component of the response. A typical example is shown in Fig. 8. Comparing the tone-delay functions at BF the ITD sensitivity of the first spike showed the same feature as the ITD sensitivity of the whole response. In 12 of the 16 neurons (75%), we found the first spike to have a similar sensitivity to ITDs as the ongoing component of the response.

We tested for correlations between types of ITD sensitivity three features: the frequency tuning of the neurons (data not shown), the temporal response pattern (Table 2, *top part*), and the binaural response type (Table 2, *bottom part*). Note that this subgroup is representative as it has the same distribution of different ITD-sensitive types as the entire sample. We could not find differences in the frequency tuning of the neurons dependent on the type of ITD sensitivity. Also, the temporal response patterns were not specific for any of the groups. Interestingly, the response pattern could change for different ITDs (Fig. 4). The neurons tended to respond to unfavorable ITDs with onset response pattern and to favorable ITDs with sustained response pattern. The response patterns were tested with pure tones at zero ITD, a common standard procedure that obviously leads to a somewhat arbitrary classification for binaural neurons. Around 80% of the peak and intermediate peak-type neurons showed clear signs of binaural excitation. Some intermediate trough- and trough-type neurons were binaurally excited, but the combined number of EI and IE neurons was much higher in these groups.

Distribution of ITDs across frequency

The head width of adult gerbils creates ITDs ranging from 0 μ s for sounds emanating straight ahead to ~ 120 μ s for sounds located 90° laterally (Maki and Furukawa 2005). Hence, the maximal ITDs gerbils can experience range from -120 to $+120$ μ s (= "physiological range"). However, the best ITDs of the peak-type neurons when tested at BF were distributed between $+527$ and -470 μ s as shown in Fig. 9. The average mean interaural phase of the peak-type neurons was 0.13 cycles (± 0.1 cycles). The majority of peak-type neurons had best ITDs well outside the physiological range of ITDs (Fig. 9A). In contrast to the peaks, the points of steepest slopes of the functions were distributed around 0 ITD and almost all within the physiological relevant range (Fig. 9B). This holds not only for contralateral but also for ipsilateral peak-type neurons, although the latter had a larger variance in their distribution.

DNLL neurons are sensitive to ITDs evoked with brief chirps

A model based on the circuitry of the MSO suggested that contralateral preceding inhibition from the medial nucleus of the trapezoid body (MNTB) might shape the ITD functions (Brand et al. 2002). Here we utilized chirp stimuli that could provide some evidence for the existence of a leading contralateral inhibition. The first panel in Fig. 10 shows separate responses evoked by stimulation of each ear at an ITD of -900 μ s (contralateral signal lagging). The shaded areas depict the expected time of response derived from monaural stimulation of the ipsilateral (left \square) and contralateral (right \blacksquare) ear, respectively. The response to contralateral stimulation was influenced by the leading ipsilateral stimulus, as it was slightly delayed compared with the monaural response, whereas the response to the leading ipsilateral stimulus occurs within the expected time frame. When the contralateral signal was lagging by 600 μ s, the contralateral response was almost absent. Note that shortening the lag of the contralateral stimulus led to a remarkable decline in the accuracy of the ipsilaterally evoked response although the response to the leading (ipsi) stimulus still occurred several hundred microseconds before the expected response to the lagging (contra) stimulus. The SD of the latency at 900 μ s ITD was 58.7 μ s and increased to 313.0 μ s at the ITD of 600 μ s for this example neuron. The most significant feature occurred when the contralateral stimulus lagged the ipsilateral signal by 300 μ s (3rd panel). Now the leading inhibition evoked by the contralateral ear suppressed almost all discharges evoked by the ipsilateral signal. When both stimuli were presented simultaneously (4th panel), the cell responded with a single spike, and with re-established excellent temporal accuracy (SD of latency 69.2 μ s, variance 4.8 μ s).

We tested 24 EE cells for contralateral inhibition preceding excitation with these chirp stimuli. In 14 of those neurons (58%), presentation of a contralateral chirp shortly after an ipsilateral chirp changed the response to the ipsilateral stimulation even though the contralateral net excitation always occurred clearly after the ipsilateral one. In 12 of the 14 cells, the influence was seen as a substantial decrease of the spike rate to the ipsilateral chirp ($>50\%$ to maximum spike rate; average decrease of 12 cells was 88.5%) as depicted in Fig. 10.

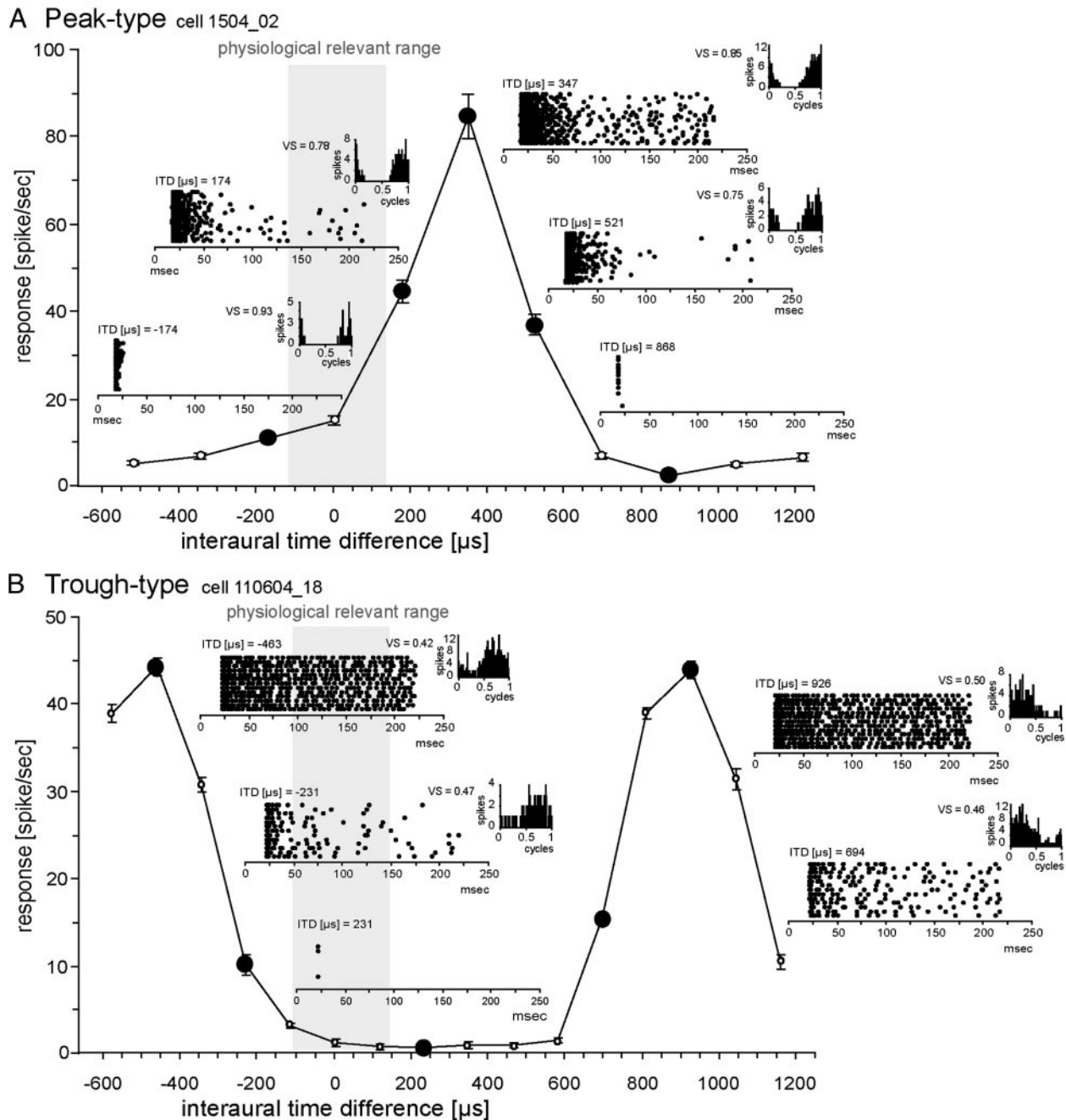


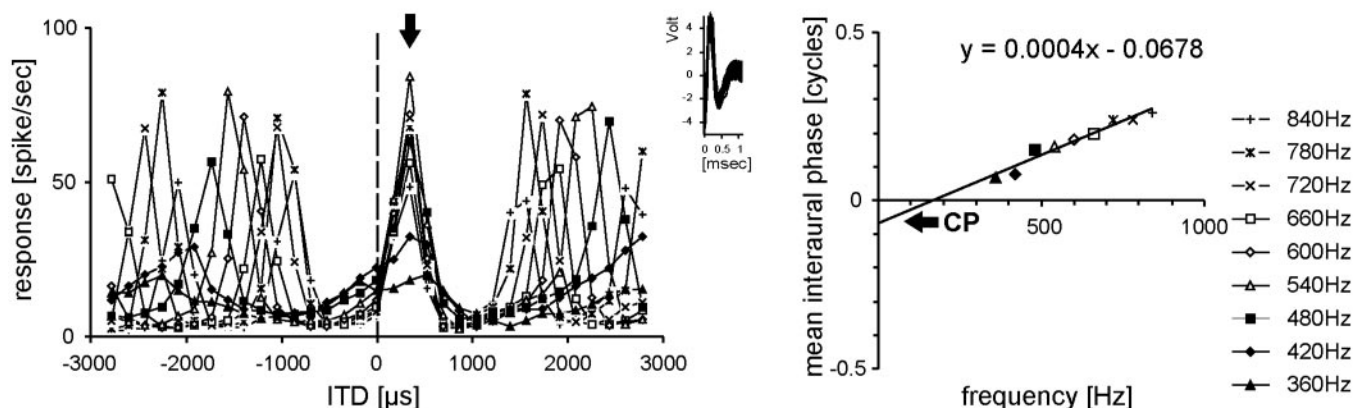
FIG. 4. Interaural time difference (ITD)-sensitive responses of a typical EE (A) and EI neuron (B). The dot raster plots (corresponding to the ITDs marked as black dots) reveal the neuron's sustained response to favorable ITDs and its onset-response to unfavorable ITDs. *Inset*: period histograms show that the sustained response as well as the onset response are phase-locked to the same phase angle. A: neuron's ITD-sensitivity was tested at BF (600 Hz) 20 dB above threshold and the ITD-sensitivity classified as peak-type response (see response of the same neuron to different frequencies Fig. 5A). B: neuron was tested at BF (700 Hz) 20 dB above threshold, and the ITD-sensitivity classified as trough-type response (see response of the same neuron to different frequencies Fig. 5B). The shaded areas indicate the physiologically relevant range of ITDs for the gerbil. Error bars = SE.

In two cells, no decrease in the response was detected, but a strong increase in the jitter of the timing of the response was observed (increase of the SD of the average response latency by >60%, the average increase in jitter was 66.0%). This effect was furthermore accompanied in these two neurons by a sudden but consistent increase of the average latency. Three cells showed both an increase in latency simultaneously with a decrease in spike rate and one neuron showed an increase in jitter and a decrease in spike rate.

IID neurons in the DNLL

Although we were mainly concerned with ITD processing in this study, we also tested 106 cells for sensitivity to IIDs by holding the intensity at the contralateral ear constant and varying the intensity at the ipsilateral ear. Of the 106 cells, 46 (43%) were sensitive to IIDs, which were all of EI aural type. IID-sensitive EI cells had BFs that ranged from 200 to 5,400 Hz (average $2,011.5 \pm 1167$ Hz). Sixty-one percent

A Peak-type cell 1504_02



B Trough-type cell 160104_018

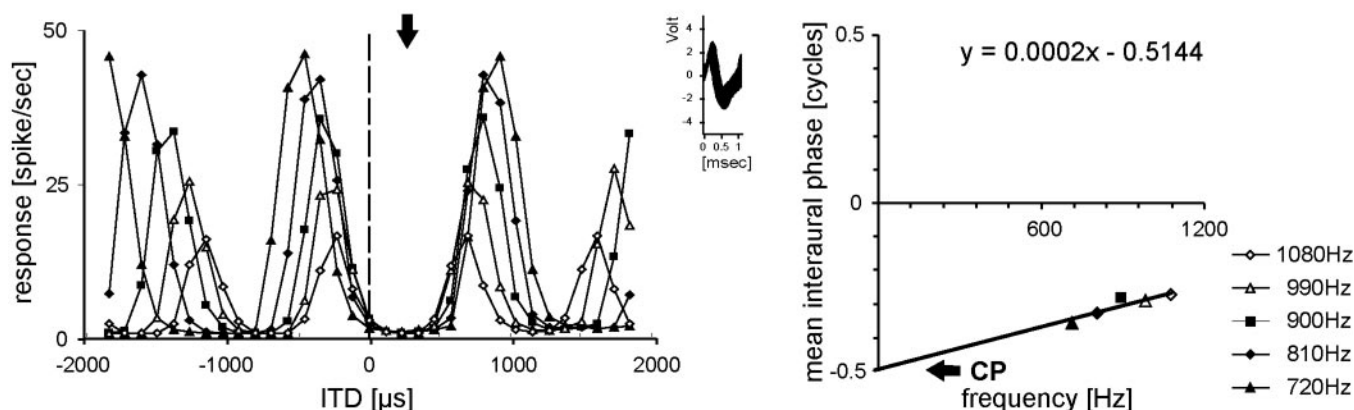


FIG. 5. A: Typical peak-type ITD sensitivity in response to different test frequencies (same neuron as in Fig. 3A). *Left*: neuron exhibited a maximum discharge at an ITD of 350 μ s (contralateral stimulus leading, \downarrow) independent of test frequency. All other peaks and troughs of the cyclic ITD functions change systematically (according to the length of the cycle) with test frequency. B: trough-type response (same neuron as in Fig. 3B) exhibited a minimal discharge at ~ 200 μ s (contralateral stimulus leading, \downarrow), independent of test frequency. The shapes of the action potentials of all spikes recorded for this stimulation are shown as *insets*. *Right*: frequency phase plot is shown. For each test frequency, the best interaural phase difference (IPD) was calculated via a vector analysis of the IPD function. The intercept with the y axis gives the characteristic phase (CP). For the neuron shown in A, the CP is close to 0, indicating the peak-type characteristic of the neuron's ITD sensitivity. In B, the CP around ± 0.5 indicates a trough type characteristic (B, *right*). The slope of the regression line gives the characteristic delay (400 μ s for the peak-type neuron and 200 μ s for the trough-type neuron in B).

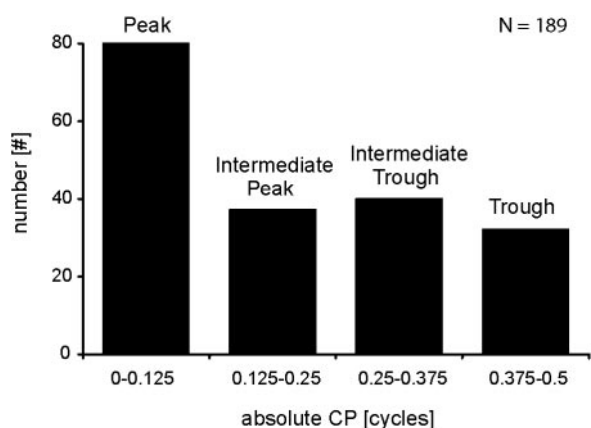


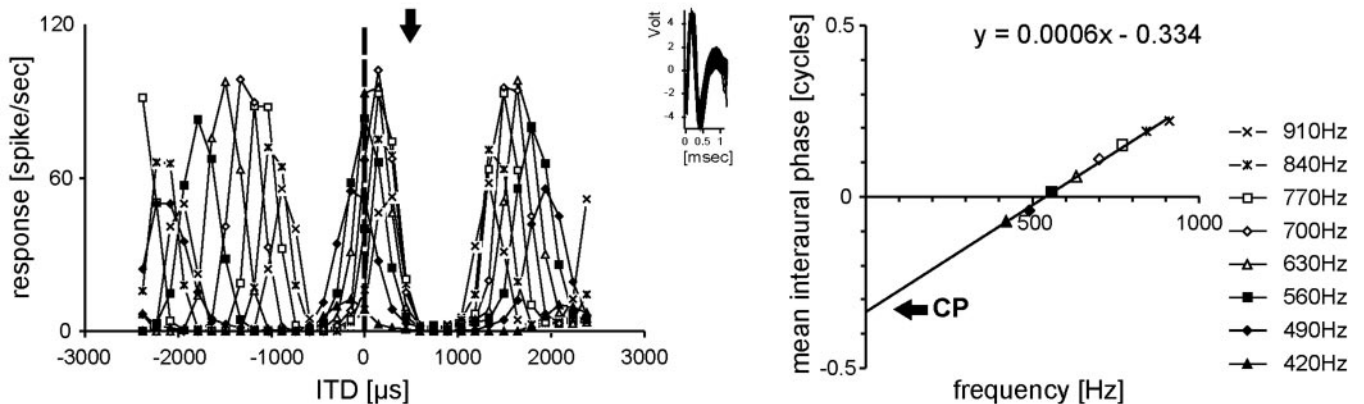
FIG. 6. Distribution of different types of ITD sensitivity found in the population of DNLL cells tested. See text for details.

(28/46) of the cells had BFs <2,000 Hz and were therefore in the low-frequency range.

We measured three features of IID functions for 45 EI cells. We determined the maximal inhibition as a percent of the peak response to binaural stimulation, the point of 50% inhibition of the IID function, and the point of maximal inhibition (Fig. 11). No significant differences could be found in the IID characteristics of low- and high-frequency neurons. Note that our "high-frequency" cells had BFs still in the range of frequencies that, under natural conditions in the free field, would only create significant IIDs in the near field (Maki and Furukawa 2005).

More than three-quarters of the neurons (35/45) showed a reduction in the response rate of 90% or more, and 19 of these units (42%) exhibited a total inhibition of spikes (Fig. 12A). The response of five neurons could not be inhibited by >80% by ipsilateral stimulation. Almost three-quarters of the cells (33/45, 73%) showed 50% points between IIDs of +10 and

A Intermediate-type cell 1504_03



B Peak-type (ipsilateral leading peak) cell 2105_04

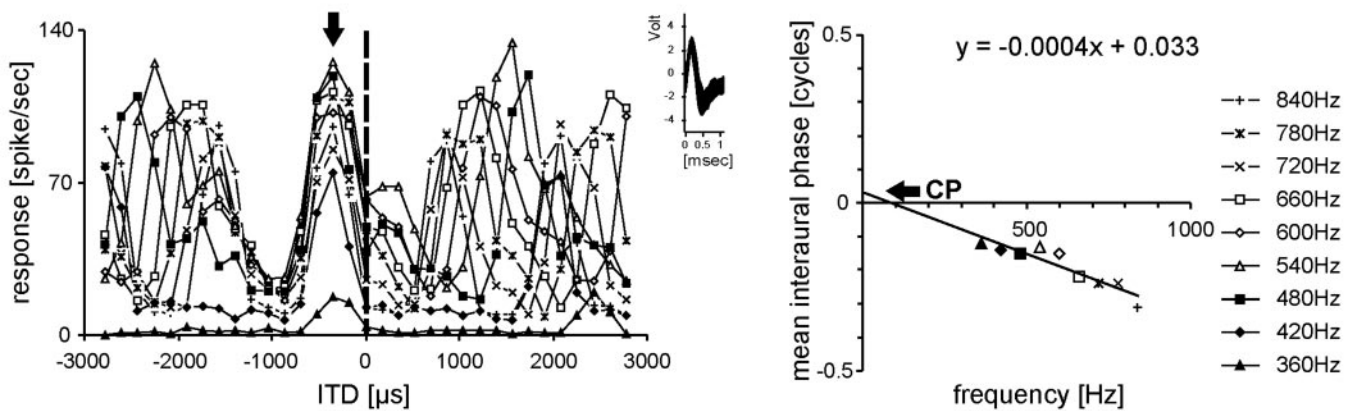


FIG. 7. A: ITD sensitivity of a neuron that showed neither a stable peak nor a stable trough across different test frequencies. The frequency phase-plot shows a CP far from 0.5 and 0, confirming the intermediate type of the ITD sensitivity. The neuron's BF was 700 Hz. B: ITD sensitivity of a neuron representative of a small population of cells that had stable peaks at negative ITDs (ipsilateral stimulus leading) with a small 2nd-peak at positive ITDs, particularly when tested with frequencies close to BF (540 Hz). Format as in Fig. 5.

−14 dB. The peak of the distribution was at slightly negative values as 18 units had 50% points between −5 and −14 dB (Fig. 12B). The average point of 50% inhibition was at −3 dB (± 10.8 dB). The point of maximal inhibition for the majority of the neurons (25/45, 55.6%) ranged between −30 and −39 dB (Fig. 12C). Two cells were already inhibited maximally for ITDs > −10 dB.

Anatomy

We injected retrograde tracers bilaterally in the DNLLs of three animals to evaluate the projections of the SOC to the DNLL. After recording from the DNLL, we injected a mixture of biotin and fluorescein-dextran in the left DNLL and tetramethylrhodamine-dextran in the right DNLL (Fig. 13B). The injections on both sides were made in locations that evoked strong activity to low frequencies. Nevertheless, as almost the whole nucleus was filled by the injections, we are not able to comment on any frequency dependence in the staining. We counted the labeled neurons in the SOC of all three animals under the microscope. In all three cases, we found labeled cells in the contralateral DNLL and in various nuclei of the SOC on both sides (Fig. 13, A and B; Table 3). In agreement with

previous studies, strong labeling was found in the ipsilateral MSO (174 of 195 labeled MSO neurons). However, we also found a much smaller number of labeled cells in the contralateral MSO (11%, 21/195). Interestingly, there were also a few double-labeled MSO cells (7%, 14/195), suggesting that some MSO cells project bilaterally to the DNLL (Fig. 13C). Large numbers of labeled cells were found in both the contra- and ipsilateral LSOs with about equal numbers of labeled cells in each LSO (contralateral: 44%, 248/641; ipsilateral: 56%, 357/641). Note that we focused on the MSO projections; those sections are shown in Fig. 13 that support the notion that MSO projects bilaterally to the DNLL. Because LSO and MSO only partially overlap in the sections, only a small portion of the LSO is shown (under representing the labeling of LSO cells). As with the MSO (Fig. 13C), some LSO cells were also double labeled (5%, 37/696). Many labeled cells were located in the nuclei of the trapezoid body with the strongest labeling in the ipsilateral MNTB (95%, 380/401), whereas 5% of the labeled cells were found in the contralateral MNTB (21/401). All labeled MNTB neurons were principle neurons. Much weaker labeling was seen in the other nuclei of the trapezoid body. 24 labeled cells were found in the lateral nuclei of the trapezoid

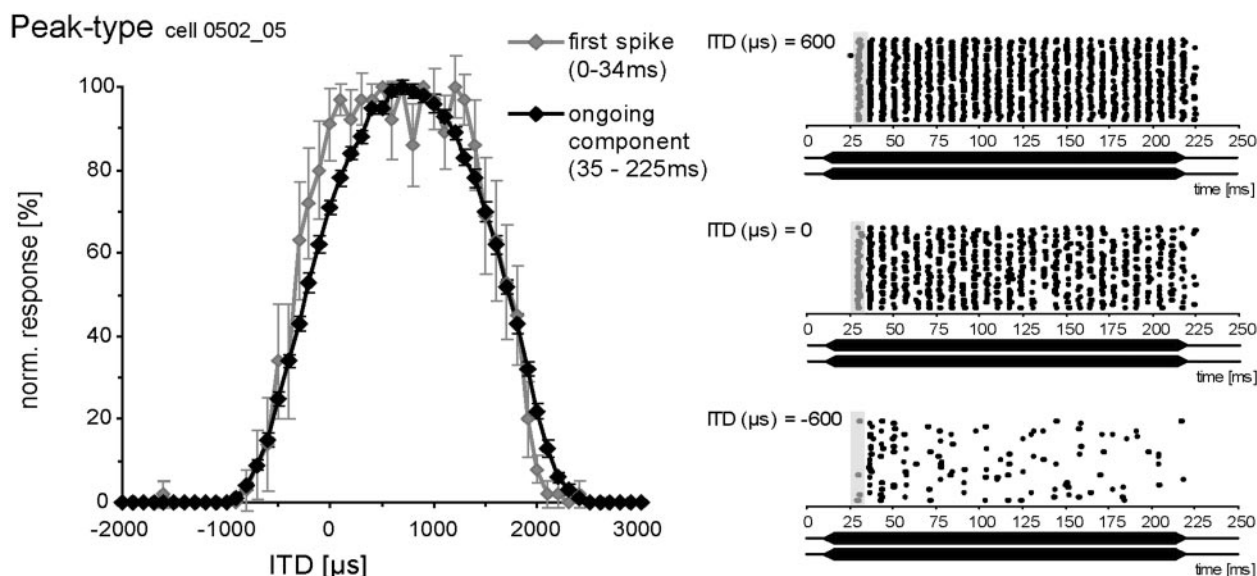


FIG. 8. ITD sensitivity of the 1st spike of the response of a peak-type neuron in comparison with the ITD sensitivity of the ongoing response. The figure shows the neuronal response to a tone-delay stimulation at BF (BF = 200 Hz). *Right*: poststimulus time histograms (PSTHs) of the response to 3 different ITDs. The shaded area indicates the area of the 1st spike. Error bars = SE.

body (LNTB) at both sides, 15 cells in the ipsilateral ventral nucleus of the trapezoid body (VNTB) and 41 cells in the ipsilateral superior paraolivary nucleus (SPN).

DISCUSSION

We found the majority of low-frequency ITD-sensitive cells to show either peak- or trough-type characteristics. Peak-type responses were more prevalent than other response types, indicating a dominance of pure MSO input characteristics. Some cells' responses, however, seemed to reflect pure LSO inputs, and a substantial number of ITD-sensitive cells were neither pure peak-type nor pure trough-type neurons but rather met criteria for intermediate types. Some neurons, mostly trough- and intermediate-type, showed secondary peaks in their ITD-functions, a feature not reported for cells in the SOC. In 2/3 of the peak-type neurons, maximal responses occurred at ITDs that correspond to sound sources in the contralateral sound field. However, a subpopulation of DNLL neurons preferred ipsilateral sounds, a finding that may correspond to

the weaker but nevertheless substantial contralateral MSO input found in the tracer experiments. Best ITDs of most peak-type neurons were evoked at ITDs that gerbils would never experience, at least not as direct irradiation. However, the slopes of their ITD functions were steepest in the physiological range of ITDs.

The abundance of low-frequency cells we found in the DNLL is consistent with the well-developed low-frequency hearing capabilities in the Mongolian gerbil (Ryan 1976). It is, however, important to stress that we actively focused on low-frequency neurons. Normally, the distribution of BFs in the DNLL reflects the entire audiogram of an animal (mustache bat: Markovitz and Pollak 1993; big brown bat: Covey 1993; free-tailed bat: Burger and Pollak 2001; rat: Bajo et al. 1998; cat: Aitkin et al. 1970), and our unpublished results confirm the existence of a large number of high-frequency neurons in the gerbils DNLL (M Pecka and B Saunier-Rebori, unpublished observation).

Most of the binaural neurons we found were binaurally excited. This is consistent with findings in the DNLL of cats and rabbits, which, like gerbils, are well adapted to hear low frequencies (Brugge et al. 1970; Kuwada et al. 2005). In contrast, EI type neurons have been found to dominate in animals that do not hear low frequencies like rats (Bajo et al. 1998; Kelly et al. 1998) and bats (Covey 1993; Markovitz and Pollak 1994).

We found phase-locked sustained discharge patterns to clearly dominate in the gerbil DNLL. These discharge patterns, however, may change depending on the binaural context. Changes of discharge patterns have been suggested to contribute in sound localization (Koch and Grothe 2000; Middlebrooks et al. 1994) but were not systematically investigated in the present study.

Peak- and trough-type DNLL neurons inherit their ITD features from the SOC

The ITD functions of the peak- and trough-type neurons we found in DNLL are similar to the ITD functions reported in

TABLE 2. Correlation between type of ITD sensitivity, response pattern, and aurality

Response pattern/ Aurality	Type of ITD Sensitivity			
	Peak Type	Intermediate Peak Type	Intermediate Trough Type	Trough Type
Onset	7 (20)	5 (33)	1 (5)	1 (8)
Sustained (phase-locked)	18 (51)	6 (40)	13 (65)	9 (75)
Sustained (tonic/primary-like)	10 (29)	4 (27)	6 (30)	2 (17)
EO	2 (6)	3 (20)	2 (10)	1 (8)
EE	31 (89)	11 (73)	10 (50)	6 (50)
IE	1 (3)	0 (0)	2 (10)	1 (8)
EI	1 (3)	1 (7)	6 (30)	4 (33)

n = 35, 15, 20, and 12 for peak type, intermediate peak type, intermediate trough type, and trough type, respectively. Percentages in parentheses.

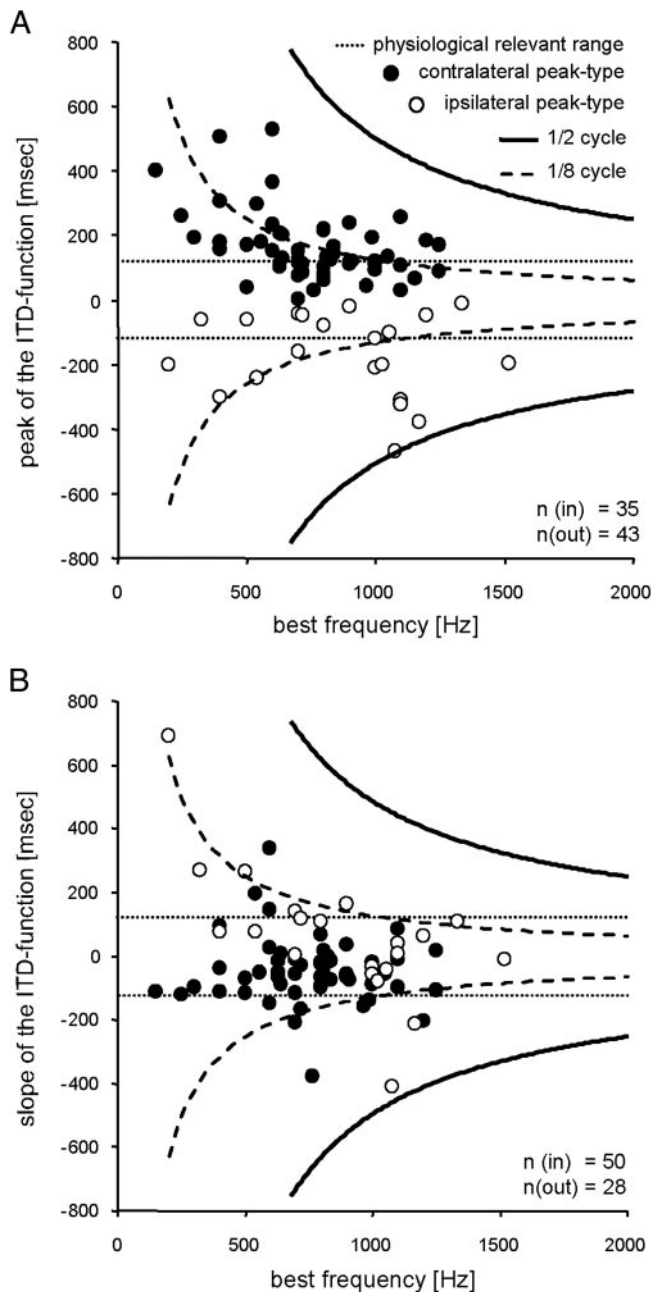


FIG. 9. Peaks and slopes of the ITD functions of peak-type neurons as a function of BF. Values derived from the ITD functions measured at BF., range of ITDs gerbils can experience naturally (about $\pm 120 \mu\text{s}$). **A**: best ITDs as a function of the neurons' BFs. Note that best ITDs are not independent of BF and that most best ITDs are outside the physiological range of ITDs. **B**: points of steepest slopes of ITD functions as a function of the neurons' BFs. Points of steepest slopes are independent of BF (in contrast to the best ITDs). The majority of points of steepest slopes are close to 0 ITD and well within the physiological range of ITDs. $n(\text{out})$ = number of point outside the physiological relevant range, $n(\text{in})$ = number of point inside the range.

previous studies for MSO and LSO neurons. As for MSO cells, the maximal responses (i.e., peaks) in peak-type neurons were evoked at the same ITD across frequency, and thus their phase-frequency plots were linear with a characteristic phase at or around 0.0 cycles (Batra et al. 1997a,b; Brand et al. 2002; Spitzer and Semple 1995; Yin and Chan 1990), indicative of binaural excitation (EE). Similarly, the minimal responses (i.e.,

troughs) of trough-type neurons were evoked at a common ITD across frequency as has been reported for low-frequency LSO cells and as indicative of an interaction of excitation and inhibition (Batra et al. 1997a,b; Brand et al. 2004; Joris and Yin 1998; Tollin and Yin 2005). The peak responses of DNLL trough-type neurons also had linear phase-frequency plots with a characteristic phase at or around 0.5 cycles. In addition to these features, we observed that in most peak-type neurons the maximal responses were evoked by ITDs generated in the contralateral sound field, which is consistent with the strong projections to the DNLL deriving from the ipsilateral SOC (Glendenning et al. 1981; Oliver 2000; Shneidermann et al. 1988). In a small number of peak-type neurons, the maximal

cell 261103_068; BF:1100Hz

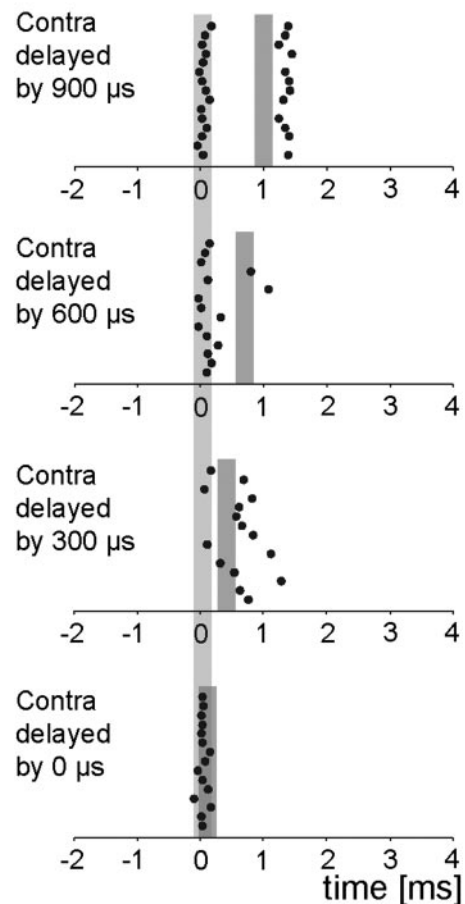


FIG. 10. Example neuron (EE) with apparent inhibition from the contralateral side preceding contralaterally driven excitation. Raster plots show the occurrence of single action potentials in response to "chirps." The stimulus amplitude was set to a level that elicited 1 spike/stimulus when presented monaurally at either ear. □, expected response based on monaural stimulation to the ipsilateral (left □) or contralateral ear (right □). When the contralateral stimulus was delayed by 900 μs , both stimuli elicited spikes. Note that the response to the lagging, contralateral stimulus was already influenced by the leading stimulus in that it was slightly delayed. A decrease of the interaural delay to 600 μs caused the lagging response to the contralateral stimulus to vanish. Also the response to the ipsilateral stimulus became less accurate (higher jitter), although the response to the contralateral stimulus is expected to occur long after the response to the ipsilaterally evoked response. At an interaural delay of 300 μs , the ipsilaterally evoked response was strongly suppressed. Coincidence of the 2 excitatory inputs seems to occur at 0 ITD, resulting in 1 spike/stimulus but with higher accuracy (lower jitter) compared with the monaural responses.

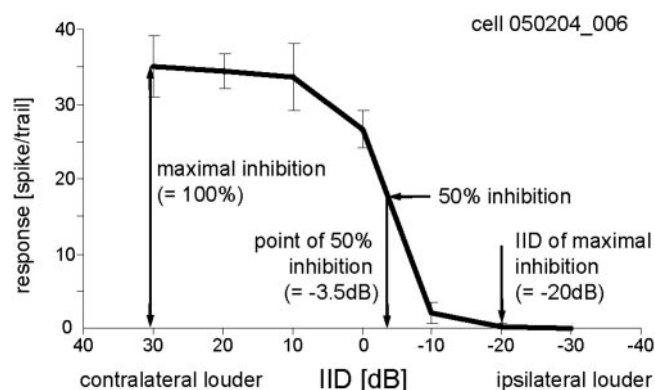


FIG. 11. IID-function of a typical EI neuron. The maximal inhibition occurred when the ipsilateral (inhibitory) stimulus was ≥ 20 dB more intense than the contralateral (excitatory) stimulus. The response was inhibited by $\sim 50\%$ when the stimulus level at the inhibitory ear was ~ 3.5 dB more intense (-3.5 dB IID, extrapolated from the IID function). The contralateral stimulus intensity was kept constant (30 dB above threshold) for all values. BF: 2,400 Hz.

responses were, however, evoked by sounds that would emanate from the ipsilateral side. This finding can be explained by the contralateral projection we found by tracer injections or by the fact that at least a small number of MSO cells has been found to prefer ipsilaterally leading sounds (Batra et al. 1997a; Yin and Chan 1990). Contralateral projections from the MSO, particularly to the IC, are not uncommon, but there is a remarkable species-specific difference concerning their prevalence (review: Grothe 2000). We also found a substantial number of ipsilateral trough-type neurons, responding minimally to a sound in the ipsilateral sound field, consistent with studies of the SOC of rabbits (Batra et al. 1997a,b). This may reflect differences in the latencies of the excitatory and inhibitory inputs to LSO neurons (Irvine et al. 2001; Park et al. 1996). Such latency differences would not only lead to different positions of troughs but also to a widespread distribution of the IIDs of maximal inhibition as found for EI DNLL cells in this study and previously shown for LSO neurons (Markovitz and Pollak 1994; Park 1998). All of these features are consistent with the hypothesis that peak- and trough-type neurons in the DNLL inherit their basic ITD properties from the MSO and LSO, respectively. Kuwada et al. (2005) found a similar distribution of ITD properties in the rabbit DNLL with a large number of neurons showing peak-type sensitivity with maximal responses mostly for stimuli generated in the contralateral sound field. They also found a small number of peak-type neurons that would prefer sounds in the ipsilateral sound field. As in our experiments, the peak- and trough-type sensitivity in the rabbit DNLL could not be exclusively explained by the binaural properties of the neurons. Nevertheless, both studies show that most EE neurons show peak-type and most EI neurons trough-type characteristics.

Although many DNLL neurons seem to simply reflect their SOC input, it is important to note that DNLL cells receive not only excitatory inputs from LSO and MSO but also glycinergic inputs from the LSO and GABAergic innervation from the opposite DNLL via the commissure of Probes (for review, Schwartz 1992). In addition, our data confirm the strong glycinergic input from the ipsilateral MNTB earlier shown for cats and rats (Glendenning et al. 1981; Sommer et al. 1993; Spangler et al. 1985). It appears likely that projections from the

opposite DNLL or from sources other than the MSO and LSO may affect processing in DNLL, although the nature of this influence requires further study. To date, two interpretations are available. The first by Kuwada and colleagues (Fitzpatrick and Kuwada 2001; Kuwada et al. 2005) suggests that ITD functions are sharpened along the ascending auditory pathway and that first signs of this sharpening are visible in the DNLL. However, their analysis comes from a dataset that does not account for the BF of neurons. As long as ITD functions are simply created by pure EI and EE interactions and as long as these binaural inputs are perfectly matched in terms of their

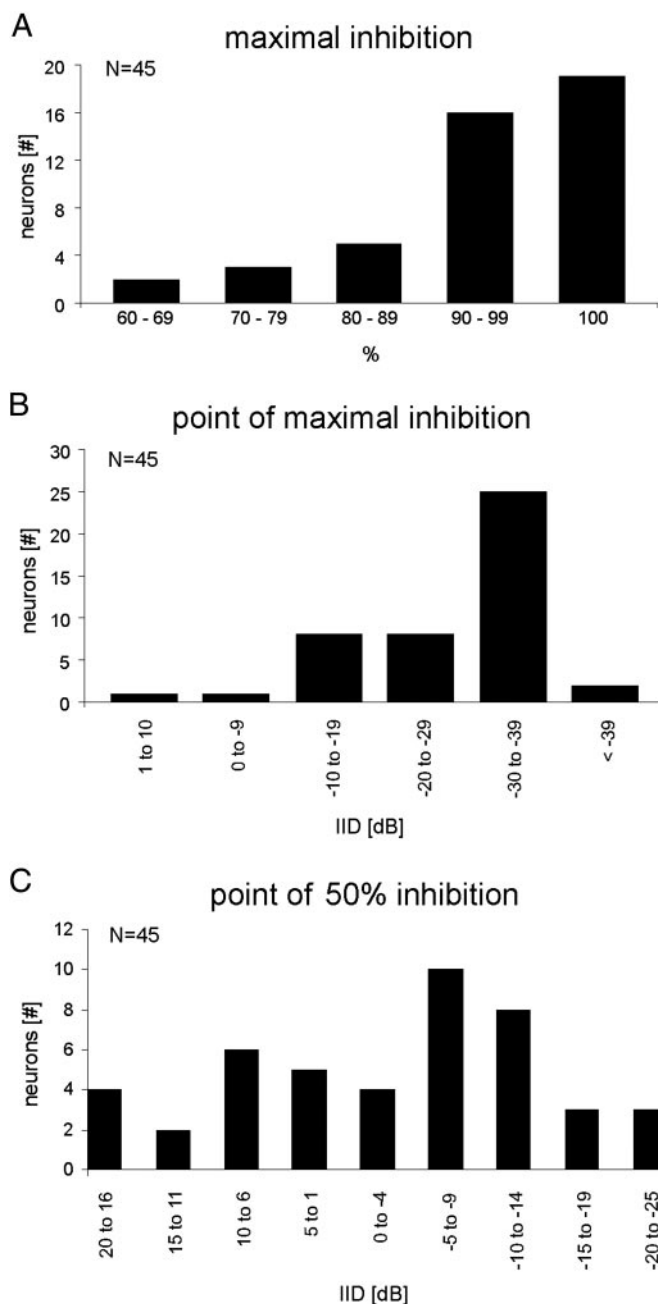


FIG. 12. Quantification of the interaural intensity difference (IID) functions measured. A: degree of maximal suppression (in percentage). B: IID of maximal suppression. In the majority of cells the response could be reduced by at most 100%, preferable at negative IIDs (ipsilateral stimulus more intense). C: IIDs of 50% inhibition (IID in dB) showing a rather broad distribution.

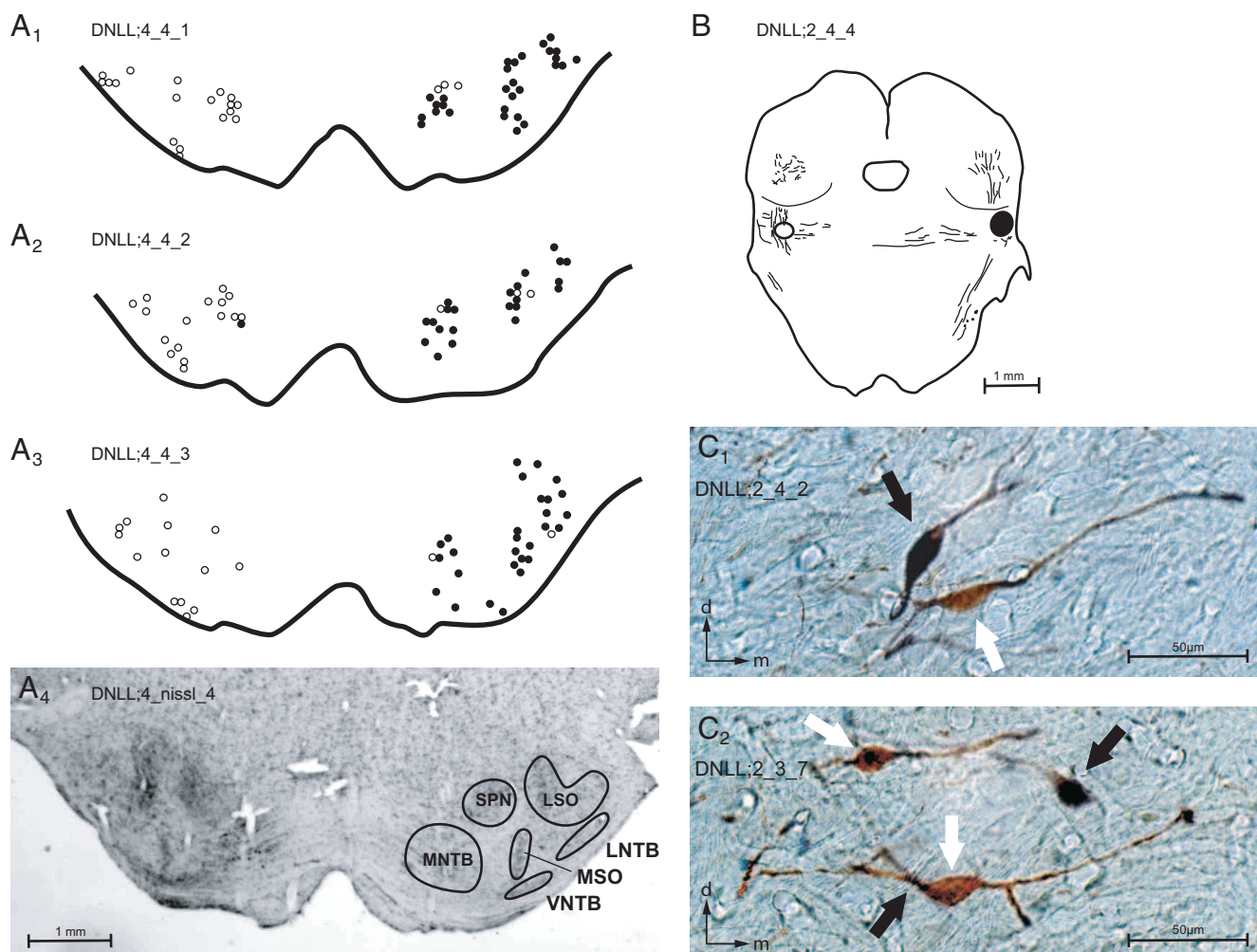


FIG. 13. Retrograde labeling in the superior olivary complex (SOC) after bilateral tracer injections into the DNLL on both sides. Biotin/flourescein-dextran was injected into the left DNLL, tetramethylrodamine-dextran into the right DNLL. Injection sites are given in B. A, 1–3: biotin (white circle) and rodamine (black circle) labeled somata of neurons in the SOC in 3 consecutive sections (from rostral to caudal). A4: Nissl-counterstained section of the SOC. The principal nuclei are outlined. C, 1 and 2: retrogradely labeled medial superior olive (MSO) neurons showing the typical bipolar outline with the dendrites oriented orthogonally to the dorsoventral axis of the nucleus. In some cases, biotin (white arrow)- and rodamine-labeled cells (black arrow) could be found in juxtaposed positions in one MSO. C2: a double-labeled cell (white and black arrow). Quantifications are given in Table 3. d, dorsal; m, medial.

frequency tuning, one could see such a sharpening in the population statistic irrespective of BF. There is, however, abundant evidence for inhibitory input to all MSO neurons (review: Grothe 2003), and even the simple EI model for LSO function has become questionable (Kil et al. 1995; Magnusson et al. 2005b). Therefore a quantitative analysis of the ITD width has to account for BF and cannot be performed far from BF where small differences in the frequency tuning of the multiple inputs may account for significant changes in the ITD functions due to different cochlear delays (compare Shamma et al. 1989). Rather, our data suggest that the straightforward processing of ITDs during static tone bursts, in anesthetized animals, is a simple reflection of the processing in the MSO for peak-type neurons and in the LSO for trough-type neurons. Furthermore, our data may suggest a second possible explanation. High-frequency DNLL neurons have been shown to inherit their IID sensitivity from the LSO. What distinguishes them from LSO neurons may not be the response to static stimuli, but the response in a more complex temporal spatial context. Pollak and colleagues (review: Pollak et al. 2003)

concluded that DNLL neurons may be involved in echo suppression. Alternatively, they may be involved in processing other dynamic changes in the spatiotemporal domain. Further studies are necessary to elucidate these processes.

ITD tuning of peak-type neurons in the DNLL

The maxima of the ITD functions are clearly outside of the physiologically relevant range for direct sound irradiation for the majority of cells tested. It should be noted, however, that they become more complex when reverberations are present. They, via de-correlation, may create larger ITDs. This could be one possible explanation for finding large best ITDs. However, if maximal ITDs matter as such, one would expect the highest density at ITDs that correspond to the highest behavioral resolution, namely around 0 ITD (Hafer et al. 1975; Makous and Middlebrooks 1990). The fact that only few maxima are found around 0 ITD stipulates a different interpretation. The key issue seems to be that, in contrast to the maxima, the slopes of almost all ITD functions cross the midline (ITD = 0). This finding is consistent with studies in the kangaroo rat and gerbil

TABLE 3. *Retrograde labeling of SOC neurons*

Nucleus	Number of Labeled Cells		
	Ipsilateral	Contralateral	Double
LSO	+++ (357)	+++ (284)	+
MSO	++ (160)	+	+
MNTB	+++ (380)	+	–
VNTB	+	–	–
LNTB	+	+	–
SPN	+	(+)	–

Number of labeled cells in the superior olivary complex (SOC) after injecting biotin/fluorescein-dextran into the left and tetramethylrhodamine-dextran into the right dorsal nucleus of the lateral lemniscus of three Mongolian gerbils. LNTB, lateral nucleus of the trapezoid body; LSO, lateral superior olive; MNTB, medial nucleus of the trapezoid body; MSO, medial superior olive; SPN, superior paraolivary nucleus; VNTB, ventral nucleus of the trapezoid body, +++, heavy labeling (>200 cells); ++, moderate labeling (>100 cells), +, weak labeling (>10 cells), (+), few cells labeled (<10 cells), –, no labeling. Data pooled from three experiments.

MSO, the IC in guinea pigs and cats (Brand et al. 2002; Crow et al. 1978; Hancock and Delgutte 2004; McAlpine et al. 2001) but appears to be in contrast to the recently published study on the rabbit DNLL that describes most peaks to be within the physiological range (Kuwada et al. 2005). However, Kuwada et al. do not distinguish between best ITDs recorded at BF and those recorded at other stimulus frequencies, and they do not provide any data concerning the slopes of ITD functions for the stimuli that drive a neuron best (BF). Recording in the low-frequency tail of high-frequency neurons (as discussed by Kuwada et al. 2005) might lead to a very different distribution of best ITDs than recording from neurons with low BFs, in particular if BFs and best ITDs are correlated to adjust the slopes of ITD functions to the physiologically relevant range. If the response peaks underlies ITD coding rather than slopes, it would be difficult to interpret the contribution of low-frequency trough-type neurons (also described for the rabbit DNLL) for which best ITDs change as a function of test frequency. Theoretical considerations suggest that a coding strategy with the maximal slopes close to ITD = 0 would be of considerable advantage at least for low frequencies and, in particular, for small animals because it optimizes the change in firing rate in face of small changes in ITD (Harper and McAlpine 2004; Leibold and van Hemmen 2003; Skottun et al. 2001). Common standards for dealing with ITD data will be needed to determine if the differences observed in studies of ITD coding are species specific. The existence of different coding strategies would imply that different principles of neuronal representations of ITDs are used by different groups of animals, whereas similar observations would suggest that all mammals use a common strategy.

This incompleteness of our current knowledge also concerns the role of the inhibitory MSO inputs in ITD processing. There is increasing evidence that the MSO output does not reflect a perfect cross-correlation based on binaural excitation (Batra and Yin 2004). Several anatomical (Cant and Hyson 1992; Clark 1969; Kuwabara and Zook 1992; Perkins 1973) as well as in vivo studies proposed an involvement of inhibitory inputs in ITD coding (Brand et al. 2002; Carney and Yin 1989; Goldberg and Brown 1969; Grothe and Park 1998; Moushegian et al. 1964; Spitzer and Semple 1995). Specific roles of synaptic inhibition have been suggested based on in vitro

recordings (Grothe and Sanes 1993, 1994; Magnusson et al. 2005a) and modeling (Batra et al. 1997a; Brand et al. 2002; Han and Colburn 1993; Zhou et al. 2005). The model by Brand et al. (2002) suggests fast contralateral inhibition preceding excitation driven by the same ear that delays the effective contralateral excitatory postsynaptic potentials, to be an important element in the ITD-encoding neuronal circuit in the MSO (Brand et al. 2002; Grothe 2003). However, an alternative model by Zhou and colleagues (2005) assumes a comparatively slow inhibition but still reliably simulates the effects observed during blockade of inhibition in the MSO (Brand et al. 2002). The fact that we found the first spike of the response to be as sensitive to ITDs as the ongoing component speaks for an immediate and fast effect of the inhibition, but direct evidence of a fast preceding inhibition at the MSO is lacking.

Carney and Yin (1989) showed a suppressive effect they called “early inhibition,” which preceded contralateral excitation in ITD-sensitive cells in the IC in response to clicks. The time courses of suppression they found were similar to the effects we obtained in the DNLL by using chirp stimuli. While Carney and Yin hypothesized that preceding inhibition could be generated in the IC, our results show that this inhibition is already present below the midbrain. The fact that both the IC and the DNLL receive prominent inputs from the MSO supports the idea that preceding inhibition is already created at the MSO, the initial site of ITD processing.

One problem in interpreting the time course of the apparent inhibition elicited by broad-band stimuli like clicks or chirps is the possible involvement of cochlear delays. Because of the time course of the traveling wave in the cochlea, high frequencies elicit earlier responses than low frequencies (Ruggero 1992). Therefore a mismatch in the frequency tuning of MSO inputs could cause a precedence of one of the inputs due to shorter cochlear delays (compare Shamma et al. 1989). The use of downward frequency modulated chirps in the present study might even enhance such effects. However, a comparison of ITD functions measured with pure tones and noise in the MSO itself revealed similar ITD tuning for both stimuli (Yin and Chan 1990), a finding that can hardly be explained by cochlear delays.

Intermediate type ITD sensitivity

It is unclear to what extent intermediate type ITD sensitivity in DNLL is a result of interactions of multiple inputs and to what extent it is imposed by SOC inputs. Spitzer and Semple (1995) as well as Batra and colleagues (1997a,b) found intermediate-type neurons in the SOC of gerbils and rabbits, respectively. They might be a result of convergence of at least three inputs (Batra et al. 1997b). Similarly, intermediate-type neurons have been found at higher stations like the IC (Fitzpatrick and Kuwada 2001; McAlpine et al. 1998; Yin and Kuwada 1983b), but there is evidence that convergence at the level of the IC itself can account for intermediate type ITD sensitivity at least in some neurons (McAlpine et al. 1998). Our present study was not designed to, and therefore cannot distinguish between, the two possible alternatives.

The feature that is likely to be constructed in the DNLL, and not inherited, is the occurrence of secondary peaks that we observed in many ipsilateral peak-type and intermediate peak- and trough-type neurons. A simple explanation for this would

be that these cells received inputs from several cells that had the same BF, but the CD of at least one of the inputs was slightly different from the CD of the other inputs or even at the opposite side (via contralateral MSO inputs) and, therefore caused a second peak in the ITD-function. Such second peaks have not been seen in the ITD functions of SOC neurons and thus are almost surely a property created in the DNLL.

In summary, it appears that pure peak- and trough-type neurons express ITD sensitivity and other properties that are nearly identical to those seen in the MSO and LSO. This suggests that peak- and trough-type neurons in the DNLL may be appropriate substitutes for the SOC, although the connections from other sources suggest the processing may be different in these neurons with stimuli more complex than tones like multiple or dynamic stimuli.

ACKNOWLEDGMENTS

We thank T. Marquardt for help with computer programming and calibration procedures as well as for interesting and stimulating discussions. We thank G. D. Pollak for intense discussions and J. H. Casseday, H. Meffin, and M. Burger for critical comments of the manuscript. Many thanks to M. Malmierca for valuable advice concerning double-labeling experiments.

Present addresses: A. H. Seidl, Virginia Merrill Bloedel Hearing Research Center, University of Washington, Box 357923, Seattle, WA 98195; and S. Baudoux, MRC Institute of Hearing Research Nottingham University Section, University Park, Nottingham, NG7 2RD, UK.

GRANTS

This work was supported by the Max Planck Society, German Research Foundation Grants GR 1205/12-1 and GR 1205/11-3, the Deutsche Studienstiftung (stipend for I. Siveke), and European Molecular Biology Organization (stipend for S. Baudoux).

REFERENCES

- Aitkin LM, Anderson DJ, and Brugge JF. Frequency organization and response characteristics of single neurons in nuclei of lateral lemniscus of cat. *J Acoust Soc Am* 47: 59–8, 1970.
- Bajo VM, Villa AE, de Ribaupierre F, and Rouiller EM. Discharge properties of single neurons in the dorsal nucleus of the lateral lemniscus of the rat. *Brain Res Bull* 47: 595–610, 1998.
- Batra R, Kuwada S, and Fitzpatrick DC. Sensitivity to interaural temporal disparities of low- and high- frequency neurons in the superior olivary complex. I. Heterogeneity of response. *J Neurophysiol* 78: 1222–1236, 1997a.
- Batra R, Kuwada S, and Fitzpatrick DC. Sensitivity to interaural temporal disparities of low- and high- frequency neurons in the superior olivary complex. II. Coincidence detection. *J Neurophysiol* 78: 1237–1247, 1997b.
- Batra R and Yin TCT. Cross correlation by neurons of the medial superior olive: a reexamination. *J Assoc Res Otolaryngol* 5: 238–252, 2004.
- Batschelet E. *Circular Statistics in Biology*. London, UK: Academic, 1991.
- Boudreau JC and Tsuchitani C. Binaural interaction in the cat superior olive S segment. *J Neurophysiol* 33: 442–54, 1968.
- Brand A, Behrend O, Marquardt T, McAlpine D, and Grothe B. Precise inhibition is essential for microsecond interaural time difference coding. *Nature* 417: 543–547, 2002.
- Brand A, Grothe B, and Park T. Interaural time difference sensitivity in the lateral superior olive of a small mammal, the Mongolian gerbil. *Assoc Res Otolaryngol Abstr* 7: 1389, 2004.
- Brugge JF, Anderson DJ, and Aitkin LM. Responses of neurons in the dorsal nucleus of the lateral lemniscus of cat to binaural tonal stimulation. *J Neurophysiol* 33: 441–458, 1970.
- Burger RM and Pollak GD. Reversible inactivation of the dorsal nucleus of the lateral lemniscus reveals its role in the processing of multiple sound sources in the inferior colliculus of bats. *J Neurosci* 21: 4830–4843, 2001.
- Cai H, Carney LH, and Colburn HS. A model for binaural response properties of inferior colliculus neurons. I. A model with interaural time difference-sensitive excitatory and inhibitory. *J Acoust Soc Am* 103: 475–493, 1998a.
- Cai H, Carney LH, and Colburn HS. A model for binaural response properties of inferior colliculus neurons. II. A model with interaural time difference-sensitive excitatory and inhibitory inputs and an adaptation mechanism. *J Acoust Soc Am* 103: 494–506, 1998b.
- Caird D and Klinke R. Processing of interaural time and intensity differences in the cat inferior colliculus. *Exp Brain Res* 68: 379–392, 1987.
- Cant NB and Hyson RL. Projections from the lateral nucleus of the trapezoid body to the medial superior olivary nucleus in the gerbil. *Hear Res* 58: 26–34, 1992.
- Carney LH and Yin TCT. Response of low-frequency cells in the inferior colliculus to interaural time differences of clicks: Excitatory and inhibitory components. *J Neurophysiol* 62: 144–161, 1989.
- Clark GM. The ultrastructure of nerve endings in the medial superior olive of the cat. *Brain Res* 14: 293–305, 1969.
- Covey E. Response properties of single units in the dorsal nucleus of the lateral lemniscus and paralemnic zone of an echolocating bat. *J Neurophysiol* 69: 842–859, 1993.
- Crow G, Rupert AL, and Moushegian G. Phase locking in monaural and binaural medullary neurons: implications for binaural phenomena. *J Acoust Soc Am* 64: 493–501, 1978.
- D'Angelo WR, Sterbing SJ, Ostapoff EM, and Kuwada S. Role of GABAergic inhibition in the coding of interaural time differences of low-frequency sounds in the inferior colliculus. *J Neurophysiol* 93: 3390–400, 2005.
- Field KJ and Siebold AL. *Hamster and Gerbil*. London, UK: CRC, 1999.
- Fitzpatrick DC and Kuwada S. Tuning to interaural time differences across frequency. *J Neurosci* 21: 4844–4851, 2001.
- Glendenning KK, Brunso-Bechtold JK, Thompson GC, and Masterton RB. Ascending auditory afferents to the nuclei of the lateral lemniscus. *J Comp Neurol* 197: 673–703, 1981.
- Goldberg JM and Brown PB. Functional organization of the dog superior olivary complex: an anatomical and electrophysiological study. *J Neurophysiol* 31: 639–656, 1969.
- Grothe B and Park TJ. Sensitivity to interaural time differences in the medial superior olive of a small mammal, the Mexican free-tailed bat. *J Neurosci* 18: 6608–22, 1998.
- Grothe B. New roles for synaptic inhibition in sound localization. *Nat Revs Neurosci* 4: 540–550, 2003.
- Grothe B. The evolution of temporal processing in the medial superior olive, an auditory brainstem structure. *Prog Neurobiol* 61: 581–610, 2000.
- Grothe B and Sanes DH. Bilateral inhibition by glycinergic afferents in the medial superior olive. *J Neurophysiol* 69: 1192–1196, 1993.
- Grothe B and Sanes DH. Synaptic inhibition influences the temporal coding properties of medial superior olivary neurons: an in vitro study. *J Neurosci* 14: 1701–1709, 1994.
- Haft ER, De Maio J, and Hellman WS. Difference thresholds for interaural delay. *J Acoust Soc Am* 57: 181–7, 1975.
- Han Y and Colburn HS. Point-neuron model for binaural interaction in MSO. *Hear Res* 68: 115–30, 1993.
- Hancock KE and Delgutte B. A physiologically based model of interaural time difference discrimination. *J Neurosci* 24: 7110–7117, 2004.
- Harper NS and McAlpine D. Optimal neural population coding of an auditory spatial cue. *Nature* 430: 682–686, 2004.
- Heffner RS and Heffner HE. Sound localization and use of binaural cues by the gerbil (*Meriones unguiculatus*). *Behav Neurosci* 102: 422–428, 1988.
- Irvine DR. Physiology of the auditory brain stem. In: *The Mammalian Auditory Pathway: Neurophysiology*, edited by Popper AN and Fay RR. New York: Springer, 1992, p. 153–231.
- Irvine DR, Park VN, and McCormick L. Mechanisms underlying the sensitivity of neurons in the lateral superior olive to interaural intensity differences. *J Neurophysiol* 86: 2647–2666, 2001.
- Joris PX and Yin TC. Envelope coding in the lateral superior olive. I. Sensitivity to interaural time differences. *J Neurophysiol* 73: 1043–1062, 1995.
- Joris PX and Yin TC. Envelope coding in the lateral superior olive. III. Comparison with afferent pathways. *J Neurophysiol* 79: 253–269, 1998.
- Kelly JB, Buckthought AD, and Kidd SA. Monaural and binaural response properties of single neurons in the rat's dorsal nucleus of the lateral lemniscus. *Hear Res* 122: 25–40, 1998.
- Kidd SA and Kelly JB. Contribution of the dorsal nucleus of the lateral lemniscus to binaural responses in the inferior colliculus of the rat: interaural time delays. *J Neurosci* 16: 7390–7397, 1996.

- Kil J, Kageyama GH, Semple MN, and Kitzes LM.** Development of ventral cochlear nucleus projections to the superior olivary complex in gerbil. *J Comp Neurol* 353: 317–40, 1995.
- Koch U and Grothe B.** Interdependence of spatial and temporal coding in the auditory midbrain. *J Neurophysiol* 83: 2300–2314, 2000.
- Kuwabara N and Zook JM.** Projections to the medial superior olive from the medial and lateral nuclei of the trapezoid body in rodents and bats. *J Comp Neurol* 324: 522–538, 1992.
- Kuwada S, Fitzpatrick DC, Batra R, and Ostapoff EM.** Sensitivity to interaural time differences in the dorsal nucleus of the lateral lemniscus of the unanesthetized rabbit: comparison with other structures. *J Neurophysiol* 94: 000–000, 2005.
- Kuwada S, Stanford TR, and Batra R.** Interaural phase-sensitive units in the inferior colliculus of the unanesthetized rabbit: effects of changing frequency. *J Neurophysiol* 57: 1338–1360, 1987.
- Kuwada S and Yin TCT.** Binaural interaction in low-frequency neurons in inferior colliculus of the cat. I. Effects of long interaural delays, intensity, and repetition rate on interaural delay function. *J Neurophysiol* 50: 981–999, 1983.
- Leibold C and van Hemmen JL.** Synaptic plasticity determines the character of interaural-time-difference representation. *Neurocomputing* 52: 321–326, 2003.
- Loskota WJ, Lomax P and Verity MA.** *A Stereotaxic Atlas of the Mongolian Gerbil Brain*. Ann Arbor, MI: Ann Arbor Science Publishers, 1974.
- Magnusson AK, Kapfer C, Grothe B, and Koch U.** Maturation of glycinergic inhibition in the gerbil medial superior olive after hearing onset. *J Physiol* 568: 497–512, 2005a.
- Magnusson AK, Koch U, Brand A, Heise I, Grothe B, and Park TJ.** GABA_B receptors modulate binaural response properties in LSO neurons. *Soc Neurosci Abstr* 44.8., 2005b.
- Maki K and Furukawa S.** Acoustical cues for sound localization by the Mongolian gerbil, *Meriones unguiculatus*. *J Acoust Soc Am* 118: 872–886, 2005.
- Makous JC and Middlebrooks JC.** Two-dimensional sound localization by human listeners. *J Acoust Soc Am* 87: 2188–200, 1990.
- Malmierca MS, Merchant MA, Henkel CK, and Oliver DL.** Direct projections from cochlear nuclear complex to auditory thalamus in the rat. *J Neurosci* 22: 10891–10897, 2002.
- Markovitz NS and Pollak GD.** The dorsal nucleus of the lateral lemniscus in the mustache bat: monaural properties. *Hear Res* 71: 51–63, 1993.
- Markovitz NS and Pollak GD.** Binaural processing in the dorsal nucleus of the lateral lemniscus. *Hear Res* 73: 121–140, 1994.
- McAlpine D, Jiang D, and Palmer AR.** A neural code for low-frequency sound localization in mammals. *Nat Neurosci* 4: 396–401, 2001.
- McAlpine D, Jiang D, Shackleton TM, and Palmer AR.** Convergent input from brain stem coincidence detectors onto delay-sensitive neurons in the inferior colliculus. *J Neurosci* 18: 6026–6039, 1998.
- McAlpine D and Palmer AR.** Blocking GABAergic inhibition increases sensitivity to sound motion cues in the inferior colliculus. *J Neurosci* 22: 1443–1453, 2002.
- Middlebrooks JC, Clock AE, Xu L, and Green DM.** A panoramic code for sound location by cortical neurons. *Science* 264: 842–844, 1994.
- Moushegian G, Rupert A, and Whitcomb MA.** Brain-stem neuronal response patterns to monaural and binaural tones. *J Neurophysiol* 27: 1174–1191, 1964.
- Oliver DL.** Ascending efferent projections of the superior olivary complex. *Microsc Res Tech* 51: 355–363, 2000.
- Oliver DL, Beckius GE, Bishop DC, and Kuwada S.** Simultaneous anterograde labeling of axonal layers from lateral superior olive and dorsal cochlear nucleus in the inferior colliculus of cat. *J Comp Neurol* 382: 215–229, 1997.
- Oliver DL and Huerta MF.** Inferior and superior colliculi. In: *The Mammalian Auditory Pathway: Neuroanatomy*, edited by Webster DB, Popper AN, and Fay RR. New York: Springer, 1992, p. 168–221.
- Park TJ.** IID sensitivity differs between two principal centers in the interaural intensity difference pathway: the LSO and the IC. *J Neurophysiol* 79: 2416–2431, 1998.
- Park TJ, Grothe B, Pollak GD, Schuller G, and Koch U.** Neural delays shape selectivity to interaural intensity differences in the lateral superior olive. *J Neurosci* 16: 6554–6566, 1996.
- Perkins RE.** An electron microscopic study of synaptic organization in the medial superior olive of normal and experimental chinchillas. *J Comp Neurol* 148: 387–415, 1973.
- Pollak GD, Burger RM, and Klug A.** Dissecting the circuitry of the auditory system. *Trends Neurosci* 26: 33–39, 2003.
- Rayleigh LJ.** On our perception of sound direction. *Philos Mag* 13: 214–232, 1907.
- Rhode WS and Greenberg S.** Physiology of the cochlear nuclei. In: *The Mammalian Auditory Pathway: Neurophysiology*, edited by Webster DB, Popper AN, and Fay RR. New-York: Springer, 1992, p. 94–152.
- Rose JE, Gross NB, Geisler CD, and Hind JE.** Some neural mechanisms in the inferior colliculus of the cat which may be relevant to localization of a sound source. *J Neurophysiol* 29: 288–314, 1966.
- Ruggero MA.** Physiology and coding of sound in the auditory nerve. In: *The Mammalian Auditory Pathway: Neurophysiology*, edited by Webster DB, Popper AN, and Fay RR. New-York: Springer, 1992, p. 34–93.
- Ryan A.** Hearing sensitivity of the mongolian gerbil, *Meriones unguiculatus*. *J Acoust Soc Am* 59: 1222–1226, 1976.
- Schuller G, Radtke Schuller S, and Betz M.** A stereotaxic method for small animals using experimentally determined reference profiles. *J Neurosci Methods* 18: 339–350, 1986.
- Schwartz IR.** The superior olivary complex and lateral lemniscal nuclei. In: *The Mammalian Auditory Pathway: Neuroanatomy*, edited by Webster DB, Popper AN, and Fay RR. New York: Springer, 1992, p. 117–167.
- Seidl AH and Grothe B.** Development of sound localization mechanisms in the Mongolian gerbil is shaped by early acoustic experience. *J Neurophysiol* 94: 1028–36, 2005.
- Shamma SA, Shen NM, and Gopalaswamy P.** Stereausis: binaural processing without neural delay. *J Acoust Soc Am* 86: 989–1006, 1989.
- Shneiderman A, Oliver DL, and Henkel CK.** Connections of the dorsal nucleus of the lateral lemniscus: an inhibitory parallel pathway in the ascending auditory system? *J Comp Neurol* 276: 188–208, 1988.
- Skottun BC, Shackleton TM, Arnott RH, and Palmer AR.** The ability of inferior colliculus neurons to signal differences in interaural delay. *Proc Natl Acad Sci USA* 98: 14050–14054, 2001.
- Sommer I, Lingenhoehl K, and Friauf E.** Principal cells of the rat medial nucleus of the trapezoid body: an intracellular in vivo study of their physiology and morphology. *Exp Brain Res* 95: 223–239, 1993.
- Spangler KM, Warr WB, and Henkel CK.** The projections of principal cells of the medial nucleus of the trapezoid body in the cat. *J Comp Neurol* 238: 249–262, 1985.
- Spitzer MW and Semple MN.** Neurons sensitive to interaural phase disparity in gerbil superior olive: diverse monaural and temporal response properties. *J Neurophysiol* 73: 1668–1690, 1995.
- Stecker GC, Harrington IA, and Middlebrooks JC.** Location coding by opponent neural populations in the auditory cortex. *PLoS Biol* 3: 520–528, 2005.
- Thompson SP.** On the function of the two ears in the perception of space. *Philos Mag* 13: 406–416, 1882.
- Tollin DJ and Yin T.** Interaural phase and level difference sensitivity in low-frequency neurons in the lateral superior olive of the cat. *J Neurosci* 25: 10648–10657, 2005.
- Yin TC.** Neural mechanisms of encoding binaural localization cues. In: *Integrative Functions in the Mammalian Auditory Pathway*, edited by Oertel D, Fay RR, and Popper AN. New York: Springer, 2002, p. 99–159.
- Yin TC and Chan JC.** Interaural time sensitivity in medial superior olive of cat. *J Neurophysiol* 64: 465–488, 1990.
- Yin TC and Kuwada S.** Binaural interaction in low-frequency neurons in inferior colliculus of the cat. II. Effects of changing rate and direction of interaural phase. *J Neurophysiol* 50: 1000–1019, 1983.
- Yin TC and Kuwada S.** Binaural interaction in low-frequency neurons in inferior colliculus of the cat. III. Effects of changing frequency. *J Neurophysiol* 50: 1020–1042, 1983b.
- Xie RL, Meitzen J, and Pollak GD.** Differing roles of inhibition in hierarchical processing of species-specific calls in auditory brainstem nuclei. *J Neurophysiol* 94: 4019–37, 2005.
- Zhou Y, Carney LH, and Colburn HS.** A model for interaural time difference sensitivity in the medial superior olive: Interaction of excitatory and inhibitory synaptic inputs, channel dynamics, and cellular morphology. *J Neurosci* 25: 3046–3058, 2005.

CHAPTER 3

Synaptic Transmission at the Calyx of Held Under In Vivo–Like Activity Levels

Joachim Hermann,¹ Michael Pecka,¹ Henrike von Gersdorff,^{1,2} Benedikt Grothe,¹ and Achim Klug¹

¹Ludwig-Maximilians-University, Munich, Germany; and ²The Vollum Institute, Oregon Health and Science University, Portland, Oregon

Submitted 29 March 2007; accepted in final form 13 May 2007

Hermann J, Pecka M, von Gersdorff H, Grothe B, Klug A. Synaptic transmission at the calyx of Held under in vivo–like activity levels. *J Neurophysiol* 98: 807–820, 2007. First published May 16, 2007; doi:10.1152/jn.00355.2007. One of the hallmarks of auditory neurons in vivo is spontaneous activity that occurs even in the absence of any sensory stimuli. Sound-evoked bursts of discharges are thus embedded within this background of random firing. The calyx of Held synapse in the medial nucleus of the trapezoid body (MNTB) has been characterized in vitro as a fast relay that reliably fires at high stimulus frequencies (≤ 800 Hz). However, inherently due to the preparation method, spontaneous activity is absent in studies using brain stem slices. Here we first determine in vivo spontaneous firing rates of MNTB principal cells from Mongolian gerbils and then reintroduce this random firing to in vitro gerbil brain stem synapses at near-physiological temperature. After conditioning synapses with afferent fiber stimulation for 2 min at Poisson averaged rates of 20, 40, and 60 Hz, we observed a number of differences in the properties of synaptic transmission between conditioned and unconditioned synapses. Foremost, we observed reduced steady-state EPSC amplitudes that depressed even further during an embedded short-stimulation train of 100, 300, or 600 Hz (a protocol that thus simulates in vitro what probably occurs at the in vivo MNTB after a short sound stimulus in a silent background). Accordingly, current-clamp, dynamic-clamp, and loose-patch recordings revealed a number of action potential failures at the postsynaptic cell during high-frequency-stimulation trains, although the initial onset of evoked activity was still transmitted with higher fidelity. We thus propose that some in vivo auditory synapses are in a tonic state of reduced EPSC amplitudes as a consequence of high spontaneous spiking and this in vivo–like conditioning has important consequences for the encoding of signals throughout the auditory pathway.

INTRODUCTION

The calyx of Held is a large synaptic terminal innervating principal neurons of the medial nucleus of the trapezoid body (MNTB) (Forsythe 1994; Held 1893; Kuwabara et al. 1991; Smith et al. 1991). MNTB neurons sign-invert calyceal excitation into glycinergic inhibition to various nuclei in the auditory brain stem (Banks and Smith 1992; Bledsoe et al. 1990; Moore and Caspary 1983; Spangler et al. 1985; Thompson and Schofield 2000). In vitro, the signal derived from the calyx generates large excitatory postsynaptic currents (EPSCs) with a short synaptic delay (Barnes-Davies and Forsythe 1995; Borst and Sakmann 1996; Sakaba and Neher 2001; Taschenberger et al. 2002). Speed and fidelity of synaptic transmission are considered very reliable up to several hundred Hertz in mature animals (Futai et al. 2001; Joshi et al. 2004; Taschenberger and von Gersdorff 2000; Wu and Kelly

1993), leading to a view of the calyx of Held as a very reliable relay synapse.

All the in vitro work mentioned earlier was performed in brain slices. Inherently, auditory brain slice preparations differ from intact brains in various parameters, including spontaneous activity. In vivo, neurons of the auditory brain stem fire spontaneously at frequencies that vary from >1 to ≥ 100 Hz, a property that results mainly from the dynamics of the transduction channels in the cochlear hair cells (Geisler et al. 1985; Hudspeth 1997; Kiang 1965; Liberman 1978; Roberts et al. 1988), resulting in spontaneous firing of the auditory nerve (Geisler et al. 1985; Liberman 1978). Spontaneous firing can also be observed in many brain stem nuclei including the cochlear nucleus (Brownell 1975; Goldberg and Brownell 1973; Joris et al. 1994; Schwarz and Puil 1997; Spirou et al. 1990, 2005) and MNTB (Kadner et al. 2006; Kopp-Scheinpflug et al. 2003; Smith et al. 1998; Sommer et al. 1993).

In an intact brain, MNTB neurons fire spontaneously at levels, which might be suitable to chronically induce some forms of short-term plasticity, such as synaptic depression or facilitation (Schneggenburger et al. 2002; von Gersdorff and Borst 2002). Sound stimuli, i.e., streams of high-frequency activity embedded in this spontaneous firing (Klyachko and Stevens 2006), would then be processed by the synapse on the background of chronic depression and/or facilitation (Fig. 1A). Because of the nature of the brain slice preparation, spontaneous activity and its potential effects on short-term plasticity might be lost in standard in vitro recordings (Fig. 1B). If that were the case, properties of synaptic transmission in the calyx of Held under in vivo conditions may be different from those commonly observed in vitro.

This study investigates synaptic transmission in the calyx of Held under in vivo–like spontaneous activity levels. We first measured the rates and statistical properties of spontaneous firing in the MNTB of Mongolian gerbils (*Meriones unguiculatus*) in vivo. Subsequently, we stimulated the afferent fibers that give rise to calyceal inputs in gerbil MNTB brain slices at physiological temperature for prolonged periods of time with stimuli that mimicked the random spontaneous activity as closely as possible (Fig. 1C). We assessed changes in synaptic transmission resulting from this long-term stimulation, such as synaptic currents, the degree of depression, recovery from depression, and finally the spiking properties of “spontaneously active” neurons.

Address for reprint requests and other correspondence: A. Klug, Neurobiology Group, Dept. Biology II, Grosshaderner Strasse 2, 82152 Martinsried, Germany (E-mail: achim.klug@lmu.de).

The costs of publication of this article were defrayed in part by the payment of page charges. The article must therefore be hereby marked “advertisement” in accordance with 18 U.S.C. Section 1734 solely to indicate this fact.

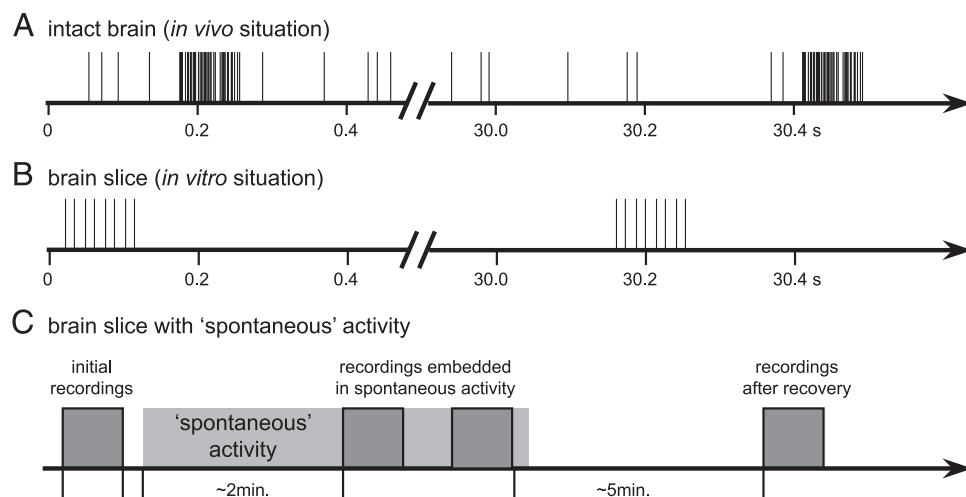


FIG. 1. *A*: illustration of in vivo activity in the medial nucleus of the trapezoid body (MNTB). In the intact brain, MNTB neurons are chronically spontaneously active. Responses to sound stimuli, indicated by high-frequency bursts, are embedded in the background activity. *B*: in a typical slice preparation, the background activity is not present, such that trains of high-frequency stimuli used to imitate responses to sound are embedded in periods of complete silence. *C*: our experimental approach attempted to bring the spontaneous activity back into slice preparations. Responses to simulated sound stimuli were tested to obtain a baseline of synaptic properties, then spontaneous activity was simulated for several minutes, then the same "sound stimuli" were tested again while they were embedded in background activity. At the end of data collection, the cell was allowed to recover and the same set of simulated sound stimuli was tested again to assess the level of recovery.

METHODS

In vivo recordings

Auditory responses from 36 single neurons were recorded in 16 Mongolian gerbils (*Meriones unguiculatus*) of both sexes, aged between 21 and 60 days. We found no systematic differences in aurality, firing frequency, threshold, characteristic frequency, or other response parameters of neurons, which depended on the age of the animal (data not shown), and thus the data from all 36 neurons were pooled. In our sample there was also no covariation between spontaneous activity and auditory threshold or between spontaneous activity and a neuron's characteristic frequency (regression analyses; data not shown). For experimental reasons, the reported in vivo data were recorded from MNTB postsynaptic neurons, not calyces of Held or globular bushy cells in the anteroventral cochlear nucleus. The underlying assumption is that the spontaneous activity in the MNTB is not high enough to induce synaptic failures at the calyx of Held synapse, such that the presynaptic spike frequency is identical to the postsynaptic activity.

Data were collected simultaneously for this study and a different project involving MNTB response properties (data not shown). All experiments complied with institutional guidelines and were approved by the appropriate government authorities (Reg. Oberbayern AZ 55.2-1-54-2531-57-05).

SURGICAL PROCEDURES. Before surgery, animals were anesthetized by an initial intraperitoneal injection (0.5 ml/100 g body weight) of ketamine (20%) and xylazine (2%, both in physiological NaCl). During surgery and recordings, a dose of 0.05 ml of the same mixture was applied subcutaneously in scheduled intervals that were based on the animal's body weight. Constant body temperature was maintained using a thermostatically controlled heating blanket.

Skin and tissue covering the upper part of the skull were removed and a small metal rod was mounted to the frontal part of the skull using UV-sensitive dental-restorative material (Charisma, Heraeus Kulzer, Hanau, Germany). Custom-made earphone holders were attached to the gerbil head, allowing for the safe insertion of earphones or probe tube microphones into the ear canal. The animal was then transferred to a sound-attenuated chamber and mounted in a custom-made stereotaxic instrument (Schuller et al. 1986). The animal's position in the recording chamber was standardized with reference to stereotaxic landmarks on the skull (Loskota et al. 1974). For electrode

penetrations to the MNTB, a small hole of approximately 1 mm² was cut into the skull lateral to the lambdoid suture. Micromanipulators were used to position the recording electrode according to landmarks on the brain surface and a reference point, which was used for all penetrations. The meninges overlying the cortex were removed and saline was applied to the opening to prevent dehydration of the brain.

Typical recording sessions lasted 10–14 h. After successful recordings, the animal was killed by injection of an overdose of chloral hydrate (Sigma–Aldrich Chemie, Munich, Germany). The last electrode position was then marked with a current-induced lesion (20 μ A for 80–120 s). The head was fixated in 4% paraformaldehyde and prepared for anatomical processing. Transverse sections were cut and Nissl-stained to verify the recording sites. An example of an anatomical verification is shown in Supplemental Fig. 1C.¹ The lesion site can be clearly seen in the center of the left MNTB.

RECORDINGS OF NEURAL ACTIVITY. Single-unit responses were recorded extracellularly using 10-M Ω glass electrodes filled with 1 M NaCl. The recording electrode was advanced under remote control, using a piezodriven (Inchworm controller 8200, EXFO Burleigh Products Group, Victor, NY). Extracellular action potentials were recorded by an electrometer (npi electronics, Tamm, Germany or Electro 705, WPI, Berlin, Germany), a 50/60-Hz noise eliminator (Humbug, Quest Scientific Instruments, North Vancouver, BC, Canada), a band-pass filter (VBF/3, Bortolin Kemo, Porcia, Italy), and an amplifier (model 7607, Toellner Electronic Instrumente, Herdecke, Germany) and subsequently fed into the computer by an A/D-converter [RP2-1, Tucker-Davis Technologies (TDT), Alachua, FL]. Clear isolation of action potentials from a single neuron (signal-to-noise ratio >5) was achieved by visual inspection on a spike-triggered oscilloscope and by off-line spike-cluster analysis (Brainware, TDT). Two examples of recorded single-cell spike waveforms are shown in Supplemental Fig. 1, *A* and *B*. The unit in supplemental Fig. 1A is an example of a neuron with a low spontaneous rate (10 Hz), whereas supplemental Fig. 1B shows an example of a neuron with a very high spontaneous rate (107 Hz). Both units were recorded from the same animal; histological verification of the recording site is shown in Supplemental Fig. 1C.

STIMULUS PRESENTATION AND RECORDING PROTOCOLS. Stimuli were generated at a 50-kHz sampling rate using TDT System III.

¹ The online version of this article contains supplemental data.

Digitally generated stimuli were converted to analog signals (DA3-2/RP2-1, TDT), attenuated (PA5, TDT), and delivered to earphones (MDR-EX70LP, Sony, Berlin, Germany).

The standard stimulus was a 200-ms toneburst with a rise/fall time of 5 ms, presented at a repetition rate of 2 Hz. Stimulus presentation was randomized. To search for acoustically evoked responses, noise stimuli were delivered binaurally. When an auditory neuron was encountered, we first determined its best frequency (BF) and absolute threshold audiovisually to set stimulus parameters subsequently controlled by the computer. The frequency that elicited responses at the lowest sound intensity was defined as BF, the lowest sound intensity evoking a noticeable response at BF as threshold. These properties were confirmed by off-line analysis of the frequency versus level response areas. Monaural pure tones to each ear and binaural pure tones without interaural intensity or time differences were presented to define the aurality of the neuron. MNTB neurons responded to stimulation of the contralateral ear only, with a tonic/primary-like firing pattern, and were not affected by stimulation of the ipsilateral ear.

Spontaneous activity of a neuron was determined by recording action potentials in several 5-s-long intervals without sound stimulation and averaging the measured firing rate. All quantifications in this study are based on off-line analysis with the software packages Brainware (TDT), Matlab (The MathWorks, Natick, MA), and IGOR (WaveMetrics, Lake Oswego, OR).

In vitro recordings

Slices of brain stem were prepared from Mongolian gerbils (*Meriones unguiculatus*) aged 14 to 19 days (posthearing animals). Data from these different ages were pooled because no age-dependent variations in synaptic amplitudes, degree of depression, response to conditioning, or firing probability were observed (data not shown).

SLICE PREPARATION. Animals were briefly anesthetized by isoflurane inhalation (Isoflurane Curamed, Curamed Pharma, Karlsruhe, Germany) and decapitated. The brain stem was dissected out under ice-cold dissection ringer (125 mM NaCl, 2.5 mM KCl, 1 mM MgCl₂, 0.1 mM CaCl₂, 25 mM glucose, 1.25 mM NaH₂PO₄, 25 mM NaHCO₃, 0.4 mM ascorbic acid, 3 mM myoinositol, 2 mM pyruvic acid; all chemicals from Sigma-Aldrich). Sections (200–250 μ m) were cut with a vibratome (VT1000S, Leica, Wetzlar, Germany). Slices were transferred to an incubation chamber containing extracellular solution (ECS) (125 mM NaCl, 2.5 mM KCl, 1 mM MgCl₂, 2 mM CaCl₂, 25 mM glucose, 1.25 mM NaH₂PO₄, 25 mM NaHCO₃, 0.4 mM ascorbic acid, 3 mM myoinositol, 2 mM pyruvic acid; all chemicals from Sigma-Aldrich) and bubbled with 5% CO₂-95% O₂. Slices were incubated for 1 h at 37°C, after which the chamber was brought to room temperature. Recordings were obtained within 4–5 h of slicing.

WHOLE CELL RECORDINGS. All recordings were performed at 36–37°C. After incubation, slices were transferred to a recording chamber and continuously superfused with ECS at 3–4 ml/min through a gravity-fed perfusion system. MNTB neurons were viewed through a Zeiss Axioskop 2 FS microscope equipped with DIC optics and a $\times 40$ water-immersion objective (Zeiss, Oberkochen, Germany). Whole cell recordings were made with an EPC 10 double amplifier (HEKA Instruments, Lambrecht/Pfalz, Germany). Signals were filtered at 5–10 kHz and subsequently digitized at 20–100 kHz using Patchmaster Version 2.02 software (HEKA). Uncompensated series resistance, between 5.5 and 15 M Ω , was compensated to values between 2.1 and 5.8 M Ω with a lag time of 10 μ s. Potential changes in series resistance were monitored throughout the recordings and data collection was discontinued whenever series resistance changed by >2 M Ω . All voltages are corrected for a -12 -mV junction potential.

Patch pipettes were pulled from 1.2-mm borosilicate glass (WPI) or 1.5-mm borosilicate glass (Harvard Instruments, Kent, UK) using a

Sutter P-97 electrode puller (Sutter Instrument, Novato, CA) or a DMZ Universal Puller (Zeitz Instruments, Munich, Germany). Pipettes were filled with potassium gluconate-based internal solution for current-clamp recordings (120 mM K-gluconate, 4 mM MgCl₂, 10 mM HEPES, 5 mM EGTA, 10 mM tris-phosphocreatine, 4 mM Na₂-ATP, 0.3 mM tris-GTP, 0.5 mM CaCl₂; all chemicals from Sigma-Aldrich) or cesium methanesulfonate-based solution for voltage-clamp recordings (125 mM CsMeSO₃, 4.5 mM MgCl₂, 9 mM HEPES, 5 mM EGTA, 14 mM tris-phosphocreatine, 4 mM Na₂-ATP, 0.3 mM tris-GTP, 1.5 mM CaCl₂, all chemicals from Sigma-Aldrich).

During all recordings, 500 nM strychnine hydrochloride (Sigma-Aldrich) and 20 μ M SR95531 were added to the bath to block glycinergic and GABA_A-ergic inhibition, respectively. During voltage-clamp recordings, 5 mM QX-314 (Alomone Labs, Jerusalem, Israel) was added to the pipette fill to eliminate sodium currents.

STIMULATION OF SYNAPTIC INPUTS. Synaptic currents were elicited by midline stimulation of the calyceal input fiber bundle with a 5-M Ω bipolar stimulation electrode (matrix electrodes with 270- μ m distance; FHC, Bowdoinham, ME). Stimuli were 100- μ s-long square pulses of 10 to 40 V delivered with an STG 2004 computer-controlled four-channel stimulator (Multi Channel Systems, Reutlingen, Germany) and a stimulation isolation unit (Iso-flex, AMPI, Jerusalem, Israel). The stimulator permitted completely independent uploading and operation of the four channels, allowing the seamless integration and thus true embedding of simulated auditory signals (i.e., high-frequency bursts) in the simulated spontaneous activity. Spontaneous activity was simulated by using 20-, 40-, and 60-Hz Poisson-distributed stimulus trains (see Figs. 1 and 2, C and E). Sound-evoked activity was simulated by short trains consisting of 20 stimuli at 100, 300, or 600 Hz.

CONDUCTANCE-CLAMP EXPERIMENTS. Excitatory conductances were simulated with an SM-1 amplifier (Cambridge Conductance, Cambridge, UK). The 10–90% rise of the current output in response to a voltage change for this amplifier was 290 ns. Reversal potentials were set to 0 mV for the excitatory postsynaptic conductances (EPSCs). The conductance waveforms used were previously recorded as EPSCs in voltage-clamp mode. After extrapolating the artifacts, EPSCs were normalized. All conductance values correspond to peak conductances. In experiments in which background leak was added, a constant step command was fed from the computer into the conductance-clamp amplifier by a separate channel and the reversal potential for this channel was set to -60 mV. The separately calculated output of both channels was added together and fed to the HEKA amplifier.

STATISTICAL ANALYSIS. Data were analyzed in IGOR 5 (WaveMetrics), MS Excel 2004 (Microsoft, Redmond, WA), and Matlab 7 (The MathWorks). Unless otherwise noted, all errors are reported as standard error. Statistical significance was tested with a Student's *t*-test, unless otherwise noted. Significant differences are marked with a single asterisk for values of $P < 0.05$ and with a double asterisk for $P < 0.01$.

RESULTS

In vivo spontaneous firing rates of MNTB cells

The first goal was to determine the spontaneous firing rates of MNTB neurons in the intact brain of Mongolian gerbils (*Meriones unguiculatus*). Neural activity was recorded in vivo from single cells in the MNTB with standard extracellular recording techniques. When a neuron was encountered and isolated, its basic response features such as aurality, auditory threshold, and frequency tuning were assessed. Among the 36 neurons from which activity was recorded, thresholds for sound stimulation ranged from 0 to 60 dB SPL (mean = 32 \pm

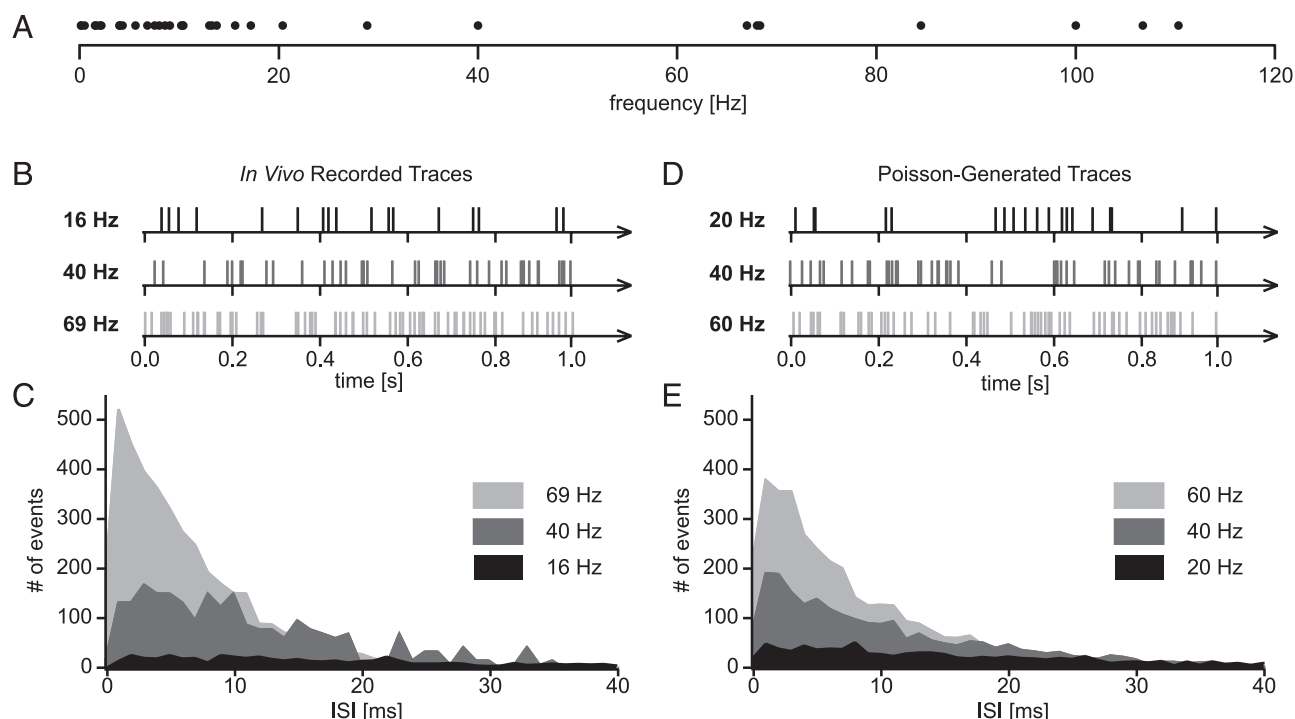


FIG. 2. *A*: distribution of spontaneous firing rates measured among our sample of 36 neurons. Each dot represents the average spontaneous firing rate of one neuron. Mean spontaneous firing rate among the 36 neurons was 24.9 ± 5.5 Hz. *B* and *C*: in vivo recordings of spontaneous activity from 3 MNTB neurons; clips of original trace (*B*); interspike interval (ISI) distribution (*C*). Although the spontaneous firing rates differed between the neurons and were 16, 40, and 69 Hz, the ISI distribution could be described by a single-exponential curve, and thus was near-Poisson-distributed in each case. *D* and *E*: based on the results from *B* and *C*, 3 stimulation protocols of simulating spontaneous activity in brain slices at 20, 40, and 60 Hz were created. ISI distribution was designed to be near-Poisson.

2.8 dB SPL) and characteristic frequencies were between 486 Hz and 16.8 kHz. Consistent with known input patterns to the MNTB, all neurons could be excited when sound was presented to the ear contralateral to the recording site. None of the neurons showed any effects of ipsilateral stimulation.

After a neuron's basic response properties to auditory stimulation were assessed, its spontaneous firing rate in the absence of sound stimulation was measured over ≥ 50 s and average discharge rates were calculated and defined as the neuron's spontaneous firing rate. Among the 36 neurons, spontaneous firing rates ranged from 0.15 to 110 Hz (Fig. 2*A*). The mean spontaneous rate was 24.9 ± 5.5 Hz. Short clips of spike trains are shown in Fig. 2*B*. The spontaneous rates of these neurons were 16, 40, and 69 Hz, respectively. An analysis of the interspike intervals (ISIs) revealed that the spikes are near-Poisson distributed with the exception that very short ISIs (< 1 ms) are underrepresented (three ISI histograms in Fig. 2*C*).

Introducing spontaneous rates into slice preparations of the MNTB

Based on these in vivo data, three representative frequencies of spontaneous rates were chosen for stimulation of the in vitro brain slice preparations: 20, 40, and 60 Hz (Fig. 2*D*). Distribution of the spike events in each one of these trains was chosen to be near-Poisson, to imitate the in vivo spontaneous activity as closely as possible (Fig. 2*E*). MNTB calyceal input fibers were stimulated with these spike trains for prolonged periods of time (≥ 2 min) and voltage-clamp recordings were performed from MNTB principal neurons. During the 2-min

conditioning, 7,200 Poisson-distributed stimuli were presented in case of the 60-Hz train, 4,800 stimuli in the case of the 40-Hz train, and 2,400 stimuli in the case of the 20-Hz conditioning train.

Effects of "spontaneous" firing on excitatory synaptic currents in the calyx of Held

At the beginning of each experiment, a synapse was "rested" or completely recovered, i.e., no stimuli had been given to the input fibers for ≥ 5 min. During the 2-min conditioning period with Poisson-distributed activity, EPSCs depressed substantially with at least two exponential components. The three graphs in Fig. 3, *A–C* show EPSC amplitudes of three different neurons in response to 2-min conditioning stimuli at 20, 40, and 60 Hz (Fig. 3, *A*, *B*, and *C*, respectively). Each dot in the graphs represents the amplitude of one EPSC and the solid lines represent double-exponential fits.

The initial EPSC amplitudes in the three examples were between about 5 and 9 nA, fairly typical values of rested calyx of Held/MNTB recordings in animals of this age group (e.g., Taschenberger and von Gersdorff 2000; von Gersdorff and Borst 2002). We term this value the "initial amplitude" or " A_0 ." The synaptic current then depressed substantially during the first few events of the stimulus train (*insets* in Fig. 3, *A–C*, initial steep declines of amplitudes), then declined much slower (later shallow decline of amplitudes), and then stabilized during the second half of the 2-min train to values between about 2 and 3 nA.

We were interested in these steady-state values measured during the second half of the conditioning period because

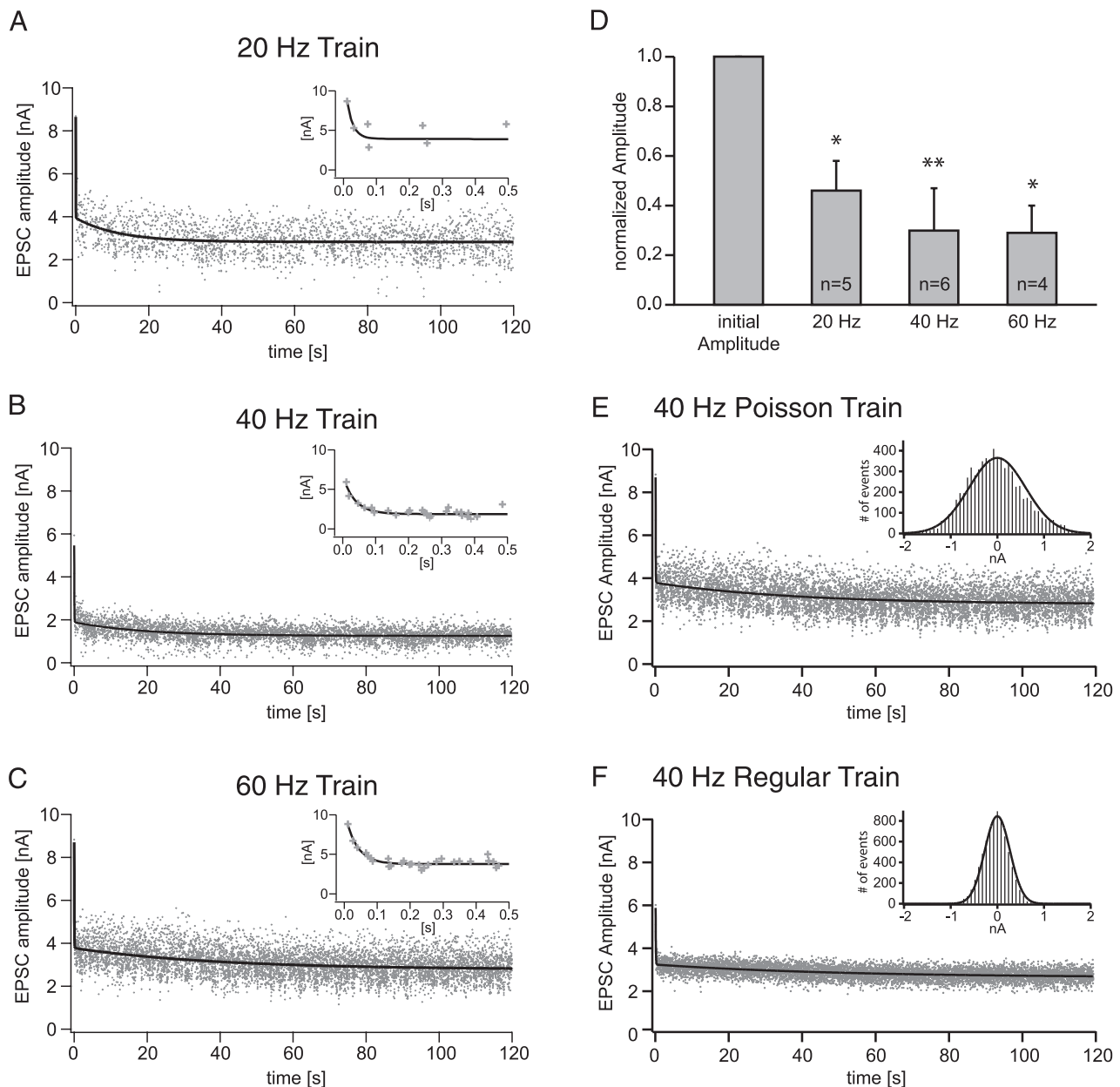


FIG. 3. A–C: excitatory postsynaptic current (EPSC) amplitudes of 3 representative neurons that were stimulated with 20, 40, and 60 Hz “spontaneous” Poisson-distributed activity, respectively. Graphs show the changes of EPSC amplitudes during the 2-min conditioning period. Each dot represents the amplitude of one EPSC. Insets: magnification of events during the first 0.5 s of conditioning. Solid lines represent double-exponential fits with the following time constants: 20 Hz: $\tau_{\text{fast}} = 18.3$ ms, $\tau_{\text{slow}} = 11.7$ s; 40 Hz: $\tau_{\text{fast}} = 36.5$ ms, $\tau_{\text{slow}} = 19.1$ s; 60 Hz: $\tau_{\text{fast}} = 35.6$ ms, $\tau_{\text{slow}} = 39.3$ s. D: comparison of initial EPSC amplitudes, termed “rested A_0 values,” and EPSC amplitudes after the 2-min conditioning protocol with Poisson-distributed activity for our sample of neurons. For the 20-Hz conditioning protocol, the *in vivo* A_0 value was 46% of the rested A_0 , for the 40-Hz conditioning it was 30%, and for the 60-Hz conditioning it was 29%. An asterisk next to a bar indicates a significantly different mean compared with the control (unconditioned) situation (Student’s *t*-test). Average initial, rested A_0 values of EPSC amplitudes for the 3 groups were: 20-Hz group: 7.17 ± 0.82 nA; 40-Hz group: 6.76 ± 0.74 nA; 60-Hz group: 6.41 ± 0.66 nA; these values were not significantly different from each other (ANOVA). E and F: comparison of EPSC variability for one neuron in response to a Poisson-distributed 40-Hz stimulus train (B) and a regular 40-Hz stimulus train (C). In both cases, synaptic current amplitudes converge to the same value, although the variability in response to the Poisson-distributed stimuli are about twice the variability in response to regularly spaced stimuli of the same frequency.

we hypothesize that these values represent the normal state of the “rested” synapse *in vivo*. The reason is that an *in vivo* gerbil calyx of Held presumably would fire spontaneously at frequencies similar to the conditioning frequencies used in this experiment and thus synaptic currents, even in the absence of any sound input, would be chronically depressed to values similar to those measured during the steady-state period of the conditioning phase. Therefore we term these

steady-state current values the “*in vivo* initial amplitude” or “*in vivo* A_0 .”

Figure 3D compares “rested A_0 ” values to “*in vivo* A_0 ” values for our sample of neurons, suggesting that typical synaptic amplitudes in the calyx of Held might be much smaller *in vivo* than those observed in standard *in vitro* experiments.

To assess the effects of the Poisson distribution, five neurons were tested with trains composed of Poisson-distributed stimuli

versus trains with regularly spaced stimuli of identical frequencies. The type of stimulus train did not affect the time course of synaptic depression or the value of the observed *in vivo* A_0 (Fig. 3, *E* and *F*). The difference of A_0 values within each pair was not statistically different (*t*-test, $P = 0.74$). However, the variability of synaptic currents was much larger in the case of Poisson-distributed stimuli compared with evenly spaced stimuli (Fig. 3, *E* and *F*, Gaussian curve *insets*). On average, the standard deviation of synaptic currents was 0.04 when stimuli with regularly spaced intervals were used. Presumably, one physiological basis of this variability is the stochastic nature of vesicle release. In contrast, the SD of current amplitudes was 0.08 when stimuli were Poisson distributed. Most likely, the reason for this larger variability is the additional effect of changing interspike intervals, which is added to the variability caused by stochastic release. However, note that the type of stimulus train used does not appear to affect the final observed *in vivo* A_0 .

Effects of simulated tone bursts on “rested” versus “spontaneously” active synapses

Our next goal was to determine the effects of the “spontaneous” activity on the processing of high-frequency trains by the calyx of Held synapse. The high-frequency trains attempt to simulate simple sound-evoked activity, such as short tones. We tested trains of 20 pulses at 100, 300, and 600 Hz, which simulated pure tones of 200-, 67-, and 33-ms duration, respectively. Effects of each stimulus train were tested before the conditioning period, i.e., on the “rested” synapse, and then after the conditioning period while the simulated tone activity was embedded in the “spontaneous activity,” and a third time ≥ 5 min after the “spontaneous” stimulation was stopped. Figure 4*A* (black trace) shows an EPSC train recorded in response to a 300-Hz, 20-pulse-stimulus train from a “rested” neuron. The synaptic current measured in response to the first event was about 6.9 nA. Subsequently, the synaptic current depressed during the stimulus train, such that the current measured in response to stimulus number 20 was depressed to 1.6 nA, i.e., the EPSC was now only 23% of the initial current.

After the synapse had been conditioned with “spontaneous” activity of 60 Hz, the synaptic current in response to the first stimulus of the same 300-Hz train was about 2.1 nA and thus substantially lower than that in the “rested” condition (Fig. 4*B*, first event). More interestingly, the relative depression induced by the 300-Hz train was substantially less than it was under control conditions, such that the synaptic current at stimulus number 20 was still about 1.1 nA. Therefore in the preconditioned synapse, the current was depressed to only 54% of the value of the first stimulus in the train, suggesting that the degree of relative synaptic depression under *in vivo* conditions might be substantially smaller than that measured by *in vitro* recordings from “rested” synapses.

Afterward the cell was allowed to recover for 5 min (i.e., it received no stimulation) and the synaptic amplitudes and depression ratios recovered to preconditioning values (Fig. 4*A*, gray trace), suggesting that the observed effects shown in Fig. 4*B* are reversible and specific and cannot be attributed to synaptic rundown or other damaging effects of the intense stimulation protocol.

Synaptic amplitudes in response to the first and last events of the various 20-pulse-test trains are shown in Fig. 4*C*. For each group of bars, the amplitude of the first event (dark gray bar) is compared with the amplitude of the 20th event after a 100-,

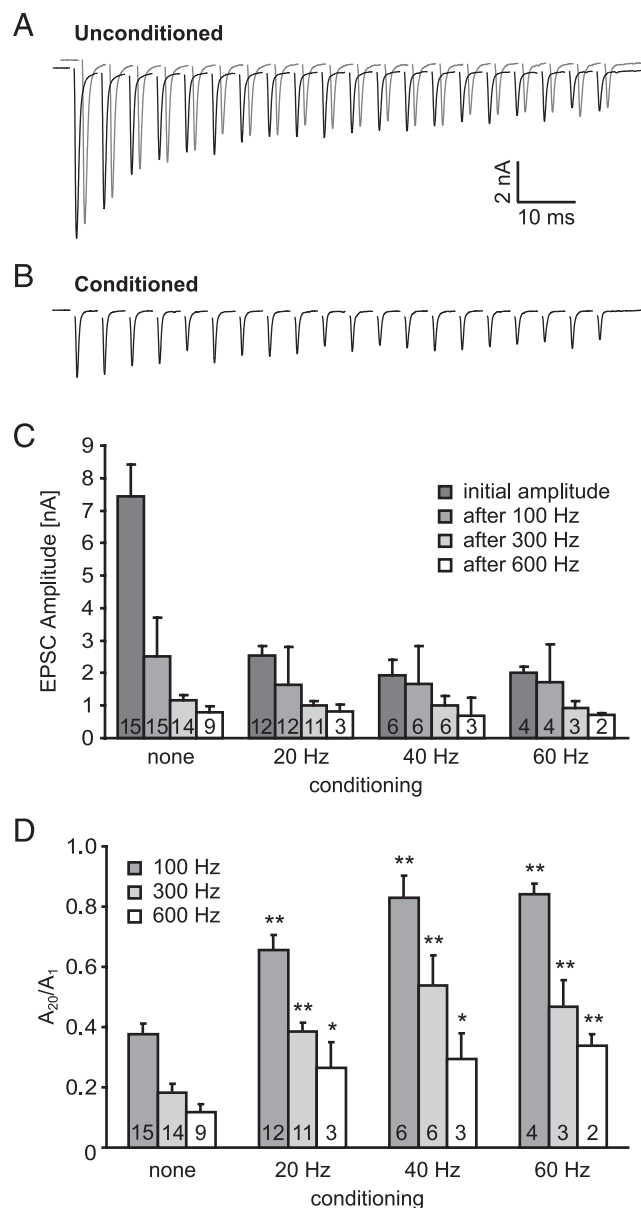


FIG. 4. *A* and *B*: responses of one neuron to the same 300-Hz, 20-pulse stimulus train before conditioning with spontaneous activity (*A*, black line), whereas the 300-Hz train was embedded in 60-Hz spontaneous activity (*B*), and about 5 min after the “spontaneous” activity was ended (*A*, gray line). *C*: absolute EPSC amplitudes with various conditioning and test frequencies. Trains of 100, 300, and 600 Hz were tested with 20 stimuli in the trains in each case. Dark bars labeled “initial amplitude” refer to the EPSC amplitude of the first event of a train (similar for 100-, 300-, and 600-Hz stimulus trains), whereas the bars labeled “after 100/300/600 Hz” refer to the amplitude of the 20th event in the train of the respective frequency. Numbers in the bars indicate sample size. *D*: ratios of synaptic current amplitudes in response to the last stimulus over the current of the synaptic response to the first stimulus of the 20-pulse trains. Low ratios indicate substantial relative depression during the 20-pulse-stimulus trains, whereas high ratios indicate low relative synaptic depression. Numbers in the bars indicate sample size. An asterisk next to a bar indicates a significantly different mean compared with the respective control (= unconditioned) condition, which is shown by the same color bar in the group “none” (Student’s *t*-test).

300-, and 600-Hz stimulus train. Note that the difference in amplitudes between event 1 and event 20 is greatest in unconditioned synapses and smallest in synapses that have been conditioned with 60 Hz of Poisson activity.

Figure 4D shows the amount of relative synaptic depression induced by the various 20-pulse trains. The bars represent the ratio of the 20th over the first postsynaptic current amplitude of the train; i.e., small values indicate that at event 20 only a small portion of the initial synaptic current was measured and therefore synaptic depression caused by the train was substantial. High values indicate that the high-frequency trains induced a much smaller amount of relative depression because the current measured at event 20 of the train was more similar to the initial current.

Overall, the 100-Hz trains induced the lowest amount of synaptic depression (dark gray bars) and the 600-Hz trains the highest amount (white bars). More interestingly, the same high-frequency train induced a much smaller amount of relative depression when the synapse was previously conditioned with spontaneous activity. In all cases the high-frequency trains induced a significantly smaller amount of relative synaptic depression when the synapses were previously conditioned with “spontaneous activity.”

Recovery of firing is very fast under in vivo-like conditions

Our next goal was to determine the recovery from synaptic depression in “spontaneously active” synapses. Recovery from depression is a critical property, especially in highly active auditory brain stem synapses, because the speed of recovery determines how well the neuron can respond to acoustic events that occur shortly after the first event. We first measured the recovery of firing patterns of MNTB neurons in vivo (Fig. 5A). Two identical tone bursts of 200-ms duration were presented to single MNTB units with a variable pause between them. The first tone burst elicited a certain firing rate and firing pattern in the neuron. When the second, identical tone burst was presented after only a very short pause, it elicited a lower response rate in the neuron, which was most apparent during the onset portion of the response (Fig. 5A, top). As the pause between the two tones was increased, neural responses to the second tone recovered progressively and at some point resembled the responses measured to the first tone (Fig. 5A, bottom). The in vivo recovery time course of six MNTB neurons is plotted in Fig. 5B. Among these six neurons, the average in vivo recovery time constant was 82 ± 23 ms, suggesting that recovery of neural responses in the MNTB to acoustic stimuli in vivo is typically very short.

This finding raises a dilemma because recovery from synaptic depression has been measured in the calyx of Held in vitro, with very different results. In these experiments, the presynaptic vesicle pool was depleted, either with a depleting high-frequency stimulus or by voltage clamping the presynaptic terminal to a positive potential. After this pool depletion, test stimuli were given at distinct time intervals to assess the degree of recovery. These experiments typically found recovery time constants at the order of several seconds, not milliseconds (e.g., von Gersdorff et al. 1997; Wang and Kaczmarek 1998).

The in vivo data and the in vitro data are not directly comparable because of additional recoveries at the level of the

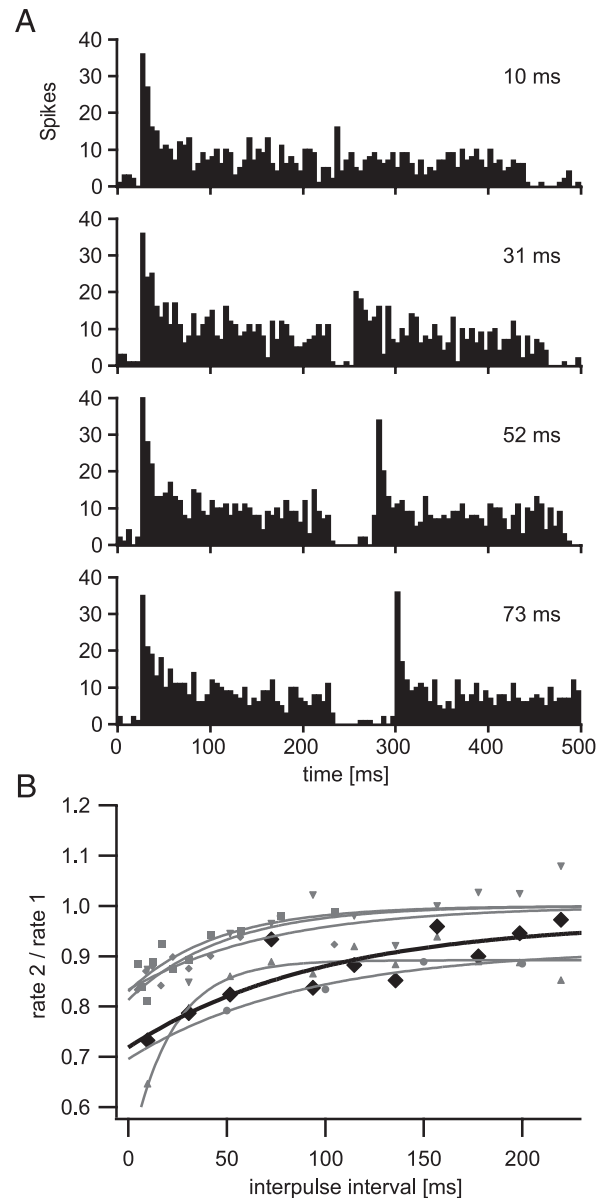


FIG. 5. A: poststimulus time histograms of a single MNTB neuron's in vivo responses to 2 identical best frequency (BF) tone bursts of 200-ms duration with varying ISIs. As the ISI was increased, the neuron's responses to the second tone recovered back to a point where the responses to the second tone were comparable to the neuron's firing pattern in response to the first tone. Tones were presented at 1,200 Hz and 30 dB above threshold. Firing frequencies in response to the first tone were about 260 Hz for the onset response only (= first 15 ms) and about 80 Hz for the sustained part of the response. For the second tone, the onset response varied between 90 and 260 Hz (10- and 73-ms ISI, respectively), whereas the sustained part varied between 52 and 72 Hz (10- and 73-ms ISI, respectively). B: time constants of in vivo recovery of firing of 6 single MNTB units. Neuron presented in A is indicated by the bold black line.

hair cells, auditory nerve (e.g., Spassova et al. 2004), and cochlear nucleus, as well as potential effects of inhibition. However, the in vivo recovery shown in Fig. 5B has to present an upper limit for the vesicular recovery at the level of the calyx of Held because the calyx of Held is one element of the network tested with the in vivo experiment. Therefore the in vivo data suggest that recovery from synaptic depression at the calyx of Held should occur with time constants of no longer than about 80 ms.

Recovery from depression is very fast in spontaneously active synapses

To test this, we measured recovery from depression *in vitro*. Recovery time constants were determined initially in unconditioned neurons by depleting the vesicle pool with a high-frequency train, then allowing the synapse to recover for a specified amount of time, and finally measuring the relative amplitude of a test EPSC. An example of a synapse in which the time course of recovery was determined with this method is shown in Fig. 6, *A* and *B*. Figure 6*A* shows data points on a magnified time axis, following a recovery time course that was best described with an exponential that had a time constant of 72 ms. The average fast time constant of our sample of neurons was 87 ± 16 ms. However, the fast time constant accounted for only about half of the recovery. Complete recovery to the rested A_0 value could best be described with double-exponential fits (Fig. 6*B*). The slow time constant of the same synapse shown in Fig. 6*A* was 1.84 s (Fig. 6*B*), whereas the average slow time constant of our sample of neurons was 1.59 ± 0.17 s. In each case tested, the two time constants together could account for the complete amplitude of the rested A_0 value.

Because of the nature of the experimental protocol, recovery from depression could not be measured in conditioned synapses with the same method as used earlier because the required time intervals (up to several seconds) would be far longer than the amount of time that a neuron is nonactive during "spontaneous activity". Therefore the time course of recovery in conditioned neurons was measured by fitting an exponential function to the time course of EPSC amplitude

recovery as a function of the preceding interpulse interval. The various interpulse intervals, which inherently occur during a Poisson-distribution of spikes, yield a suitable range of time periods to measure the fast recovery time constant. When this was done, we found fast time constants very similar to those found in unconditioned synapses. Figure 6*C* shows an example of a cell in which recovery from depression was measured with the described method. For events where the test stimulus followed shortly after a previous stimulus, the EPSC amplitude of the test EPSC was small. As the time interval before the test stimulus increased, the amplitude of the EPSC progressively increased, presumably as a result of recovery from depression. For this synapse, the time constant of recovery from depression was 74 ms. The average recovery time constant for our sample of neurons was 90 ± 15 ms. As for the unconditioned synapse, the relative contribution of the fast time constant to overall recovery accounted for about half of the rested A_0 amplitude. Therefore we assume that the (missing) slow component of recovery in conditioned synapses might be similar to that of unconditioned synapses, although we were unable to measure this parameter for the reason described earlier.

The fast recovery time constants of both unconditioned and conditioned synapses are very similar to the recovery time constants measured *in vivo* shown in Fig. 5, suggesting that recovery from activity in the calyx of Held occurs at a time course similar to that of the recovery of other components of the circuit. Although we also found a slow component of recovery that was in a range similar to that described previously by other groups, our *in vivo* data suggest that the

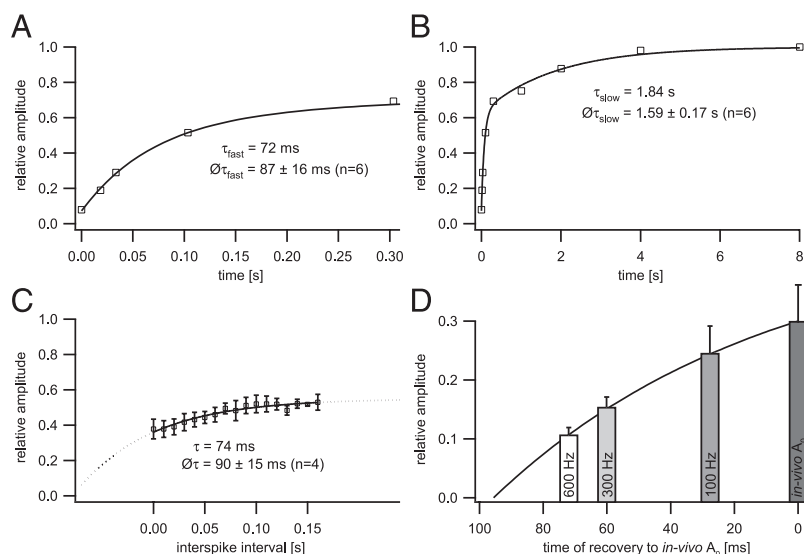


FIG. 6. *A* and *B*: recovery from depression in unconditioned synapses. Data were obtained with a protocol that depletes the vesicle pool with a 300-Hz, 20-pulse-stimulus train, followed by a pause of variable time to allow for pool refilling, followed by a test stimulus. Amplitudes plotted in graphs refer to the amplitudes measured in response to the test stimulus. Recovery could be best described with double-exponential fits that had fast time constants of 87 ± 16 ms and slow time constants of 1.59 ± 0.17 s. *C*: recovery from depression in conditioned synapses. In contrast to *A* and *B*, recovery was assessed by analyzing the variable ISIs inherently contained in the Poisson-distributed trains. Only the fast component was measured here and was found to be very similar to the fast component of unconditioned synapses. *D*: illustration of recovery from depression in active synapses, which happens within milliseconds. In *in vivo* A_0 point is indicated at *time* = 0; the amplitude of the bar is based on data in Fig. 3*D*. This amplitude represents the state of a synapse after it has been conditioned with a 60-Hz Poisson train for several minutes, but has not received a high-frequency stimulation. Presumably, this situation compares to the state of a synapse in an intact brain, while the animal is not receiving sound stimulation. Typical values for synaptic currents after 100-, 300-, and 600-Hz 20-pulse stimulus trains are presented in the graph. These amplitudes presumably compare to the state of a synapse after a short tone burst has just been played to the animal. Naturally, synaptic amplitudes are lower than those in the *in vivo* A_0 state, as a result of the recent high-frequency activity. Position of the bars along the *x*-axis is chosen such that the respective amplitudes correspond to the value of the exponential curve at the same time. Time of recovery indicates the time it would take for the synapse to recover *in vivo* from one of the mentioned 20-pulse-stimulus trains back to the *in vivo* A_0 point. Time constant of exponential = 90 ms, corresponding to the average value presented in Fig. 6*C*; values of bars correspond to last group of bars in Fig. 4*C*.

short time constant might be the dominant one for in vivo recovery.

This point is further illustrated in Fig. 6D. The general idea of this cartoon is that recovery in vivo does not proceed up to the point of a completely full pool, i.e., the rested A_0 seen in silenced synapses in brain slices. Rather, in vivo, recovery of the calyx progresses up to the in vivo A_0 , the value of synaptic current that is typically available to a spontaneously active and thus chronically depressed synapse for the processing of high-frequency sound stimuli. The graph in Fig. 6D plots a typical exponential time course of recovery with a time constant of 90 ms, as determined earlier. The typical “in vivo A_0 ” point of a synapse, which is spontaneously active at 60 Hz without acoustic input, is marked at time 0 (value = 29% of the rested A_0 ; see Fig. 3D). When the synapse now processes a tone burst of 20 pulses at 100, 300, or 600 Hz, the synaptic amplitude depresses even further, typically to the values indicated by the respective bars (values of amplitudes based on data from Fig. 4D). At the end of the tone burst, the synapse recovers back to the in vivo A_0 value, which takes longer or less long, depending on the frequency of the tested stimulus and the resulting depression. In this example, which assumes an exponential time course of 90 ms for vesicle pool refilling, the recovery of the synapse back to the in vivo A_0 point would take between 25 and 74 ms. In other words, a spontaneously active synapse might need only 25–74 ms to recover from a high-frequency sound input because the synapse is chronically depressed by the spontaneous activity and thus recovers only partially back to the steady-state level.

Reduced synaptic reliability in active calyces

The data presented so far suggest that synaptic currents produced by the calyx of Held under simulated in vivo conditions are considerably smaller than those typically measured in vitro in “rested” or silent brain slices. The very large synaptic currents produced by rested calyces in older animals are known to bring postsynaptic neurons well above threshold for firing and thus allow for secure synaptic transmission (e.g., Taschenberger and von Gersdorff 2000). In light of the synaptic currents seen under the simulated in vivo conditions, presented earlier, we next asked the question whether these reduced currents are still suitable for fail-safe synaptic transmission.

This question was addressed with three different techniques. First, current-clamp data were obtained from MNTB neurons, whereas the calyceal fiber bundle was stimulated, with stimulation protocols equivalent to those used for the voltage-clamp experiments shown earlier. Figure 7A shows the firing pattern of a representative neuron in response to a 300-Hz, 20-pulse-stimulus train. Consistent with previous reports, the neuron responded faithfully to the 300-Hz train—i.e., it fired one action potential in response to each synaptic event—when the slice was rested. However, after the neuron was conditioned with 60 Hz of “spontaneous activity” as described earlier, the same 300-Hz stimulus train elicited a substantial number of synaptic failures (Fig. 7B). For those events where the neuron failed to fire an action potential, a small excitatory postsynaptic potential (EPSP) could be observed in the voltage trace, suggesting that the calyx of Held fired an action potential and produced a synaptic current in response to the stimulus. However, the synaptic current appears to have been subthreshold.

The probability of a failure to occur increased with the number of the event in the 20-pulse train. Events early in the train were less likely to fail than events in the latter part of the stimulus train.

Among our sample of neurons tested with this method, we observed some variability in the number of failures as well as other response characteristics. For example, some neurons showed fewer failures, whereas others showed a higher number. Also, in some neurons stimulation of the fiber pathway with 300 Hz resulted in a small plateau from which action potentials to the stimuli were fired (Fig. 7A), whereas the plateau was absent in other neurons. Also, we observed some variation in the height of the action potential. Differences in channel complement or best frequency to which the neuron was tuned might account for this variability.

For our sample of neurons, the probability of a postsynaptic spike was tested as a function of the position of the event in the train. Firing probability was defined as the number of spikes fired in response to a given stimulus in the train over the number of repetitions presented. In the unconditioned synapse, the firing probability was almost 100% throughout the 300-Hz stimulus train; very few failures occurred toward the end of the stimulus train (Fig. 7H, black dotted line and open circles, $n = 5$). However, when synapses were conditioned with 60 Hz of spontaneous activity, the number of failures during the 300-Hz train increased (Fig. 7H, black solid line and closed circles, $n = 5$). In most cases, postsynaptic neurons still answered reliably during the initial three or four events of the train, although the reliability declined afterward.

The reliability of synaptic transmission was also tested with conductance-clamp recordings. The advantage of conductance clamp was twofold: First, this method does not rely on the presynaptic axons and the calyx to follow the intense stimulation protocol. Therefore synaptic failures arising from axonal failures can be ruled out more reliably than with the technique presented earlier. Second, conductance clamp offers the possibility of combining simulated synaptic currents with added background leaks to reduce the neuron’s input resistance (see following text). In our recordings, EPSC waveforms derived from 300-Hz EPSC trains were used to simulate calyceal synaptic currents in response to a 300-Hz stimulus train. Two waveforms were used in these experiments: a 300-Hz, 20-pulse EPSC waveform that simulated synaptic currents of a rested calyx (Fig. 7C, bottom) and an EPSC waveform that simulated the response of a calyx to the same stimulus train embedded in spontaneous activity (Fig. 7D, bottom). Both waveforms were previously recorded as EPSC waveforms from an MNTB neuron under voltage-clamp conditions, while electrically stimulating the input fibers to the calyx. The waveforms were chosen to reflect the observation that peak EPSC currents are larger in rested than in conditioned synapses (Fig. 3D) and that synaptic depression within a high-frequency train is reduced in active synapses (Fig. 4, A and B). Conductance-clamp recordings with these two waveforms were performed on seven MNTB neurons. The neurons reliably fired action potentials when excitatory synaptic currents typical for a rested calyx were injected (Fig. 7C, top). In the rare case that failures could be observed, they occurred toward the end of the train (Fig. 7H, red dotted line and open squares, $n = 7$). However, when currents typical for a spontaneously active synapse were used, failures in the neuron’s response to the 300-Hz, 20-pulse EPSC

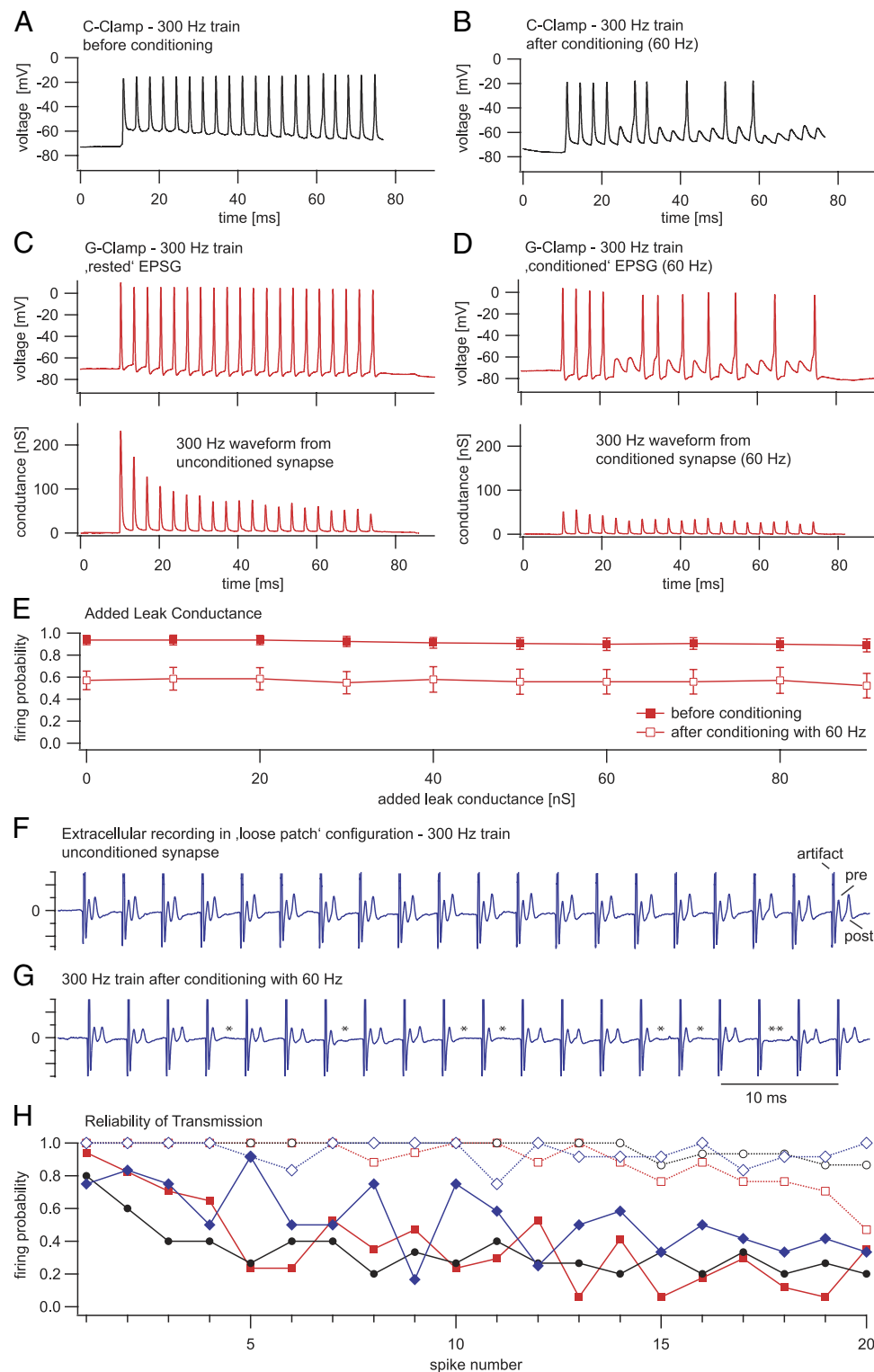


FIG. 7. Reliability of synaptic transmission in spontaneously active synapses. *A*: current-clamp recording of MNTB neuron while the calyceal input fibers were stimulated with a 300-Hz, 20-pulse train; the neuron responded to each stimulation with one action potential. *B*: after the slice was conditioned with 60 Hz of spontaneous activity, a number of failures could be observed during the same 300-Hz train. For each failure, an excitatory postsynaptic potential can be observed in the place of the missing action potential, suggesting that the failure was postsynaptic. *C*, *top*: responses of MNTB neuron when a 300-Hz conductance waveform was used to simulate currents of a rested synapse; the neuron responded to each event with one action potential, similar to that observed when the calyceal fibers were stimulated. Conductance waveform is shown in the *bottom panel*. Peak conductance was 232 nS. *D*, *top*: responses of MNTB neuron when a 300-Hz conductance waveform was used to simulate currents of a synapse that was conditioned with 60 Hz of spontaneous activity; the neuron failed to respond to a number of events. Corresponding conductance waveform is shown in the *bottom panel*. Peak conductance was 56 nS. *E*: various levels of background leak were added to the EPSP waveforms under conductance-clamp conditions, effectively reducing the input resistance of the neurons to values that are closer to input resistances observed in neurons under in vivo conditions. *F* and *G*: example of a loose-patch recording of a MNTB neuron while calyceal input fibers were

train could be observed (Fig. 7*D*, top). These failures tended to occur more frequently toward the end of the EPSC waveform, but could sometimes also be observed early in the train (Fig. 7*H*, red solid line and closed squares, $n = 7$).

Interestingly, the firing probabilities and frequencies for conditioned synapses shown in Fig. 7*E* closely match those observed in vivo. For both current-clamp and conductance-clamp experiments, the firing probability of the first few events in the train was 0.7 to 1.0, based on the calculation method described earlier. For a train frequency of 300 Hz, this corresponds to a firing frequency of about 200 to 300 Hz. The onset portion of the in vivo spike trains shown in Fig. 5*A* had a firing frequency of about 260 Hz (considered is the response to first tone of the pair only). The average firing frequency of the neuron in response to the latter part of the 200-ms tone was about 80 Hz. This corresponds well to the in vitro data shown in Fig. 7*E*, where the firing probability of the neuron to the latter portion of the train is about 1/3, i.e., about 100 Hz.

A number of studies have observed that a neuron's input resistance is substantially higher in brain slices than in the intact brain (e.g., Bernander et al. 1991; Paré et al. 1998). The main reason for this observation is probably that neurons in the intact brain receive a large number and variety of synaptic inputs. When these inputs are activated at different points in time, postsynaptic receptors open and thus decrease the neuron's input resistance. In brain slices, many of these inputs are silent and/or cut, with the result that the neuron's input resistance increases. It is unknown whether and how much the input resistance of an MNTB neuron differs in brain slices compared with the intact brain because the projection pattern to MNTB neurons is much simpler than in the case of, say, cortical neurons. However, prominent glycinergic inhibition to MNTB has been described in vitro (Awatramani et al. 2004). These inputs, when activated, will decrease the input resistance of postsynaptic neurons. An artificially high-input resistance in neurons of MNTB brain slices would facilitate the neuron's responses to synaptic events. In this case, the synaptic failures shown in Fig. 7, *A–E* would be an underestimate of the true in vivo failure rates. We attempted to address this issue by adding a background leak to MNTB neurons during presentation of the EPSC waveforms. The background leak had a constant amplitude of 10–90 nS with a reversal potential of -60 mV and effectively reduced the input resistance of the postsynaptic neuron up to fivefold. Figure 7*F* shows the overall firing probability of six MNTB neurons, when EPSC waveforms of 300-Hz trains plus various amounts of background leak were tested. As expected, the firing probability decreased with increasing background leak, although the effect was minor.

The last approach to test the reliability of synaptic transmission was to use "loose-patch" extracellular recordings. For these experiments, an MNTB neuron in a brain slice was only

loosely patched without obtaining a gigaseal and no break-in into the neuron was performed, such that the recordings were effectively extracellular. In some recordings, action potentials of both the calyx of Held (termed "prepotential") and the postsynaptic principal neuron could be observed. An example is shown in Fig. 7, *F* and *G*. In this recording, stimulation of the calyceal input fibers produced three peaks in response to each event. The first one was the stimulation artifact (labeled "artifact"), followed by the prepotential (labeled "pre"), and then followed by the postsynaptic action potential (labeled "post"). The advantage of this method is that the interior environment of the postsynaptic cell is left undisturbed. For whole cell recordings, a common concern is that the perfusion of the neuron with artificial intracellular fluid might change the firing properties of the neuron, which would result in inaccurate measurements of failure rates. However, even when the postsynaptic neuron was left intact, transmission failures could be observed in the calyx of Held synapse when the slice was driven at in vivo-type activity levels. Figure 7*F* shows a loose-patch recording of a rested brain slice. Consistent with the data shown earlier, the synapse was appreciably fail-safe when a 300-Hz, 20-pulse train was tested, i.e., each prepotential was followed by a postsynaptic action potential (Fig. 7*F*). However, when the slice was conditioned with 60-Hz spontaneous activity, a substantial amount of failures could be observed in response to the same 300-Hz test train (Fig. 7*G*; postsynaptic failures are indicated by single asterisks). In one case, neither a prepotential nor a postpotential could be observed (marked by a double asterisk), suggesting that for this event, the failure must have occurred in the calyceal input fiber. The blue lines in Fig. 7*H* show the average reliability of transmission measured with this technique (blue dotted line and open diamonds: unconditioned synapses, $n = 6$; blue solid line and closed diamonds: conditioned synapses, $n = 6$).

Furthermore, the latency of synaptic transmission was increased when synapses were spontaneously active (Fig. 7, *F* and *G*). In this cell, the synaptic latency increased by 0.19 ms when the synapse was conditioned. For all 11 neurons from which spike-latency data were available, the average latency increase was 0.4 ± 0.13 ms. This discrepancy matches well with the discrepancy between published values for in vitro synaptic latency (Taschenberger et al. 2002; von Gersdorff and Borst 2002) versus in vivo latency (Guinan and Li 1990; Kopp-Scheinpfug et al. 2003) at the calyx of Held. These data suggest that highly active calyces have a longer synaptic latency than previously reported in vitro, but also that our conditioning protocol might be suited to transform calyces into a functional state that more closely resembles the functional state of an active in vivo calyx of Held.

In summary, the data presented in Fig. 7 suggest that the calyx of Held synapse shows a substantial amount of synaptic

stimulated. In loose patch recordings, no gigaseal is formed and no break-in into the cell is performed. Because the recording is effectively extracellular, the internal environment of the postsynaptic cell is undisturbed. Even under these conditions, MNTB neurons exhibited a substantial number of failures in response to a 300-Hz train, when the slice was conditioned with 60 Hz of spontaneous activity. Artifact = stimulation artifact; pre = prepotential = presynaptic action potential; post = postsynaptic action potential. Postsynaptic failures are indicated by a single asterisk. For one event, neither a prepotential nor a postpotential could be observed (double asterisk), suggesting an axonal failure for that event. *H*: firing probability as a function of the number of the event in the 20-pulse train. Black graphs with circular symbols represent data from 5 neurons tested with current clamp as described in *A* and *B*. Red graphs with squared symbols represent data from 7 neurons tested under conductance clamp conditions, as described in *C* and *D*. Blue graphs with diamond symbols represent data from 6 neurons tested with extracellular, loose-patch recordings. For all experimental methods, few failures could be observed under conditions that correspond to a rested synapse, and occurred toward the end of the 20-pulse train (open symbols and dotted lines). However, for situations that correspond to a spontaneously active synapse, the same 300-Hz trains elicited a substantial number of failures (solid symbols and solid lines). Firing probability of a given neuron was defined as the ratio of number of action potentials per 3 stimulations. Presented in graph are average firing probabilities of 5–7 neurons per method, as described earlier.

failures, after cells were stimulated for several minutes with Poisson-distributed activity. One possible interpretation of these results is that in vivo, the MNTB might not be the simple and reliable relay that is commonly observed under standard in vitro conditions.

DISCUSSION

The main question addressed in this study is the question of how synaptic transmission in the calyx of Held synapse changes when synapses are stimulated for prolonged periods of time with Poisson-distributed activity, which, we hypothesize, imitates naturally occurring spontaneous activity. There are four main findings. First, the introduction of "spontaneous" activity into in vitro preparations of the calyx of Held considerably depresses synaptic currents, even at relatively low spontaneous frequencies of 20 Hz. Second, in these "spontaneously active" synapses, the degree of additional depression induced by high-frequency trains (i.e., simulated sound inputs) is reduced considerably. Third, recovery from synaptic depression is very fast. Data from corresponding in vivo extracellular recordings also show fast recovery of firing and are consistent with these in vitro findings. Fourth, in chronically active synapses with reduced synaptic currents, the reliability of transmission is reduced during high-frequency bursts of afferent input.

Background firing in MNTB neurons

Spontaneous activity in the lower auditory system is a widespread phenomenon. It is assumed that this activity is explained by the probabilistic behavior of the transduction channels of the inner hair cells and the resulting chronic transmitter release at the hair cell synapse. The spontaneous activity is still present at the level of the cochlear nucleus (Brownell 1975; Goldberg and Brownell 1973; Joris et al. 1994; Schwarz and Puil 1997; Spirou et al. 1990, 2005) and most auditory brain stem nuclei, such as MSO in bats (Grothe 1994), MNTB in cats (Smith et al. 1998), MNTB in gerbils (Kopp-Scheinpflug et al. 2003), and MNTB in rats (Sommer et al. 1993). Consistent with our data presented here, studies of spontaneous activity in the lower auditory system typically report a large variability of rates among neurons, even within the same species or the same nucleus. One possible explanation for this large variability is that different neurons receive inputs from different classes of auditory nerve fibers with low, medium, or high spontaneous rates (Liberman 1978), which would give rise to auditory brain stem neurons with very diverse spontaneous firing rates.

For the experiments presented here, three frequencies of Poisson-distributed activity were chosen for stimulation of brain slices: 20, 40, and 60 Hz. Although the mean spontaneous firing rate in our sample of neurons was 24.9 Hz and thus closer to the lowest of these frequencies, the three frequencies chosen for stimulation successfully cover the spectrum of observed in vivo spontaneous rates (see Fig. 2A; see also Kopp-Scheinpflug et al. 2003). However, because of the nature of the brain slice preparation, the original in vivo spontaneous firing rate of a given neuron is unknown. Therefore it is possible or even likely that an originally low spontaneously active neuron was stimulated with a high-frequency stimulus

train and vice versa. However, all neurons in our in vitro sample responded stereotypically and in a very similar fashion to our various stimulus protocols and no responses were observed that could be explained by the use of an inappropriate background stimulation rate.

Measurements of spontaneous activity presented in this study were performed under anesthesia. As with almost every type of anesthesia, the ketamine–xylazine mixture used in this study might have depressed the neurons' spontaneous activity to a certain degree (Destexhe et al. 2003). Therefore the actual spontaneous firing rates in MNTB neurons of behaving gerbils might be higher than those shown in this study. On the other hand, the values for spontaneous activity determined here match closely with findings of other studies using various species and various types of anesthesia or, in some cases, no anesthesia at all (e.g., Irvine 1992; Kiang 1965; Ryan and Miller 1978). We therefore conclude that the values presented here are representative or, at worst, a conservative lower limit of the true effects induced by spontaneous activity.

We also note that double-walled sound-attenuated rooms by themselves create the biologically unnatural situation of complete absence of sound. Natural auditory environments always contain a certain level of background noise, which contributes to the background activity of auditory neurons. Therefore the effects of chronic activity on synaptic transmission in behaving animals might be even larger, but are not likely to be smaller than presented here.

Prolonged spontaneous spiking changes properties of synaptic transmission

Our data show that prolonged stimulation even at a frequency of 20 Hz decreases synaptic currents to less than half of the original value, whereas stimulation with frequencies of 60 Hz reduces currents to about one third. It might be surprising to find that such low frequencies cause such a high degree of depression because all brain slices were prepared from animals well past the onset of hearing and recordings were performed at physiological temperature. α -Amino-3-hydroxy-5-methyl-4-isoxazolepropionic acid (AMPA) receptor desensitization as well as *N*-methyl-D-aspartate (NMDA) currents, although playing a substantial role in preparations from young animals (Neher and Sakaba 2001; Sakaba and Neher 2001), play only a very minor role in animals past the age of hearing onset (Futai et al. 2001; Renden et al. 2005; Taschenberger et al. 2005). Under these conditions, MNTB neurons can follow stimulation frequencies of ≥ 600 Hz for at least short periods (Futai et al. 2001; Taschenberger and von Gersdorff 2000; Wu and Kelly 1993). The depression we observed in response to long-term stimulation progressed with at least two time constants: an initial, fast time constant, which can be seen during the first few stimulus pulses, and a much slower time constant. The mechanisms for the slow time constant are unclear, but are likely to be multiple and will be studied in the future. When the processing of high-frequency trains was tested in rested versus spontaneously active synapses, the observed relative degree of synaptic depression caused by the high-frequency train was much larger in the rested than in the active synapse. This might have important functional implications at the calyx of Held, which sustains high levels of activity.

Our findings also suggest that recovery from synaptic depression is very fast under biologically relevant activity levels. These time constants of about 90 ms are an order of magnitude shorter than previously reported values for rested synapses, which are in the range of several seconds (e.g., von Gersdorff et al. 1997: 4.2 s; see also Ishikawa and Takahashi 2001; Schneggenburger et al. 2002; Wang and Kaczmarek 1998; Wu and Borst 1999). Age, temperature, and species differences might account for some of this discrepancy. However, there is strong evidence suggesting that calcium accumulation in the presynaptic terminal through high-frequency firing may play a role in speeding up the recovery from depression (Wang and Kaczmarek 1998). It appears that this faster recovery plays a dominant role in active synapses.

Reliability of synaptic transmission

In vitro studies of the calyx of Held in animals past hearing onset have reported very reliable synaptic transmission and a number of cellular specializations to increase synaptic reliability. Our data are consistent with the view that “rested” calyces produce large synaptic currents and have a high transmission reliability. However, we show that in chronically active synapses, the synaptic currents are much smaller. Our current-clamp, conductance-clamp, and extracellular action potential recordings all suggest that spontaneously active synapses may show synaptic failures during periods of high-frequency activity. Therefore the calyx of Held may not always show the reliable 1:1 transmission postulated from in vitro experiments in rested synapses. This finding is consistent with previous in vivo results from the MNTB. Among the in vivo studies performed in the MNTB only those where both presynaptic and postsynaptic activity have been recorded simultaneously can address the question of transmission failures at the calyx of Held synapse. To our knowledge, two studies report simultaneous pre- and postsynaptic recordings at the MNTB and both agree on the occurrence of postsynaptic failures (Guinan and Li 1990; Kopp-Scheinpflug et al. 2003) in vivo. However, the two studies differ in the number of failures observed. Guinan and Li (1990) found failures mainly with prolonged high-frequency stimulation of the afferent fiber bundle and only occasionally with sound stimulation, whereas Kopp-Scheinpflug et al. (2003) found a substantial number of failures with sound stimulation. Species differences might account for some of this discrepancy, but note that these recordings were performed with intact synaptic inhibition and under anesthesia. Because MNTB neurons are known to receive a substantial amount of glycinergic inhibition (Awatramani et al. 2004), it is possible that some of these failures are the result of spike suppression by inhibition and that some of the difference observed in the two studies arises from differential recruitment of synaptic inhibition. Nevertheless, the presence of synaptic inhibition alone also questions the interpretation of the calyx of Held as a fail-safe “relay” synapse. This view has been formed by previous in vitro studies performed in slices from animals past hearing onset, where EPSCs well above action potential threshold have been measured even in response to stimulus frequencies of several hundred Hertz. However, these stimulus trains typically consisted of no more than 20–50 stimuli, with considerable recovery time of several seconds between trials. Our experimental setup avoided these periods of silence because

they do not occur under in vivo conditions. Presumably the lack of prolonged periods of recovery keeps calyces in a chronic state of synaptic depression and causes transmission to fail during periods of embedded high-frequency activity.

In conclusion, the aim of this study was to perform a first description of the effects of prolonged “spontaneous activity” on synaptic transmission at the calyx of Held synapse. We conclude from our data that synaptic transmission in the calyx of Held differs in a number of significant ways when synapses are stimulated with a Poisson-distributed stimulus train for prolonged periods of time. Future studies will determine the specific contribution of multiple modulators, receptors, or channel types in the calyx of Held synapse to the “rested” or the “spontaneously active” synaptic state.

ACKNOWLEDGMENTS

We thank F. Felmy, G. Pollak, L. Trussell, and J. Gittelmann for critical comments on the manuscript.

GRANTS

H. von Gersdorff was funded by a “Mercator Professor” award from Deutsche Forschungsgemeinschaft (DFG) and National Institute on Deafness and Other Communication Disorders Grant R01 DC-04274. The research was funded by DFG Grant KL-1842 to A. Klug.

REFERENCES

- Awatramani GB, Turecek R, Trussell LO. Inhibitory control at a synaptic relay. *J Neurosci* 24: 2643–2647, 2004.
- Banks MI, Smith PH. Intracellular recordings from neurobiotin-labeled cells in brain slices of the rat medial nucleus of the trapezoid body. *J Neurosci* 12: 2819–2837, 1992.
- Barnes-Davies M, Forsythe ID. Pre- and postsynaptic glutamate receptors at a giant excitatory synapse in rat auditory brainstem slices. *J Physiol* 488: 387–406, 1995.
- Bernander O, Douglas RJ, Martin KA, Koch C. Synaptic background activity influences spatiotemporal integration in single pyramidal cells. *Proc Natl Acad Sci USA* 88: 11569–11573, 1991.
- Bledsoe SC Jr, Snead CR, Helfert RH, Prasad V, Wenthold RJ, Altschuler RA. Immunocytochemical and lesion studies support the hypothesis that the projection from the medial nucleus of the trapezoid body to the lateral superior olive is glycinergic. *Brain Res* 517: 189–194, 1990.
- Borst JG, Sakmann B. Calcium influx and transmitter release in a fast CNS synapse. *Nature* 383: 431–434, 1996.
- Brownell WE. Organization of the cat trapezoid body and the discharge characteristics of its fibers. *Brain Res* 94: 413–433, 1975.
- Destexhe A, Rudolph M, Paré D. The high-conductance state of neocortical neurons in vivo. *Nat Rev Neurosci* 4: 739–751, 2003.
- Forsythe ID. Direct patch recording from identified presynaptic terminals mediating glutamatergic EPSCs in the rat CNS, in vitro. *J Physiol* 479: 381–387, 1994.
- Futai K, Okada M, Matsuyama K, Takahashi T. High-fidelity transmission acquired via a developmental decrease in NMDA receptor expression at an auditory synapse. *J Neurosci* 21: 3342–3349, 2001.
- Geisler CD, Deng L, Greenberg SR. Thresholds for primary auditory fibers using statistically defined criteria. *J Acoust Soc Am* 77: 1102–1109, 1985.
- Goldberg JM, Brownell WE. Discharge characteristics of neurons in anteroventral and dorsal cochlear nuclei of cat. *Brain Res* 64: 35–54, 1973.
- Grothe B. Interaction of excitation and inhibition in processing of pure tone and amplitude-modulated stimuli in the medial superior olive of the mustached bat. *J Neurophysiol* 71: 706–721, 1994.
- Guinan JJ Jr, Li RY. Signal processing in brainstem auditory neurons which receive giant endings (calyces of Held) in the medial nucleus of the trapezoid body of the cat. *Hear Res* 49: 321–334, 1990.
- Held H. Die centrale Gehörleitung. *Archiv Anat Physiol Anat Abteil* 1893: 201–247, 1893.
- Hudspeth AJ. How hearing happens. *Neuron* 19: 947–950, 1997.
- Irvine DRF. Physiology of the auditory brainstem. In: *The Mammalian Auditory Pathway: Neurophysiology*, edited by Popper AN, Fay RR. New York: Springer-Verlag, 1992, p. 153–231.

- Ishikawa T, Takahashi T.** Mechanisms underlying presynaptic facilitatory effect of cyclothiazide at the calyx of Held of juvenile rats. *J Physiol* 533: 423–431, 2001.
- Joris PX, Carney LH, Smith PH, Yin TC.** Enhancement of neural synchronization in the anteroventral cochlear nucleus. I. Responses to tones at the characteristic frequency. *J Neurophysiol* 71: 1022–1036, 1994.
- Joshi I, Shokralla S, Titis P, Wang LY.** The role of AMPA receptor gating in the development of high-fidelity neurotransmission at the calyx of Held synapse. *J Neurosci* 24: 183–196, 2004.
- Kadner A, Kulesza RJ Jr, Berrebi AS.** Neurons in the medial nucleus of the trapezoid body and superior paraolivary nucleus of the rat may play a role in sound duration coding. *J Neurophysiol* 95: 1499–1508, 2006.
- Kiang NY-S.** *Discharge Patterns of Single Fibers in the Cat's Auditory Nerve.* Cambridge, MA: MIT Press, 1965.
- Klyachko VA, Stevens CF.** Excitatory and feed-forward inhibitory hippocampal synapses work synergistically as an adaptive filter of natural spike trains. *PLoS Biol* 4: e207, 2006.
- Kopp-Scheinpflug C, Lippe WR, Dorrscheidt GJ, Rubsamen R.** The medial nucleus of the trapezoid body in the gerbil is more than a relay: comparison of pre- and postsynaptic activity. *J Assoc Res Otolaryngol* 4: 1–23, 2003.
- Kuwabara N, DiCaprio RA, Zook JM.** Afferents to the medial nucleus of the trapezoid body and their collateral projections. *J Comp Neurol* 314: 684–706, 1991.
- Lieberman MC.** Auditory-nerve response from cats raised in a low-noise chamber. *J Acoust Soc Am* 63: 442–455, 1978.
- Loskota W, Lomax P, Verity M.** *A Stereotaxic Atlas of the Mongolian Gerbil Brain.* Ann Arbor, MI: Ann Arbor Science, 1974.
- Moore MJ, Caspary DM.** Strychnine blocks binaural inhibition in lateral superior olivary neurons. *J Neurosci* 3: 237–242, 1983.
- Neher E, Sakaba T.** Combining deconvolution and noise analysis for the estimation of transmitter release rates at the calyx of Held. *J Neurosci* 21: 444–461, 2001.
- Paré D, Shink E, Gaudreau H, Destexhe A, Lang EJ.** Impact of spontaneous synaptic activity on the resting properties of cat neocortical pyramidal neurons in vivo. *J Neurophysiol* 79: 1450–1460, 1998.
- Renden R, Taschenberger H, Puente N, Rusakov DA, Duvoisin R, Wang LY, Lehre KP, von Gersdorff H.** Glutamate transporter studies reveal the pruning of metabotropic glutamate receptors and absence of AMPA receptor desensitization at mature calyx of held synapses. *J Neurosci* 25: 8482–8497, 2005.
- Roberts WM, Howard J, Hudspeth AJ.** Hair cells: transduction, tuning, and transmission in the inner ear. *Annu Rev Cell Biol* 4: 63–92, 1988.
- Ryan A, Miller J.** Single unit responses in the inferior colliculus of the awake and performing rhesus monkey. *Exp Brain Res* 32: 389–407, 1978.
- Sakaba T, Neher E.** Quantitative relationship between transmitter release and calcium current at the calyx of Held synapse. *J Neurosci* 21: 462–476, 2001.
- Schneggenburger R, Sakaba T, Neher E.** Vesicle pools and short-term synaptic depression: lessons from a large synapse. *Trends Neurosci* 25: 206–212, 2002.
- Schuller G, Radtke-Schuller S, Betz M.** A stereotaxic method for small animals using experimentally determined reference profiles. *J Neurosci Methods* 18: 339–350, 1986.
- Schwarz DW, Puil E.** Firing properties of spherical bushy cells in the anteroventral cochlear nucleus of the gerbil. *Hear Res* 114: 127–138, 1997.
- Smith PH, Joris PX, Carney LH, Yin TC.** Projections of physiologically characterized globular bushy cell axons from the cochlear nucleus of the cat. *J Comp Neurol* 304: 387–407, 1991.
- Smith PH, Joris PX, Yin TC.** Anatomy and physiology of principal cells of the medial nucleus of the trapezoid body (MNTB) of the cat. *J Neurophysiol* 79: 3127–3142, 1998.
- Sommer I, Lingenhoehl K, Friauf E.** Principal cells of the rat medial nucleus of the trapezoid body: an intracellular in vivo study of their physiology and morphology. *Exp Brain Res* 95: 223–239, 1993.
- Spangler KM, Warr WB, Henkel CK.** The projections of principal cells of the medial nucleus of the trapezoid body in the cat. *J Comp Neurol* 238: 249–262, 1985.
- Spassova MA, Avissar M, Furman AC, Crumling MA, Saunders JC, Parsons TD.** Evidence that rapid vesicle replenishment of the synaptic ribbon mediates recovery from short-term adaptation at the hair cell afferent synapse. *J Assoc Res Otolaryngol* 5: 376–390, 2004.
- Spirou GA, Brownell WE, Zidanic M.** Recordings from cat trapezoid body and HRP labeling of globular bushy cell axons. *J Neurophysiol* 63: 1169–1190, 1990.
- Spirou GA, Rager J, Manis PB.** Convergence of auditory-nerve fiber projections onto globular bushy cells. *Neuroscience* 136: 843–863, 2005.
- Taschenberger H, Leao RM, Rowland KC, Spirou GA, von Gersdorff H.** Optimizing synaptic architecture and efficiency for high-frequency transmission. *Neuron* 36: 1127–1143, 2002.
- Taschenberger H, Scheuss V, Neher E.** Release kinetics, quantal parameters and their modulation during short-term depression at a developing synapse in the rat CNS. *J Physiol* 568: 513–537, 2005.
- Taschenberger H, von Gersdorff H.** Fine-tuning an auditory synapse for speed and fidelity: developmental changes in presynaptic waveform, EPSC kinetics, and synaptic plasticity. *J Neurosci* 20: 9162–9173, 2000.
- Thompson AM, Schofield BR.** Afferent projections of the superior olivary complex. *Microsc Res Tech* 51: 330–354, 2000.
- von Gersdorff H, Borst JG.** Short-term plasticity at the calyx of Held. *Nat Rev Neurosci* 3: 53–64, 2002.
- von Gersdorff H, Schneggenburger R, Weis S, Neher E.** Presynaptic depression at a calyx synapse: the small contribution of metabotropic glutamate receptors. *J Neurosci* 17: 8137–8146, 1997.
- Wang LY, Kaczmarek LK.** High-frequency firing helps replenish the readily releasable pool of synaptic vesicles. *Nature* 394: 384–388, 1998.
- Wu LG, Borst JG.** The reduced release probability of releasable vesicles during recovery from short-term synaptic depression. *Neuron* 23: 821–832, 1999.
- Wu SH, Kelly JB.** Response of neurons in the lateral superior olive and medial nucleus of the trapezoid body to repetitive stimulation: intracellular and extracellular recordings from mouse brain slice. *Hear Res* 68: 189–201, 1993.

CHAPTER 4

Inhibiting the Inhibition: A Neuronal Network for Sound Localization in Reverberant Environments

Michael Pecka,^{1*} Thomas P. Zahn,^{1*} Bernadette Saunier-Rebori,^{1*} Ida Siveke,¹ Felix Felmy,¹ Lutz Wiegrebe,¹ Achim Klug,¹ George D. Pollak,² and Benedikt Grothe¹

¹Division of Neurobiology, Department of Biology II, Ludwig-Maximilians-Universität Munich, D-82152 Martinsried, Germany, and ²Section of Neurobiology, The University of Texas at Austin, Austin, Texas 78712

The precedence effect describes the phenomenon whereby echoes are spatially fused to the location of an initial sound by selectively suppressing the directional information of lagging sounds (echo suppression). Echo suppression is a prerequisite for faithful sound localization in natural environments but can break down depending on the behavioral context. To date, the neural mechanisms that suppress echo directional information without suppressing the perception of echoes themselves are not understood. We performed *in vivo* recordings in Mongolian gerbils of neurons of the dorsal nucleus of the lateral lemniscus (DNLL), a GABAergic brainstem nucleus that targets the auditory midbrain, and show that these DNLL neurons exhibit inhibition that persists tens of milliseconds beyond the stimulus offset, so-called persistent inhibition (PI). Using *in vitro* recordings, we demonstrate that PI stems from GABAergic projections from the opposite DNLL. Furthermore, these recordings show that PI is attributable to intrinsic features of this GABAergic innervation. Implementation of these physiological findings into a neuronal model of the auditory brainstem demonstrates that, on a circuit level, PI creates an enhancement of responsiveness to lagging sounds in auditory midbrain cells. Moreover, the model revealed that such response enhancement is a sufficient cue for an ideal observer to identify echoes and to exhibit echo suppression, which agrees closely with the percepts of human subjects.

Key words: echo suppression; precedence effect; Clifton effect; GABA; dorsal nucleus of the lateral lemniscus; inferior colliculus; binaural processing; modeling; persistent inhibition

Introduction

Faithful localization of an initial sound source in the presence of a multitude of its echoes is a fundamental challenge to our auditory system. The system copes with this challenge by suppressing the directional information of echoes (echo suppression) without eliminating their overall perception. Thus, we are aware of the presence of echoes but do not localize them. This phenomenon is referred to as “precedence effect” and applies when lagging sounds trail leading sounds in the range of 2 to 10–20 ms (depending on the nature of the sound). Two sounds delayed by <2 ms are spatially fused and are heard as a single sound located midway between the two. Sounds temporally segregated by >10–20 ms exceed the so-called “echo threshold” and are perceived as independent entities with their own spatial location (Zurek, 1987; Blauert, 1997; Litovsky et al., 1999). Moreover, depending on the context, echo suppression can break down

[“Clifton effect” (Clifton, 1987)], indicating facultative processing of echoes in higher brain centers.

The neural mechanisms underlying the precedence effect have to match three criteria: first, the circuitry has to be part of the binaural system, because interaural disparities are the main cues for sound localization (Rayleigh, 1907; Erulkar, 1972). Second, it has to operate on a time scale in the range of ~2–20 ms, hence on a different time scale than the binaural disparity detectors, which operate on a microsecond time scale. Third, the circuitry must be able to either specifically suppress the directional information of the trailing sound or identify and tag it as an echo for additional context-dependent processing.

A candidate circuitry that matches at least two of these criteria has been described for echo-locating bats (Pollak, 1997). The key structure in this circuit is the dorsal nucleus of the lateral lemniscus (DNLL) (Fig. 1). First, many DNLL neurons respond to sounds from the contralateral ear but are inhibited by sounds from the ipsilateral ear and thus are sensitive to interaural intensity differences (IIDs), a feature they inherit from the lateral superior olive (LSO) (Glendenning et al., 1981; Shneiderman et al., 1988). Second, in bats, DNLL neurons display an additional characteristic not known from the LSO: depending on the spatiotemporal succession of stimuli, their response can be suppressed for tens of milliseconds as a result of GABAergic inhibition (Yang and Pollak, 1994a,b, 1998; Burger and Pollak, 2001). It has been hypothesized that such “persistent inhibition” (PI) is derived

Received Sept. 7, 2006; revised Jan. 9, 2007; accepted Jan. 11, 2007.

This work was supported by The Max Planck Society (B.G.), the German Research Foundation (Grants Gr1205/12-1 and GRK 1091), and the Bernstein Center for Computational Neuroscience. We thank R. Michael Burger and H. von Gersdorff for helpful discussions and comments on this manuscript. We also thank Hamish Meffin for his assistance on the quantification of the model readout as well as for helpful comments.

*M.P., T.P.Z., and B.S.-R. contributed equally to this work.

Correspondence should be addressed to Prof. Dr. Benedikt Grothe, Department of Biology II, Biocenter, Ludwig-Maximilians-University of Munich, Grosshaderner Strasse 2, D-82152 Martinsried, Germany. E-mail: grothe@lmu.de.

DOI:10.1523/JNEUROSCI.5335-06.2007

Copyright © 2007 Society for Neuroscience 0270-6474/07/271782-09\$15.00/0

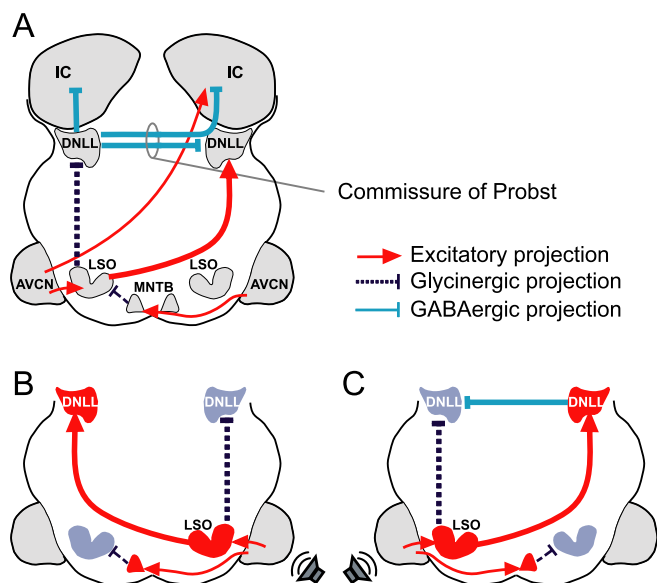


Figure 1. The DNLL circuit. **A**, DNLL neurons are excited by contralateral sounds via an excitatory input from the contralateral LSO. Additionally, they receive two inhibitory inputs driven by ipsilateral sounds, one from the ipsilateral LSO (glycinergic) and one from the contralateral DNLL (GABAergic). DNLL neurons send inhibitory (GABAergic) projections to the opposite DNLL and to the IC on both sides. LSO cells are driven by ipsilateral stimulation (via AVCN) and inhibited by contralateral stimuli (via AVCN and the glycinergic MNTB). The AVCN also sends excitatory projections to the contralateral IC. **B**, For sounds that are louder on the right ear (indicated by the loudspeaker symbol), the left DNLL is excited by the right LSO. The left LSO gets inhibited by sounds from the right via the left MNTB, which is innervated by the right AVCN. **C**, For sounds that are louder on the left ear, the left DNLL is inhibited by the left LSO. The left LSO also sends excitatory projections to the right DNLL, which then provides an additional inhibition to the left DNLL. MNTB, Medial nucleus of the trapezoid body.

from the opposite DNLL via the commissure of Probst (Yang and Pollak, 1998) (Fig. 1A).

Here, we show the existence of PI in the DNLL of the Mongolian gerbil, a choice mammalian animal model for high- and low-frequency hearing, and prove that its cellular basis derives from GABAergic innervation provided by the opposite DNLL. Based on these findings, we developed a model that explains how the DNLL output can generate context-dependent suppression of directional information of lagging sounds in the auditory mid-brain. Finally, we report results from a psychophysical echo-suppression test with human subjects that closely matches the predictions of the model.

Materials and Methods

In vivo recordings. All experiments were approved according to the German Tierschutzgesetz (AZ 211-2531-40/01). Mongolian gerbils (*Meriones unguiculatus*; 2–3 months of age) were anesthetized by an initial intraperitoneal injection (0.5 ml/100 g of body weight) of a physiological NaCl solution containing ketamine (20%) and xylazine (2%), with supplementary doses of 0.05 ml of the same mixture given subcutaneously every 30 min. The animal was then transferred to a sound-attenuated chamber and mounted in a custom-made stereotaxic instrument (Schulter et al., 1986). A small hole was cut into the skull ($\sim 1 \text{ mm}^2$), and the dura was removed. Ringer's solution was frequently applied to the opening to prevent dehydration of the brain. Constant body temperature ($37\text{--}39^\circ\text{C}$) was maintained using a thermostatically controlled heating blanket. After recordings (10–12 h), the animals were killed (injection of 0.2 ml of T61). For some recording sessions, current-induced lesions (5 mA for 5 s) using metal electrodes (5 M Ω) were made to mark the recording site after successful experiments. The brains of these animals were fixed, sliced, and Nissl stained by standard methods.

Acoustic stimuli were digitally generated at a sampling rate of 50 kHz

by TDT System III (Tucker-Davis Technologies, Alachua, FL), converted to analog signals (DA3-2/RP2-1; Tucker-Davis Technologies), attenuated (PA5; Tucker-Davis Technologies), and delivered to the earphones [Stereo Dynamic Earphones (MDR-EX70LP; Sony, Tokyo, Japan) or EC1 electrostatic speaker (Tucker-Davis Technologies); for details and calibration procedures, see Siveke et al. (2006)]. All signals had rise-fall times (RFTs) of 5.0 ms and were presented at a repetition rate of 4 Hz unless stated differently. Action potentials from single cells were recorded extracellularly using tungsten electrodes (5 M Ω ; World Precision Instruments, Berlin, Germany) or glass electrodes filled with 1 M NaCl ($\sim 10 \text{ M}\Omega$). The recording electrode was advanced under remote control, using a motorized micromanipulator (Digimatic; Mitutoyo, Neuss, Germany) and a piezodrive (Inchworm controller 8200; EXFO Burleigh Products Group, Fishers Victor, NY). Spikes were amplified, filtered, and fed to an analog-to-digital converter (RP2-1; Tucker-Davis Technologies), and the digitized signals were fed to the computer. To search for acoustic responses, 200 ms uncorrelated noise bursts were delivered binaurally with equal intensities at the two ears (IID = 0 dB). When a neuron was encountered, its best frequency (BF) (the frequency that elicited response at the lowest intensity) and absolute threshold were determined audiovisually (IID = 0). BFs ranged from 650 Hz to 18 kHz. Sixty-four percent of the neurons (32 of 50) were tuned to “high” frequencies (BF > 2 kHz). Binaural and monaural pure tones were presented to determine the binaural properties of the neuron. IID sensitivity was assessed by holding the intensity on the excitatory ear constant at 20 dB above the threshold of the cells while varying the intensity on the inhibitory ear in 10 dB steps between 10 dB below and 50 dB above threshold. Neurons were defined as IID sensitive if ipsilateral stimulation at BF reduced the maximal response elicited by contralateral stimulation by >50%.

To test an IID-sensitive neuron for PI, we evoked a steady response by presenting a tone burst (200 ms at BF) at 20 dB above threshold on the excitatory ear. Additionally, we presented shorter tone bursts (10 or 20 ms at BF) with several different intensities on the inhibitory ear midway through the excitatory stimulus. Stimuli were \cos^2 -function gated with RFTs of 5 ms for the contralateral and 2 ms for the ipsilateral side (if not stated otherwise). A DNLL neuron was defined as persistently inhibited if the duration of total suppression of responses to contralateral stimulation exceeded ipsilateral stimulus duration by at least 5 ms. The duration of PI was evaluated from peristimulus-time histograms of 1 ms bin width.

In vitro recordings. Coronal slices of DNLL were prepared from 14- to 19-d-old Mongolian gerbils (*M. unguiculatus*). Animals were anesthetized by isoflurane inhalation (Isofluran Curamed; Curamed Pharma, Karlsruhe, Germany) and decapitated. The brainstem was dissected out in ice-cold dissection Ringer's solution [(in mM) 125 NaCl, 2.5 KCl, 1 MgCl₂, 0.1 CaCl₂, 25 glucose, 1.25 NaH₂PO₄, 25 NaHCO₃, 0.4 ascorbic acid, 3 myo-inositol, and 2 pyruvic acid; all chemicals from Sigma (Deisenhofen, Germany)]. Sections of 200 μm were cut with a vibratome (VT1000S; Leica, Nussloch, Germany). Slices were transferred to an incubation chamber containing extracellular solution (ECS) [(in mM) 125 NaCl, 2.5 KCl, 1 MgCl₂, 2 CaCl₂, 25 glucose, 1.25 NaH₂PO₄, 25 NaHCO₃, 0.4 ascorbic acid, 3 myo-inositol, and 2 pyruvic acid; all chemicals from Sigma], bubbled with 5% CO₂–95% O₂, and incubated for 1 h at 37°C .

All recordings were performed at $\sim 36^\circ\text{C}$. After incubation, slices were transferred to a recording chamber and continuously superfused with ECS at 3–4 ml/min through a gravity-fed perfusion system. DNLL neurons were viewed at $40\times$ through a Zeiss (Oberkochen, Germany) Axioskop 2 FS microscope equipped with differential interference contrast optics. Whole-cell recordings were made with an EPC 10 double amplifier (HEKA Instruments, Lambrecht/Pfalz, Germany). Signals were filtered at 5–10 kHz and subsequently digitized at 20–100 kHz using Patchmaster version 2.02 software (HEKA Instruments). During recordings, series resistance was compensated electronically up to 60% to achieve a remaining series-resistance error <4 M Ω . All voltages are corrected for the junction potentials of the two different intracellular solutions.

Whole-cell recordings were performed with the following intracellular solutions (in mM): for current clamp, 125 K-gluconate, 5 KCl, 10 HEPES, 1 EGTA, 10 sodium-phosphocreatine, 2 Na₂-ATP, 2 Mg-ATP, 0.3 Na₂-

GTP, pH adjusted to 7.25 (all chemicals from Sigma); and for voltage clamp, 140 CsCl, 10 HEPES, 10 EGTA, 2 NaCl, 1 CaCl₂, 2 Mg-ATP, 0.3 Na₂-GTP, pH adjusted to 7.3 (all chemicals from Sigma). The Cl[−] reversal potential was estimated to be at +2 mV. Because of a holding potential of −60 mV, GABAergic chloride currents are reported as inward currents. During all recordings, 500 nM strychnine hydrochloride (Sigma) and 2.5 mM kynurenic acid were added to the bath to block glycinergic and glutamatergic transmission, respectively. During voltage-clamp recordings, 5 mM QX-314 (lidocaine *N*-ethyl bromide; Alomone Labs, Jerusalem, Israel) was added to the intracellular solution to block sodium channels, preventing action potential generation.

Synaptic currents were elicited by stimulation of the commissure of Probst with a 5 MΩ bipolar stimulation electrode (matrix electrodes with 270 μm distance; FHC, Bowdoinham, ME). Stimuli were 100-μs-long square pulses adjusted to elicit maximal responses (35–90 V) and were delivered with an STG 2004 computer-controlled four-channel stimulator (Multichannel Systems, Reutlingen, Germany) and a stimulation isolation unit (Iso-Flex; AMPI, Jerusalem, Israel).

Model. The model of the auditory brainstem is based on computational models of dynamic spiking neurons that were developed by T. P. Zahn. The cochlea base element contains a filter cascade of second-order all-pole gammatone filters (Lyon, 1997) corresponding to 16 different locations along the basilar membrane. The outputs of each of the 16 filter channels were fed to 16 hair-cell models that generated oscillatory potentials for each frequency channel (2–8 kHz). Their amplitude, phase, and frequency are coded by spike trains in the auditory nerve fibers generated by three sets of ganglion cells for each frequency channel. Thus, each of the modeled nuclei in the auditory brainstem contains 16 cell models, each tuned to a different frequency.

The neural modeling approach that we used, termed Spike Interaction Model (SIM), uses the precise spatiotemporal interaction of single spike events for coding and processing of neural information. SIM can identify and code phase, frequency, and amplitude dynamics on the time resolution of 10 μs. The model exclusively uses single spike events for information coding, transfer, and interpretation. The basic elements are integrate-and-fire neurons extended by specially designed dynamic transfer functions. SIM extends the kernel transfer function of synapses and neurons by dynamic properties, leading to nonuniform dynamic responses depending on the firing history of the elements and their surroundings. The main synaptic features simulated for each synapse were depolarization time and slope, repolarization time and slope, transmitter availability, and overall synaptic efficiency. The dynamic features of the cells included dendritic delay and decay, dendritic spatial and temporal summation, somatic summation, dynamic firing threshold of the axon hillock, afterhyperpolarization, and axonal delay. The SIM model that we used consists exclusively of Neural Base Elements of a specifically designed Neural Base Library that extends the commercially available environment of MATLAB/Simulink (The MathWorks, Natick, MA) by a set of neural models intended to simulate the intrinsic dynamic properties of neurons, synapses, dendrites, and axons. To create PI in the model DNLL neurons, hyperpolarization of the cell membrane potential caused by the inhibitory inputs of the contralateral DNLL and ipsilateral LSO were modeled with different time constants of 12 and 5 ms, respectively. Detailed information about model parameters can be found in supplemental Tables 1 and 2 (available at www.jneurosci.org as supplemental material) [for additional details, see Zahn et al. (1997) and Zahn (2003)].

To quantify the responses of the left and right model inferior colliculi (ICs) for the first and the second signal independently, we used discrete time bins in which spikes were counted. Time bins were of the same duration as the signals. For delays in which the leading and lagging signal were partially overlapping, only nonoverlapping periods of the respective time bins were quantified. Responses to 12 distinct recordings were averaged for each lead–lag delay. We determined the ratios of average responses of the left and right model IC in the respective time bins for all delays. The leading signal was always presented from the left, and the lagging signal was always presented from the right. To create an ideal observer, we introduced a directional sensor that assigned “right” to the lagging sound if the ratio of left-to-right IC response was ≥ 2 , thereby modeling the ability of a listener to localize the lagging sound. For smaller

ratios, the sensor assigned “left” to the signal to model a listener’s perception of the lagging sound at the location of the leading sound as a result of spatial fusion. Use of this particular threshold provided the best match to the perceptual data.

Psychoacoustical experiment. The psychophysical experiments were designed to determine both the detection and localization ability of a lagging tone burst. Binaural free-field tone bursts with a frequency of 4 kHz (10 ms in duration; 2 ms RFT) were computer generated, digital–analog converted (Fireface 800; RME-Audio, Haimhausen, Germany), amplified (TA-FE 330R; Sony), and broadcast by two speakers [Canton (Weilrod, Germany) Plus XS], located 45° to the left and right of the head of the subject at a distance of 1.5 m in a sound-attenuated, anechoic chamber (2 × 3 × 2.2 m). The tone bursts from the speakers were identical, except that the leading signal was always broadcast from the left speaker. The delays between the left and right speaker were varied from 0.5 to 32 ms in 13 steps with exponential increments. Stimuli were presented at an average level of 80 dB SPL, randomly roving within ± 10 dB.

The experiment was executed in two versions with identical stimuli but with different instructions given to the listeners: in the first version, listeners were instructed to indicate whether a second tone burst with a distinct location was perceived. In the second version, listeners were instructed to indicate whether one or two tone bursts were perceived, independent of location. Whereas the first version leads to an estimate of echo threshold as defined by Blauert (1997) and Litovsky et al. (1999), the second instruction leads to an estimate of lag detectability. The lead–lag delay for each trial was selected at random from the 13 delays. For each delay and experimental version, 33 decisions were obtained.

Ten normal-hearing listeners (two female, eight male; 25–46 years of age) completed both versions of the experiment. Performance was averaged across listeners, and a sigmoid function was fitted to the psychometric function. The 50% values of these fits were taken as threshold.

The signals as they arrived at the ears of the subjects were recorded by two Sennheiser (Old Lyme, CT) K6 capacitor microphones placed directly between the tragus and the antitragus of the subjects’ ears. The shadowing of the head and ears created an interaural level disparity of ~ 13 dB at 4 kHz. The signals recorded from the microphone in each ear were amplified (Eurorack MX 802A; Behringer, Willich, Germany), digitized (Digi 96/8 PST Sound Card; RME-Audio), and stored as stereo .wav files. Subsequently, the stored files were converted into a MATLAB-readable format, digitally amplified, and fed to the left and right inputs of the model.

Results

In vivo physiology reveals persistent inhibition

We tested 70 neurons in the left DNLL of Mongolian gerbils, of which 70% exhibited PI. All of these neurons responded to monaural tones at the right ear with sustained discharge trains that had durations that match the duration of the tone bursts evoking them. When neurons were stimulated binaurally, the discharges evoked by stimulation of the right ear were progressively suppressed by increasing stimulus intensities at the left ear and thus were sensitive to IIDs. On average, neurons exhibited 50% reduction in spike rate at an IID of 3.3 ± 1.3 (SEM) dB. The average difference between the IID eliciting maximal and the IID eliciting minimal spike counts was 29.8 ± 2 (SEM) dB ($n = 41$). Because these DNLL neurons were excited by sound from the right ear and inhibited by the left ear, they are termed excitatory/inhibitory (EI).

We evaluated PI in 30 DNLL neurons by driving the cells with a 200 ms tone burst at the BF of the neuron presented to the excitatory ear, while simultaneously presenting a 20 ms BF tone burst to the inhibitory ear, temporally embedded in the long stimulus (Fig. 2A). The intensity of the long, excitatory tone burst was held constant, whereas the intensity of the shorter, inhibitory tone was varied from 20 dB below to 20 dB above the intensity at the excitatory ear (Fig. 2A). With increasing levels of the inhibitory tone burst, a progressive suppression was evident as gaps in

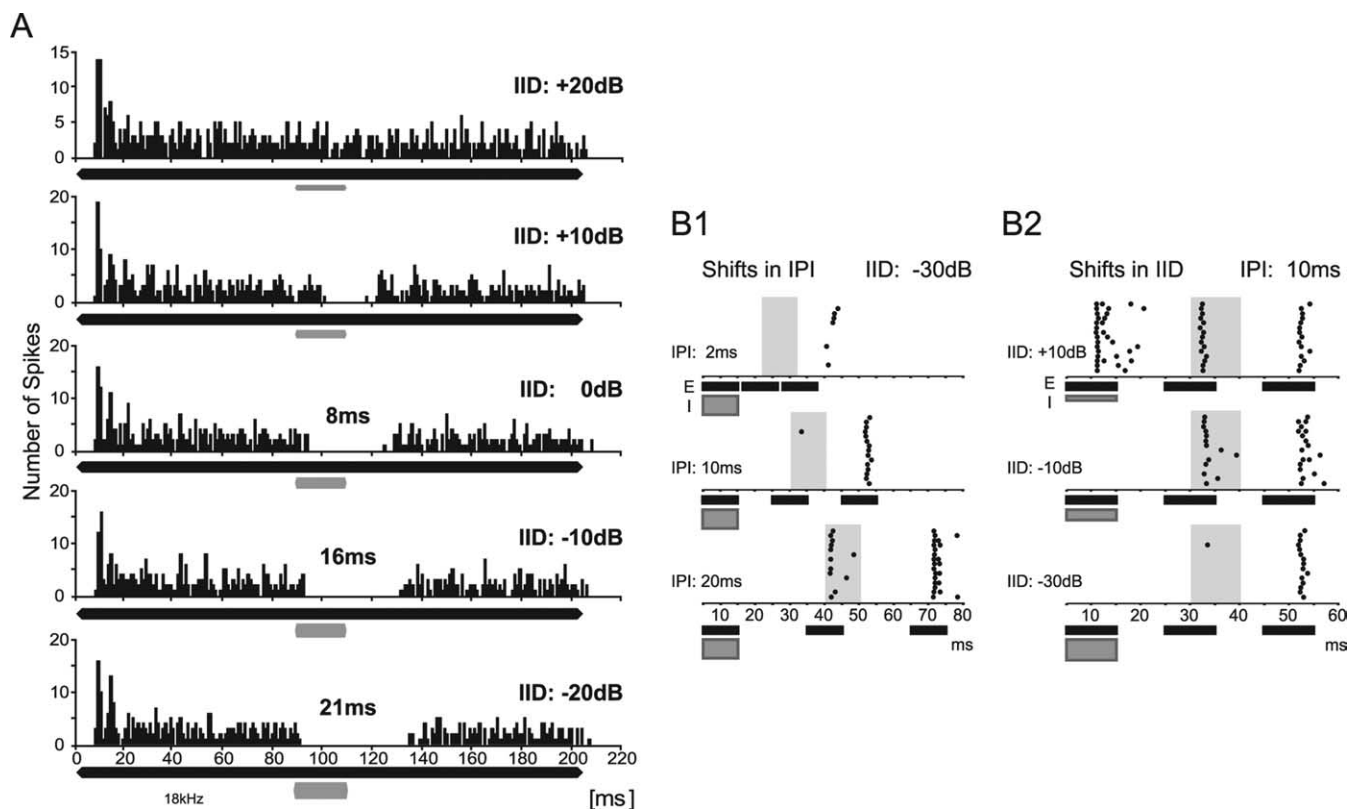


Figure 2. PI evoked *in vivo* by ipsilateral stimulation. **A**, Peristimulus-time histograms (bin size, 1 ms) showing the responses of a DNLL neuron to an excitatory pure tone on the right ear (200 ms at BF of 18 kHz; 20 dB above threshold; black bar) plus a 20-ms-long inhibitory tone burst on the left ear (at BF; gray bar) delayed by 90 ms. Sound intensity on the left ear was varied in 10 dB steps to create IIDs between +20 dB (louder on the right ear) and -20 dB (louder on the left ear). At an IID of +20 dB (top), the neuron exhibited a sustained response during the entire duration of the excitatory stimulus. By increasing the intensity at the inhibitory ear by 10 dB (IID, +10 dB; second panel), the response was suppressed for the duration of the inhibitory stimulus. At an IID of 0 dB, the duration of inhibition increased to 28 ms, persisting 8 ms longer than the inhibitory stimulus (20 ms) (third panel). The duration of PI was further increased to 16 and 21 ms for IIDs of -10 and -20 dB, respectively (fourth and fifth panels). **B**, Suppression of responses to trailing sounds. **B1**, Dependency of PI on IPI. Raster displays of the responses to a sequence of three sounds are shown. First, a binaural sound favoring the left, inhibitory ear (IID, -30 dB; gray bar; I) was presented, followed by two monaural sounds presented only to the right, excitatory ear (black bars; E). Time periods during which responses to the first monaural excitatory sound were expected are illustrated by gray shaded areas. At an IPI of 2 ms (top), the neuron responded neither to the initial inhibitory sound nor to the first monaural sound at the right ear. The neuron responded weakly and with a long delay to the second monaural sound. At an IPI of 10 ms (middle), the response to the first monaural sound was still suppressed, and the response to the second monaural sound was strong and occurred with a short latency. For IPIs of 20 ms (bottom), the cell had overcome PI and responded to both monaural sounds at the right ear. **B2**, Dependency of PI on IID. Raster displays of the responses of the same neuron as in **B1** to different initial IIDs at a fixed IPI (10 ms). When the initial sound was presented at an IID of +10 dB, the neuron responded to all three stimuli. At an IID of -10 dB, the initial sound did not elicit a response, but the cell responded to both trailing monaural sounds (middle). At even more negative IIDs of the leading sound (bottom), PI was created by the leading sound, and hence the response to the first trailing sound was suppressed.

the spike trains that elongated with more negative IIDs. In the example neuron (Fig. 2), the maximal duration of spike suppression exceeded the inhibitory stimulus duration by 21 ms (IID = -20 dB) (Fig. 2A, bottom) (i.e., created PI of 21 ms). On average, the maximum duration of PI, derived from the PI duration at the most negative IID tested, was 17.4 ± 1.5 (SEM) ms, ranging between 6 and 38 ms ($n = 30$).

The above findings demonstrate that binaural sounds that favor the inhibitory ear (negative IIDs) create PI, which suppresses contralateral excitation several milliseconds longer than the duration of the sound. Thus, trailing excitatory sounds (simulating echoes) should be subject to similar suppression if they arrive within the time of PI. We presented a binaural sound (at BF; 10 ms) that favored the inhibitory ear and created PI in the cell followed by two monaural sounds (at BF; 10 ms) only presented to the excitatory ear at different interpulse intervals (IPIs). In Figure 2B1, the initial binaural sound with an IID of -30 dB was followed by two trailing, monaural sounds with a 2 ms IPI (top). Importantly, the PI created by the initial sound completely suppressed the responses to the first trailing sound (the periods for which responses to the first monaural sound were expected

are illustrated by the gray shaded areas) and also affected the response to the second trailing sound. As the IPI was lengthened to 10 ms (middle), the second trailing sound evoked robust discharges but not the first. The response to the first trailing sound only recovered when the IPI was 20 ms (bottom). Within our sample of neurons ($n = 20$), full recovery of the response to the first trailing sound ranged from 5 to 30 ms.

The suppression of responses to the trailing sounds was dependent on the IID of the initial sound (Fig. 2B2). When the IPI was held constant at 10 ms and the IID of the initial sound was positive, the discharges evoked by the trailing sounds were not suppressed. However, if the initial sound had a more negative IID than -10 dB, it generated a PI that suppressed the excitation evoked by the trailing sounds.

***In vitro* physiology identifies the source of persistent inhibition**

The *in vivo* results show that initial binaural signals with IIDs favoring the inhibitory ear generate PI at the DNLL in gerbils, similarly to bats (Pollak, 1997). The PI in the bat DNLL, moreover, has been shown to be mediated by GABAergic inhibition

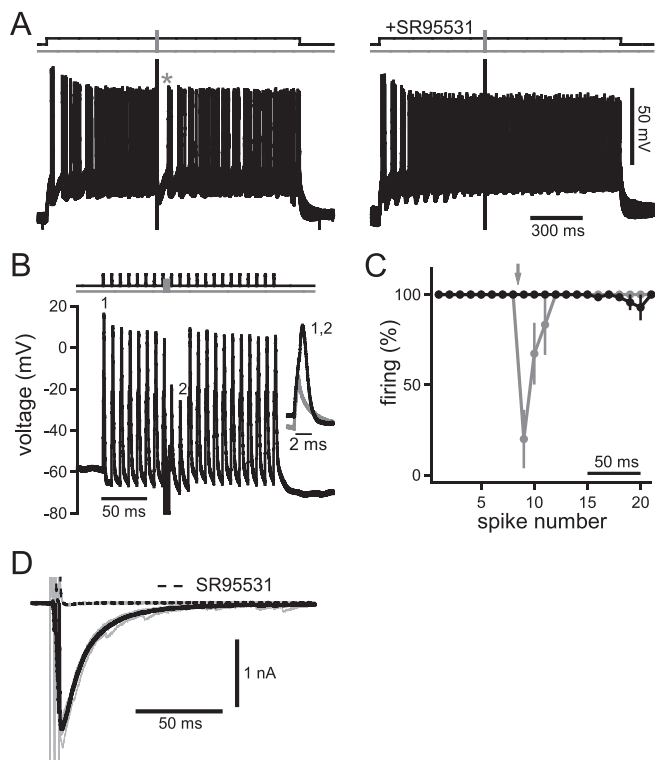


Figure 3. PI evoked *in vitro* by the contralateral GABAergic synaptic inputs. **A**, Overlay of 10 traces of current-clamp recording from a DNLL neuron. Spikes were elicited via a continuous current injection of 200 pA for 1500 ms (top, black line). The fibers of the commissure of Probst were stimulated with a short train of three pulses at 500 Hz (top, gray line) to activate the GABAergic inhibitory input from the contralateral DNLL. Left, After the end of the fiber stimulation, the cell showed persistent spike suppression (63.3 ms; indicated by asterisk). Right, Bath application of the GABA_A receptor blocker SR95531 eliminated spike suppression. **B**, Simulation of sound-evoked excitatory inputs by repetitive 0.5 ms current injections (1–2 nA; at 100 Hz; top, black line), each eliciting one action potential (first indicated as “1”). When the commissure was stimulated by the same three-pulse protocol used above (top, gray line), action potentials to the two following current injections were suppressed (second failure indicated as “2”). The inset shows blowups of the first spike (1) and the second failure (2). **C**, Firing probability of six neurons before and after the recruitment of the GABAergic inhibition by the three-pulse protocol (gray line and symbols). The fiber stimulation (as in **B**) is indicated by the arrow. Black line, Control without fiber stimulation showing the high spiking fidelity of the neurons. Spikes were elicited every 10 ms. Error bars represent SEM. **D**, Voltage-clamp recordings from a DNLL neuron showing inhibitory postsynaptic currents in response to the same three-pulse fiber stimulation described above. Fiber stimulation elicited an IPSC of ~2 nA whose decay could best be described by fitting a double exponential with time constants of 12.3 and 43.7 ms. Solid black line, Average of 10 traces; gray lines, single traces. The current could be blocked by SR95531 (dashed black line).

(Yang and Pollak, 1994b). Because the majority of inhibitory inputs to the DNLL arise from its contralateral counterpart (Glendenning et al., 1981; Shneiderman et al., 1988), the possibility is raised that PI is mediated by the opposite DNLL. However, no prolonged or strongly delayed firing, which could explain the persistent nature of the inhibition, has been observed (Covey, 1993; Bajo et al., 1998; Siveke et al., 2006). We therefore used *in vitro* whole-cell patch-clamp recordings to test the hypothesis that PI results from properties of the GABAergic transmission in the DNLL.

To imitate excitatory input to DNLL cells in the brain slices, action potentials were elicited via continuous current injections (Fig. 3A). Midway through the current injection, fibers in the commissure of Probst were stimulated with a short train of three pulses at 500 Hz. This procedure elicited apparent suppression of spikes (Fig. 3A, left, asterisk) for 55.6 ± 9.4 ms ($n = 11$) after the

end of the fiber stimulation. However, because of the underlying average firing frequency of the cells of 43.2 ± 10.3 Hz (resulting in interspike intervals of ~23 ms), the effective spike suppression was ~32 ms. Application of the GABA_A receptor blocker 2-(3-carboxyl)-3-amino-6-(4-methoxyphenyl)-pyridazinium bromide (SR95531) (Hamann et al., 1988) eliminated this PI ($n = 5$), indicating that it was caused by the GABAergic projections of the commissure of Probst (Fig. 3A, right). We next tested effects of PI on simulated sound-evoked phase-locked excitation. To do so, 0.5-ms-long current injections presented every 10 ms (100 Hz) were applied to the soma of principal DNLL neurons. Each of these simulated excitatory input trains was adjusted to elicit one action potential per pulse (Fig. 3B). Fiber stimulation of the commissure (three pulses at 500 Hz; 6 ms duration, as in Fig. 3A) elicited suppression of spikes for the following two current injections. Hence, PI lasted for at least 14 ms after cessation of fiber stimulation. On average, PI was found to last for 19.4 ± 3.2 ms at 90% recovery ($n = 6$) (Fig. 3C).

If PI is produced synaptically by GABAergic inhibition, the kinetics of postsynaptic GABA currents would resemble the time course of PI on a cellular level. We assessed the kinetics of GABAergic IPSC elicited by the same three-pulse fiber-stimulation paradigm as above. The IPSC decay of the example depicted in Figure 3D was best described by a double-exponential fit with fast and slow time constants of 12.3 and 43.7 ms, respectively. The average time constants were 12.6 ± 0.5 and 39.5 ± 5.1 ms ($n = 5$). In the same five cells, blocking GABA_A receptors with SR95531 reduced the IPSCs by $96.3 \pm 1.7\%$. Using one instead of three pulses yielded results (11.8 ± 1.1 ms for the slow and 26.6 ± 5.6 ms for the fast time constant; $n = 8$) that were not significantly different ($p_{\text{fast}} = 0.599$; $p_{\text{slow}} = 0.143$; two-tailed paired t test). Comparing the time course of spike suppression (Fig. 3A–C) and IPSC kinetics (Fig. 3D) suggests that the fast component of the IPSC is the main source of PI. In summary, our *in vitro* data suggest that GABAergic inhibition provided by the contralateral DNLL through the commissure of Probst is sufficient to explain PI.

Modeling the processing of binaural signals and “echoes”

The DNLL sends inhibitory projections mainly to the contralateral IC, the major integration site in the auditory midbrain. Thus, we next ask what effect PI has on the response of IC cells innervated by the DNLL. To predict responses of such IC cells to leading and trailing sounds, we used an SIM based on dynamic integrate-and-fire neurons, which interacted exclusively through single spike events (for details, see Materials and Methods). The model simulated the frequency decomposition and neural coding of sound stimuli into 16 tonotopically organized auditory nerve fibers for the left and right cochlea–ganglion complex separately. A tonotopic organization into 16 frequency channels (2–8 kHz) was maintained for all nuclei of the model, illustrated as horizontal block lines in Figure 4A. Sound-evoked spikes at both anteroventral cochlear nuclei (AVCNs) were transferred to LSO, DNLL, and IC via the known excitatory and inhibitory connections (Figs. 1, 4A). The model was restricted to a specific population of IC neurons, as described by pharmacological studies (Li and Kelly, 1992; Burger and Pollak, 2001): these IC cells receive an excitatory projection from the contralateral AVCN in combination with an inhibitory projection from the contralateral DNLL. This interaction creates EI properties, and hence IID sensitivity, in the IC *de novo*. PI was incorporated as an intrinsic feature of the DNLL–DNLL interaction via a slowly decaying hyperpolarization with a time constant of 12 ms, as determined *in vitro*. De-

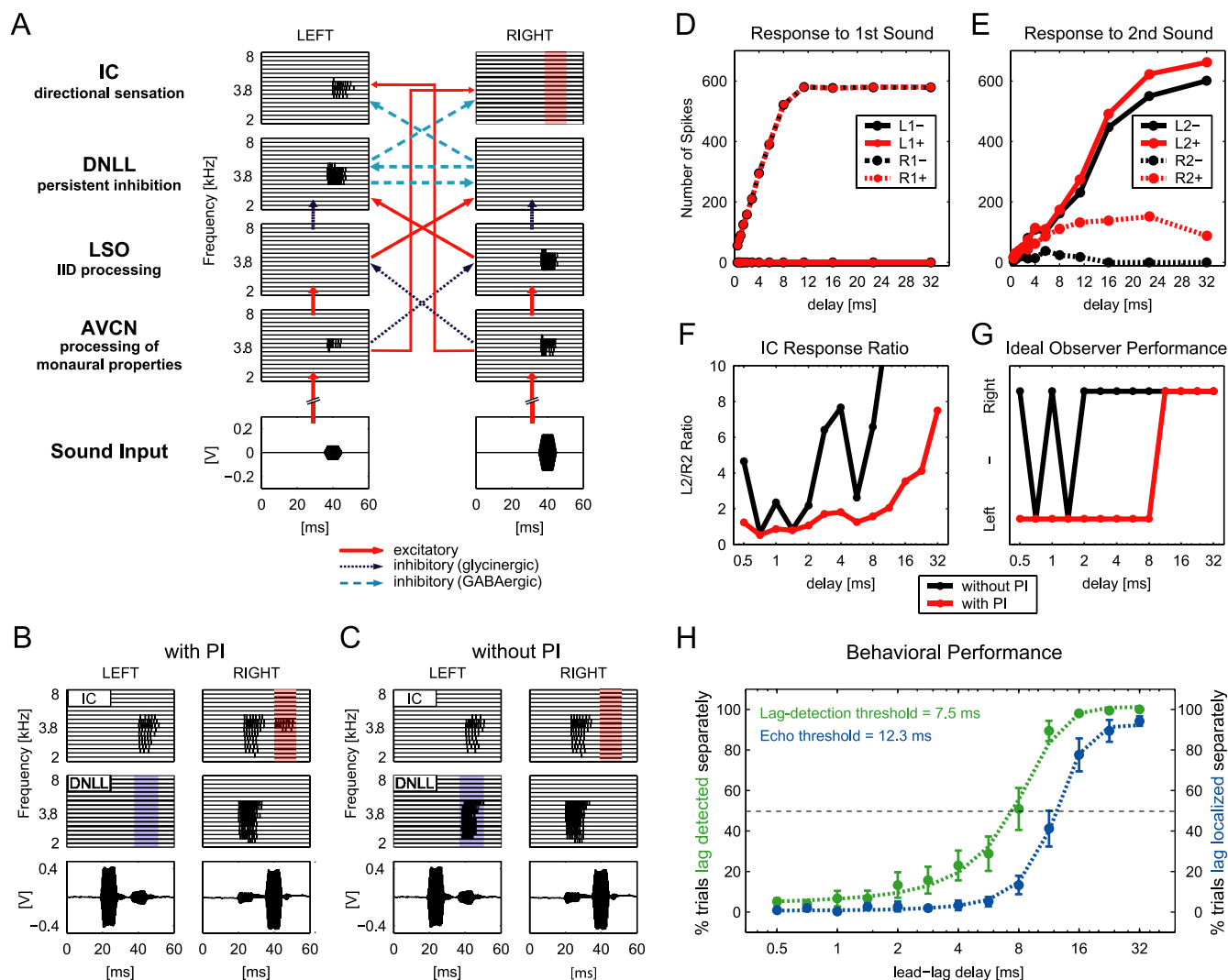


Figure 4. A model of the DNLL circuitry can explain human behavioral performance. **A**, Analogous to the auditory brainstem pathway, the model includes cochlear hair cells (data not shown) and four pairs of nuclei (left and right). Each nucleus is represented by 16 neurons (horizontal block lines), each tuned to a different frequency between 2 and 8 kHz. Spiking in each model neuron is represented by vertical lines. The stimuli are depicted at the bottom. For a detailed explanation, see Results. **B**, **C**, Model response pattern of DNLL and IC to two 4 kHz tone bursts recorded by microphones placed in the ears of a human subject. The two bursts were played from symmetric locations to the left and right side of the subject with a delay of 16 ms, left speaker leading. **B**, The first tone burst created PI in the left DNLL (blue shaded area), relieving the right IC of its inhibition. Thus, the right IC was able to respond to the second tone burst (red shaded area). **C**, When PI was removed from the model DNLL neurons, the second tone burst was able to elicit responses in the left DNLL (blue shaded area), which in turn suppressed responses to the second tone burst in the right IC (red shaded area). **D**, **E**, Quantitative analyses of IC response patterns. Average numbers of spikes evoked by the first and second tone burst are plotted. Spikes were counted independently in time slots of 10 ms in each IC for each tone burst. For delays in which the first and second tone burst partially overlapped in time, only nonoverlapping periods of the respective time slots were quantified. **D**, Response of the left and right IC to the leading sound did not change with and without PI. **E**, The right IC responded to the second tone burst when PI was included in the model (R2+; dashed red line). Without PI, no responses were elicited by the second tone burst in the right IC (R2-; dashed black line). **F**, Ratios of L2+/R2+ (red line) and L2-/R2- (black line) over different lead-lag delays. Values >10 are not shown. **G**, Localization performance of an ideal observer based on an L2/R2-ratio threshold equal to 2 with and without PI (red and black lines, respectively). **H**, Performance of 10 human subjects in a psychophysical lag-detection and echo-threshold test. The dashed green line depicts the fitted average response of all subjects when asked whether one or two tones were perceived (lag detection). The dashed blue line depicts the fitted average response of all subjects to the same stimuli when asked to indicate whether they were able to localize two tones with distinct locations (echo threshold). The dashed black line marks the 50% level. Green and blue symbols mark average responses of all subjects \pm SEM for the two tests, respectively.

tailed information about all model parameters can be found in supplemental Tables 1 and 2 (available at www.jneurosci.org as supplemental material). It is important to note that the model output was extremely robust to parameter variations. For instance, synaptic strength of the DNLL–DNLL inhibition may range between 0.1 and 0.5 to yield similar IC responses. Figure 4A shows the spike trains generated in each frequency channel of each nucleus up to the IC for a single digitally created binaural tone burst of 4 kHz favoring the right ear. Note that because of the inhibition from the left DNLL, the right IC does not respond to the sound (red shaded area), despite the monaural excitatory input from the left AVCN.

In Figure 4B, the model responses of DNLL and IC cells to two 10 ms binaural tone bursts separated by a delay of 16 ms (resulting in an IPI of 6 ms) are shown. The tone bursts were acoustic stimuli (10 ms; 4 kHz) recorded with probe microphones inserted into the ear canals of a human subject while the subject was performing a typical echo-detection task (see below). The first binaural tone burst had an IID of \sim 13 dB favoring the left ear, whereas the IID of the trailing sound favored the right ear (\sim 13 dB). Recall that IIDs that favor the right ear suppress responses in the right IC (Fig. 4A). In the modeled responses shown in Figure 4B, the first binaural sound favoring the left ear generated PI in the left DNLL. The trailing binaural sound had an IID that fa-

vored the right ear, and hence, should evoke a response in the left DNLL. However, because of the PI generated by the first sound, the left DNLL failed to respond to the trailing sound (blue shaded area). Therefore, it failed to inhibit the right IC, as it would without the preceding sound. As a consequence, the right IC responded to both the first and the trailing sound (red shaded area), although the second sound evoked no activity in the right IC when presented alone (compare Fig. 4A).

Thus, whether or not the IC responded to the trailing sound depended on its recent history, which was determined by the IID of the initial sound and its temporal separation from the trailing sound. These features are consistent with a previous study that determined responses to initial and trailing sounds in EI cells that are innervated by the DNLL in the IC of bats (Burger and Pollak, 2001). We used the model to investigate how the IC response patterns changed when PI was not incorporated as an intrinsic feature of the DNLL–DNLL interaction. The model predicts that the activation of the right IC in response to the second tone burst was dependent on PI in the left DNLL (Fig. 4C). Omitting PI from the model system enabled the left DNLL to respond to the trailing tone burst (blue shaded area). This activity in the left DNLL suppressed all responses to the trailing tone burst in the right IC (red shaded area).

We next tested different lead–lag combinations of delays between 0.5 and 32 ms (the left speaker always led) and quantified the IC responses in 10 ms bins. Response bins in the left IC to the leading and trailing tone bursts were termed L1 and L2, and responses in the right IC were termed R1 and R2. This analysis was performed with (+) and without (–) PI implemented in the model circuit. Figure 4D displays the averaged number of spikes in the left and right IC in response to the first tone burst for both conditions. A total alignment of the values for L1+ and L1– as well as for R1+ and R1– shows that the responses of both ICs to the first stimulus is unaffected by the exclusion of PI from the circuit. However, analysis of the response to the second tone burst revealed the significance of PI for the response formation in the IC (Fig. 4E). Although the left IC response to the trailing sound was similar for both model conditions (L2+ and L2–), there were substantial differences in the responses of the right IC to this signal with and without PI in the DNLL (R2+ and R2–). Because of PI in the left DNLL, the right IC was deprived of its inhibition by the left DNLL, enabling the trailing tone burst to elicit a substantial number of spikes in the right IC (R2+). If PI was removed from the model circuitry (R2–), no responses were elicited in the right IC. Importantly, the responses of neurons in the right IC to a sound favoring the right ear were not observed when presented alone (compare Fig. 4A), but only when a sound from the left preceded the sound from the right. Together, the model predicts that during PI in the DNLL, the contralateral IC displays an enhancement of responsiveness to trailing sounds that were not excitatory if presented alone.

We tested whether such response enhancement, which depends on the spatiotemporal stimulus configuration, would be a sufficient cue for higher-order centers to achieve suppression of directional information carried by trailing sounds based on IC rate code evaluation. Because we were particularly interested in the ability to localize a trailing signal (or the lack thereof), we calculated the ratio of responses to the trailing signal in the left IC to the responses to the trailing signal in the right IC (L2/R2) (Fig. 4F). Without PI (black line), the ratios changed even for very small delays from values >4 to ~ 1 . When PI was present (red line), the ratio was <2 for all delays smaller than 10 ms. Thus, because of PI, the right IC response was $>50\%$ of the response

observed in the left IC at small delays, although no response would be seen to the trailing sound in the right IC if presented alone.

We used the ratio data to introduce an ideal observer to the model. To do so, we established a localization threshold based on the ratios of responses in the two ICs to define localization capabilities. We chose a threshold of 2, meaning that for ratios of >2 (response in left IC at least twice as high as in right IC), the trailing sound was localized on the right side by the observer. For ratios <2 , the trailing sound was not localized but fused to the location of the leading sound on the left side (Fig. 4G). Clearly, Figure 4G shows that when PI was present in the model (red line), the trailing sound was not localized independently for delays ≤ 8 ms but fused to the location of the leading sound. At delays >8 ms, however, the ratio was >2 , enabling the ideal observer to localize the second sound. This continuity and unambiguity in the analysis was only seen when PI was included. Without PI, the ideal observer failed to identify the trailing sound as an echo and to suppress the directional information, even at very small delays. Thus, the ideal observer was able to exhibit suppression-like behavior of directional information of lagging sounds based on the response ratio between the ICs, which in turn was dependent on PI in the DNLL. It is noteworthy that regardless of the ratio threshold, such behavior of the observer was not achievable without PI.

Determination of echo threshold and lag-detection threshold of human subjects

Finally, we tested whether the time course of the suppression of directional information in lagging sounds of the ideal observer corresponds to human perception. Human listeners ($n = 10$) performed a perceptual free-field echo-threshold test, hearing the same sounds that were presented to the model. A leading sound was presented from a speaker 45° to the left from midline followed by a sound with varying delays between 0.5 and 32 ms from a speaker 45° to the right. The subjects had to indicate whether a second tone burst with a distinct location was perceived. The results of this perceptual test are depicted in Figure 4H (blue line). In most of the trials, subjects were not able to independently localize the trailing sound when it was delayed by 8 ms or less. In contrast, for delays of >16 ms, two sounds with distinct locations were perceived in most of the trials. The echo threshold of the 10 subjects for perceiving two tones with distinct locations (50% criterion) was a lead–lag delay of 12.3 ms. Evidently, the time course of suppression of directional information of lagging sounds was similar in ideal observer and human subjects [Fig. 4, compare G (red line), H (blue dashed line)].

The model also predicts that at lead–lag delays shorter than echo threshold, information about the presence of the lag is still existent at the level of the IC. Hence, the model predicts that human listeners should be able to detect lagging tones at delays shorter than the echo threshold. We tested this prediction by performing the same experiment as we did for echo-threshold determination but with different instructions given to the subjects: now, subjects had to indicate whether one or two tones were perceived, regardless of the ability to resolve their location. The average results of this lag-detection test are depicted in Figure 4H (green dashed line and symbols). The lag-detection threshold of the 10 subjects (50% criterion) was a lead–lag delay of 7.5 ms. Thus, on average, listeners were able to detect the presence of a lagging tone at delays almost 5 ms shorter than required for localizing the lagging tone (Fig. 4H, compare green and blue dashed lines).

Discussion

The DNLL fulfills the three criteria laid down in the introduction that characterize a circuit sufficiently to explain the context-dependent phenomenon of the precedence effect. First, as in other mammals, it is part of the binaural pathway and contains many EI cells (Brugge et al., 1970; Covey, 1993; Markovitz and Pollak, 1993; Kelly et al., 1998). Second, many EI cells in the gerbil DNLL show persistent inhibition evoked by binaural signals that favor the ear ipsilateral to the DNLL. This causes the suppression of lagging sounds that would normally evoke discharges. We suggest that PI is a feature of the auditory system in all mammals, because it now has been described in rodents (this study) as well as in bats (Yang and Pollak, 1994a; Burger and Pollak, 2001). Our *in vitro* recordings infer that PI is a feature of the GABAergic transmission of the commissure of Probst and, for the first time, imply a cellular basis for PI. Fiber stimulation persistently inhibited action potential generation by pulsed current injections for ~20 ms, similar to our observations under *in vivo* conditions (17 ms). Additional work has to identify presynaptic or postsynaptic cellular properties as the underlying source of PI. Third, implementing the DNLL circuitry (including its target cells in the IC) and the intrinsic features of the GABAergic inhibition into a model revealed IC response properties to lagging sounds that correspond to features of the precedence effect derived from human psychophysical studies.

The dynamic integrate-and-fire model accurately simulated the discharge patterns of neurons in each nucleus found in *in vivo* recordings, including the responses in the IC to trailing signals, which were virtually the same as those found in the IC of bats (Burger and Pollak, 2001). Moreover, the IC population response was sufficient to produce precedence-like precepts in an ideal observer similar to the percepts of human subjects when presented with the same stimuli. The model of the IC population response is oversimplified in that it only includes the inputs of one functional circuitry, and certainly the information that the IC presents to higher nuclei is far more complex than simulated (Aitkin, 1986). Nevertheless, the results provide strong evidence for the role of the DNLL in echo suppression and show the high potential of the model for predicting responses of auditory brainstem structures to all kind of complex stimuli.

The psychophysical results demonstrate that the stimuli used in the *in vivo* experiments do evoke precedence in human listeners. A direct comparison of lag-detection threshold and echo threshold with the exact same stimulation and listeners further shows that listeners can detect the presence of a lagging sound at considerably shorter delays than they can localize the lagging sound separately from the lead. These psychophysical findings are well reflected by the response behavior of our model, because IC responses to the lagging sound are present also at delays smaller than the ideal observer's echo threshold (compare Fig. 4E). Hence, the distinctive feature of our model is that information about a lagging sound is not suppressed at the level of the IC but rather echoes are identified as such by additional activity of a subpopulation of IC neurons.

Previous studies concerned with physiological mechanisms of the precedence effect have been mainly conducted in the IC of rabbits and cats (Yin, 1994; Fitzpatrick et al., 1995, 1999; Litovsky and Delgutte, 2002; Tollin et al., 2004). In those studies, the response to the lagging sound was suppressed by the leading sound, and the studies focused on the interstimulus delay at which the lag responses recovered. The assumption in those studies is that the suppression of the response to the trailing sound corresponds

to a change in the coding of the location of that sound source. The suppression of responsiveness to trailing sounds as a result of the presentation of a leading sound is exactly the opposite effect from that found in the bat IC and from the modeled IC responses we obtained in this study. Here, we showed an enhancement of the responsiveness to trailing sounds in IC neurons as a result of DNLL PI evoked by a leading sound. We suggest that these differences in IC responses evoked by similar stimulus configurations were a consequence of recordings from different types of IC cells. For instance, we focused on high-frequency EI cells, whereas the majority of cells reported in previous studies were tuned to low frequencies and were most likely EE cells. This is significant because the circuits that create the binaural properties of EE cells are different from those that create EI cells. One recent study from behaving cats showed suppression of responses to trailing sounds in high-frequency IC cells (Tollin et al., 2004). However, these cells responded briskly to sounds presented from the ipsilateral and contralateral side and therefore were not EI and not processed by the IID circuitry. This difference in the processing of high- and low-frequency stimuli is also noteworthy in regard to psychophysical experiments. We conducted our tests using 4 kHz tones, which forced the subjects to use IID cues processed by EI neurons of the LSO. In contrast, many previous studies used broadband signals (cf. Blauert, 1997), in which substantial energy is present in low-frequency bands, and therefore spatial processing is dominated by the EE circuitry via the medial superior olive.

Our interpretation of these results is that correlates of precedence at the IC are a consequence of multiple processes. The periods of suppression of responses to trailing sounds in some types of IC cells is one feature that contributes to precedence (Yin, 1994; Fitzpatrick et al., 1995, 1999; Litovsky and Delgutte, 2002; Tollin et al., 2004). However, such a mechanism alone cannot account for the fact that the precedence effect is facultative. For example, in humans, precedence breaks down when the lead-lag arrangement is switched [Clifton effect (Clifton, 1987)]. In bats, echo suppression occurs while the animal is passively listening to communication calls (Schuchmann and Wiegand, 2005), but not while bats are actively echo locating (Schuchmann et al., 2006).

Our model suggests an alternative or additional mechanism that is compatible with the context-dependent nature of the precedence effect. The model shows how PI in the DNLL could change the coding of directional information conveyed by lagging sounds in IC cells whose EI properties are formed or shaped by DNLL projections. The circuitry is reconfigured by the initial sound such that the neurons respond to lagging sounds from spatial positions that would not elicit responses to single sounds. Hence, compared with leading sounds, the IC population response to a trailing sound contains an additional subgroup of firing neurons. Higher centers should be able to interpret this additional firing as a tag indicating an echo. Because other parallel pathways still convey the binaural information, the system thereby can weight spatial information in a context-dependent manner.

References

- Aitkin L (1986) The auditory midbrain: structure and function of the central auditory pathway. Clifton, NJ: Humana.
- Bajo VM, Villa AE, de Ribaupierre F, Rouiller EM (1998) Discharge properties of single neurons in the dorsal nucleus of the lateral lemniscus of the rat. *Brain Res Bull* 47:595–610.
- Blauert J (1997) Spatial hearing with multiple sound sources and in en-

- closed spaces. In: *Spatial hearing: the psychophysics of human sound localization* (revised edition), pp 201–287. Cambridge, MA: MIT.
- Brugge JF, Anderson DJ, Aitkin LM (1970) Responses of neurons in the dorsal nucleus of the lateral lemniscus of cat to binaural tonal stimulation. *J Neurophysiol* 33:441–458.
- Burger RM, Pollak GD (2001) Reversible inactivation of the dorsal nucleus of the lateral lemniscus reveals its role in the processing of multiple sound sources in the inferior colliculus of bats. *J Neurosci* 21:4830–4843.
- Clifton RK (1987) Breakdown of echo suppression in the precedence effect. *J Acoust Soc Am* 82:1834–1835.
- Covey E (1993) Response properties of single units in the dorsal nucleus of the lateral lemniscus and paralemniscal zone of an echolocating bat. *J Neurophysiol* 69:842–859.
- Erulkar SD (1972) Comparative aspects of sound localization. *Physiol Rev* 52:237–360.
- Fitzpatrick DC, Kuwada S, Batra R, Trahiotis C (1995) Neural responses to simple simulated echoes in the auditory brain stem of the unanesthetized rabbit. *J Neurophysiol* 74:2469–2486.
- Fitzpatrick DC, Kuwada S, Kim DO, Parham K, Batra R (1999) Responses of neurons to click-pairs as simulated echoes: auditory nerve to auditory cortex. *J Acoust Soc Am* 106:3460–3472.
- Glendenning KK, Brunso-Bechtold JK, Thompson GC, Masterton RB (1981) Ascending auditory afferents to the nuclei of the lateral lemniscus. *J Comp Neurol* 197:673–703.
- Hamann M, Desarmenien M, Desaulles E, Bader MF, Feltz P (1988) Quantitative evaluation of the properties of a pyridazinyl GABA derivative (SR 95531) as a GABAA competitive antagonist. An electrophysiological approach. *Brain Res* 442:287–296.
- Kelly JB, Buckthought AD, Kidd SA (1998) Monaural and binaural response properties of single neurons in the rat's dorsal nucleus of the lateral lemniscus. *Hear Res* 122:25–40.
- Li L, Kelly JB (1992) Inhibitory influence of the dorsal nucleus of the lateral lemniscus on binaural responses in the rat's inferior colliculus. *J Neurosci* 12:4530–4539.
- Litovsky RY, Delgutte B (2002) Neural correlates of the precedence effect in the inferior colliculus: effect of localization cues. *J Neurophysiol* 87:976–994.
- Litovsky RY, Colburn HS, Yost WA, Guzman SJ (1999) The precedence effect. *J Acoust Soc Am* 106:1633–1654.
- Lyon RF (1997) All-pole models of auditory filtering. In: *Diversity in auditory mechanics*, pp 205–211. Hackensack, NJ: World Scientific Publishing.
- Markovitz NS, Pollak GD (1993) The dorsal nucleus of the lateral lemniscus in the mustache bat: monaural properties. *Hear Res* 71:51–63.
- Pollak GD (1997) Roles of GABAergic inhibition for the binaural processing of multiple sound sources in the inferior colliculus. *Ann Otol Rhinol Laryngol* 106:44–54.
- Rayleigh L (1907) On our perception of sound direction. *Philos Mag* 13:214–232.
- Schuchmann M, Wiegand L (2005) Echo suppression in echolocating bats: influence of semantic meaning? *Assoc Res Otolaryngol Abstr* 28:958.
- Schuchmann M, Hubner M, Wiegand L (2006) The absence of spatial echo suppression in the echolocating bats *Megaderma lyra* and *Phyllostomus discolor*. *J Exp Biol* 209:152–157.
- Schuller G, Radtke Schuller S, Betz M (1986) A stereotaxic method for small animals using experimentally determined reference profiles. *J Neurosci Methods* 18:339–350.
- Shneiderman A, Oliver DL, Henkel CK (1988) Connections of the dorsal nucleus of the lateral lemniscus: an inhibitory parallel pathway in the ascending auditory system? *J Comp Neurol* 276:188–208.
- Siveke I, Pecka M, Seidl AH, Baudoux S, Grothe B (2006) Binaural response properties of low-frequency neurons in the gerbil dorsal nucleus of the lateral lemniscus. *J Neurophysiol* 96:1425–1440.
- Tollin DJ, Populin LC, Yin TCT (2004) Neural correlates of the precedence effect in the inferior colliculus of behaving cats. *J Neurophysiol* 92:3286–3297.
- Yang L, Pollak GD (1994a) Binaural inhibition in the dorsal nucleus of the lateral lemniscus of the mustache bat affects responses for multiple sounds. *Audiot Neurosci* 1:1–17.
- Yang L, Pollak GD (1994b) The roles of GABAergic and glycinergic inhibition on binaural processing in the dorsal nucleus of the lateral lemniscus of the mustache bat. *J Neurophysiol* 71:1999–2013.
- Yang L, Pollak GD (1998) Features of ipsilaterally evoked inhibition in the dorsal nucleus of the lateral lemniscus. *Hear Res* 122:125–141.
- Yin TC (1994) Physiological correlates of the precedence effect and summing localization in the inferior colliculus of the cat. *J Neurosci* 14:5170–5186.
- Zahn TP (2003) Neural architecture for echo suppression during sound source localization based on spiking neural cell models. Retrieved January 16, 2007, from http://www.bibliothek.tu-ilmenau.de/elektr_medien/dissertationen/2003/Zahn_Thomas/.
- Zahn TP, Izak R, Trott K, Paschke P (1997) A paced analog silicon model of auditory attention. In: *Neuromorphic systems: engineering silicon from neurobiology* (Smith LS, Hamilton A, eds), pp 99–112. Hackensack, NJ: World Scientific Publishing.
- Zurek PM (1987) The precedence effect. In: *Directional hearing* (Yost WA, Gourevitch G, eds), pp 85–105. New York: Springer.

GENERAL DISCUSSION

It was already mentioned in the introduction that glycinergic and GABAergic inhibition exhibit different receptor kinetics, leading to distinct functional roles for the two transmitters. The results of this thesis clearly illustrated such a differentiation for glycine and GABA in processing auditory information. Below, the functional roles as found in the studies of this thesis will be discussed in comparison to other known functional roles of glycinergic and GABAergic inhibition.

Functional roles of inhibition in coincidence detection

MSO neurons (as well as low frequency LSO cells) represent an extreme example of temporal precision, both in that the kinetics of glycinergic inhibition in these neurons are the fastest reported so far and in that these neurons are sensitive to ITDs in the microsecond range (Goldberg and Brown, 1969; Finlayson and Caspary, 1991; Magnusson et al, 2005, Smith et al 2000). We showed in our pharmacological experiments that the glycinergic inputs to the MSO were crucial for defining the binaural coincidence window of the MSO neurons (the range of ITDs that are able to elicit responses), most probably by acting in sub-millisecond events (i.e. in cycle-by-cycle manner). In our proposed scenario, the glycinergic inputs interact with the synaptic integration of the excitatory inputs and thereby refine the width of the coincidence window. Therefore, glycinergic inhibition in the MSO is not only well-timed itself, but it also increases the overall temporal sensitivity of MSO neurons. This functional role of controlling temporal sensitivity and defining the coincidence window of excitatory inputs is a recurring functional role of inhibition also in other neuronal systems, albeit on less extreme time scales. In the cerebellum, for instance, it was shown that the temporal summation of excitatory inputs from parallel fibers onto Purkinje cells is restrained by a delayed GABAergic input stemming from an interneuron that is activated by the same parallel fibers (Mittmann et al., 2005). This feed-forward inhibition is able to refine the coincidence window of the Purkinje cell from <30ms to less than 2ms, thereby establishing the temporal precision of the cerebellar output that is crucial for the coordination of movements. A similar feed-forward inhibitory pathway is also found in cortical and hippocampal pyramidal cells and here, likewise to the cerebellum, GABAergic, trailing inhibitory inputs refine the coincidence window of multiple excitatory inputs to a range of a few milliseconds (Buzsaki 1984; Pouille and Scanziani 2001; Gabernet et al., 2005). Notably, feed-forward inhibitory inputs in the hippocampus synapse mainly onto somatic regions of the pyramidal cell, reminiscent to the arrangement found in the MSO (Pouille and Scanziani 2001; Kapfer et al., 2002). However, the requirements in temporal precision of the glycinergic

inputs to the MSO seem to be an order of magnitude higher than in the compared GABAergic feed-forward pathways.

Next to feed-forward inhibition to increase temporal sensitivity, another prominent role of inhibition is gain control. Gain control is typically achieved by a negative feedback loop to control the excitatory input strength, thereby assuring a broad dynamic range regardless of the stimulus intensity. Such robustness against changes in intensity is particularly important in ITD processing because the ability of the detector neurons to remain unresponsive to out-of-phase ITDs independent of their input strength is crucial for neuronal coincidence detection. However, the amplitude of a net EPSP of all incoming inputs increases with increasing intensities, as more inputs are recruited at higher intensities (Reed and Durbeck 1995;Pena et al., 1996). At some point the depolarization that is produced by the net EPSP from either the ipsi- or the contralateral ear alone might be supra-threshold and elicit spikes. Hence, the neuron could potentially lose ITD sensitivity at high intensities if it also responded to out-of-phase ITDs (Reed and Durbeck 1995). In the avian ITD detection system, to prevent these so-called “monaural responses”, a gain control circuit consisting of GABAergic inhibitory inputs to the NL reduces the amplitude of excitatory inputs and shortens their duration, thereby ensuring consistent ITD sensitivity across intensity levels (Pena et al., 1996;Dasika et al., 2005). Importantly, the inhibition in NL neurons is not timed (it is decoupled from the phase-locked excitation; Yang et al., 1999), and it actually has a depolarizing effect on the NL cells (due to a high intracellular Cl^- concentration), which in turn activates low-threshold potassium-channels that lead to shunting of the cell (Hyson et al., 1995;Yang et al., 1999;Burger et al., 2005b). Moreover, the superior olivary nucleus (SON), which is the source of this GABAergic inhibition in the NL (Lachica et al., 1994), shares the same input source with the NL and is additionally innervated by NL neurons, creating a differential gain control circuit for the NL (Monsivais and Rubel, 2001;Burger et al 2005a).

In the MSO, the inhibitory inputs seem not to fulfill a classical gain control function. Our results in chapter 1 suggest that the phase-locked glycinergic inputs create short intervals of hyper-polarization that are precisely aligned relative to the excitatory intervals and thereby refine the range of ITDs at which incoming EPSPs are able to exceed spiking threshold. However, by refining the binaural coincidence window, the inhibition should also be able to prevent out-of-phase responses at any given intensity. Recent studies in the lab of Benedikt Grothe showed that ITD sensitivity in the MSO is indeed very robust against changes in intensity (Pecka et al., 2008, abstract), yet it is an open question what fraction of this robustness can be attributed to the effects of the timed inhibition rather than to the specific morphology and channel composition of MSO neurons. It was shown that the presence of low-threshold potassium channels in MSO neurons mediate the generation of very fast and small action potentials that only allow supra-threshold depolarization when multiple PSPs

coincide at the spike-initiating zone (Svirskis et al., 2003; Scott et al., 2005). Modeling studies additionally suggested that the distinct dendritic morphology of the MSO (and NL) neurons promotes binaural coincidences and reduces the summation of monaural inputs (Grau-Serrat et al., 2003, Svirskis et al., 2003; Dasika et al., 2005). It has also been suggested that synaptic depression of the excitatory inputs helps to preserve ITD sensitivity across intensities (Cook et al., 2003). Nevertheless, at least in NL neurons, which have similar cellular specializations, a gain control mechanism seems to be fundamental for maintaining ITD sensitivity at high intensities (Pena et al., 1996; Dasika et al., 2005). Therefore, it seems likely that glycinergic inhibition may account not only for tuning ITD sensitivity in the MSO, but also contributes to establish robustness of the coincidence mechanism against changes in intensity. Both of these functional roles are accomplished by the preservation of a defined width of the ITD window, allowing supra-threshold depolarization only by coincidence of binaural inputs.

Finally, it is noteworthy that glycinergic inhibition in the MSO serves an additional functional role during development that is not accomplished by the tonic inhibition in the NL: During maturation of an animal, the correct neuronal representation of sound sources in space demands a learning mechanism that calibrates the system. In both the MSO and the avian auditory system, such experience-dependent developmental plasticity is conveyed by inhibition, but the mechanisms are very different. In the avian system, the auditory topographic map that is created in the midbrain is eventually merged with the visual map in the optic tectum (review: Knudsen, 2002). Thereby the accuracy of the auditory map can be supervised during development by visual input and, if necessary, re-calibrated. Knudsen and colleagues showed in owls that the ability to shift the auditory maps to match the visual maps is dependent on GABAergic inputs that are created during a critical period of plasticity (Zheng and Knudson 1999, 2001). Importantly, these GABAergic inputs are formed in the midbrain, not in the NL. Hence, the spatial sensitivity of single NL cells is determined only by their specific excitatory innervation (i.e. the offset of the delay lines), while the inhibition-mediated calibration takes place at the level of the midbrain, the site of convergence with the visual map. In contrast, the auditory localization ability of mammals is not based on maps in which activity of single neurons is read out, but information is encoded in the overall activity level in a population of neurons (McAlpine et al., 2001; Hancock and Delgutte, 2004). Consequently, all neurons of a particular nucleus need to be tuned to assure monotonic response modulation across the range of physiological ITDs. This tuning mechanism is provided already at the level of the MSO by the glycinergic inhibition, as was explicitly demonstrated in this thesis (chapter 1). It is important to mention that this tuning is also experience dependent and restricted to a critical period: ITD functions in the gerbil DNLL were shown to be adjusted to the physiological range during a period shortly after hearing

onset that coincided with a period in which a refinement of inhibitory synapses to the somatic area of MSO neurons takes place (Seidl and Grothe 2005; Kapfer et al 2002). These maturation processes were absent when animals did not experience directional auditory input during the critical period.

In summary, the glycinergic inputs to the MSO and the GABAergic inputs to the NL both generate a gain control for the coincidence-detection mechanism. However, only glycinergic inhibition in the MSO has the essential function of refining ITD sensitivity. The underlying mechanisms facilitating the functional roles in the two systems are, accordingly, very different for the two systems and strongly coupled to the different receptor kinetics of the respective transmitters. The effectiveness of the inhibitory inputs in the MSO is crucially linked to their precise timing relative to the excitatory inputs and, hence, demands very fast kinetics as found for glycinergic inhibition (Gingrich et al, 1995; Smith et al., 2000; Legendre, 2001; Magnusson et al, 2005). In contrast, in the avian ITD detection system a sustained activity of inhibition rather than timing is required, promoting GABA as inhibitory transmitter. Next, the role of GABAergic transmission in mediating sustained inhibition of activity will be examined in more detail.

Sustained inhibition as a functional role for GABAergic transmission

In contrast to the glycinergic inhibition to the MSO that precisely influenced synaptic integration in a cycle-by-cycle manner, the GABAergic PI in the DNLL that we investigated (chapter 4) influenced the responsiveness of a population of cells via reconfiguration of an entire network, and the characteristic feature of this GABAergic inhibition was its tonic persistence for tens of milliseconds. Generally, one can observe that GABAergic transmission exhibits clear tendencies in its kinetics towards tonic hyper-polarization rather than towards a fast inhibition: Next to the A-type receptors (GABA_AR), the two additional existing types of GABA receptors (called the B- and C-type) are considerably slower. For instance, GABA_BRs are metabotropic receptors and thus signal transduction is G-protein mediated, which exhibits much slower kinetics than ionotropic signaling (review: Couve et al., 2000). The prolonged effectiveness of GABA_BRs are known to be involved for instance in retrograde signaling in order to modulate synaptic input strength (Scholz and Miller, 1991; Sakaba and Neher, 2003; Magnusson et al., 2008). Moreover, additional mechanisms of prolonged activation in GABAergic transmission are known. One of these mechanisms is the asynchronous (and hence prolonged) release of vesicles into the synaptic cleft due to pre-synaptic Ca²⁺ accumulation, which was shown to lead to slow repolarization kinetics of IPSCs (Goda and Stevens, 1994; Lu and Trussel 2000; Hefft and Jonas, 2005). The second

mechanism is called “spillover” and describes an additional, delayed activation of extra-synaptic receptors due to diffusion of GABA from the synaptic cleft (Destexhe and Sejnowski, 1995; Dittman and Regehr, 1997). Both of these synaptic mechanisms achieve a tonic, ongoing hyper-polarization in the target cell. One main difference between a series of phasic inhibitory events and spillover or asynchronous release is that the latter two create an residual concentration of GABA in or around the synaptic cleft. Therefore, integration of pre-synaptic activity takes place before the post-synaptic cell, eliminating the chance for precise temporal processing (review: Farrant and Nusser 2005). Instead, the activation of a few GABAergic inputs is able to achieve tonic and relatively duration-independent hyper-polarization of the target neuron that results in suppression of all excitatory inputs that arrive not only during but also after the activation of the inhibitory inputs. Knowing these properties of tonic GABAergic transmission it comes as no surprise that a recently conducted *in vitro* study in the lab of Benedikt Grothe identified both spillover and asynchronous release as the responsible mechanisms for generating PI in the DNLL (Saunier-Rebori 2008). Next, the functional impact of PI on the generation and transmission of information in the auditory system will be discussed.

Gain of information by disinhibition: Implications on coding strategies

Our study on echo suppression in the DNLL (chapter 4) explained how temporary release from inhibition can provide a gain of information that eventually results in increased precision in a behavioral task, in this case the localization of a sound source in the presence of echoes. The general scheme of this functional mechanism is the disinhibition of a particular brain area for a defined time period during which a task is performed. Such a scheme is also found in other areas of the brain, most prominently perhaps in the basal ganglia of the efferent motor system. Here, precise execution of a voluntary movement is mediated by a temporary release from inhibition of the neurons that are involved in producing the desired movement while the inhibition of those neurons responsible for related, potentially compromising movements is held up or even strengthened (review: Mink, 1996). Thus, both in the basal ganglia and in the IC, a sub-group of neurons are released from inhibition for the period of time during which a task is performed. However, the mechanism that leads to the increased behavioral precision of the task is very different: In the case of the basal ganglia network, interfering movements are suppressed while the desired movement is performed by the subgroup of neurons that are released from inhibition. Thus, precision is actually achieved by suppression of those neurons that potentially might compromise the performance of the task. In contrast, the neurons in the IC that respond to a trailing sound due to disinhibition do not directly enhance localization of the original sound. Precise

localization of the sound source is in fact completed by evaluation of the binaural cues of the original sound, thus no additional activity is needed. However, the additional activity in the IC triggers the disregarding of the echo directional information and therefore ultimately secures the precision of the localization.

The question then becomes how additional activity in the IC helps to suppress the localization of the echo. One explanation would be that the additional activity simply degrades the overall localization ability for the respective echo. However, the Clifton effect strongly contradicts this explanation, as it shows that the directional information about the echo is present in the system and can be retrieved (Clifton, 1987). The ideal observer in our model identified echoes by comparing activity levels in the *de novo* E/I IC populations on both sides of the brain. If the activity ratio between the two sides fell short of a threshold value (due to additional activity during the period of PI), the sound was regarded as an echo and not localized. Such an activity-ratio based echo-identification is closely associated with a population-rate-coding strategy of IIDs, which is known to be employed in the IC of mammals (e.g. Park et al., 2004). Coding auditory space via a space map as it is found in owls (Knudsen and Konishi, 1978; note that the formation of this space map includes IID, ITD and spectral cues of the sound source), seems less adapted for our proposed concept of echo-tagging by activity in a sub-population of neurons, because additional activity within a topographic map would create ambiguity about the correct location of the sound. Hence, one could hypothesize that recalling the directional information of the echo would be unfeasible for owls or that a strategy other than our tagging-model is utilized. Unfortunately, despite recent psychophysical descriptions of the precedence effect in owls (Spitzer et al., 2003; Spitzer and Takahashi 2006), investigations on the Clifton effect have not been reported in these animals so far. It should be noted, though, that the differences in coding strategy between mammals and birds are also reflected by anatomical differences in the respective pathways, i.e. while nuclei analogous to the DNLL and IC can be found in the bird brain, it is doubtful that a connectivity similar to the PI circuit is present. Thus, it is unclear whether the ability to process echo directional information in context-dependent manner might be bound to a particular strategy of auditory space coding.

Future perspectives

While the studies of this thesis yielded coherent and comprehensive insight into the importance of synaptic inhibition in temporal processing in the auditory system, some important questions could not be addressed with the techniques employed. For instance, while the results from our pharmacological experiments in the MSO supported the predictions of the well-timed inhibition hypothesis, neither the exact (effective) time course of

the glycinergic inputs nor their sequence relative to the excitatory inputs could be investigated directly. In regard to PI in the DNLL, the similarity of the model results to the human behavior in the psychophysical tests implied a strong functional link between this circuitry and context dependent echo-suppression. However, the precedence effect consists of multiple potentially independent psychophysical effects and it is unknown what contribution the PI circuit makes on a behavioral level. Specifically, our model predicts that the context-dependent retrieval of echo-directional information (the Clifton effect) would be particularly dependent on the activity of PI circuit.

One technique that has potential to answer these questions both for ITD processing in the MSO and the PI circuit is the targeted virus transfection of particular nuclei *in vivo* (e.g. Wimmer et al., 2004). This technique utilizes viral vectors to express specific proteins in a group of cells in order to alter particular cellular properties or introduce a new property. This way, a detailed picture of the relationship between the respective cellular property and its functional relevance to the circuit can be obtained while the overall functionality of the neuronal network is maintained. Also, by choosing cell-type specific promoters, high specificity of the transfection can be assured. Most importantly, virus-mediated protein expression offers the unique possibility to test the relevance of defined physiological alterations on behavior.

Virus-mediated protein expression in the DNLL would allow the determination of the role of PI in context-dependent echo suppression in a behavioral paradigm: Since recent studies in the lab of Benedikt Grothe identified spillover and asynchronous release as the cellular mechanisms of PI in DNLL neurons (Saunier-Rebori 2008), potentially specific antagonists for these mechanisms could be over-expressed in the DNLL. Possible candidates for manipulation would be fast GABA up-take in glia cells to antagonize spill-over and slow calcium-buffering in DNLL neurons to minimize asynchronous release. Subsequently, echo suppression and ultimately Clifton-effect-like behavior in animals trained to report the detection of trailing sounds (compare Schuchmann et al., 2007) could be evaluated before and after DNLL transfection. However, these experiments are technically extremely challenging. As a first step, the reversible blockade of the DNLL using pharmacological methods (e.g. by using infusion pumps to deliver drugs, see Cunningham et al., 2008) would also be a promising paradigm within a behavioral framework.

Regarding the role of glycinergic inhibition in the MSO, a decoupling of the timing of the inhibitory MSO inputs from the excitatory MSO inputs could verify the relevance of precise timing of inhibition in the coincidence-detection mechanism. For instance, degrading the phase-locking precision of the MNTB neurons, for example by modifying post-synaptic glutamate-receptor density, could address two important issues: the importance of the MNTB

input as source of inhibition in the MSO (compared to the LNTB), and the hypothesis that the MNTB input precedes the contralateral excitation.

Finally, synergistic effects of GABA to speed up the kinetics of glycinergic transmission at the MNTB were recently reported (Lu et al., 2008). It is unknown if such a mechanism is also present in the glycinergic inputs of the MSO, but this can be readily examined with *in vitro* experiments as well as immunochemistry to check for GABA/Glycine co-release. So far, the measured kinetics of glycinergic inhibition in the MSO are already as fast as ever reported for glycine alone (Magnusson et al., 2005), but a further acceleration would be in favor of the preceding inhibition scenario (Brand et al., 2002). Interestingly, the occurrence of GABAergic transmission at the MSO is supported by the findings of ongoing studies in the lab, which indicate the presence of pre-synaptic GABA_B receptors for both inhibitory and excitatory MSO inputs (Ursula Koch, personal communication). Similar GABA_BR staining on LSO inputs was recently investigated in the lab and it was shown physiologically that GABA_B signaling serves as retrograde messenger between LSO neurons and their inputs (Magnusson et al., 2008). Specifically, dendritic release of GABA from LSO neurons enabled modulation of the synaptic inputs in dependence of the prevailing environmental sound conditions (i.e. post-synaptic activity). Similar function for GABA_B signaling can be assumed for the MSO and should be tested by a combined *in vitro* and *in vivo* approach.

In summary, in this thesis we further strengthened the hypothesis that synaptic inhibition is crucial for temporal processing on multiple levels of the auditory system. We demonstrated that different functional roles are associated with glycinergic and GABAergic transmission and that the functional differences of the two transmitters are closely associated with the temporal precision that is required in the particular processing task. We believe that a better understanding of the role(s) of inhibition is essential not only for gaining insight into the functioning of the auditory system and hearing, but also for deciphering the neuronal code of the central nervous system in general.

REFERENCES

- Adams JC (1979) Ascending projections to the inferior colliculus. *J Comp Neurol* 183:519-538.
- Adams JC, Mugnaini E (1984) Dorsal nucleus of the lateral lemniscus: a nucleus of GABAergic projection neurons. *Brain Res Bull* 13:585-590.
- Aitkin L, Schuck D (1985) Low frequency neurons in the lateral central nucleus of the cat inferior colliculus receive their input predominantly from the medial superior olive. *Hear Res* 17:87-93.
- Aprison MH, Werman R (1965) The distribution of glycine in cat spinal cord and roots. *Life Sci* 4:2075-2083.
- Bartheld CS, Code RA, Rubel EW (1989) GABAergic Neurons in Brainstem Auditory Nuclei of the Chick: Distribution, Morphology, and Connectivity. *The Journal of Comparative Neurology* 287:470-483.
- Batra R, Kuwada S, Stanford Tr (1993) High-frequency neurons in the inferior colliculus that are sensitive to interaural delays of amplitude-modulated tones: evidence for dual binaural influences. *J Neurophysiol* 70:64-80.
- Beckius GE, Batra R, Oliver DL (1999) Axons from anteroventral cochlear nucleus that terminate in medial superior olive of cat: Observations related to delay lines. *Journal of Neuroscience* 19:3146-3161.
- Bernstein LR (2001) Auditory processing of interaural timing information: new insights. *J Neurosci Res* 66:1035-1046.
- Betz H (1990) Ligand-gated ion channels in the brain: the amino acid receptor superfamily. *Neuron* 5:383-392.
- Blauert J (1997) Spatial Hearing with Multiple Sound Sources and in Enclosed Spaces. In: *Spatial Hearing: The Psychophysics of Human Sound Localization (Revised Edition)* pp 201-287. Cambridge, MA: MIT Press.
- Borst JG, Helmchen F, Sakmann B (1995) Pre- and postsynaptic whole-cell recordings in the medial nucleus of the trapezoid body of the rat. *J Physiol Lond* 489:825-840.
- Boudreau JC, Tsuchitani C (1968) Binaural interaction in the cat superior olive S segment. *Journal of Neurophysiology* 31:442-454.
- Brand A, Behrend O, Marquardt T, McAlpine D, Grothe B (2002) Precise inhibition is essential for microsecond interaural time difference coding. *Nature* 417:543-547.
- Brawer JR, Morest DK, Kane EC (1974) The neuronal architecture of the cochlear nucleus of the cat. *J Comp Neurol* 160:491-506.
- Brugge JF, Anderson DJ, Aitkin LM (1970) Responses of neurons in the dorsal nucleus of the lateral lemniscus of cat to binaural tonal stimulation. *J Neurophysiol* 33:441-458.
- Brungart DS, Rabinowitz WM (1999) Auditory localization of nearby sources. Head-related transfer functions. *J Acoust Soc Am* 106:1465-1479.
- Brunso-Bechtold JK, Thompson GC, Masterton RB (1981) HRP study of the organization of auditory afferents ascending to central nucleus of inferior colliculus in cat. *J Comp Neurol* 197:705-722.
- Burger RM, Cramer KS, Pfeiffer JD, Rubel EW (2005a) Avian superior olivary nucleus provides divergent inhibitory input to parallel auditory pathways. *J Comp Neurol* 481:6-18.

- Burger RM, Pfeiffer JD, Westrum LE, Bernard A, Rubel EW (2005b) Expression of GABA(B) receptor in the avian auditory brainstem: ontogeny, afferent deprivation, and ultrastructure. *J Comp Neurol* 489:11-22.
- Burger RM, Pollak GD (2001) Reversible inactivation of the dorsal nucleus of the lateral lemniscus reveals its role in the processing of multiple sound sources in the inferior colliculus of bats. *J Neurosci* 21:4830-4843.
- Buzsaki G (1984) Feed-forward inhibition in the hippocampal formation. *Prog Neurobiol* 22:131-153.
- Cant NB (1991) Projections to the lateral and medial superior olivary nuclei from the spherical and globular bushy cells of the anteroventral cochlear nucleus. In: *Neurobiology of hearing: The central auditory system* (Altschuler RA, Bobbin RP, Clopton BM, Hoffman DW, eds), pp 99-119. New York: Raven Press.
- Cant NB, Casseday JH (1986) Projections from the anteroventral cochlear nucleus to the lateral and medial superior olivary nuclei. *J Comp Neurol* 247:457-476.
- Cant NB, Hyson RL (1992) Projections from the lateral nucleus of the trapezoid body to the medial superior olivary nucleus in the gerbil. *Hear Res* 58:26-34.
- Cant NB, Morest DK (1984) The structural basis for stimulus coding in the cochlear nucleus of the cat. In: *Hearing Science: recent Advances* pp 371-421. San Diego: College-Hill Press.
- Carr CE, Fujita I, Konishi M (1989) Distribution of GABAergic neurons and terminals in the auditory system of the barn owl. *J Comp Neurol* 286:190-207.
- Carr CE, Konishi M (1988) Axonal delay lines for time measurement in the owl's brainstem. *Proc Natl Acad Sci U S A* 85:8311-8315.
- Carr CE, Konishi M (1990) A circuit for detection of interaural time differences in the brain stem of the barn owl. *J Neurosci* 10:3227-3246.
- Clark GM (1969) Vesicle shape versus type of synapse in the nerve endings of the cat medial superior olive. *Brain Research* 15:548-551.
- Clifton RK (1987) Breakdown of echo suppression in the precedence effect. *J Acoust Soc Am* 82:1834-1835.
- Cook DL, Schwindt PC, Grande LA, Spain WJ (2003) Synaptic depression in the localization of sound. *Nature* 421:66-70.
- Couve A, Moss SJ, Pangalos MN (2000) GABAB receptors: a new paradigm in G protein signaling. *Mol Cell Neurosci* 16:296-312.
- Crow G, Rupert AL, Moushegian G (1978) Phase locking in monaural and binaural medullary neurons: implications for binaural phenomena. *J Acoust Soc Am* 64:493-501.
- Cunningham MG, Ames HM, Donalds RA, Benes FM (2008) Construction and implantation of a microinfusion system for sustained delivery of neuroactive agents. *J Neurosci Methods* 167:213-220.
- Curtis DR, Hosli L, Johnston GA (1968) A pharmacological study of the depression of spinal neurones by glycine and related amino acids. *Exp Brain Res* 6:1-18.
- Dasika VK, White JA, Carney LH, Colburn HS (2005) Effects of inhibitory feedback in a network model of avian brain stem. *J Neurophysiol* 94:400-414.

- Destexhe A, Sejnowski TJ (1995) G protein activation kinetics and spillover of gamma-aminobutyric acid may account for differences between inhibitory responses in the hippocampus and thalamus. *Proc Natl Acad Sci U S A* 92:9515-9519.
- Dittman JS, Regehr WG (1997) Mechanism and kinetics of heterosynaptic depression at a cerebellar synapse. *J Neurosci* 17:9048-9059.
- Farrant M, Nusser Z (2005) Variations on an inhibitory theme: phasic and tonic activation of GABA(A) receptors. *Nat Rev Neurosci* 6:215-229.
- Feddersen WE, Sandel TT, Teas DC, Jeffress LA (1957) Localization of high-frequency tones. *J Acoust Soc Am* 29:988-991.
- Finlayson PG, Caspary DM (1991) Low-frequency neurons in the lateral superior olive exhibit phase-sensitive binaural inhibition. *J Neurophysiol* 65:598-605.
- Fitzpatrick DC, Kuwada S (2001) Tuning to Interaural Time Differences across Frequency. *J Neurosci* 21:4844-4851.
- Friauf E, Kandler K, Lohmann C, Kungel M (1997) Inhibitory and excitatory brainstem connections involved in sound localization: how do they develop? In: *Acoustical Signal Processing in the Central Auditory System* (Syka J, ed), pp 181-191. New York: Plenum Press.
- Friauf E, Ostwald J (1988) Divergent projections of physiologically characterized rat ventral cochlear nucleus neurons as shown by intra-axonal injection of horseradish peroxidase. *Experimental Brain Research* 73:263-284.
- Funabiki K, Koyano K, Ohmori H (1998) The role of GABAergic inputs for coincidence detection in the neurones of nucleus laminaris of the chick. *J Physiol Lond* 508:851-869.
- Gabernet L, Jadhav SP, Feldman DE, Carandini M, Scanziani M (2005) Somatosensory integration controlled by dynamic thalamocortical feed-forward inhibition. *Neuron* 48:315-327.
- Galambos R, Davis H (1943) The response of single auditory-nerve fibres to acoustic stimulation. *Journal of Neurophysiology* 6:39-57.
- Geurts FJ, De SE, Dieudonne S (2003) Unraveling the cerebellar cortex: cytology and cellular physiology of large-sized interneurons in the granular layer. *Cerebellum* 2:290-299.
- Gingrich KJ, Roberts WA, Kass RS (1995) Dependence of the GABAA receptor gating kinetics on the alpha-subunit isoform: implications for structure-function relations and synaptic transmission. *J Physiol* 489 (Pt 2):529-543.
- Glendenning KK, Baker BN, Hutson KA, Masterton RB (1992) Acoustic Chiasm .5. Inhibition and Excitation in the Ipsilateral and Contralateral Projections of Lso. *Journal of Comparative Neurology* 319:100-122.
- Glendenning KK, Brunso-Bechtold JK, Thompson GC, Masterton RB (1981) Ascending auditory afferents to the nuclei of the lateral lemniscus. *J Comp Neurol* 197:673-703.
- Goda Y, Stevens CF (1994) Two components of transmitter release at a central synapse. *Proc Natl Acad Sci U S A* 91:12942-12946.
- Goldberg JM, Brown PB (1969) Response of binaural neurons of dog superior olivary complex to dichotic tonal stimuli: some physiological mechanisms of sound localization. *J Neurophysiol* 32:613-636.
- Grau-Serrat V, Carr CE, Simon JZ (2003) Modeling coincidence detection in nucleus laminaris. *Biol Cybern* 89:388-396.

- Grothe B (1994) Interaction of excitation and inhibition in processing of pure tone and amplitude-modulated stimuli in the medial superior olive of the mustached bat. *J Neurophysiol* 71:706-721.
- Grothe B (2000) The evolution of temporal processing in the medial superior olive, an auditory brainstem structure. *Prog Neurobiol* 61:581-610.
- Grothe B (2003) New roles for synaptic inhibition in sound localization. *Nature Reviews Neuroscience* 4:540-550.
- Grothe B, Covey E, Casseday JH (2001) The medial superior olive in the big brown bat: neuronal response to pure tones, amplitude modulations, and pulse trains. *J Neurophysiol* 86:2219-2230.
- Grothe B, Park TJ (1998) Sensitivity to interaural time differences in the medial superior olive of a small mammal, the Mexican free-tailed bat. *J Neurosci* 18:6608-6622.
- Grothe B, Sanes DH (1993) Bilateral inhibition by glycinergic afferents in the medial superior olive. *J Neurophysiol* 69:1192-1196.
- Guinan JJ, Jr., Guinan SS, Norris BE (1972) Single Auditory Units in the Superior Olivary Complex I: Responses to Sounds and Classifications Based on Physiological Properties. *Intern J Neuroscience* 4:101-120.
- Guinan JJ, Jr., Li RY (1990) Signal processing in brainstem auditory neurons which receive giant endings (calyces of Held) in the medial nucleus of the trapezoid body of the cat. *Hear Res* 49:321-334.
- Hamill OP, Bormann J, Sakmann B (1983) Activation of multiple-conductance state chloride channels in spinal neurones by glycine and GABA. *Nature* 305:805-808.
- Hancock KE, Delgutte B (2004) A physiologically based model of interaural time difference discrimination. *Journal of Neuroscience* 24:7110-7117.
- Harper NS, McAlpine D (2004) Optimal neural population coding of an auditory spatial cue. *Nature* 430:682-686.
- Hefft S, Jonas P (2005) Asynchronous GABA release generates long-lasting inhibition at a hippocampal interneuron-principal neuron synapse. *Nat Neurosci* 8:1319-1328.
- Held H (1893) Die zentrale Gehörleitung. *Arch Anat u Physiol* 17:201-248.
- Huang ZJ, Di CG, Ango F (2007) Development of GABA innervation in the cerebral and cerebellar cortices. *Nat Rev Neurosci* 8:673-686.
- Hyson RL, Reyes AD, Rubel EW (1995) A depolarizing inhibitory response to GABA in brainstem auditory neurons of the chick. *Brain Res* 677:117-126.
- Jeffress LA (1948) A place theory of sound localization. *J Comp Physiol Psychol* 41:35-39.
- Kapfer C, Seidl AH, Schweizer H, Grothe B (2002) Experience-dependent refinement of inhibitory inputs to auditory coincidence-detector neurons. *Nat Neurosci* 5:247-253.
- Kelly JB, Buckthorpe AD, Kidd SA (1998) Monaural and binaural response properties of single neurons in the rat's dorsal nucleus of the lateral lemniscus. *Hear Res* 122:25-40.
- Kiang NY, Watanabe T, Thomas C, Clark LF (1965) Discharge patterns of single fibres in the cat's auditory nerve. Cambridge, MA: MIT Press.
- Kirsch J (2006) Glycinergic transmission. *Cell Tissue Res* 326:535-540.

- Knudsen EI (2002) Instructed learning in the auditory localization pathway of the barn owl. *Nature* 417:322-328.
- Knudsen EI, Konishi M (1978) A neural map of auditory space in the owl. *Science* 200:795-797.
- Kopp-Scheinpflug C, Lippe WR, Dorrscheidt GJ, Rubsamen R (2003) The medial nucleus of the trapezoid body in the gerbil is more than a relay: comparison of pre- and postsynaptic activity. *J Assoc Res Otolaryngol* 4:1-23.
- Krnjevic K, Schwartz S (1967) The action of gamma-aminobutyric acid on cortical neurones. *Exp Brain Res* 3:320-336.
- Kudo M (1981) Projections of the nuclei of the lateral lemniscus in the cat: an autoradiographic study. *Brain Res* 221:57-69.
- Kuwabara N, Zook JM (1992) Projections to the medial superior olive from the medial and lateral nuclei of the trapezoid body in rodents and bats. *J Comp Neurol* 324:522-538.
- Kuwada S, Fitzpatrick DC, Batra R, Ostapoff EM (2006) Sensitivity to interaural time differences in the dorsal nucleus of the lateral lemniscus of the unanesthetized rabbit: comparison with other structures. *J Neurophysiol* 95:1309-1322.
- Lachica EA, Rubsamen R, Rubel EW (1994) GABAergic terminals in nucleus magnocellularis and laminaris originate from the superior olivary nucleus. *J Comp Neurol* 348:403-418.
- Laurent G (2002) Olfactory network dynamics and the coding of multidimensional signals. *Nat Rev Neurosci* 3:884-895.
- Legendre P (2001) The glycinergic inhibitory synapse. *Cell Mol Life Sci* 58:760-793.
- Lindsey BG (1975) Fine structure and distribution of axon terminals from the cochlear nucleus on neurons in the medial superior olivary nucleus of the cat. *J Comp Neurol* 160:81-103.
- Litovsky RY, Colburn HS, Yost WA, Guzman SJ (1999) The precedence effect. *J Acoust Soc Am* 106:1633-1654.
- Lorente de No (1933) Anatomy of the eighth nerve. III. General plan of structure of the primary cochlear nuclei. *Laryngoscope* 43:327-377.
- Lu T, Rubio ME, Trussell LO (2008) Glycinergic transmission shaped by the corelease of GABA in a mammalian auditory synapse. *Neuron* 57:524-535.
- Lu T, Trussell LO (2000) Inhibitory transmission mediated by asynchronous transmitter release. *Neuron* 26:683-694.
- Magnusson AK, Kapfer C, Grothe B, Koch U (2005) Maturation of glycinergic inhibition in the gerbil medial superior olive after hearing onset. *Journal of Physiology-London* 568:497-512.
- Magnusson AK, Park TJ, Pecka M, Grothe B, Koch U (2008) Retrograde GABA signaling adjusts sound localization by balancing excitation and inhibition in the brainstem. *Neuron* 59:125-137.
- Maki K, Furukawa S (2005) Acoustical cues for sound localization by the Mongolian gerbil, *Meriones unguiculatus*. *Journal of the Acoustical Society of America* 118:872-886.
- Malosio ML, Marqueze-Pouey B, Kuhse J, Betz H (1991) Widespread expression of glycine receptor subunit mRNAs in the adult and developing rat brain. *EMBO J* 10:2401-2409.
- Markovitz NS, Pollak GD (1994) Binaural processing in the dorsal nucleus of the lateral lemniscus. *Hear Res* 73:121-140.

- Masterton RB, Diamond IT (1967) Medial superior olive and sound localization. *Science* 155:1696-1697.
- Matsubara JA (1990) Calbindin D-28K immunoreactivity in the cat's superior olivary complex. *Brain Res* 508:353-357.
- McAlpine D, Jiang D, Palmer AR (2001) A neural code for low-frequency sound localization in mammals. *Nat Neurosci* 4:396-401.
- McAlpine D, Jiang D, Shackleton TM, Palmer AR (1998) Convergent input from brainstem coincidence detectors onto delay-sensitive neurons in the inferior colliculus. *J Neurosci* 18:6026-6039.
- Mink JW (1996) The basal ganglia: focused selection and inhibition of competing motor programs. *Prog Neurobiol* 50:381-425.
- Mittmann W, Koch U, Hausser M (2005) Feed-forward inhibition shapes the spike output of cerebellar Purkinje cells. *J Physiol* 563:369-378.
- Monsivais P, Rubel EW (2001) Accommodation enhances depolarizing inhibition in central neurons. *J Neurosci* 21:7823-7830.
- Moore BCJ (2004) London: Academic Press.
- Moore JK, Moore RY (1987) Glutamic acid decarboxylase-like immunoreactivity in brainstem auditory nuclei of the rat. *J Comp Neurol* 260:157-174.
- Moore MJ, Caspary DM (1983) Strychnine blocks binaural inhibition in lateral superior olivary neurons. *J Neurosci* 3:237-242.
- Morest DK (1968) The growth of synaptic endings in the mammalian brain: a study of the calyces of the trapezoid body. *Z Anat Entwicklungsgesch* 127:201-220.
- Moushegian G, Rupert AL, Gidda JS (1975) Functional characteristics of superior olivary neurons to binaural stimuli. *J Neurophysiol* 38:1037-1048.
- Osen KK (1969) Cytoarchitecture of the cochlear nuclei in the cat. *Journal of Comparative Neurology* 136:453-484.
- Overholt E, Rubel EW, Hyson RL (1992) A circuit for coding interaural time differences in the chick brainstem. *J Neurosci* 12:1698-1708.
- Park TJ, Grothe B, Pollak GD, Schuller G, Koch U (1996) Neural delays shape selectivity to interaural intensity differences in the lateral superior olive. *J Neurosci* 16:6554-6566.
- Park TJ, Klug A, Holinstat M, Grothe B (2004) Interaural level difference processing in the lateral superior olive and the inferior colliculus. *Journal of Neurophysiology* 92:289-301.
- Park TJ, Pollak GD (1993) Gaba shapes sensitivity to interaural intensity disparities in the mustache bat's inferior colliculus: implications for encoding sound location. *J Neurosci* 13:2050-2067.
- Park TJ, Pollak GD (1994) Azimuthal receptive fields are shaped by gabaergic inhibition in the inferior colliculus of the mustache bat. *J Neurophysiol* 72:1080-1102.
- Parks TN, Rubel EW (1975) Organization and development of brain stem auditory nuclei of the chicken: organization of projections from n. magnocellularis to n. laminaris. *J Comp Neurol* 164:435-448.
- Pecka M, Grothe B (2008) Interaural Time Difference Processing in the Medial Superior Olive of the Gerbil: Invariance to Changes in Absolute Intensity.

- Pena JI, Viète S, Albeck Y, Konishi M (1996) Tolerance to sound intensity of binaural coincidence detection in the nucleus laminaris of the owl. *The Journal of Neuroscience* 16:7046-7054.
- Perkins RE (1973) An electron microscopic study of synaptic organization in the medial superior olive of normal and experimental chinchillas. *J Comp Neurol* 148:387-415.
- Pollak GD (1988) Time is traded for intensity in the bat's auditory system. *Hear Res* 36:107-124.
- Pollak GD, Burger RM, Klug A (2003) Dissecting the circuitry of the auditory system. *Trends Neurosci* 26:33-39.
- Pollak GD, Burger RM, Park TJ, Klug A, Bauer EE (2002) Roles of inhibition for transforming binaural properties in the brainstem auditory system. *Hear Res* 168:60-78.
- Pouille F, Scanziani M (2001) Enforcement of temporal fidelity in pyramidal cells by somatic feed-forward inhibition. *Science* 293:1159-1163.
- Rampon C, Luppi PH, Fort P, Peyron C, Jouvet M (1996) Distribution of glycine-immunoreactive cell bodies and fibers in the rat brain. *Neuroscience* 75:737-755.
- Rayleigh L (1907) On our perception of sound direction. *Philos Mag* 13:214-232.
- Reed MC, Durbeck L (1995) Delay Lines and Auditory Processing. *Comments Theoretical Biology* 3:441-461.
- Rhode WS, Smith PH (1986) Encoding timing and intensity in the ventral cochlear nucleus of the cat. *J Neurophysiol* 56:261-286.
- Roberts RC, Ribak CE (1987) GABAergic neurons and axon terminals in the brainstem auditory nuclei of the gerbil. *J Comp Neurol* 258:267-280.
- Rose JE, Galambos R, Hughes JR (1959) Microelectrode studies of the cochlear nuclei of the cat. *Bull Johns Hopkins Hops* 104:211-251.
- Rose JE, Gross NB, Geisler CD, Hind JE (1966) Some neural mechanisms in the inferior colliculus of the cat which may be relevant to localization of a sound source. *J Neurophysiol* 29:288-314.
- Rubel EW, Parks TN (1975) Organization and development of brain stem auditory nuclei of the chicken: tonotopic organization of n. magnocellularis and n. laminaris. *J Comp Neurol* 164:411-433.
- Ryugo DK, Sento S (1991) Synaptic connections of the auditory nerve in cats: relationship between endbulbs of held and spherical bushy cells. *J Comp Neurol* 305:35-48.
- Sabatini BL, Regehr WG (1999) Timing of synaptic transmission. *Annu Rev Physiol* 61:521-542.
- Saint Marie RL, Baker RA (1990) Neurotransmitter-specific uptake and retrograde transport of [3H]glycine from the inferior colliculus by ipsilateral projections of the superior olivary complex and nuclei of the lateral lemniscus. *Brain Res* 524:244-253.
- Sakaba T, Neher E (2003) Direct modulation of synaptic vesicle priming by GABA(B) receptor activation at a glutamatergic synapse. *Nature* 424:775-778.
- Saunier-Rebori B (2008) The neural mechanisms of persistent inhibition in the DNLL of the Gerbil (*Meriones unguiculatus*). Thesis. LMU München.
- Scholz KP, Miller RJ (1991) GABAB receptor-mediated inhibition of Ca²⁺ currents and synaptic transmission in cultured rat hippocampal neurones. *J Physiol* 444:669-686.

- Schuchmann M, Hubner M, Wiegube L (2006) The absence of spatial echo suppression in the echolocating bats *Megaderma lyra* and *Phyllostomus discolor*. *J Experim Biol* 209:152-157.
- Schwartz IR (1992) The superior olivary complex and lateral lemniscal nuclei. In: *The mammalian auditory pathway: Neuroanatomy* (Webster DB, Popper AN, Fay RR, eds), pp 117-167. New York: Springer.
- Scott LL, Mathews PJ, Golding NL (2005) Posthearing developmental refinement of temporal processing in principal neurons of the medial superior olive. *J Neurosci* 25:7887-7895.
- Seidl AH, Grothe B (2005) Development of sound localization mechanisms in the mongolian gerbil is shaped by early acoustic experience. *J Neurophysiol* 94:1028-1036.
- Shneiderman A, Oliver DL, Henkel CK (1988) Connections of the dorsal nucleus of the lateral lemniscus: an inhibitory parallel pathway in the ascending auditory system? *J Comp Neurol* 276:188-208.
- Siveke I, Pecka M, Seidl AH, Baudoux S, Grothe B (2006) Binaural response properties of low-frequency neurons in the gerbil dorsal nucleus of the lateral lemniscus. *J Neurophysiol* 96:1425-1440.
- Smith AJ, Owens S, Forsythe ID (2000) Characterisation of inhibitory and excitatory postsynaptic currents of the rat medial superior olive. *J Physiol* 529:681-698.
- Smith PH, Joris PX, Carney LH, Yin TC (1991) Projections of physiologically characterized globular bushy cell axons from the cochlear nucleus of the cat. *J Comp Neurol* 304:387-407.
- Smith PH, Joris PX, Yin TC (1993) Projections of physiologically characterized spherical bushy cell axons from the cochlear nucleus of the cat: evidence for delay lines to the medial superior olive. *J Comp Neurol* 331:245-260.
- Smith PH, Joris PX, Yin TC (1998) Anatomy and physiology of principal cells of the medial nucleus of the trapezoid body (MNTB) of the cat. *Journal of Neurophysiology* 79:3127-3142.
- Spitzer MW, Bala AD, Takahashi TT (2003) Auditory spatial discrimination by barn owls in simulated echoic conditions. *J Acoust Soc Am* 113:1631-1645.
- Spitzer MW, Semple MN (1995) Neurons sensitive to interaural phase disparity in gerbil superior olive: diverse monaural and temporal response properties. *J Neurophysiol* 73:1668-1690.
- Spitzer MW, Takahashi TT (2006) Sound localization by barn owls in a simulated echoic environment. *J Neurophysiol* 95:3571-3584.
- Stotler WA (1953) An experimental study of the cells and connections of the superior olivary complex of the cat. *Journal of Comparative Neurology* 98:401-432.
- Sullivan WE, Konishi M (1986) Neural map of interaural phase difference in the owl's brainstem. *Proc Natl Acad Sci U S A* 83:8400-8404.
- Svirskis G, Dodla R, Rinzel J (2003) Subthreshold outward currents enhance temporal integration in auditory neurons. *Biol Cybern* 89:333-340.
- Thompson GC, Cortez AM, Lam DM (1985) Localization of GABA immunoreactivity in the auditory brainstem of guinea pigs. *Brain Research* 339:119-122.
- Tollin DJ, Yin TCT (2005) Interaural phase and level difference sensitivity in low-frequency neurons in the lateral superior olive. *Journal of Neuroscience* 25:10648-10657.

- Tretter V, Jacob TC, Mukherjee J, Fritschy JM, Pangalos MN, Moss SJ (2008) The clustering of GABA(A) receptor subtypes at inhibitory synapses is facilitated via the direct binding of receptor alpha 2 subunits to gephyrin. *J Neurosci* 28:1356-1365.
- Tsuchitani C, Boudreau JC (1969) Stimulus level of dichotically presented tones and cat superior olive S-segment cell dcharge. *J Acoust Soc Am* 46:979-988.
- Vater M, Habbicht H, Kössl M, Grothe B (1992) The functional role of gaba and glycine in monaural and binaural processing in the inferior colliculus of horseshoe bats. *J Comp Physiol A* 171:541-553.
- von Békésy G. (1947) The variations of phase along the basilar membrane with sinusoidal vibrations. *J Acoust Soc Am* 19:452-460.
- von Gersdorff H, Borst JG (2002) Short-term plasticity at the calyx of held. *Nat Rev Neurosci* 3:53-64.
- Warr WB (1966) Fiber degeneration following lesions in the anterior ventral cochlear nucleus of the cat. *Experimental Neurology* 14:453-474.
- Wentholt RJ, Huie D, Altschuler RA, Reeks KA (1987) Glycine immunoreactivity localized in the cochlear nucleus and superior olivary complex. *Neuroscience* 22:897-912.
- Wimmer VC, Nevian T, Kuner T (2004) Targeted in vivo expression of proteins in the calyx of Held. *Pflugers Arch* 449:319-333.
- Wu WL, Ziskind-Conhaim L, Sweet MA (1992) Early development of glycine- and GABA-mediated synapses in rat spinal cord. *J Neurosci* 12:3935-3945.
- Yang L, Pollak GD (1998) Features of ipsilaterally evoked inhibition in the dorsal nucleus of the lateral lemniscus. *Hear Res* 122:125-141.
- Yang L, Pollak GD (1994b) The roles of gabaergic and glycinergic inhibition on binaural processing in the dorsal nucleus of the lateral lemniscus of the mustache bat. *J Neurophysiol* 71:1999-2013.
- Yang L, Pollak GD (1994a) Binaural Inhibition in the Dorsal Nucleus of the Lateral Lemniscus of the Mustached Bat Affects Responses for Multiple Sounds. *Audit Neurosci* 1:1-17.
- Yang LC, Monsivais P, Rubel EW (1999) The superior olivary nucleus and its influence on nucleus laminaris: A source of inhibitory feedback for coincidence detection in the avian auditory brainstem. *Journal of Neuroscience* 19:2313-2325.
- Yin TC, Chan JC (1990) Interaural time sensitivity in medial superior olive of cat. *J Neurophysiol* 64:465-488.
- Zheng W, Knudsen EI (2001) Gabaergic inhibition antagonizes adaptive adjustment of the owl's auditory space map during the initial phase of plasticity. *J Neurosci* 21:4356-4365.
- Zheng WM, Knudsen EI (1999) Functional selection of adaptive auditory space map by GABA(A)-mediated inhibition. *Science* 284:962-965.
- Ziskind-Conhaim L (1998) Physiological functions of GABA-induced depolarizations in the developing rat spinal cord. *Perspect Dev Neurobiol* 5:279-287.

List of abbreviations

AVCN	anteroventral cochlear nucleus
BF	best frequency (the frequency that elicited the highest response at the central peak of the ITD function)
dB	decibel
CF	characteristic frequency (the frequency that elicited responses at the lowest intensity for binaural stimulation with IID=0 and ITD=0)
DNLL	dorsal nucleus of the lateral lemniscus
E/E	excitatory/excitatory (contra/ipsi)
E/I	excitatory/inhibitory (contra/ipsi)
EPSP	excitatory post-synaptic potential
GABA	gamma-amino-butyric acid
Hz	Hertz
IID	interaural intensity difference
IPD	interaural phase difference
IPSP	inhibitory post-synaptic potential
ITD	interaural time difference
LSO	lateral superior olive
MNTB	medial nucleus of the trapezoid body
MSO	medial superior olive
NL	nucleus laminaris
PI	persistent inhibition
SOC	superior olivary complex
VCN	ventral cochlear nucleus
VS	vector strength

Curriculum Vitae

Family name: Pecka
Given name: Michael
Address: Lochhauserstrasse 5A; 82178 Puchheim
Email: pecka@zi.biologie.uni-muenchen.de
Nationality: Germany
Date of Birth: 11.09.1977
Gender: male
Marital status: married since September 2005
first son born in May 2008
Education: 09/1984 – 07/1988 Elementary school in Puchheim
09/1988 – 07/1997 Gymnasium in Puchheim
07/1997 Abitur
10/1998 – 07/2004 Study of Biology at the Ludwig
Maximilian University of Munich
10/2003 – 07/2004 Diploma work at the Max Planck
Institute of Neurobiology in
Martinsried
07/2004 Diploma (Graduation, Major:
Neurobiology)
since 01/05 PhD student at the LMU Munich
since 10/05 Member of the International Max-
Planck Research School for
molecular and cellular Life
Sciences
Professional experience: 10/1997 – 09/1998 Community service at
Johanniter Unfall-Hilfe e.V.
Research experience 04/2003 – 04/2004 Student assistant at the Max
Planck Institute of Neurobiology

List of publications

- Siveke I, Pecka M, Seidl AH, Baudoux S, and Grothe B. Binaural response properties of low-frequency neurons in the gerbil dorsal nucleus of the lateral lemniscus (2006) *Journal of Neurophysiology* 96:1425-1440.
- Hermann J, Pecka M, von Gersdorff H, Grothe B, and Klug A. Synaptic transmission at the calyx of Held under in vivo-like activity levels (2007) *Journal of Neurophysiology* 98:807-820.
- Pecka M, Zahn TP, Saunier-Rebori B, Siveke I, Felmy F, Wiegrebe L, Klug A, Pollak GD, and Grothe B. Inhibiting the inhibition: a neuronal network for sound localization in reverberant environments (2007) *Journal of Neuroscience* 27(7):1782-1790.
- Pecka M, Brand A, Behrend O, and Grothe B. Interaural time difference processing in the medial superior olive: the role of glycinergic inhibition (2008). *Journal of Neuroscience* 28(27):6914-25.
- Magnusson AK, Park TJ, Pecka M, Grothe B and Koch U. Retrograde GABA signalling adjusts sound localization by balancing excitation and inhibition in the brainstem (2008). *Neuron* 59(1):125-37.

Acknowledgments

First and foremost, I thank Prof. Dr. Benedikt Grothe for his excellent guidance throughout my entire time in his lab. Benedikt, I am very grateful to you for numerously expressing your belief in me by helping me to develop scientifically as well as personally.

I would like to thank all present and former members of the Grothe, Wiegrebe and Leibold labs for an extremely warm and kind working atmosphere, which was crucial for me to succeed. In particular, I want to acknowledge the following people that significantly contributed to this work: Drs. Ida Siveke, Felix Felmy, Achim Klug, Ursula Koch, Lutz Wiegrebe, Nick Lesica and Profs. Christian Leibold, Mike Burger and George Pollak:

Ida, thank you for clarifying and also for sometimes sharing my confusion regarding ITD processing in our countless discussions.

Felix, even though our data didn't make it into this thesis (IRES stinks!), I really enjoyed working with you and benefited a lot from it.

Achim, Ursula and Lutz, thank you for the valuable advises and fruitful discussions throughout the years.

Nick, thank you for being my Matlab godfather (I still hate structures!) and paper editor. Also, our football/basketball/running work-breaks were much needed to stay sane during the time I performed the MSO experiments (although my throwing shoulder still hurts...).

Christian, your curative expertise was well appreciated every time I knocked on your door suffering from severe CD/CP confusion.

Mike, your help with the preparation was crucial for my MSO adventures to turn out successful.

George, I am sincerely grateful for your enormous support and the thoughtful discussion we had. Thank you for giving me the opportunity to work on PI with you.

Finally, I thank my parents and especially my wife. Laura, I could not have done this without your support.

Ehrenwörtliche Erklärung

Hiermit versichere ich, Michael Pecka, dass die vorliegende Arbeit von mir selbstständig und nur unter Verwendung der angegebenen Hilfsmittel angefertigt wurde.